ISTITUTO NAZIONALE DI FISICA NUCLEARE
Laboratori Nazionali di Frascati

LNF-86/48

G. Barbiellini and C. Santoni:
EXPERIMENTAL STATUS OF WEAK INTERACTIONS.

Estratto da:
Nuovo Cimento Vol.9 n.2 (1986).

Servizio Documentazione
dei Laboratori Nazionali di Frascati
Cas. Postale 13 - Frascati (Roma)

2

La Rivista del Nuovo Cimento
della Società Italiana di Fisica
1986

G. BARBIELLINI and C. SANTONI

Experimental status of weak interactions

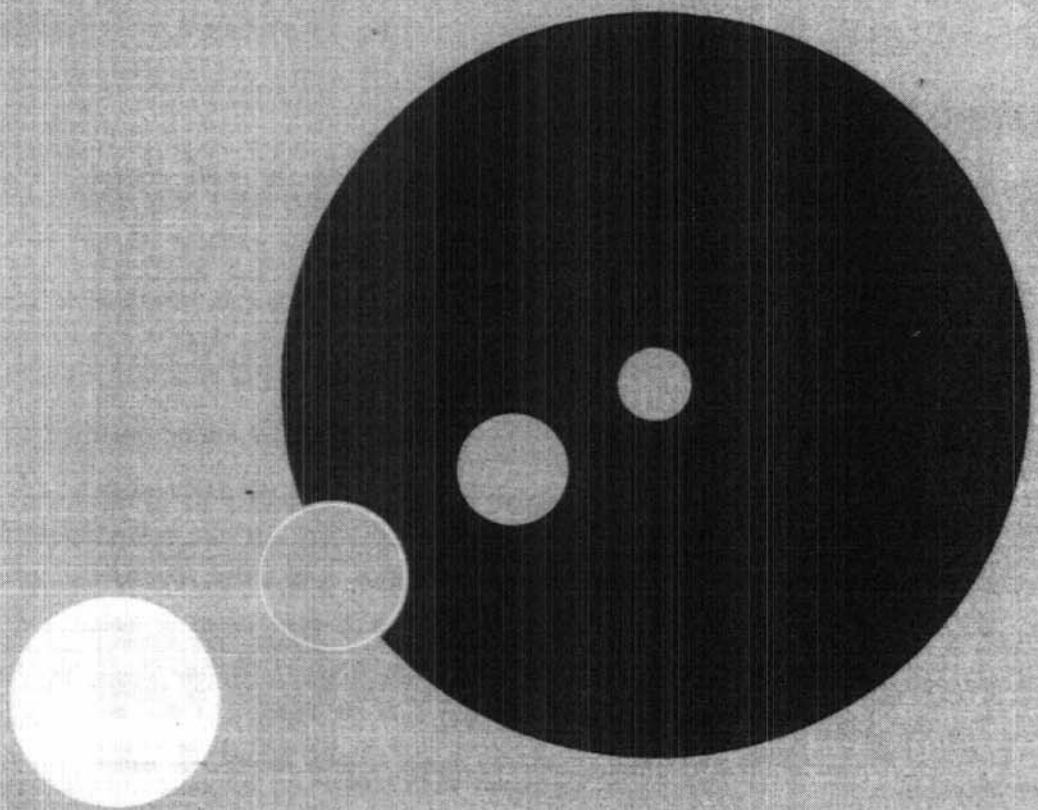

Editrice Compositori Bologna

IL NUOVO CIMENTO

rivista internazionale di fisica

fondata a Pisa nel 1855 da C. MATTEUCCI e R. PIRIA
dal 1897 Organo della Società Italiana di Fisica

pubblicata
sotto gli auspici del Consiglio Nazionale delle Ricerche

La collaborazione alla *Rivista del Nuovo Cimento* è esclusivamente su invito. I lavori possono essere scritti in francese, inglese, italiano, spagnolo o tedesco.

Si prega vivamente d'inviare i lavori destinati alla pubblicazione, in duplice copia, direttamente al **Direttore del Nuovo Cimento, via degli Andalò, 2 - 40124 Bologna.** Ciascuna copia, scritta a macchina su un solo lato del foglio, deve essere corredata di disegni, fotografie e bibliografia con i nomi e le iniziali di tutti gli autori; una serie di disegni originali in inchiostro di China su carta da lucidi deve essere allegata alle copie del lavoro; le eventuali fotografie devono essere stampate su carta bianca lucida pesante. Non si accettano manoscritti in una sola copia od incompleti. I manoscritti non si restituiscono.

Di regola le bozze sono inviate agli autori una sola volta, salvo che non siano state esplicitamente richieste seconde bozze.

Gli autori non hanno spese di pubblicazione, salvo quelle per correzioni dovute ad insufficienze del manoscritto inviato per la pubblicazione, modifiche del testo originario, modifiche o rifacimenti di figure, ecc.

Gli estratti (eventualmente con copertine stampate e montate apposta) possono essere forniti a richiesta secondo la tariffa che la Redazione comunicherà agl'interessati. L'importo di tali estratti, unitamente a quello delle correzioni, sarà fatturato dall'**Editrice Compositori, viale XII Giugno, 1 - 40124 Bologna.**

Norme più dettagliate si trovano nella « Guida per gli Autori », che viene inviata dietro versamento di L. 1.000.

Contribution to *Rivista del Nuovo Cimento* is by invitation only. Papers may be written in English, French, German, Italian or Spanish.

Manuscripts submitted for publication should be sent in duplicate and only to the **Director of Il Nuovo Cimento, via degli Andalò, 2 - I 40124 Bologna (Italy).** Each copy, typewritten on one side of the sheets only, must be complete with drawings, photographs and references with the names and initials of all the authors; a set of original drawings in India ink on tracing paper must be enclosed with the copies of the manuscript; photographs must be on heavy-weight glossy white paper. Manuscripts either in single copies or incomplete will not be accepted. Manuscripts will not be returned.

Proofs will be sent only once unless second proofs are specifically requested for by the authors.

Authors will be charged only for corrections due to lack of clarity of the manuscript submitted, modifications to the original text, modifications or remaking of figures, etc.

Reprints as well as covers printed to order may be supplied on payment. The Editorial Office will give the corresponding prices on request. The cost of reprints and the charges for corrections will be invoiced by **Editrice Compositori, viale XII Giugno, 1 - I 40124 Bologna (Italy).**

Further details are contained in the « Guide for the Authors », which will be sent against payment of US $ 1.00.

Direzione e Redazione Via degli Andalò, 2 40124 Bologna

G. BARBIELLINI and C. SANTONI

Experimental Status of Weak Interactions.

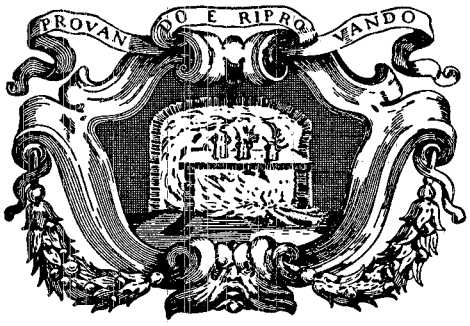

RIVISTA DEL NUOVO CIMENTO VOL. 9, N. 2 1986

Experimental Status of Weak Interactions.

G. BARBIELLINI

CERN - Geneva, Switzerland
Istituto Nazionale di Fisica Nucleare - Laboratori Nazionali di Frascati, Italia

C. SANTONI

CERN - Geneva, Switzerland,
Istituto Nazionale di Fisica Nucleare - Sezione Sanità
Istituto Superiore di Sanità - Roma, Italia

(ricevuto il 31 Agosto 1985)

1. – Introduction.

1·1. *The standard model of weak interactions.* – Weak interactions are responsible for many phenomena in Nature, such as beta-decay of nuclei, muon decay, interactions of neutrinos, etc. In contrast with the strong and electromagnetic interactions, they violate a number of conservation laws such as space parity P, charge conjugation C, combined inversion of charge and parity CP, strangeness, charm, and others.

Until now, all the experimental evidence has been in favour of the so-called standard model [1]. In particular, the discovery of the predicted weak neutral currents [2] and, recently, the detection, at the CERN SPS (*) $p\bar{p}$ Collider [3], of the bosons $W^{\pm}$ and Z^0 responsible for weak interactions, with the expected masses, are amongst the most important physical results of the last decade.

The standard model is a renormalizable theory [4] which allows the unification of weak and electromagnetic interactions.

The sources of the weak and electromagnetic forces are fermions: neutral neutrinos (ν_e, ν_μ, ν_τ), negatively charged leptons (electron (e), muon (μ), tau (τ)) and quarks with charge $\frac{2}{3}$ (up (u), charm (c), top (t)) and $-\frac{1}{3}$ (down (d), strange (s), bottom (b)) in units of the electron charge. Each particle has a

(*) For the sake of simplicity, the names of laboratories and Collaborations or experiments have been abbreviated in the text. They are shown in full in the appendix.

corresponding antiparticle. They are naturally grouped in three families characterized by the lepton and quark flavours: $((\nu_e, e), (u, d))$, $((\nu_\mu, \mu), (c, s))$ and $((\nu_\tau, \tau), (t, b))$. The lepton and quark members of the same family have an electric charge that differs by one.

In order to take into account the fact that the charged-current (CC) interactions are of the $V - A$ form (V = vector, A = axial-vector), the left-handed fermion fields are put into weak-isospin doublets $(f, f')_L$:

$$(1.1) \qquad \begin{cases} \begin{pmatrix} \nu_e \\ e' \end{pmatrix}_L \begin{pmatrix} \nu_\mu \\ \mu' \end{pmatrix}_L \begin{pmatrix} \nu_\tau \\ \tau' \end{pmatrix}_L & \text{(leptons)}, \\ \begin{pmatrix} u \\ d' \end{pmatrix}_L \begin{pmatrix} c \\ s' \end{pmatrix}_L \begin{pmatrix} t \\ b' \end{pmatrix}_L & \text{(quarks)}. \end{cases}$$

The right-handed fields are members of weak-isospin singlets (f_R), (f'_R):

$$(1.2) \qquad \begin{cases} e'_R, \quad \mu'_R, \quad \tau'_R & \text{(leptons)}, \\ u_R, \quad c_R, \quad t_R, \quad d'_R, \quad s'_R, \quad b'_R & \text{(quarks)}. \end{cases}$$

Right-handed neutrinos do not exist. The fields e', μ', τ' coincide with the mass eigenstates, whilst d', s' and b' are related to the mass eigenstates of charge $-\frac{1}{3}$ quarks by a unitary transformation (see sect. **3**).

The left- and right-handed fermion fields are defined by

$$(1.3) \qquad f_L(f'_L) = \tfrac{1}{2} \times (1 + \gamma_5) f(f'), \quad f_R(f'_R) = \tfrac{1}{2} \times (1 - \gamma_5) f(f').$$

Three vector bosons for the $SU_{2,L}$ group ($W_\mu^{1,2,3}$) and one vector boson for the U_1 group (B_μ) are introduced, requiring a local symmetry of the free-fermion field Lagrangian for phase transformation of all fields and a rotation of the isospin left-handed doublets. The couplings of the W_μ and of the B_μ to the fermions are defined by two constants, g and g', corresponding to the two symmetry groups $SU_{2,L}$ and U_1, respectively. The strength depends on the fermion representation (see eqs. (1.1) and (1.2)).

An undiscovered neutral Higgs particle is believed to be at the origin of all the particle masses except its own, through the so-called spontaneous-symmetry-breaking mechanism [5].

The Lagrangian which describes the interactions of vector bosons with the fermion fields f and f' contains three terms:

$$(1.4) \qquad L = L^{CC} + L^{e.m.} + L^{NC}.$$

The charged-current term (L^{CC}) is given by

$$(1.5) \qquad L^{CC} = (g/2\sqrt{2})(J^\mu_{CC} W^-_\mu + \text{h.c.}).$$

The expression

$$J^{\mu}_{\mathrm{CC}} = \bar{f}_{\mathrm{L}} \gamma^{\mu} f'_{\mathrm{L}} \tag{1.6}$$

is the fermion CC (the fields f_{L} and f'_{L} represent the members of the weak isodoublet (1.1) with the third component equal to $\frac{1}{2}$ and $-\frac{1}{2}$, respectively). The charged boson fields are

$$W^{\pm}_{\mu} = (W^{1}_{\mu} \pm i W^{2}_{\mu})/\sqrt{2} \,. \tag{1.7}$$

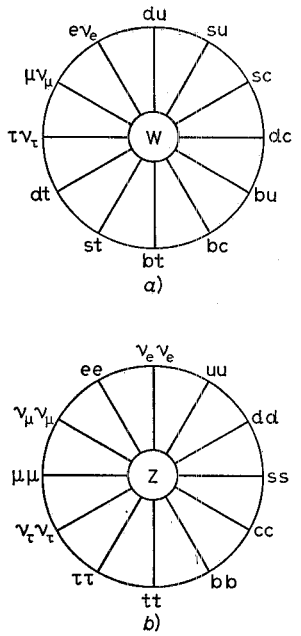

Fig. 1. – Scheme of the coupling of lepton and quark CC to the W (a)) and NC to the Z^0 (b)).

The coupling of the fermion with the charged vector bosons is schematized in fig. 1a). A comparison of eq. (1.5) with the local $V - A$ Lagrangian for μ decay yields

$$g^2/8m^2_{\mathrm{W}} = G/\sqrt{2} \,, \tag{1.8}$$

where $G = 1.17 \cdot 10^{-5}\ (\mathrm{GeV})^{-2}$ is the Fermi constant and m_{W} is the charged-boson mass.

Assuming the existence of six quarks, the quark sector of the CC Lagrangian

(1.5) can be written in the form

$$L^{CC} = (g/2\sqrt{2})\left\{\left[(\bar{u},\ \bar{c},\ \bar{t})\,\gamma^{\mu}(1+\gamma^{5})\,U\begin{pmatrix} d \\ s \\ b \end{pmatrix}\right] W_{\mu}^{-} + \text{h.c.}\right\}. \tag{1.9}$$

The unitary matrix U describing the weak coupling of $+\frac{2}{3}$ quarks with $-\frac{1}{3}$ quarks depends on four parameters. The Kobayashi-Maskawa representation of the matrix U [6] is given by

$$U = \begin{pmatrix} c_1 & s_1 c_3 & s_1 s_3 \\ -s_1 c_2 & c_1 c_2 c_3 - s_2 s_3 \exp[i\delta] & c_1 c_2 s_3 + s_2 c_3 \exp[i\delta] \\ s_1 s_2 & -c_1 s_2 c_3 - c_2 s_3 \exp[i\delta] & -c_1 s_2 s_3 + c_2 c_3 \exp[i\delta] \end{pmatrix}, \tag{1.10}$$

where s_i and c_i are the sine and the cosine of the mixing angles θ_i. In particular, the angle $\theta_1 = \theta_C$, defining the interaction of the up and down quarks, is the Cabibbo angle [7] ($\cos\theta_C = 0.9733$). The phase δ could possibly be the origin of CP violation. The second term in eq. (1.4) describes the electromagnetic Lagrangian,

$$L^{\text{e.m.}} = g \sin\theta_w (J^{\mu}_{\text{e.m.}} A_{\mu} + \text{h.c.}). \tag{1.11}$$

The electromagnetic current $J^{\mu}_{\text{e.m.}}$ is given by

$$J^{\mu}_{\text{e.m.}} = q_f \bar{f}\gamma^{\mu} f + q_{f'} \bar{f}'\gamma^{\mu} f', \tag{1.12}$$

where q_f ($q_{f'}$) is the fermion charge. The photon field A_{μ} is obtained by a linear combination of the fields B_{μ} and W^3_{μ}. The weak angle θ_w is defined by

$$\sin^2\theta_w = g'^2/(g^2 + g'^2). \tag{1.13}$$

From eq. (1.11) it follows that

$$e = g \sin\theta_w, \tag{1.14}$$

where e is the electron charge.

The third term in eq. (1.4), L^{NC}, is the weak neutral-current (NC) Lagrangian:

$$L^{NC} = (e/\sin\theta_w \cos\theta_w)(J^{\mu}_{NC} Z_{\mu} + \text{h.c.}). \tag{1.15}$$

The NC is given by

$$J^{\mu}_{NC} = \varepsilon(f_L)\bar{f}_L\gamma^{\mu} f_L + \varepsilon(f_R)\bar{f}_R\gamma^{\mu} f_R + \varepsilon(f'_L)\bar{f}'_L\gamma^{\mu} f'_L + \varepsilon(f'_R)\bar{f}'_R\gamma^{\mu} f'_R. \tag{1.16}$$

The Z^0-boson is described by the field Z_μ obtained by a linear combination of the B_μ and W^3_μ fields, orthogonal to A_μ. In eq. (1.16) the NC chiral couplings are defined by

$$\varepsilon(f_L[f'_L]) = I^3 - q\sin^2\theta_w\,, \qquad \varepsilon(f_R[f'_R]) = -q\sin^2\theta_w\,. \tag{1.17}$$

In eqs. (1.17) q is the charge of the fermion and I^3 is the third component of the weak isospin. Table I shows the values of $\varepsilon(f_L[f'_L])$ and $\varepsilon(f_R[f'_R])$ predicted by the standard model. The coupling of the fermions to the Z^0 is schematized in fig. 1*b*).

TABLE I. – *Values of* $\varepsilon(f_L)$ *and* $\varepsilon(f_R)$ *predicted by the standard model.*

Particle	$\varepsilon(f_L)$	$\varepsilon(f_R)$
ν	$\frac{1}{2}$	0
e, μ, τ	$-\frac{1}{2}+\sin^2\theta_w$	$\sin^2\theta_w$
u, c, t	$\frac{1}{2}-\frac{2}{3}\sin^2\theta_w$	$-\frac{2}{3}\sin^2\theta_w$
d, s, b	$-\frac{1}{2}+\frac{1}{3}\sin^2\theta_w$	$\frac{1}{3}\sin^2\theta_w$

The J^μ_{NC} can also be given as a sum of a vector ($f\gamma^\mu f$) and an axial-vector ($f\gamma^\mu\gamma_5 f$) term. The relative couplings g^t_V and g^t_A are related to the couplings (1.17) according to

$$g^{t,t'}_V = \varepsilon(f_L[f'_L]) + \varepsilon(f_R[f'_R])\,, \qquad g^{t,t'}_A = \varepsilon(f_L[f'_L]) - \varepsilon(f_R[f'_R])\,. \tag{1.18}$$

As the mixing matrix U (eq. (1.10)) is unitary, it does not appear in the quark sector of the NC Lagrangian (eq. (1.15)). This is the Glashow, Iliopoulos and Maiani (GIM) mechanism [8] for which there are no flavour-changing NCs in the standard model.

The $SU_{2,L}\times U_1$ model unifies weak and electromagnetic interactions in the sense that A_μ and Z_μ are intimately related to each other and to $W^\pm_\mu$. Since $\sin^2\theta_w \approx 1$, the weak and the electromagnetic couplings are of the same order (eq. (1.14)), and the differences in the strengths of these interactions are due to the differences of the intermediate-vector-boson masses:

$$m_\gamma = 0\,, \tag{1.19}$$

$$m_W = (\pi\alpha/\sqrt{2}G\sin^2\theta_w)^{\frac{1}{2}} = 37.3\ \mathrm{GeV}/\sin\theta_w\,, \tag{1.20}$$

$$m_Z = m_W/\cos\theta_w\,. \tag{1.21}$$

The value of the fine-structure constant α at $Q^2 = m_e^2$ is 1/137. Relation (1.21) is obtained assuming that the Higgs fields are members of the weak-isospin doublet [9] (see eqs. (1.26) and (1.27)).

In general in the $SU_{2,L} \times U_1$ frame the weak neutral interactions are described by two parameters: the weak angle θ_w and the ratio of the NC and CC overall strengths,

$$\varrho = m_W^2/m_Z^2 \cos^2 \theta_w . \tag{1.22}$$

The chiral coupling constants are then given by

$$\varepsilon(f_L[f'_L]) = \varrho(I^3 - q \sin^2 \theta_w) , \quad \varepsilon(f_R[f'_R]) = \varrho(-q \sin^2 \theta_w) . \tag{1.23}$$

In the standard model the Higgs particles are members of the isospin doublet [9]

$$\Phi = \begin{pmatrix} \Phi^+ \\ \Phi^0 \end{pmatrix}, \quad \Phi_+ = 1/\sqrt{2}\,(\Phi_1 + i\Phi_2) , \quad \Phi^0 = 1/\sqrt{2}\,(\Phi_3 + i\Phi_4) . \tag{1.24}$$

In the case of the spontaneous breakdown of the symmetry, the Higgs Lagrangian, invariant under a local transformation of the $SU_{2,L} \times U_1$ group, is

$$L = \left[\left(\frac{\partial}{\partial x^\mu} - ig\,\frac{\sigma}{2}\,W^\mu - ig' y B^\mu\right)(\Phi - v)\right]^2 + V(\Phi) . \tag{1.25}$$

Here σ's are the Pauli matrices and y is a constant; $V(\Phi) = -\mu^2 \Phi^* \Phi + h(\Phi^* \Phi)^2$ is the field potential. The parameters μ^2 and h are both positive. The fact that $\mu^2 > 0$ is responsible for the spontaneous symmetry breaking of the theory. Three of the four fields in (1.24) are taken out by a gauge transformation. The mass of the particle described by the surviving field is a free parameter of the theory. The product of the ground state of Φ, v, with the linear combination of the fields W_μ and B_μ in eq. (1.25), is responsible for the W and Z masses. In terms of v we get

$$m_W^2 = \frac{g^2 v^2}{2} = \frac{e^2 v^2}{2 \sin^2 \theta_w} , \tag{1.26}$$

$$m_Z^2 = \frac{v^2 e^2}{2 \sin^2 \theta_w \cos^2 \theta_w} . \tag{1.27}$$

From these equations, $\varrho = 1$.

In a more general theory containing several scalar fields

$$\varrho = \frac{\sum (I^2 - I_3^2 + I)\, v(I, I_3)^2}{2 \sum I_3^2 v(I, I_3)^2} . \tag{1.28}$$

In eq. (1.28) the sum is performed over all the particles with isospin I and third component I_3. The quantities $v(I, I_3)$ are the vacuum expectation values [10].

The Higgs-fermion interaction Lagrangian is

$$L = 1/\sqrt{2}\,(c_f v\bar{f}f + c_{f'} v\bar{f}'f' + c_f \Phi\bar{f}f + c_{f'}\Phi\bar{f}'f')\,, \tag{1.29}$$

where c_f and $c_{f'}$ are unknown constants.

The scalar field is responsible for the fermion masses ($m_f = c_f v$, $m_{f'} = c_{f'} v$) and couples to f and f′ with a strength proportional to the mass of the fermions.

The predictions of the standard model discussed until now have been derived as the lowest order of the theory. Higher-order diagrams change the Born predictions according to the energy scale μ of the experiment and the cuts applied in the analysis of the experimental data.

The renormalized weak angle is given by [11]

$$\sin^2\theta_{w(\overline{MS})}(m_W) = \sin^2\theta_w + \delta_{exp}\,, \tag{1.30}$$

where $\sin^2\theta_w$ is the measurement result and δ_{exp} is a process (experiment)-dependent correction. The quantity $\sin^2\theta_{w(\overline{MS})}(m_W)$ is defined in the modified minimal-subtraction ($\overline{MS}$) renormalization scheme and evaluated at $\mu = m_{W,Z}$. In the case of the determination of $\sin^2\theta_w$ from the measurement of the ratio between the neutrino (antineutrino) CN and CC cross-sections, μ is a few GeV, $\sin^2\theta_w \approx 0.22$ and $\delta_{exp} \approx -0.005\,\%$ [12].

A second definition of the renormalized weak angle, valid for $\varrho = 1$, is given by [13]

$$\sin^2\theta'_w = 1 - m_W^2/m_Z^2\,. \tag{1.31}$$

The definition (1.31) is larger than (1.30) by $\approx 0.6\,\%$ [14].

First-order corrections modify the expressions of the W and Z masses (1.20) and (1.21). One gets

$$m_W = \frac{(37.2804 \pm 0.0003)\ \text{GeV}}{\sin\theta'_w(1-\Delta r)^{\frac{1}{2}}}\,, \tag{1.32}$$

where the largest contribution to Δr is due to the α renormalization. For a top mass of 36 GeV and a mass of the Higgs particle equal to the Z mass, one finds [15]

$$\Delta r = 0.0696 \pm 0.0020\,, \tag{1.33}$$

which yields

$$m_W = \frac{(38.65 \pm 0.04)\ \text{GeV}}{\sin\theta'_w} \tag{1.34}$$

and, assuming $\varrho = 1$,

$$m_Z = \frac{(77.30 \pm 0.08)\ \text{GeV}}{\sin 2\theta'_w}\,. \tag{1.35}$$

In terms of the $W^{\pm}$ and Z^0 masses, one gets

$$\Delta r = 1 - \frac{(37.28\ \mathrm{GeV})^2}{m_W^2(1 - m_W^2/m_Z^2)}. \tag{1.36}$$

Releasing the condition $\varrho = 1$, one obtains

$$\varrho = \frac{m_W^2}{m_Z^2[1 - (38.65\ \mathrm{GeV})^2/m_W^2]}. \tag{1.37}$$

Experimental efforts are today concentrated on the verification, with increasing accuracy, of the validity of the standard model. At low energy the main aim of the experiments is to test the structure of the charged and neutral currents. At Q^2, $s \ll m_{W,Z}^2$, the propagator effects are negligible, and weak interactions are described by an effective current-current Hamiltonian,

$$L_{\mathrm{eff}} = (G/\sqrt{2})(J_{\mathrm{CC}}^{\mu} J_{\mu\mathrm{CC}}^{\dagger} + \varrho J_{\mathrm{NC}}^{\mu} J_{\mu\mathrm{NC}}^{\dagger}), \tag{1.38}$$

where J_{CC}^{μ}, J_{NC}^{μ} and ϱ have been defined in eqs. (1.6), (1.16) and (1.22); and $J_{\mu\mathrm{CC}}^{\dagger}$, $J_{\mu\mathrm{NC}}^{\dagger}$ are the Hermitian conjugates of the currents.

At $p\bar{p}$ collider energies ($\sqrt{s} = 540$ GeV), tests of the standard model are based on measurements of the mass and the widths of intermediate vector bosons.

1·2. *Outline of the article.* – In sect. **2** recent results on the determination of the Lorentz structure of weak CC interactions are described. Section **3** is devoted to the determination of the mixing angles in the quark sector of the CC Lagrangian. In sect. **4** experimental evidence of *CP* violation in weak interactions is discussed. Section **5** is dedicated to the experimental status of measurements of neutrino masses and of the search for neutrino oscillations and massive neutrinos. Some recent results on the structure of NCs are discussed in sect. **6**. Particular emphasis is placed on the determination of the NC coupling of the leptons and quarks to the Z^0. In particular, experimental results on *a*) neutrino-electron scattering, *b*) electroweak interference in e^+e^- annihilation, *c*) neutrino-hadron scattering and *d*) charged lepton-hadron interactions are reported. Section **7** is dedicated to the high-energy measurements performed at the CERN SPS $p\bar{p}$ Collider. Experimental limits on the search for Higgs particles are described in sect. **8**.

2. – Structure of weakly charged currents.

In the standard model the space-time structure of the CCs is assumed to be $V - A$. This assumption is supported by many measurements of low-energy phenomena (nuclear beta-decay, μ decay, π decay, etc.). Recent ex-

perimental results on the Lorentz structure of the weak current in CC-induced reactions have been obtained from

1) the measurement of the y distribution in inelastic neutrino interactions,

2) the μ^+ polarization in the experiment $\bar{\nu}_\mu \mathrm{Fe} \to \mu^+ \mathrm{X}$ (test of helicity conservation in the CC),

3) the purely leptonic reaction $\nu_\mu e^- \to \mu^- \nu_e$,

4) the measurement of the asymmetry parameter ξ in muon decay,

5) the measurement of the Michel parameter in τ decay,

6) the inelasticity distribution of opposite-sign dimuon events (test of the family universality of the CC in neutrino interactions).

2·1. *Measurement of the y distribution in inelastic neutrino-nucleon interactions.* – The CDHS Collaboration [16] investigated the possibility of the existence of right-handed weak quark currents which couple with the usual left-handed weak lepton currents. They studied the reactions

$$\nu_\mu \mathcal{N} \to \mu^- \mathrm{X}\,, \qquad \bar{\nu}_\mu \mathcal{N} \to \mu^+ \mathrm{X}\,. \tag{2.1}$$

In the quark-parton model the neutrino-nucleon interactions are described in terms of the interaction of neutrinos with the quarks constituting the nucleons. The inclusive cross-sections are expressed in terms of the inelasticity variable y defined by

$$y = E_h/E_\nu = (E_\nu - E_\mu)/E_\nu\,, \tag{2.2}$$

where E_h is the energy of the hadronic system X, and E_ν is the energy of the incoming neutrino: $E_\nu = E_h + E_\mu$ (E_μ energy of the muon), and in terms of the fraction of the nucleon momentum x brought by the scattered quark inside the nucleon.

In the presence of left-handed and right-handed quark currents the differential cross-sections are given by

$$\frac{\mathrm{d}^2\sigma^\nu}{\mathrm{d}x\,\mathrm{d}y} \approx q_L(x) + (1-y)^2 q_R(x)\,, \qquad \frac{\mathrm{d}^2\sigma^{\bar{\nu}}}{\mathrm{d}x\,\mathrm{d}y} \approx q_R(x) + (1-y)^2 q_L(x)\,, \tag{2.3}$$

with

$$q_L(x) = q(x) + \varrho^2 \bar{q}(x)\,, \qquad q_R(x) = \bar{q}(x) + \varrho^2 q(x)\,;$$

ϱ is the ratio of the right-handed to the left-handed coupling, and the functions $q(x)$ and $\bar{q}(x)$ represent the quark and the antiquark structure functions.

Since the neutrino and antineutrino helicities are fixed (equal to -1 for neutrinos and to 1 for antineutrinos) and

$$y = (1 - \cos\theta^*)/2\,, \tag{2.4}$$

where θ^* is the angle of the outgoing lepton in the centre-of-mass system, the y distribution is determined from the conservation of the angular momentum (fig. 2). For a total angular momentum $J = 0$, one has $d\sigma/dy \approx 1$, and, for $J = 1$, $d\sigma/dy \approx (1 - y)^2$.

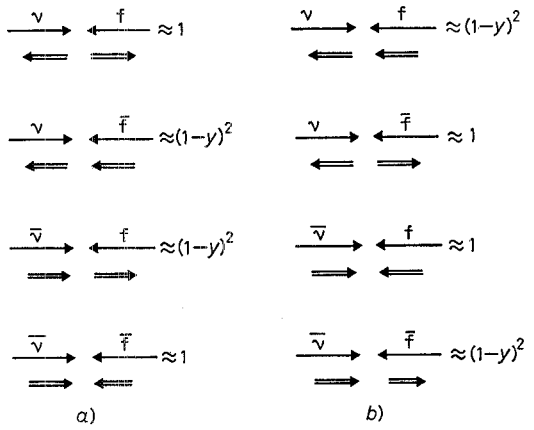

Fig. 2. – Helicity diagrams for νf ($\bar{\nu}$f) interactions in the case of *a*) left-handed and *b*) right-handed charged-fermion currents.

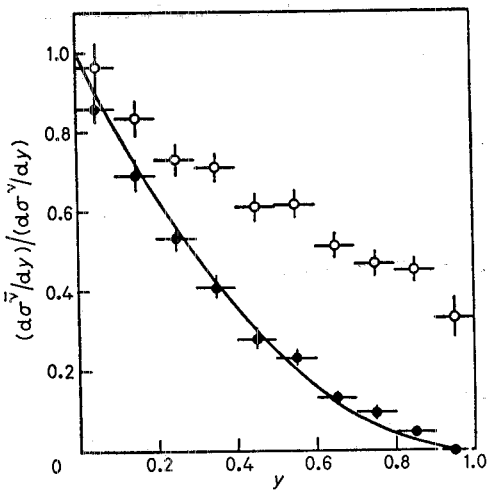

Fig. 3. – Ratio of the CC antineutrino and neutrino differential cross-sections for small and large x, as a function of the inelasticity y [16]: o $x < 0.1$, • $x > 0.4$, —— $(1 - y)^2$.

The analysis of the y measurements is based on a total sample of 175 000 $\bar{\nu}$ and 90 000 ν events collected in both wide- and narrow-band beams (WBB and NBB) in the CDHS detector at the CERN SPS. The average four-momentum transfer squared corresponding to these data is $\langle Q^2 \rangle = 33\ (\mathrm{GeV})^2/c^2$. Figure 3 shows the ratio $R = (\mathrm{d}\sigma^{\bar{\nu}}/\mathrm{d}y)/(\mathrm{d}\sigma^{\nu}/\mathrm{d}y)$ for small and large x, as a function of y. At large x, where the contribution of $\bar{\mathrm{q}}$ is negligible, R is very small, indicating that the contribution of right-handed quark current is very small. An upper limit on ϱ^2 is obtained from the ratio

$$\frac{q_R(x)}{q_L(x)} = \frac{\mathrm{d}^2\sigma^{\bar{\nu}}/\mathrm{d}x\,\mathrm{d}y - (1-y)^2\,(\mathrm{d}^2\sigma^{\nu}/\mathrm{d}x\,\mathrm{d}y)}{\mathrm{d}^2\sigma^{\nu}/\mathrm{d}x\,\mathrm{d}y - (1-y)^2\,(\mathrm{d}^2\sigma^{\bar{\nu}}/\mathrm{d}x\,\mathrm{d}y)} \tag{2.5}$$

for x and y both large. A limit of $|\varrho|^2 < 0.009$ at 90 % c.l. was found.

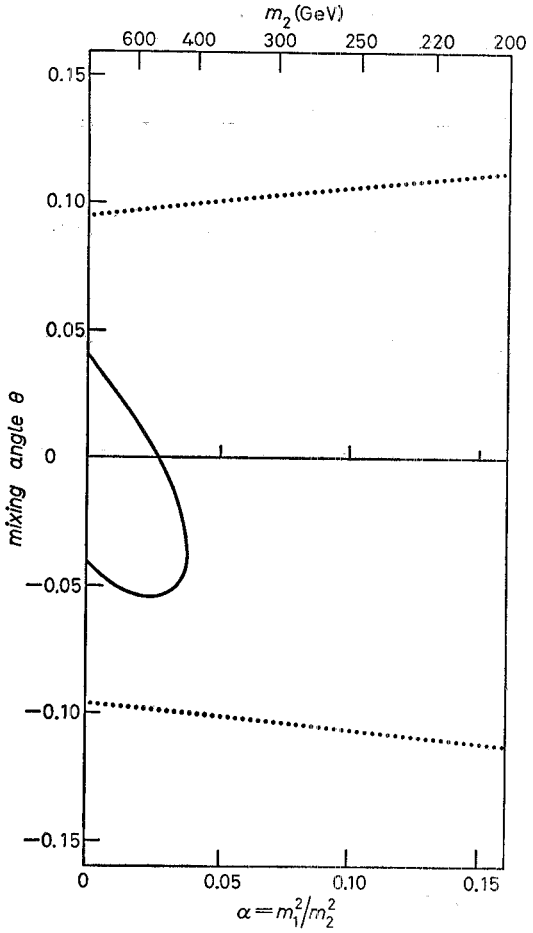

Fig. 4. – Limits on the mixing angle θ [17] as a function of $\alpha = m_1^2/m_2^2$ ($m_1 = m_{W_L}$, $m_2 = m_{W_R}$, θ = (W_L-W_R) mixing angle), $\cdots$ νFe, ——— μ decay.

The measurement puts limits on left-right symmetric models such as $SU_{2,L} \times \times SU_{2,R} \times U_1$ [17]. In this model the two intermediate vector bosons W_L and W_R are mixed in the symmetry-breaking process to yield two mass eigenstates W_1 and W_2, with mass m_1 and m_2, respectively. Figure 4 shows the constraint on the mixing angle θ as a function of $\alpha = m_1^2/m_2^2$.

2·2. *Polarization of* μ^+ *from the inclusive reaction* $\bar{\nu}_\mu \mathrm{Fe} \to \mu^+ \mathrm{X}$. – Neglecting the antiquark content in the nucleon, the most general Lagrangian, which is bilinear in the fields of the reaction, gives the following inelasticity distribution for the process $\bar{\nu}_\mu \mathcal{N} \to \mu^+ \mathrm{X}$ [18]:

$$\mathrm{d}\sigma^{\bar{\nu}}/\mathrm{d}y \approx 2(g_V - g_A)^2 + 2(g_V + g_A)^2(1-y)^2 + \\ + (|g_S|^2 + |g_P|^2)y^2 + 32|g_T|^2(1-y/2)^2 + 8\,\mathrm{Re}\,[g_T(g_S^* + g_P^*)]y(1-y/2)\,, \tag{2.6}$$

where g_i are the coupling constants of the different Lorentz-invariant combinations of the spinors participating in the reaction. The study of the y distribution at high energy is consistent with $V-A$ structure (see previous section), but the same y distribution could be obtained with a mixture of scalar (S), pseudoscalar (P) and tensor (T) terms (confusion theorem [19]). The measurement of the μ^+ helicity can resolve this ambiguity since V and A interactions conserve the helicity, whereas S, P and T interactions do not (fig. 5).

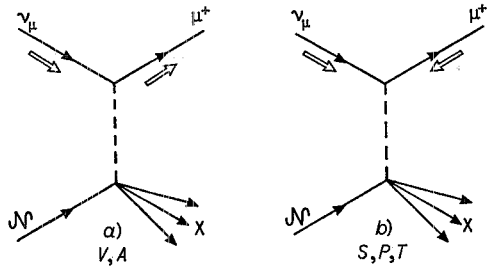

Fig. 5. – Helicity state of the incoming and the outgoing particle in antineutrino-nucleon scattering in the case of *a*) V, A currents and *b*) S, P and T currents.

The experiment was carried out at the CERN SPS WBB using the CDHS detector as an instrumented target where the antineutrino interaction took place, and the CHARM detector as a polarimeter of the stopped μ^+ (fig. 6) [20]. The polarization is derived from the measured asymmetry of the decay positron,

$$R_0(t) = \frac{N_B(t) - N_F(t)}{N_B(t) + N_F(t)} = R_0 \cos(\omega t + \varphi) + \mathrm{const}\,, \tag{2.7}$$

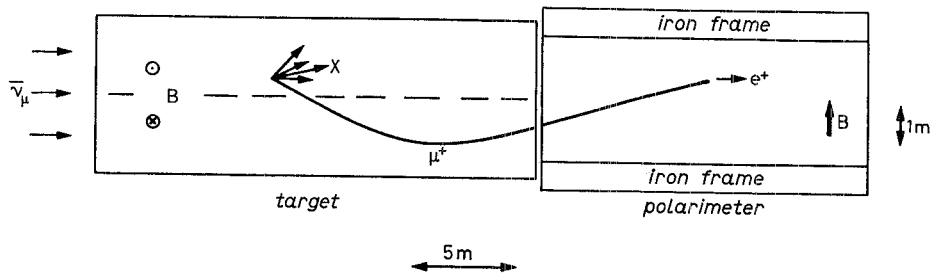

Fig. 6. – Layout of the μ^+ polarization experiment [20].

shown in fig. 7 and is determined from 17500 $\mu^+ \to e^+$ decays in the CHARM polarimeter; $N_{B,F}(t)$ are the number of decay positrons in the backward and forward directions measured at a time t after the μ^+ has stopped. The quantity ω is the muon spin precession frequency, and $R_0 = P_\mu \alpha$, where P_μ is the polarization value of the μ^+ and α is the polarimeter analysing power. The expected phase is $\varphi = 0$ for negative helicity and $\varphi = -\pi$ for positive helicity. The best fit to the data is obtained for

(2.8) $$R_0 = 0.116 \pm 0.010\,, \quad \varphi = -3.02 \pm 0.08\,.$$

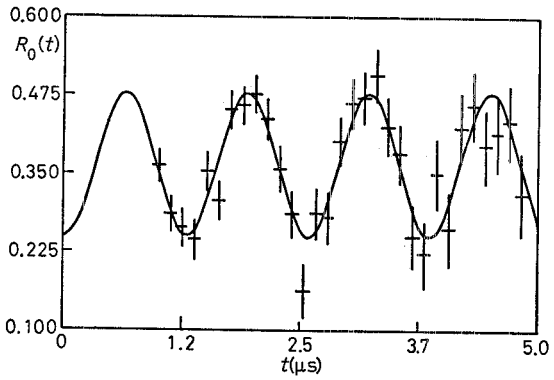

Fig. 7. – Measured asymmetry of the positron produced μ in decay as a function of time [20].

The observed phase φ is in excellent agreement with the value predicted for positive helicity, strongly supporting the hypothesis of pure V and A interactions.

Taking into account the depolarization effects, the measured value of R_0 corresponds to a polarization value

(2.9) $$P_\mu = 0.82 \pm 0.07(\text{stat.}) \pm 0.12(\text{syst.})\,.$$

This polarization value sets an upper limit to the possible S, P and T contributions to the CC reaction at $\langle Q^2 \rangle = 4.5$ (GeV)^2:

$$\sigma_{\mathrm{SPT}}/\sigma_{\mathrm{all}} < 0.20 \qquad (95\,\%\ \mathrm{c.l.}). \tag{2.10}$$

The measured R_0 is shown in fig. 8 *vs.* the inelasticity y. The data show a constant P_μ value over the explored range of y. Since the S and P interactions that contribute to the lepton spin-flip amplitude are zero at $y = 0$ (2.6), assuming the contribution of T to be negligible, the value of the polarization at small y ($y < 0.2$) can be treated as a normalization, and the value at large y ($y > 0.5$) can be used to derive a limit on the S and P contributions which is unaffected by the systematic errors on the integrated polarization value (2.9). The limit was found to be

$$\sigma_{\mathrm{SP}}/\sigma_{\mathrm{all}} < 0.07 \qquad (95\,\%\ \mathrm{c.l.}). \tag{2.11}$$

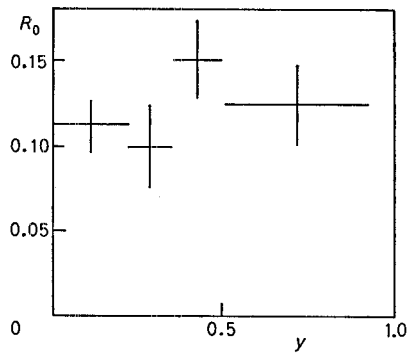

Fig. 8. – Muon precession amplitude as a function of the inelasticity y [20].

2·3. *Neutrino charged-current reactions on an electron target.* – The investigation of the reaction

$$\nu_\mu e^- \to \mu^- \nu_e \tag{2.12}$$

has been suggested by JARLSKOG [21] to complement the information on purely leptonic CC reactions, until recently only studied in muon decay: $\mu^- \to e^- \nu_\mu \bar{\nu}_e$. The centre-of-mass energy $\sqrt{s}$ of reaction (2.12) is low because of the small target mass, and the energy threshold in the laboratory system is 10.9 GeV. The differential cross-section for $s^2 > m_\mu^2$, assuming completely left-handed charged leptons and making no assumption on the helicity of the neutral leptons, is

$$\frac{\mathrm{d}\sigma}{\mathrm{d}y} = \frac{G^2 s}{4\pi} [(1+P)(1-\lambda)y^2 + (1-P)(1+\lambda)], \tag{2.13}$$

with

$$P = \frac{N(\nu_R) - N(\nu_L)}{N(\nu_R) + N(\nu_L)} = \text{neutrino polarization},$$

$$\lambda = \frac{-2 g_V g_A}{g_V^2 + g_A^2}, \qquad y = 1 - E_\mu / E_\nu,$$

where g_A and g_V are the axial-vector and vector coupling constants, respectively. The y^2 term in (2.13) describes the scattering of possible right-handed ν_μ by left-handed e^-, coupled by S and P terms in the effective Lagrangian. A pure $V - A$ structure of the interaction implies that $\lambda = 1$, and a left-handed two-component neutrino implies that $P = 1$.

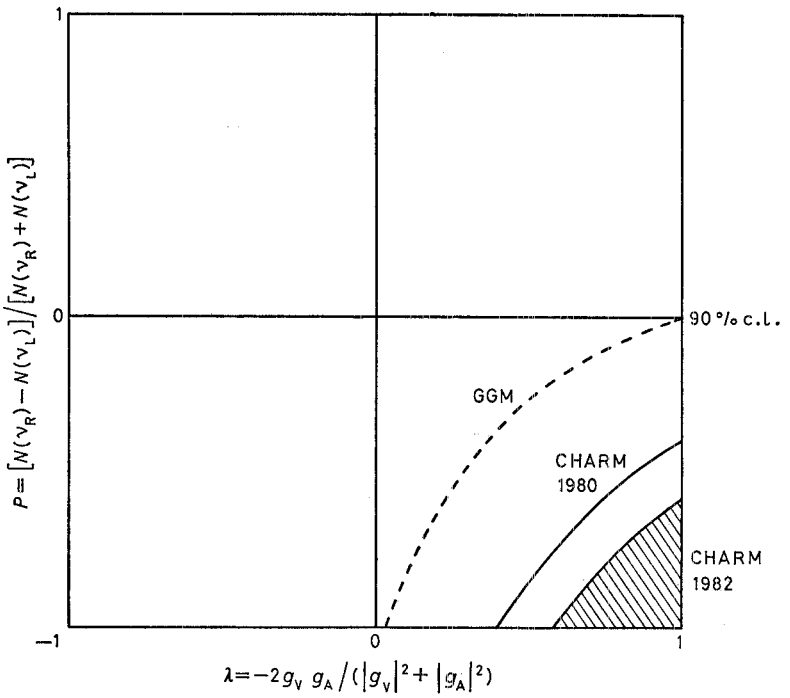

Fig. 9. – Limits on the plane (λ, P) (2.13) from the measurements of the reaction $\nu_\mu e^- \to \mu^- \nu_e$ [22].

Recent data on reaction (2.12) have been obtained by the CHARM Collaboration [22]. After correction for efficiencies, a sample of 594 ± 56 (stat.) $\pm$ ± 22 (syst.) events has been found. The ratio of the measured and the expected cross-sections is 0.98 ± 0.12, assuming pure $V - A$ interaction. Figure 9 shows the 90 % c.l. contour in the (λ, P)-plane. Previous limits from a GGM Collaboration [23] and from the CHARM Collaboration [24] are shown as well.

In the frame of the $SU_{2,L} \times SU_{2,R} \times U_1$ model [17], from this experiment the masses and the mixing of the W_1, W_2 are constrained by the limits $m_2/m_1 > 1.9$ and $\theta < 15°$ at 90 % c.l.

2·4. *Measurement of the asymmetry parameter ξ in muon decay.* – A search for right-handed currents in muon decay has recently been performed at TRIUMF [25]. This experiment measured the combination of the muon decay parameters $A = \delta\xi/\varrho$, where δ is the anisotropic angular shape parameter, ϱ is the isotropic angular shape parameter, and ξ is the asymmetry parameter. In the $V - A$ theory A is equal to 1. If right-handed currents exist, A is related to the ratio of vector-boson masses α and to the the mixing angle θ according to ref. [25],

$$1 - A \approx 2(2\alpha^2 + 2\alpha\theta + \theta^2), \tag{2.14}$$

when α and θ are $\ll 1$.

In the experiment, highly polarized μ^+'s were stopped in pure metal foils to minimize depolarization effects.

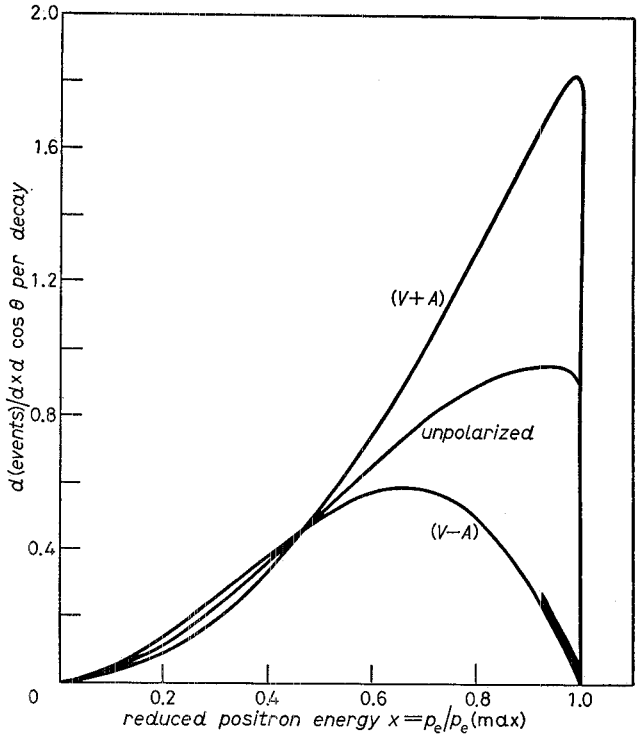

Fig. 10. – Positron momentum spectrum for μ^+ decay at rest in the direction opposite to the muon spin. The apparatus acceptance is denoted by the thick portion of the $V - A$ curve [25].

The quantity A was measured in two ways. The first method measured the rate of positrons emitted in a direction opposite to the muon's spin as a function of their momentum when the stopping target was immersed in a 1.1 T longitudinal magnetic field. As shown in fig. 10, this kinematic region is particularly sensitive to $V+A$ effects because the dominant $V-A$ interaction causes the positron rate to vanish there when $p_e/p(\max) = 1$. The second method measured the amplitude of the spin precession oscillation of the stopping muon subjected to a weak transverse magnetic field. The results obtained with both methods are consistent and were combined to get the limit

$$P_\mu A > 0.9966 \qquad (90\,\%\ \text{c.l.}), \tag{2.15}$$

where P_μ is the muon polarization. The corresponding limits on the mass of an intermediate vector boson which couples to right-handed weak currents [17] are 400 GeV, when no constraints are put on the mixing angle, and 470 GeV, if mixing is assumed to be 0 (fig. 4).

2·5. *Measurement of the Michel parameter in τ decay.* – The space-time structure of the CCs in τ decay has been determined by the DELCO experiment [26] measuring the electron momentum spectrum (fig. 11) in the reaction

$$\tau \to \mathrm{eX}\,. \tag{2.16}$$

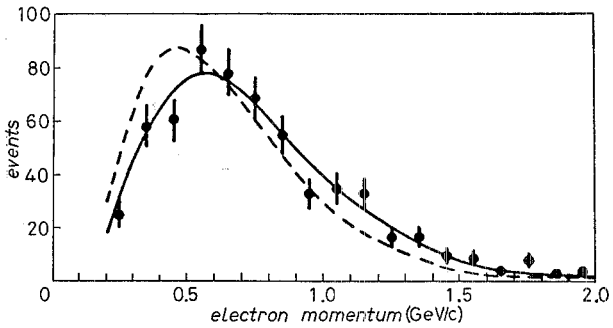

Fig. 11. – Electron momentum spectrum in the reaction $\tau \to \mathrm{eX}$ [26], 621 events, $3.57 < E_{\mathrm{c.m.}} < 7.4$(no ψ''), —— $V-A$, – – – $V+A$.

The Michel parameter ϱ obtained is

$$\varrho = 0.72 \pm 0.15\,. \tag{2.17}$$

The value of the radiatively corrected Michel parameter has been estimated elsewhere [27]. For values of $x = E_e/E(\max)$ in the range $0.3 \div 0.9$, $\varrho = 0.66$ was found for $V-A$ interactions and $\varrho = -0.15$ for $V+A$ interactions. Thus the DELCO result strongly favours $V-A$.

2·6. *Generation universality in the charged current.* – Opposite-sign dimuon (OSD) events in neutrino interactions are interpreted as being due to the following production mechanism:

$$\nu_\mu \mathcal{N} \to \mu \mathrm{D} \mathrm{X}\,, \qquad \mathrm{D} \to \mu \mathrm{Y}\,. \tag{2.18}$$

In the quark-parton model the charmed-meson neutrino production is described by the elementary neutrino-quark interactions:

$$\begin{cases} \nu_\mu \mathrm{d} \to \mu^- \mathrm{c}\,, & \nu_\mu \mathrm{s} \to \mu^- \mathrm{c}\,, \\ \bar{\nu}_\mu \bar{\mathrm{d}} \to \mu^+ \bar{\mathrm{c}}\,, & \bar{\nu}_\mu \bar{\mathrm{s}} \to \mu^+ \bar{\mathrm{c}}\,. \end{cases} \tag{2.19}$$

In the standard model, processes (2.19) are described by the $V-A$ CC Lagrangian (1.5). The y distributions are expected to be flat for both neutrinos and antineutrinos. In the more general case of the existence of left-handed $(V-A)$ and right-handed $(V+A)$ quark currents, the y distribution of reactions (2.19) can be written

$$\mathrm{d}\sigma/\mathrm{d}y = [\alpha + (1-\alpha)(1-y)^2] f(y)\,, \tag{2.20}$$

where the term proportional to α is due to the $V-A$ current and that proportional to $1-\alpha$ to the $V+A$ current; $f(y)$ represents the threshold behaviour.

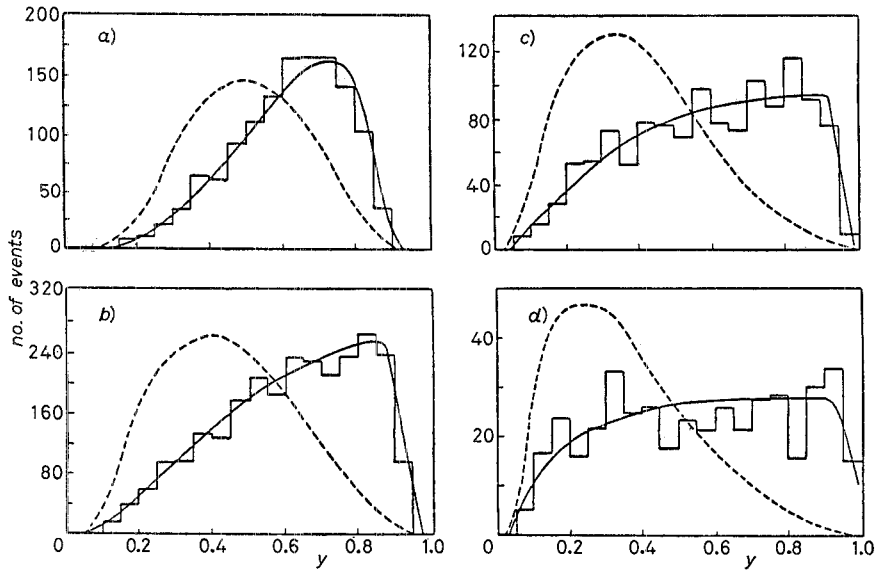

Fig. 12. – The y distribution for ν_μ opposite-sign dimuon events for different neutrino energy windows [28]: *a*) 30 GeV$< E_\nu <$ 50 GeV, *b*) 50 GeV$< E_\nu <$ 100 GeV, *c*) 100 GeV$< E_\nu <$ 150 GeV, *d*) $E_\nu >$ 150 GeV; ——— $V-A$, – – – $V+A$.

In fig. 12 the y distributions for ν_μ opposite-sign dimuon events from the CDHS [28] experiment are shown for different neutrino energy windows.

The results from the CDHS [28] and CHARM Collaborations [29] are

$$\begin{cases} \text{CDHS:} & 1-\alpha<0.07 & (95\%\ \text{c.l.}), \\ \text{CHARM:} & \alpha=0.85\pm0.10\,. \end{cases} \tag{2.21}$$

3. – Measurements of the mixing angles in the quark sector of the charged-current Lagrangian.

3'1. *Introduction.* – The masses and the interactions of the hadrons are very well interpreted in terms of the fundamental constituents called quarks: u, d, c, s, t and b (evidence for the quark t is still preliminary [30]). As we have seen in sect. **1**, the six quarks are divided into two main groups, q^+ and q^-, having an electric charge equal to $+\frac{2}{3}$ and $-\frac{1}{3}$, respectively, in units of the electron charge.

The $q^\pm$ quarks form three «families»:

$$\begin{pmatrix} u \\ d \end{pmatrix}\begin{pmatrix} c \\ s \end{pmatrix}\begin{pmatrix} t \\ b \end{pmatrix} \tag{3.1}$$

with increasing mean value of the doublet member mass.

The forces responsible for the strong interactions of the hadrons are of a gauge nature, obeying a local gauge symmetry SU_3 called quantum chromodynamics (QCD) [31]. The nature of the QCD forces suggests the confinement of the coloured quarks inside the colourless hadron bag. The strong «charge» of the quarks is given in terms of three colours. The known hadrons are made of a quark-antiquark system or of three quarks of different colours, in a combination that neutralizes the QCD charges (white hadrons). The QCD interactions are flavour-independent.

All the known weak decays of the hadrons with a charged lepton in the final state (CC interactions) are described as the transition of a left-handed quark of charge q_L^+ (q_L^-) to one of charge q_L^- (q_L^+) (eq. (1.6)). The assumption of universality of the CC weak interactions for quarks and leptons puts all the fermions in left-handed weak-isospin doublets (eq. (1.1)); the lower isodoublet member is a mixture of the q^- quark mass eigenstates.

The unitary matrix U in eq. (1.9) mixes the mass eigenstates of the quarks with mass q^- and fixes the strength of the CC transition between the q_L^+ and q_L^- states relative to the strength of the μ decay. The most general form of the U matrix is

$$U=\begin{pmatrix} U_{ud} & U_{us} & U_{ub} \\ U_{cd} & U_{cs} & U_{cb} \\ U_{td} & U_{ts} & U_{tb} \end{pmatrix}. \tag{3.2}$$

The elements of the unitary matrix U can be parametrized in terms of three rotation angles and a phase.

In the literature two special representations of the U-matrix are usually used. The first one, due to KOBAYASHI and MASKAWA (KM) [6], is the result of three successive rotations: θ_3 around the z-axis, θ_1 around the rotated x-axis and θ_2 around the new z-axis. A phase δ is introduced in the second rotation:

$$U_{\mathrm{KM}} = \begin{pmatrix} 1 & 0 & 0 \\ 0 & c_2 & s_2 \\ 0 & -s_2 & c_2 \end{pmatrix} \begin{pmatrix} c_1 & s_1 & 0 \\ -s_1 & c_1 & 0 \\ 0 & 0 & \exp[i\delta] \end{pmatrix} \begin{pmatrix} 1 & 0 & 0 \\ 0 & c_3 & s_3 \\ 0 & -s_3 & c_3 \end{pmatrix}, \tag{3.3}$$

where $c_i = \cos\theta_i$ and $s_i = \sin\theta_i$. The z, x and y axes represent the d, s and b quark mass eigenstates. The expression of the KM matrix is given in eq. (1.10).

For small mixing angles, as suggested by the experiments, we have

$$U_{\mathrm{KM}} = \begin{pmatrix} 1 & s_1 & s_1 s_3 \\ -s_1 & 1 & s_3 + s_2 \exp[\delta] \\ s_1 s_2 & -s_2 - s_3 \exp[i\delta] & \exp[i\delta] \end{pmatrix}. \tag{3.4}$$

Neglecting the phase δ and assuming $\theta_1 = \theta_2 = \theta_3 = \theta \approx 0$,

$$U_{\mathrm{KM}} \approx \begin{pmatrix} 1 & \theta & \theta^2 \\ -\theta & 1 & \theta \\ \theta^2 & \theta & 1 \end{pmatrix}. \tag{3.5}$$

This would imply strength $O(1)$ for the transition $\mathrm{q}_{\mathrm{L}}^{-}(\mathrm{q}_{\mathrm{L}}^{+}) \to \mathrm{q}_{\mathrm{L}}^{+}(\mathrm{q}_{\mathrm{L}}^{-})$ inside one flavour family, strength $O(\theta)$ for the transition from one family to the neighbouring one and strength $O(\theta^2)$ for a jump of two families. In reality the long lifetime of the beauty particles (b-quark) (see subsect. 3·2.5) suggests a non-symmetric transition between second to first family and third to second family according to the following expression of the mixing matrix (fig. 13):

$$U_{\mathrm{KM}} \approx \begin{pmatrix} 1 & \theta & \theta^3 \\ -\theta & 1 & \theta^2 \\ \theta^3 & \theta^2 & 1 \end{pmatrix}. \tag{3.6}$$

The phase δ, as originally proposed by KM, can explain the CP violation in the weak decays of the $\mathrm{K}_{\mathrm{L}}^0$ and $\mathrm{K}_{\mathrm{S}}^0$ system. The KM matrix is a generalization, to a six-quark system, of the famous mixing angle introduced by CABIBBO [7]

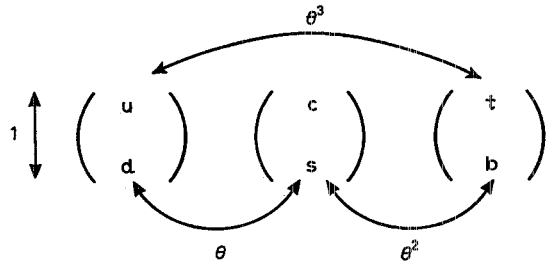

Fig. 13. – Quark transitions in CC weak interactions. The limit is valid in the approximation $\theta_1 = \theta_2 = \theta_3 = \theta \approx 0$ and $\delta = 0$.

to restore the apparent deviation of the weak universality measured in the neutron beta-decay and the strange-particle decay.

A second representation of the U-matrix, due to MAIANI (M) [32], is

$$(3.7) \qquad U_{\mathrm{M}} = \begin{pmatrix} c_\beta c_\theta & c_\beta s_\theta & s_\beta \\ -s_\gamma c_\theta s_\theta \exp[i\delta] - s_\theta c_\gamma & c_\gamma c_\theta - s_\gamma s_\beta s_\theta \exp[i\delta] & s_\gamma c_\beta \exp[i\delta] \\ -s_\beta c_\gamma c_\theta - s_\gamma s_\theta \exp[-i\delta] & -c_\gamma s_\beta s_\theta - s_\gamma c_\theta \exp[i\delta] & c_\gamma c_\beta \end{pmatrix}.$$

For β, θ, $\gamma \approx 0$ one gets

$$(3.8) \qquad U_{\mathrm{M}} \approx \begin{pmatrix} 1 & \theta & \beta \\ -\theta & 1 & \gamma \exp[i\delta] \\ -\beta & -\gamma \exp[i\delta] & 1 \end{pmatrix}.$$

The angles θ, β and γ are then approximately related to the strength of the transitions $\mathrm{u} \leftrightarrow \mathrm{s}$, $\mathrm{u} \leftrightarrow \mathrm{b}$ and $\mathrm{b} \leftrightarrow \mathrm{c}$, respectively.

The measurement of the strength of the CC quark interactions allow a determination of the square of the matrix elements $U_{\mathrm{q}^+\mathrm{q}^-}$ and is not sensitive to the phase δ.

3·2. *Present measured values of the matrix elements.*

3·2.1. The matrix element U_{ud}. The strength of the transition $\mathrm{u} \leftrightarrow \mathrm{d}$ or $\mathrm{d} \leftrightarrow \mathrm{u}$ relative to that of the μ decay is measured with high accuracy in nuclear beta-decay involving spin-zero nuclei in the initial and final states, where only the vector transitions are involved. The value U_{ud} is derived from the measurement of $fT_{\frac{1}{2}}$ in the decay of nuclei such as $^{14}\mathrm{O}$, $^{26}\mathrm{Al}$, $^{34}\mathrm{Cl}$, $^{36}\mathrm{K}$, and others (f is the integral of the Fermi function which takes into account the

finite nuclear size and the effect of screening of the nuclear charge by atomic electrons; $T_{\frac{1}{2}}$ is the nucleus half-life).

The relation between $fT_{\frac{1}{2}}$ and the beta-decay Fermi coupling constant of a vectorial transition G_v is

$$fT_{\frac{1}{2}}\,\delta = (\pi^3 \ln 2)/G_v^2 m_e^5 , \tag{3.9}$$

where m_e is the electron mass and δ takes into account the radiative and nucleus isospin corrections.

The matrix element is given by

$$|U_{ud}| = \frac{G_v}{G_\mu} . \tag{3.10}$$

The quantity G_μ is the weak-coupling constant obtained from the muon lifetime measurement [33].

From the measurements made studying the superallowed transitions of eight different nuclei [34], the $fT_{\frac{1}{2}}$ value, extrapolated to zero nuclear charge, is (3084.4 ± 1.9) s, which gives [35] $|U_{ud}| = 0.9735 \pm 0.0005$. The uncertainties on δ ($\Delta\delta = \pm 0.2\,\%$) lead to an additional uncertainty on $|U_{ud}|$ of ± 0.0010, which, added linearly to the experimental error, gives

$$|U_{ud}| = 0.9735 \pm 0.0015 . \tag{3.11}$$

Other authors [36, 37] assigned rather larger errors ($\approx \pm 0.0025$) to $|U_{ud}|$, showing the uncertainty in the estimation of the theoretical corrections.

This has been confirmed recently by MARCIANO and SIRLIN [37] calculating a more refined radiation correction that modifies the value of $|U_{ud}|$ by $\sim 1\,\%$ corresponding to almost 1σ of formula (3.11).

3·2.2. The matrix element U_{us}. The coupling of the transition $s \leftrightarrow u$ is measured in the decays of the mesons and baryons containing the strange quark.

The most precise results come from the measurement of the semi-leptonic decay of strange baryons [35] and K-mesons [36] listed below:

$$\begin{cases} \Lambda(uds) \to p\ell^-\nu , \\ \Sigma^-(dds) \to n\ell^-\nu , \\ \Xi^0(uss) \to \Sigma^+\ell^-\nu , \\ \Xi^-(dss) \to \Lambda\ell^-\nu , \\ \Xi^-(dss) \to \Sigma^0\ell^-\nu \end{cases} \tag{3.12}$$

and

$$\text{(3.13)} \qquad \begin{cases} K^{\pm}(us) \to \ell^{\pm}\nu\pi^{0}, \\ K^{0}(ds) \to \ell^{\pm}\nu\pi^{\mp}. \end{cases}$$

The relation between the experimental measurements and the value of U_{us} is complicated by the presence of the nondecay quarks, « spectators », in initial and final hadron states. The space distribution of the quark making the transition from the initial to the final hadron is described with a form factor dependence of the decay rate. The information on the form factors is derived by measuring many processes, each having different combinations of the form factors and using relations that are due to the SU_3 flavour symmetry of the hadrons.

The results of the WA2 experiment [35, 38] are summarized in table II, where f_i and g_i are the form factors (in particular f_1 and g_1 are the vector and the axial-vector form factors, respectively).

TABLE II. – *Results obtained by the* WA2 *experiments* [35].

Decay	Events	Branching ratio	g_1/f_1 ($g_2 = 0$)
$\Sigma \to \Lambda e\nu$	1650	$(0.561 \pm 0.031)\cdot 10^{-4}$	$+ 3.00 \pm 0.08$ [a]
$\Sigma \to ne\nu$	3262	$(0.96 \pm 0.05)\cdot 10^{-3}$	$- 0.34 \pm 0.05$
$\Xi \to \Lambda e\nu$	2608	$(5.64 \pm 0.31)\cdot 10^{-4}$	$+ 0.25 \pm 0.05$
$\Xi \to \Sigma e\nu$	150	$(0.87 \pm 0.17)\cdot 10^{-4}$	
$\Lambda \to pe\nu$	7111	$(8.57 \pm 0.36)\cdot 10^{-4}$	$+ 0.70 \pm 0.03$

(a) f_1/g_1 is quoted in this case.

The semi-leptonic-decay amplitudes of all the members of the lowest baryon octet are determined by only three free parameters. These are U_{us}, and the axial-vector reduced matrix elements which correspond to the antisymmetric (F) and symmetric (D) couplings of two octets to form a third octet. A fit to the WA2 data and neutron lifetime measurements [39] including radiative corrections gives [35]

$$\text{(3.14)} \qquad \begin{cases} F = 0.477 \pm 0.011, \\ D = 0.755 \pm 0.011, \\ |U_{us}| = 0.231 \pm 0.003. \end{cases}$$

Figure 14 shows the bands of allowed F and D values deduced from the measurements of g_1/f_1 and of the branching ratios. The ratio $\alpha = D/(D + F)$ is 0.613 ± 0.009; this is close to the SU_6 prediction of $\frac{3}{5}$.

It is also possible to determine $|U_{us}|$ from K_{e3} decay; compared with hyperon decay this has the advantage that only the vector current contributes. How-

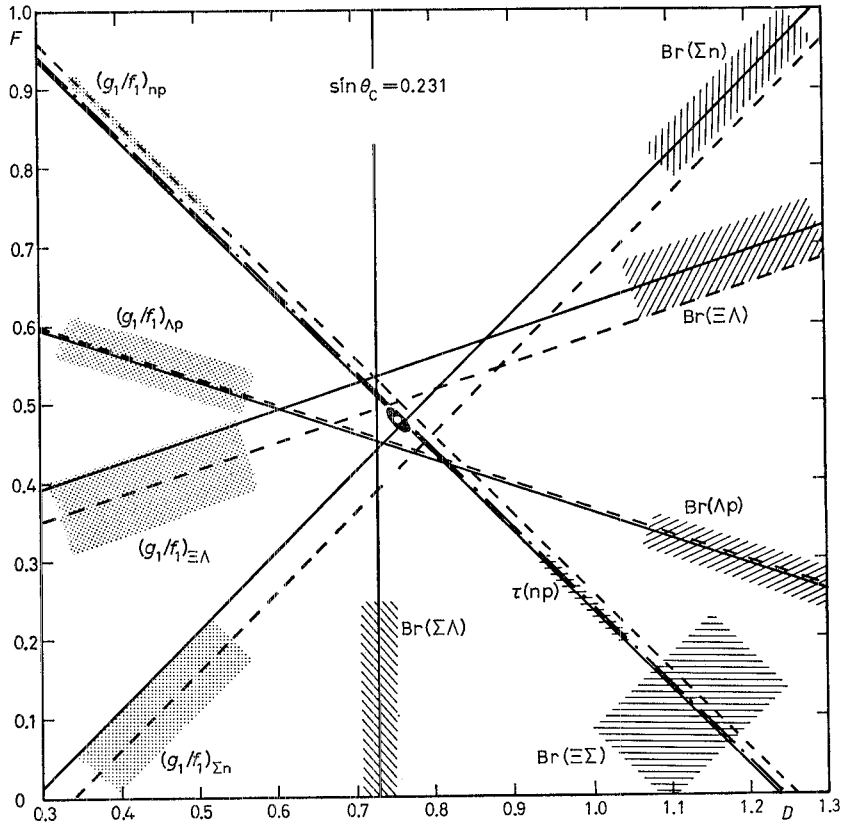

Fig. 14. – Limits on the F and D values obtained by the WA2 experiment at CERN [35].

ever, Q^2 is larger than for hyperon decay, and the SU_3 predictions apply strictly only at $Q^2 = 0$. Using the experimental branching ratios of the $K^{\pm}$ and K^0_L decays the following values were found [36]:

$$(3.15) \qquad |U_{us}|(K^{\pm}) = 0.221 \pm 0.003\,, \qquad |U_{us}|(K^0) = 0.212 \pm 0.005\,.$$

3·2.3. The matrix element U_{cd}. The experimental study of the charmed meson and baryon decays is much more difficult than that of the strange particles because of the short lifetime ($\tau_c \approx 10^{-13}$ s), the small cross-section for charmed-particle production relative to pions (with the exception of the e^+e^- annihilation) and the large number of particles produced in the decay of the charmed hadrons, whose mass is larger than 1.8 GeV. Semi-leptonic decays of charmed particles with π or ρ mesons in the final state have not yet been observed. The purely leptonic decay of the D-meson ($D \to \ell\nu$) is strongly suppressed by helicity conservation for $\ell = e$ and $\ell = \mu$, and by phase space for $\ell = \tau$. The nonleptonic decays of charmed mesons such as $D \to 2\pi$

are affected by problems of interpretation in terms of quark decay, owing to the large c-quark mass. Information on the expected small deviation of U_{cd} from $\sin\theta_C$ can hardly come from nonleptonic D decays.

The U_{cd} matrix element was measured in the neutrino interaction with nuclei.

The production of charmed particles in CC neutrino interactions has been studied experimentally in emulsion, in bubble chambers and in high-mass electronic calorimetric detectors exposed to $\bar{\nu}$ beams.

In the emulsion and bubble chamber experiments the charm signature is given by the detection of the small decay path resulting from the short lifetime and/or by the mass reconstruction of the charmed particles, mainly D and Λ_c.

The calorimeters allow the study of a large number of neutrino-induced events with two opposite-sign muons in the final state.

At the quark level the dimuon events (2.18) are interpreted as a result of reactions (2.19). In the six-quark constituent scheme the neutrino (antineutrino) dimuon cross-sections $\sigma^{\nu}_{\mu^-\mu^+}$ ($\sigma^{\bar{\nu}}_{\mu^+\mu^-}$) on isoscalar targets are

$$\begin{cases} \sigma^{\nu}_{\mu^-\mu^+} = (G^2 m E_\nu/\pi)\left[|U_{cd}|^2(U+D) + |U_{cs}|^2 2S\right], \\ \sigma^{\bar{\nu}}_{\mu^+\mu^-} = (G^2 m E_{\bar{\nu}}/\pi)\left[|U_{cd}|^2(\bar{U}+\bar{D}) + |U_{cs}|^2 2\bar{S}\right], \end{cases} \tag{3.16}$$

where m is the nucleon mass, E_ν is the incoming neutrino energy, and U, D, S and $\bar{U}$, $\bar{D}$, $\bar{S}$ are the average fractional momentum x of the u, d and s quarks and antiquarks in the nucleon target ($U_p = D_n = U$ and $D_p = U_n = D$).

Since the quantities U, D, $\bar{U}$ and $\bar{D}$ are known from the measurement of single-muon neutrino and antineutrino CC cross-sections and $S = \bar{S}$, the subtraction of $\sigma^{\nu}_{\mu^-\mu^+}$ from $\sigma^{\bar{\nu}}_{\mu^+\mu^-}$ gives information on U_{cd}.

The product of $|U_{cd}|^2$ times the branching ratio Br for the decay of the charmed particle into a muon plus anything is given by

$$\mathrm{Br}|U_{cd}|^2 = \frac{2}{3}\frac{(\sigma^{\nu}_{\mu^-\mu^+}/\sigma^{\nu}_{\mu^-}) - R(\sigma^{\bar{\nu}}_{\mu^+\mu^-}/\sigma^{\bar{\nu}}_{\mu^+})}{1-R}, \tag{3.17}$$

where $\sigma^{\nu}_{\mu^-}$ ($\sigma^{\bar{\nu}}_{\mu^+}$) are the inclusive single-muon neutrino (antineutrino) nucleon cross-sections and $R = (\sigma^{\bar{\nu}}_{\mu^+}/E_{\bar{\nu}})/(\sigma^{\nu}_{\mu^-}/E_\nu) = 0.48 \pm 0.02$ [40]. The dimuon to single-muon cross-section ratios measured by the CDHS Collaboration [28], corrected for acceptance and slow rescaling, are shown in fig. 15. The result is

$$\mathrm{Br}\,|U_{cd}|^2 = (0.41 \pm 0.07)\cdot 10^{-2}. \tag{3.18}$$

Taking $\mathrm{Br} = (7.1 \pm 1.3)\,\%$, one obtains

$$|U_{cd}| = 0.24 \pm 0.03. \tag{3.19}$$

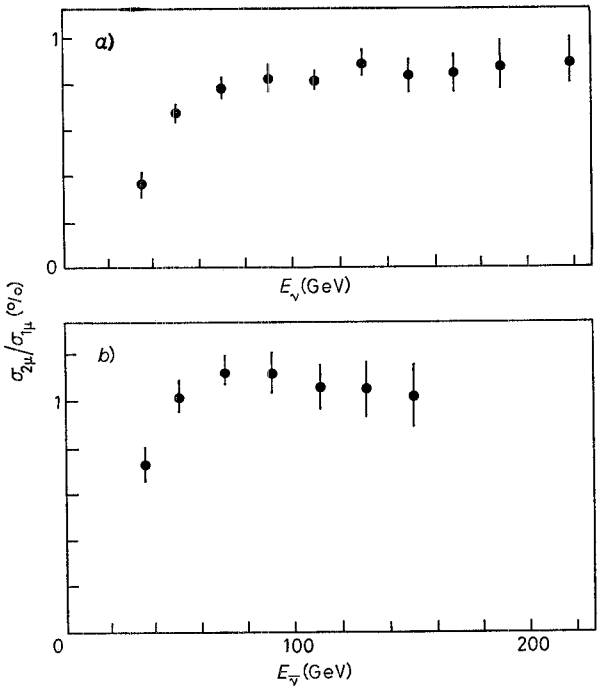

Fig. 15. – $R = \sigma_{2\mu}/\sigma_{1\mu}$ for *a*) neutrinos and *b*) antineutrinos [28], corrected for slow rescaling.

3·2.4. The matrix element U_{cs}. Information on the value of the matrix element U_{cs} can be obtained from the measurement of the x distribution of the dimuon neutrino and antineutrino events.

The x distribution of the $\bar{\nu}$-induced dimuon events shows [28] that the strange sea contained in the nucleons has the same momentum distribution as that of the antiquarks $\bar{u}$ and $\bar{d}$ as derived by the $\bar{\nu}$ inclusive μ^+ production in the region $y = E_{\text{hadron}}/E_{\bar{\nu}} \approx 1$ (fig. 16) [40].

The strange-quark contribution to the cross-section of the ν-induced dimuon events is obtained fitting the x distribution with two shapes, the first being given by the antineutrino dimuon event x-distribution, and the second by $x[u(x) + d(x)]$ as measured in the single-muon CC reactions [40]. The result of the fit, shown in fig. 17, is

$$R = \frac{|U_{cs}|^2 2S}{|U_{cd}|^2 (U + D)} = 1.19 \pm 0.09 \,. \tag{3.20}$$

From the value of R and the ratio of the valence to the sea quark [40] one gets

$$\frac{|U_{cs}|^2 2S}{|U_{cd}|^2 (\bar{U} + \bar{D})} = 9.3 \pm 1.6 \,. \tag{3.21}$$

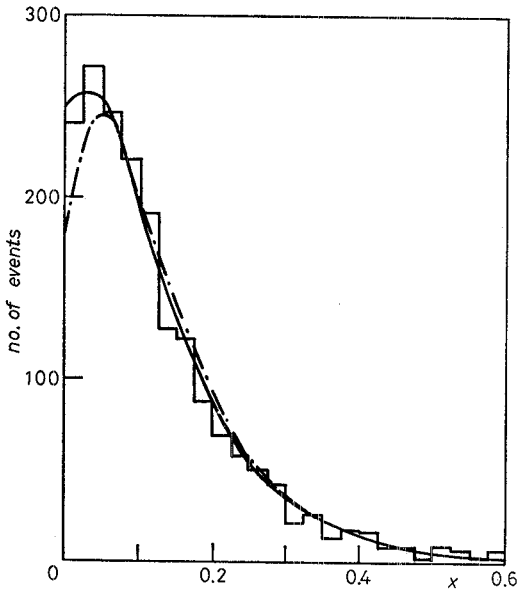

Fig. 16. – The x distribution for dimuon events induced by antineutrino interactions [28]; the solid curve is the sea distribution obtained in ref. [40], the dash-dotted curve demonstrates the effect of slow rescaling; $\bar{\nu}_\mu + \bar{s} \pm \mu^+ + \bar{c} \hookrightarrow \mu^-$, —— $x(\bar{u} + \bar{d} + 2\bar{s}) = \bar{q}^{\bar{\nu}}$, –·–·– $q^{\bar{\nu}}$ including slow rescaling ($m_c = 1.5$ GeV).

Assuming that the SU_3 symmetric hypothesis $\bar{U} + \bar{D} = 2S$ is an upper limit of the s-quarks contained in the nucleon, we get

$$|U_{cs}|^2 > (9.3 \pm 1.6)|U_{cd}|^2 \tag{3.22}$$

or

$$|U_{cs}| > 0.59 \qquad (90\,\%\ \text{c.l.}). \tag{3.23}$$

The transition element $|U_{cs}|$ can be also measured in the semi-leptonic decay of the charged D-mesons. Using the electron spectra obtained in the DELCO experiment (fig. 18) [41] together with the average values of the neutral and charged D's branching ratio Br (D $\to$ evX) = (10 $\pm$ 3) % [42] and the average of the D^0 and $D^\pm$ lifetimes $\tau(D) = (6.05 \pm 0.54) \cdot 10^{-13}$ s [43], this transition element was found [44] to be

$$|U_{cs}| = 0.92 \pm 0.08\,. \tag{3.24}$$

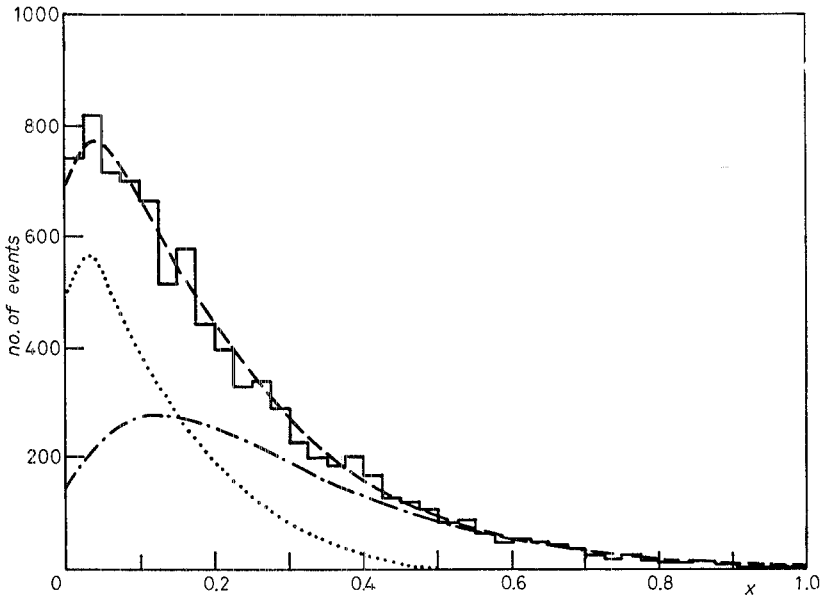

Fig. 17. – The x distribution for dimuon events induced by neutrinos [28]; the curves show the decomposition into a strange-sea contribution (48%) taken from the data of fig. 16 (dotted curve), and a quark contribution (52%) (dash-dotted curve). The dashed curve is the sum of both. $-\cdot-\cdot-$ $\nu+q \to \mu^-+c \hookrightarrow \mu^+$, $\cdots$ $\nu+s \to \mu^-+c \hookrightarrow \mu^+$, ——— $\nu+\mathcal{N} \to \mu^-+\mu^++X$ (data), — — — fit result.

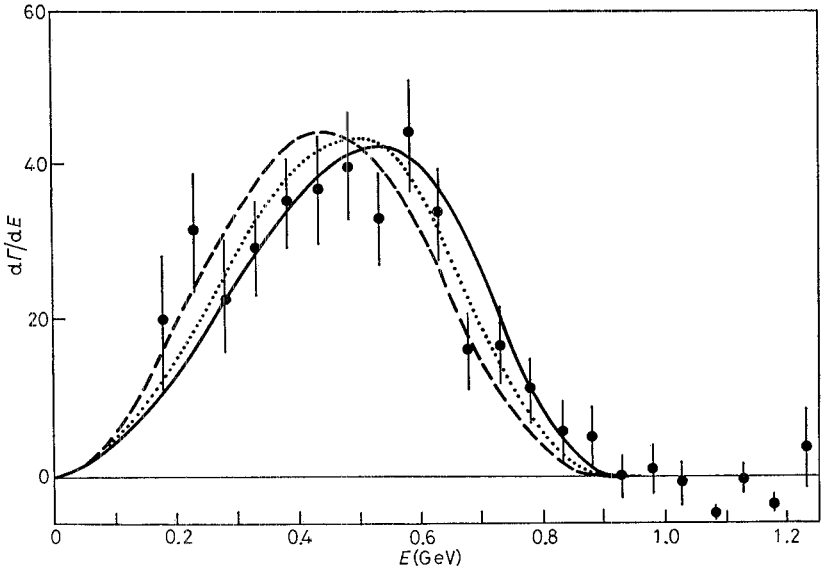

Fig. 18. – The DELCO electron spectrum on the ψ''. The curves are fits to the experimental data [44].

3·2.5. The matrix elements U_{ub} and U_{cb}. The calorimeters exposed to ν ($\bar{\nu}$) beams have detected the existence of events with two muons of the same sign [45] in the final state.

The number of the same-sign dimuon (SSD) events observed ($\approx (5 \div 10)\%$ of the OSD events; this depends on the cut in the momentum of the secondary muon, both in the ν and in the $\bar{\nu}$ beam) is larger than the standard-model expectation. In the $\bar{\nu}_\mu$-induced events, a fraction of the SSD events ($\mu^+\mu^+$) can be attributed to the production of a b-quark followed by the b $\to$ c decay and a semi-leptonic decay of the c-quark:

$$\bar{\nu}u \to \mu^+ b\,, \qquad b \to cX\,, \qquad c \to \mu^+ \nu Y\,. \tag{3.25}$$

In the ν_μ interactions the chain that can produce the SSD is the same as in eq. (3.25), but the u is replaced by the $\bar{u}$ and, therefore, strongly depressed.

Considering the SSD events in a ν_μ beam as a unknown background to be subtracted from the $\bar{\nu}_\mu$ SSD, an upper limit on the cross-section for b production by $\bar{\nu}_\mu$ on nuclei can be derived.

The cross-section limit obtained from the CDHS data [45] is translated in the limit [46]

$$|U_{ub}|^2 < 0.38 \cdot 10^{-2}\, T_c/T_b \qquad (90\,\%\ \text{c.l.}), \tag{3.26}$$

where T_c and T_b are the threshold factors due to the c and b quark masses, respectively. For $m_c = 1.5$ GeV and $m_b = 5$ GeV at the 350 GeV neutrino WBB, $T_c/T_b \approx 8$, and one gets

$$|U_{ub}| < 0.18 \qquad (90\,\%\ \text{c.l.})\,. \tag{3.27}$$

The experimental study of hadrons with a b-quark is quite recent. Most of the results on the semi-leptonic branching ratios and on the lifetime of the beauty particles are from the e^+e^- storage ring experiments.

The $4S$ resonance of the $b\bar{b}$ system produced from the e^+e^- annihilation is just above the threshold of the $B\bar{B}$ pairs and is a source of B-mesons almost at rest and with a good ratio of the B signal over the background.

The study of the lepton energy spectrum in the b decay gives the relative strength b $\to$ u over b $\to$ c. Because of the mass difference between the u and c quarks, the end-point of the lepton energy spectrum in the three-body decay (b $\to$ c$\ell\nu$) is about 600 MeV lower than that of the b $\to$ u$\ell\nu$ decay. The number of leptons with energy greater than that kinematically allowed in the b $\to$ c decay gives the upper limit of the b $\to$ u decay relative to b $\to$ c.

The energy spectra collected for the $e^\pm$ and the $\mu^\pm$ by the two experiments CUSB [47] and CLEO [48] at the Cornell e^+e^- storage ring are shown in fig. 19.

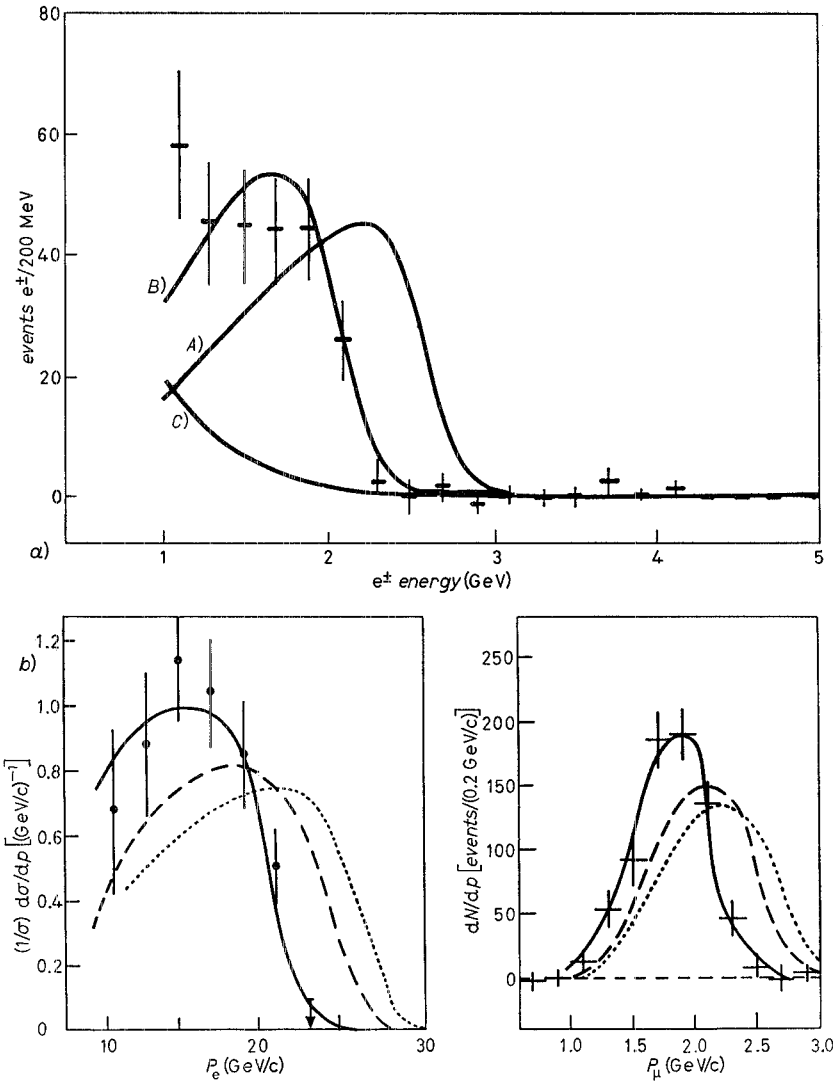

Fig. 19. – Spectrum of charged leptons produced in B decay from *a*) the CUSB experiment [47]: *A*) $m_q = 0$, *B*) $m_q = 1.8$ GeV, *C*) D's for B decays; and *b*) the CLEO experiment [48]: l.h.s.: ——— $B \to e\nu D$ (50%), $B \to e\nu D^*$ (50%); — — — $e \to e\nu X$, $M_X = 1.0$ GeV; · · · $B \to \mu\nu\pi$. R.h.s.: ——— $B \to \mu\nu D$ (50%), $B \to \mu\nu D^*$ (50%); — — — $B \to \mu\nu X$, $M_X = 1.0$ GeV; · · · $e \to \mu\nu\pi$.

The CUSB Collaboration found

$$\frac{\Gamma(b \to u\ell\nu)}{\Gamma(b \to c\ell\nu)} < 5.5\% . \tag{3.28}$$

For a mass of the hadronic system produced with the lepton, $m_X < 1.0$ GeV,

the CLEO Collaboration obtained

$$\frac{\Gamma(b \to u\ell\nu)}{\Gamma(b \to c\ell\nu)} < 4\% . \tag{3.29}$$

Using these results, the following value was obtained [49]:

$$|U_{ub}|/|U_{cb}| < 0.16 \qquad (90\% \text{ c.l.}). \tag{3.30}$$

The transition elements $|U_{ub}|$ and $|U_{cb}|$ are also related to the b lifetime. In the e^+e^- storage ring experiments at PEP and PETRA, with energy well above the $B\overline{B}$ threshold, an unexpectedly long lifetime for the B particles was found.

The technique used for the lifetime measurement in the e^+e^- storage ring experiments is the one developed for the measurement of the τ heavy-lepton lifetime. The lifetime is derived from the statistical distribution of the transverse impact parameter of the lepton relative to the average beam-crossing position. The lepton impact parameter distribution is made on an enhanced sample containing a pair of particles with beauty. The enhancement with respect to the normal e^+e^- annihilation rate is obtained requiring a lepton with high momentum transverse to the jet axis, as expected in the decay of a particle with a mass of 5 GeV.

Figure 20 shows the impact parameter distribution for leptons, *a*) in the enhanced sample of beauty particles and *b*) in the enhanced sample of charmed

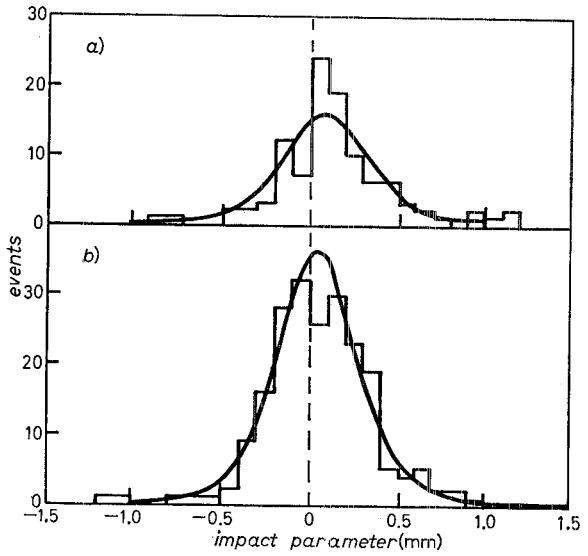

Fig. 20. – Impact parameter distribution for leptons coming from *a*) beauty particles and *b*) charmed particles measured in the MARK II experiment [50].

particles obtained in the MARK II experiment [50]. The average of the measurements from MARK II [50] and from MAC, DELCO and JADE [51] is

$$\tau(\mathrm{B}) = (1.44 \pm 0.2 \pm 0.3)\ \mathrm{ps}\,. \tag{3.31}$$

The beauty lifetime has been also measured by TASSO, studying the distribution of all charged particles from b decay [51]. The measured value is

$$\tau(\mathrm{B}) = [1.83^{+0.38}_{-0.35}(\mathrm{stat.})^{+0.37}_{-0.34}(\mathrm{syst.})]\ \mathrm{ps}\,. \tag{3.32}$$

The expected lifetime for the transition of a b-quark of 5 GeV mass to a c-quark of 1.8 GeV mass, assuming a semi-leptonic branching ratio of 12 %, is [52]

$$\tau(\mathrm{B}) \approx 2.77 \cdot 10^{-3}/|U_{\mathrm{cb}}|^2\ \mathrm{ps}\,. \tag{3.33}$$

Combining all the τ(B) measurements yields [51]

$$|U_{\mathrm{cb}}| = [0.042^{+0.003}_{-0.002}(\mathrm{stat.})^{+0.005}_{-0.004}(\mathrm{syst.})]\,. \tag{3.34}$$

Using the result (3.30) the upper limit on $|U_{\mathrm{ub}}|$ is

$$|U_{\mathrm{ub}}| < 6.7 \cdot 10^{-3} \qquad (90\ \%\ \mathrm{c.l.}). \tag{3.35}$$

Recently, the associated production of a pair of beauty particles B^- and $\overline{\mathrm{B}}^0$ by a 350 GeV π^- interaction as been observed in an emulsion target inserted in an array of silicon detectors [53]. The decay of the two beauty particles into charm particles was observed in the emulsion. Two negative muons were identified, and the transverse momentum was measured in a large muon spectrometer set behind the emulsion stacks.

The weighted mean lifetime of the B^- and $\overline{\mathrm{B}}^0$ is

$$\tau(\mathrm{B}) = 0.3^{+0.2}_{-0.1}\ \mathrm{ps}\,. \tag{3.36}$$

Using this result and the relations (3.30) and (3.33), one obtains

$$|U_{\mathrm{cb}}| = 0.09 \pm 0.03 \tag{3.37}$$

and

$$|U_{\mathrm{ub}}| < 0.02 \qquad (90\ \%\ \mathrm{c.l.}). \tag{3.38}$$

3·2.6. Evidence for the top quark. Indications in favour of the existence of the t-quark have been given by the UA1 Collaboration working at the CERN SPS Collider [30]. The production mechanism is very likely

to be the following:

$$(3.39) \qquad p\bar{p} \to WX\,, \quad W \to tb'\,, \quad t \to \ell\nu b'\,.$$

The signature for events with a t-quark is a single isolated electron or muon with high momentum transverse to the jet axis. Six candidate events have been found (three with an electron and three with a muon). The mass of the system lepton-jet$_1$-jet$_2$-(missing transverse energy) is compatible with the W mass and the mass of jet$_1$-lepton-(missing transverse energy) clusters around a common value of 40 GeV/c^2 (fig. 21). The uncertainty on the masses is mainly

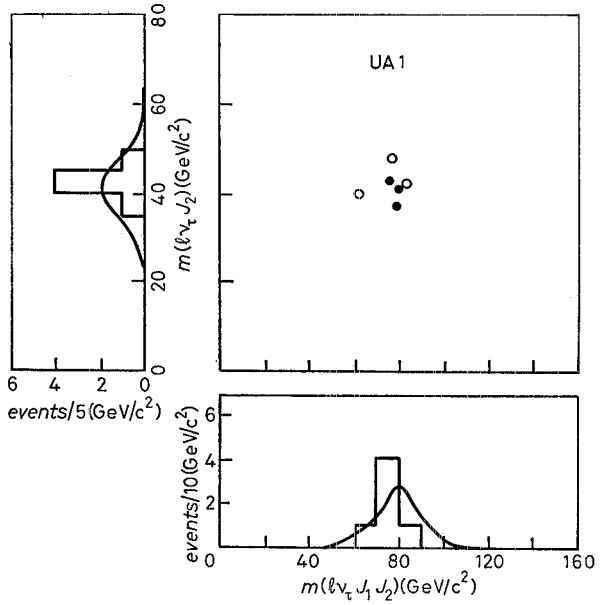

Fig. 21. – Four-body *vs.* three-body mass distribution for the six $W \to tb$ candidate events [30]: ——— $m_t = 40$ GeV/c^2, o e → 2 jets, • μ → 2 jets.

systematic because of the jet reconstruction, and is equal to ±10 GeV. The jet with lower transverse energy with respect to the $p\bar{p}$ axis is indicated by jet$_1$. The existence of particles with a t-quark, which hopefully will be confirmed by the new data recently collected at the CERN SPS $p\bar{p}$ Collider, gives strong support to the six-quark scheme, but, from the few events that can be collected at $p\bar{p}$ colliders, it is not possible to extract information on the mixing matrix elements involving the t-quark.

At future e^+e^- storage rings (SLC, LEP) the production of a heavy top-onium ($t\bar{t}$) system with mass close to the Z^0 mass will be enhanced by the Z^0 resonance, and the experimental study of the decays of a reasonable number

of produced toponia will be able to give information on U_{tb}, since the direct weak decay of one quark of the bound system will become competitive with the other decays of the onia.

3·3. *Relation between the transition elements $U_{q^+q^-}$ and the rotation angles.* – The experimental determination of the matrix elements $U_{q^+q^-}$, using the b lifetime value obtained in the e^+e^- experiments, is at present at the following stage:

$$U = \begin{pmatrix} 0.973 \pm 0.001 & 0.231 \pm 0.003 & < 6.7 \cdot 10^{-3} \\ 0.24 \pm 0.03 & 0.92 \pm 0.08 & 0.042 \pm 0.005 \\ < 0.04 & < 0.06 & > 0.998 \end{pmatrix}. \tag{3.40}$$

The values in the last line of the matrix (3.40) are limits at 90% c.l. obtained assuming the existence of six quarks.

The data indicate the pattern discussed in subsect. **3·1**, with superallowed transition within the families

$$|U_{ud}| \approx |U_{cs}| \approx |U_{tb}| \approx 1, \tag{3.41}$$

first forbidden transition between the second and the first family

$$|U_{us}| \approx |U_{cd}| \approx 0.23, \tag{3.42}$$

second forbidden transition between the third and the second family

$$|U_{cb}| < 6.7 \cdot 10^{-3}, \tag{3.43}$$

and third forbidden transition between the third and the first family

$$|U_{ub}| < 0.04. \tag{3.44}$$

Some relations between the rotation angles in the KM representation (1.10) and the $U_{q^+q^-}$ elements can be derived:

1)

$$U_{ud} = \cos\theta_1 = 0.9733 \pm 0.0015, \tag{3.45}$$

which corresponds to $\sin\theta_1 = 0.229 \pm 0.006$.

2)

$$U_{ub} = \sin\theta_1 \sin\theta_3 < 6.7 \cdot 10^{-3}, \quad \sin\theta_3 < 0.029. \tag{3.46}$$

3)

$$U_{us} = \sin\theta_1 \cos\theta_3 = 0.231 \pm 0.003, \quad \cos\theta_3 = 1.009 \pm 0.03. \tag{3.47}$$

4) The knowledge of the transition element $|U_{cb}|$ can be translated into a relation between $\sin\theta_2$ and $\sin\theta_3$, putting δ as a parameter ($U_{cb} = \sin\theta_3 + + \exp[i\delta]\sin\theta_2$). In the ($\sin\theta_2$, $\sin\theta_3$)-plane the allowed region is contained in the shaded area (fig. 22) delimited by the lines $|U_{cb}| = \sin\theta_3 \pm \sin\theta_2$, corresponding to $\delta = 0$ and $\delta = \pi$, respectively, and by the line $\sin\theta_3 = 0.029$ (eq. (3.46)).

If the b lifetime measured in the emulsion experiment is used, the matrix (3.40) changes to

$$U = \begin{pmatrix} 0.973 \pm 0.001 & 0.231 \pm 0.003 & < 0.02 \\ 0.24 \pm 0.03 & 0.92 \pm 0.08 & 0.09 \pm 0.03 \\ < 0.04 & < 0.014 & > 0.99 \end{pmatrix}. \tag{3.48}$$

The corresponding constraints in the plane $\sin\theta_2$-$\sin\theta_3$ are given by the dotted area in fig. 22.

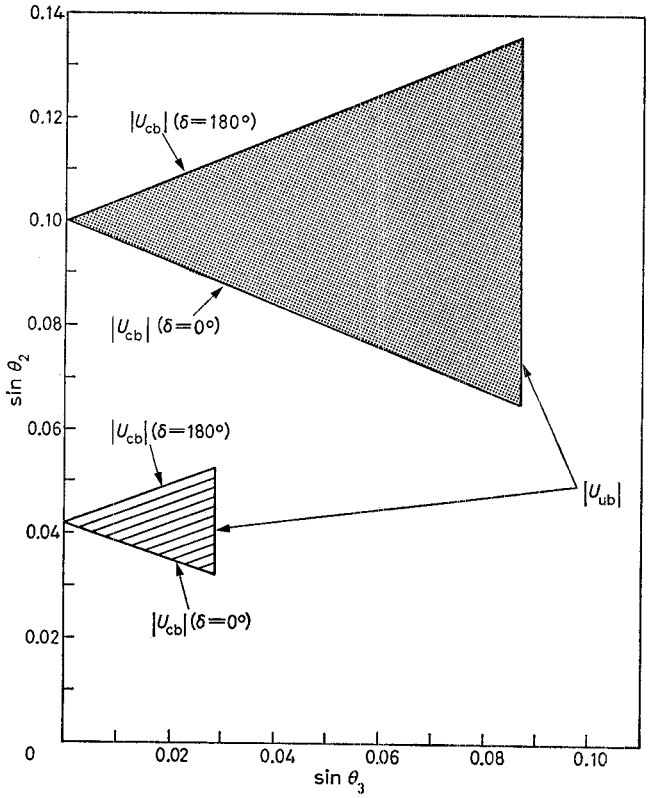

Fig. 22. – Limits on the plane $\sin\theta_2$-$\sin\theta_3$ obtained from the measurement of $|U_{cb}|$ and $|U_{ub}|$. The shaded (dotted) area shows the constraints obtained using the value of the beauty lifetime measured in the e^+e^- experiments (emulsion experiment).

In conclusion, until now the measured transition elements $U_{q^+q^-}$ have allowed the determination of θ_1 and some constraints on θ_2 and θ_3. The phase δ is not determined by the measured $U_{q^+q^-}$.

Since δ is related to *CP* violation, the study of *CP* violation processes will make it possible to test the KM scheme for the six-quark system.

A more detailed analysis of the results in terms of the KM and Maiani parametrizations can be found elsewhere [54].

4. – *CP* violation in weak interactions.

4·1. *Introduction.* – Since 1947, when ROCHESTER and BUTLER discovered a new component in the cosmic rays [55] produced with a cross-section typical of the hadron interactions (1% of the π-meson cross-section) and decaying with a lifetime corresponding to the weak interactions, the K^0 mesons have been a unique source of surprising experimental results and stimulating theoretical hypotheses that have made important contributions to the construction of the standard model.

To resolve the paradox of the strong production and the weak decay of the new particles, GELL-MANN and NAKANO and NISHIJIMA [56] suggested the existence of a new internal quantum number, the strangeness S. The K^+ and K^0 have $S = +1$ and the K^- and $\overline{K}^0$ have $S = -1$. The strangeness is conserved in the strong interactions and violated in the weak ones.

The existence of two lifetimes for the K^0 decaying into two pions (K_S) and into three pions (K_L) was one of the motivations for the criticism by LEE and YANG [57] of the validity of the parity conservation law in weak interactions.

The apparent lack of universality in the weak decay of the strange particles was solved by CABIBBO [7] with the introduction of the mixing of the d and s quarks.

The discovery that the K^0 decays into two muons at a level lower than that expected from the weak-interaction calculations involving only s, d and u quarks suggested the GIM mechanism [8]. This mechanism puts the quarks into left-handed doublets and requires the existence of a fourth quark, the charmed one, later experimentally confirmed in the famous experiments of the November '74 revolution [58].

Many of the phenomena that can only be studied with a K^0 beam are of fundamental importance for the study of the basic laws of quantum mechanics, such as the K^0_S regeneration, the interference of different K^0 states and other matter-antimatter differences in K decay.

The reasons for these peculiar characteristics of the K^0-$\overline{K}^0$ system are that the strangeness is not conserved by the weak interactions, and the transitions $K^0 \leftrightarrow \overline{K}^0$ are allowed.

Moreover, the K^0 system is the only place where a violation of the *CP* in-

variance of the laws of physics has been detected. The discovery, due to CHRISTENSON, CRONIN, FITCH and TURLAY [59], consisted in the observation of the decay of K_L^0 ($CP = -1$) into two pions ($CP = +1$).

In the beginning, the CP violation was explained with a new force [60]. In 1973, before even the experimental discovery of the charmed quark, KOBAYASHI and MASKAWA [6] suggested that the CP violation in the K_L^0 decay could be accommodated by the existing known weak interaction if the quarks were six in number and grouped in three families. The Cabibbo matrix [7] generalized to three families can be expressed in terms of a phase δ and three real parameters, the mixing angles θ_i ($i = 1, 2, 3$). The existence of an imaginary amplitude in the weak transition allows the construction of a component of the weak Hamiltonian that violates T and consequently CP if CPT is conserved.

4·2. *The discovery of CP violation.* – The discovery of CP violation was made in an experiment performed at the BNL AGS accelerator [59]. The experimental layout is shown in fig. 23. To eliminate the K_S^0 component of

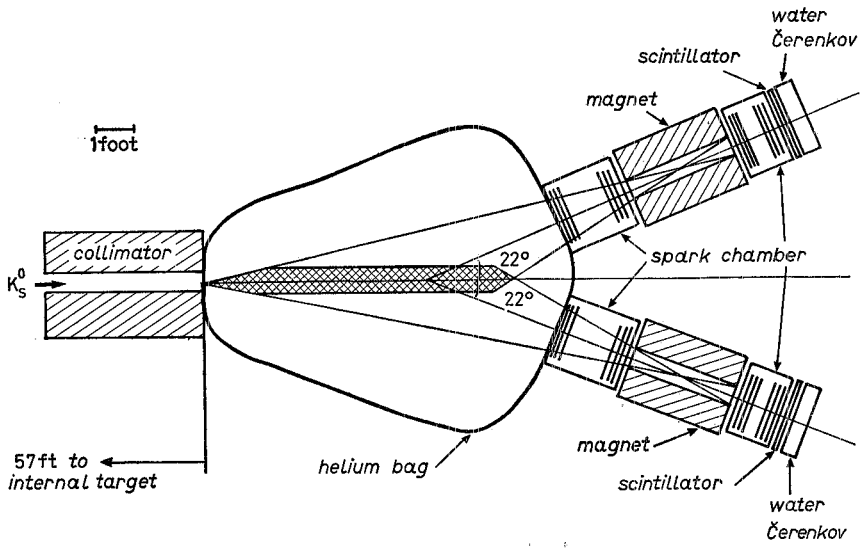

Fig. 23. – Plan view of the detector used in the experiment that discovered CP violation [59].

the beam, the detector was placed ≈ 18 m from the proton target, corresponding to ≈ 300 times the K_S^0 decay length. The detector consisted of two spectrometers, each composed of two spark chambers for track reconstruction and separated by a magnetic field of ≈ 70 kG cm. Behind the spectrometer were placed the scintillators and a water Čerenkov counter.

As obtained by a calibration using K_S^0, the reconstructed mass of the K_L^0 decaying into two pions is expected to have an average of 498 MeV and a standard deviation of 3 MeV. The K_L^0 vector momentum peaks around the forward direction with a standard deviation of 3 mrad. For the other decays of the K_L^0 ($K_L^0 \to 3\pi$, $K_L^0 \to e\pi\nu$ and $K^0 \to \mu\pi\nu$), in general the reconstructed invariant mass is not equal to the K^0 mass and the K^0 direction is different from zero.

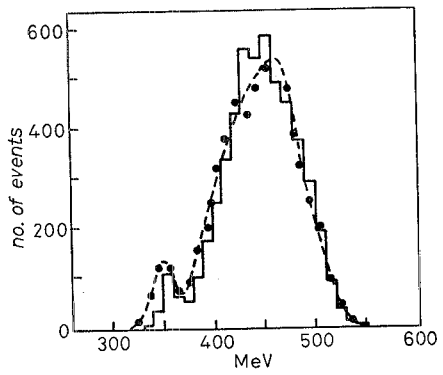

Fig. 24. – Experimental distribution of the K^0 invariant mass obtained in the experiment of ref. [59]: ——— data, 5211 events; • – – – Monte Carlo calculation.

Figure 24 shows the invariant-mass distribution for the K_L^0 decays in the fiducial volume filled with He gas. The experimental data are compared with Monte Carlo expectations. In fig. 25 is shown the angular distribution of those events with invariant mass in the range (490÷510) MeV. In the region $\cos\theta > > 0.9999$ there was found a signal of (45±9) K_L^0 events decaying into 2π over 22 700 decays into 3π, corresponding to a *CP* violation effect of $(2.0\pm0.4)\cdot10^{-3}$.

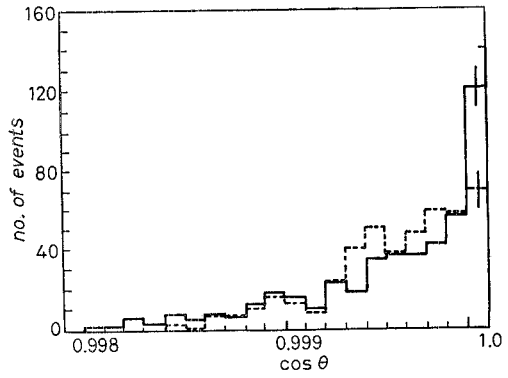

Fig. 25. – Angular distribution for the events having an invariant mass in the range (490÷510) MeV [59]. The calculated curve is normalized to the number of events in the complete sample. ——— data, – – – Monte Carlo calculation.

4·3. *The formalism of the CP violation in the* K^0-$\bar{K}^0$ *system.* – The main source of *CP* violation in the K^0 system is due to the mixing of *CP* eigenstates in the K_S^0 and K_L^0 states which is produced by the nonsymmetric transitions $K^0 \leftrightarrow \bar{K}^0$.

Assuming *CPT* invariance, the parametrization used is

$$\begin{cases} |K_S\rangle \approx |K_1\rangle + \varepsilon|K_2\rangle , \\ |K_L\rangle \approx |K_2\rangle + \varepsilon|K_1\rangle , \end{cases} \tag{4.1}$$

where ε is a complex parameter and $|K_1\rangle$ and $|K_2\rangle$ are the *CP* eigenstates:

$$\begin{cases} |K_1\rangle = (|K^0\rangle + |\bar{K}^0\rangle)/\sqrt{2} & (CP = +1), \\ |K_2\rangle = (|K^0\rangle - |\bar{K}^0\rangle)/\sqrt{2} & (CP = -1). \end{cases} \tag{4.2}$$

In terms of $|K^0\rangle$ and $|\bar{K}^0\rangle$, the $|K_S\rangle$ and $|K_L\rangle$ states are given by

$$\begin{cases} |K_S\rangle \approx (1+\varepsilon)|K^0\rangle + (1-\varepsilon)|\bar{K}^0\rangle , \\ |K_L\rangle \approx (1+\varepsilon)|K^0\rangle - (1-\varepsilon)|\bar{K}^0\rangle . \end{cases} \tag{4.3}$$

Another *CP* violation effect, in addition to that described above, can arise when there is more than one decay amplitude for the same physical state. In the case of the K^0 decay into two pions, this second effect is described by the complex quantity

$$\varepsilon' = (1/\sqrt{2})\,\mathrm{Im}\,(A_2/A_0)\exp[i(\delta_2 - \delta_0 + \pi/2)] , \tag{4.4}$$

where A_0 and A_2 are the amplitudes for a K-meson decaying into two pions with final-state isospin I equal to 0 and 2, respectively. The quantities δ_0 and δ_2 are the s-wave $\pi\pi$ scattering phase shifts at $\sqrt{s} = m_K$ for the states $I = 0$ and $I = 2$, respectively. The phases of ε and ε' are almost equal. Experimentally ε is determined by measuring the charge asymmetry δ_l [61] in the semi-leptonic decay $K_L \to l\nu\pi$:

$$\delta_l = \frac{\Gamma(K_L \to \bar{\nu}l^-\pi^+) - \Gamma(K_L \to \nu l^+\pi^-)}{\Gamma(K_L \to \bar{\nu}l^-\pi^+) + \Gamma(K_L \to \nu l^+\pi^-)} . \tag{4.5}$$

Assuming *CPT* invariance and the selection rule $\Delta S = \Delta Q$ [62], one has

$$\Gamma(K^0 \to \nu l^+\pi^-) = \Gamma(\bar{K}^0 \to \bar{\nu}l^-\pi^+) \tag{4.6}$$

and

$$A(K^0 \to \bar{\nu}l^-\pi^+) = A(\bar{K}^0 \to \nu l^+\pi^-) = 0 . \tag{4.7}$$

The charge asymmetry is then given by

$$\delta_l \approx 2 \operatorname{Re} \varepsilon . \tag{4.8}$$

The experimental study of the decay of K_L into $\pi^+\pi^-$ and $\pi^0\pi^0$ allows the measurement of ε and ε'.

The parametrization of the measurements is the following:

$$\eta_{+-} \exp [i\Phi_{+-}] = \frac{A(K_L \to \pi^+\pi^-)}{A(K_S \to \pi^+\pi^-)} \approx \varepsilon + \varepsilon' , \tag{4.9}$$

$$\eta_{00} \exp [i\Phi_{00}] = \frac{A(K_L \to \pi^0\pi^0)}{A(K_S \to \pi^0\pi^0)} \approx \varepsilon - 2\varepsilon' . \tag{4.10}$$

Experimentally the decay rates give the modulo squared of η_{+-} and η_{00}. The phases are measured by the interference of K_L and K_S decay into two pions [61].

The experimental situation is summarized in table III [63].

TABLE III. – *Experimental situation with respect to the measurement of CP violation parameters.*

$\lvert\eta_{+-}\rvert$	$(\ 2.274 \pm 0.022) \cdot 10^{-3}$
$\lvert\eta_{00}\rvert$	$(\ 2.33 \pm 0.08\ ) \cdot 10^{-3}$
Φ_{+-}	$(44.6 \pm 1.2)^\circ$
Φ_{00}	$(54 \pm 5)^\circ$
$\operatorname{Re}\varepsilon$	$(\ 1.621 \pm 0.088) \cdot 10^{-3}$

4·4. *Theoretical predictions.* – In the superweak model [60] the $\Delta S = 1$ *CP*-violating decays $K_L^0 \to 2\pi$ are forbidden and $\eta_{+-} = \eta_{00} = \varepsilon$ ($\varepsilon' = 0$).

In the standard model the asymmetry in the $K^0 \leftrightarrow \bar{K}^0$ transition amplitudes defined by ε is due to the box diagram of fig. 26*a*). The parameter ε' is due to the « penguin » diagram (fig. 26*b*)) leading to a final 2π state with isotopic spin equal to zero.

The parameters ε and ε' are expressed in terms of the mixing angle and the phase of the KM matrix.

Figure 27 shows the lower bounds on the ratio

$$\varepsilon'/\varepsilon \approx \tfrac{1}{3}\left(1 - |\eta_{00}|/|\eta_{+-}|\right) \tag{4.11}$$

obtained by GILMAN and HAGELIN [64] as a function of the top mass. The larger uncertainties in this determination come from QCD effects. In fig. 27, B parametrizes the matrix element of the $\Delta S = 2$ transition. Equation (4.11) is obtained from eqs. (4.9) and (4.10) in the limit $\varepsilon'/\varepsilon \ll 1$.

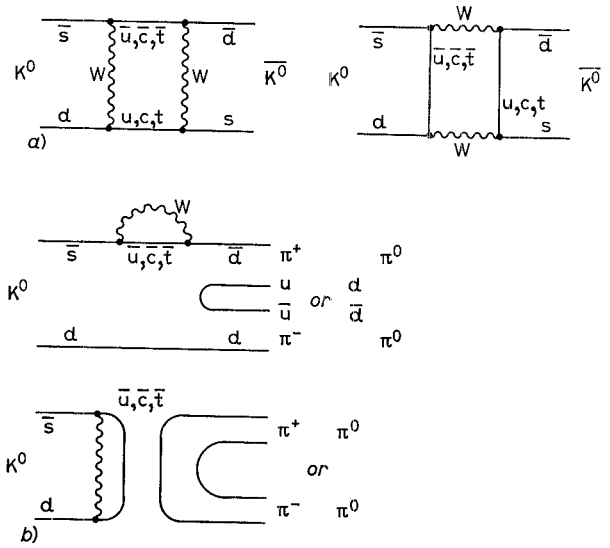

Fig. 26. – *CP* violation diagrams: *a*) diagrams responsible for the asymmetry in the $K^0 \to \overline{K}^0$ transition amplitudes, *b*) « penguin » diagrams contributing to the $K^0 \to \pi\pi$ decay.

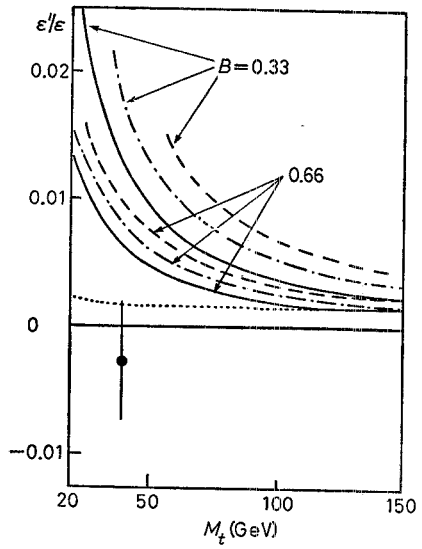

Fig. 27. – Lower bounds on ε'/ε as a function of the top mass for different lifetimes of the beauty quark: $\tau_b = 0.6 \cdot 10^{-12}$ s (solid lines), $\tau_b = 0.9 \cdot 10^{-12}$ s (dash-dotted lines), $\tau_b = 1.2 \cdot 10^{-12}$ s (dashed lines). The dotted line represents a previous limit obtained assuming $B = 0.3$ and using the short-distance contribution to $K_L \to \mu\mu$ instead of the information on the b lifetime. • Average of experimental results.

4·5. *Measurement of* ε'/ε. – Two new experimental determinations of ε'/ε have recently been obtained at FNAL [65] and BNL [66]. The quantity ε'/ε was derived measuring the $\pi^0\pi^0$ and $\pi^+\pi^-$ decays of K_L and K_S with the same detector. In the ratio measurements most of the experimental errors (acceptance, efficiency, apparatus imperfections, etc.) cancel out.

The Chicago-Saclay detector at FNAL [65] was exposed to two K_L beams simultaneously. The K_S's are provided by placing a regenerator in one of the two K_L beams. The neutral and charged decays were collected in different runs and analysed using a drift chamber spectrometer and an array of 804 lead-glass blocks, respectively. In the case of $\pi^0\pi^0$ decay, one gamma is required to convert at the end of the decay region. The reconstruction of the

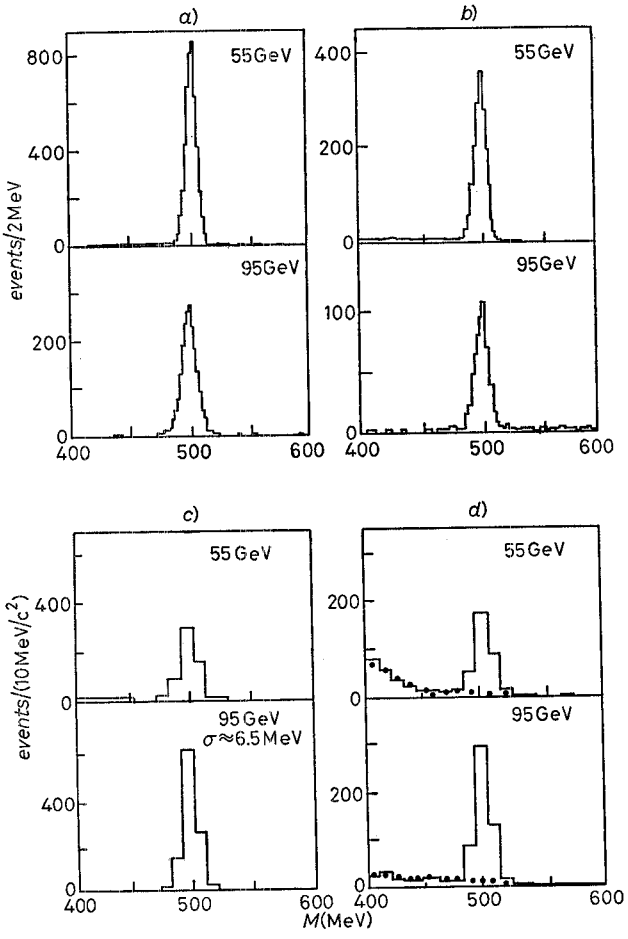

Fig. 28. – Invariant-mass distribution of the K_S and K_L decays into $\pi^+\pi^-$ for K^0 of 55 and 95 GeV measured in the Chicago-Saclay experiment at FNAL [65]. Also shown, by the points in *d*), is the expected background due to the K_L decay into $3\pi^0$. *a*) $K_S \to \pi^+\pi^-$, *b*) $K_L \to \pi^+\pi^-$, *c*) $K_S \to 2\pi^0$, *d*) $K_L \to 2\pi^0$.

decay point is crucial in order to determine from which beam the event originated.

The invariant-mass distribution for the $\pi^+\pi^-$ and $\pi^0\pi^0$ events reconstructed in the beam without the regenerator are shown in fig. 28. The $K \to \pi^+\pi^-$ mass plots are essentially free of background. The dots in fig. 28*d*) show the Monte Carlo expectation for the $K_L^0 \to 3\pi^0$ background.

The ratio of the neutral and charged decay events collected in the beams with and without a regenerator has been measured in nine K^0 momentum bins in the range (35÷135) GeV. The total events collected, after background subtraction, are shown in table IV.

TABLE IV. – *Events collected in the Chicago-Saclay experiment.*

Mode	Events
$K_L \to 2\pi^0$	3 142
$K_S \to 2\pi^0$	5 663
$K_L \to \pi^+\pi^-$	10 676
$K_S \to \pi^+\pi^-$	25 752

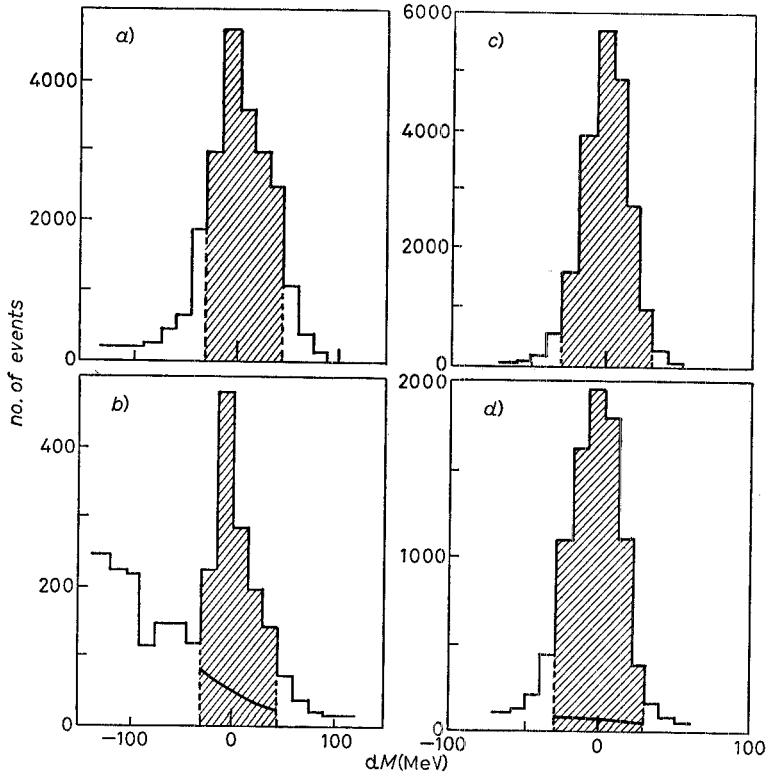

Fig. 29. – Distribution of the difference between the reconstructed mass of the K_S and K_L decays into two pions and the real K^0 mass [66]. The events in the dashed region were used in the analysis. The solid lines in the K_L^0 graphs show the expected background. *a*) $K_S \to \pi^0\pi^0$, *b*) $K_L \to \pi^0\pi^0$, *c*) $K_S \to \pi^+\pi^-$, *d*) $K_L \to \pi^+\pi^-$.

The value of ε measured in semi-leptonic charge asymmetry is used to obtain ε' from a fit of the data where also the regeneration amplitude is taken as a parameter. The result of this experiment is

$$\varepsilon'/\varepsilon = -0.0046 \pm 0.0053 \text{ (stat.)} \pm 0.0024 \text{ (syst.)} . \tag{4.12}$$

In the Yale-BNL experiment [66] the K_L and K_S decays were collected in different runs. The K_S's were produced by introducing a regenerator into the K_L beam.

The neutral and charged decay modes were measured simultaneously. In the case of the $\pi^0\pi^0$ decay, one photon was required to convert in a lead plate covering a large solid angle and placed at the end of the decay region. The $\pi^+\pi^-$ decays were observed simultaneously in the remainder of the solid angle. A complete reconstruction of both event types was performed using a magnetic spectrometer and an array of 200 lead-glass blocks.

Figure 29 shows the measured mass distributions of the four categories of events. In this figure, ΔM is the difference between the measured invariant mass and the known K mass. The final result is

$$\varepsilon'/\varepsilon = 0.0017 \pm 0.0082 , \tag{4.13}$$

where the statistical and systematic errors are combined in quadrature.

In fig. 30 the Chicago-Saclay and the Yale-BNL results [65, 66] are com-

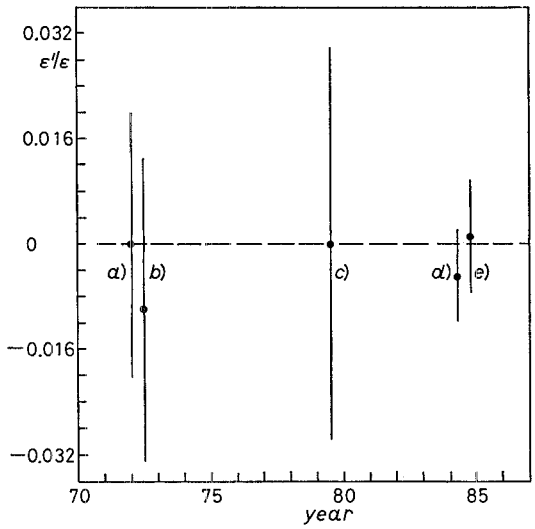

Fig. 30. – Experimental determination of ε'/ε. The results shown are from *a*) ref. [67], *b*) ref. [68], *c*) ref. [69], *d*) ref. [65] and *e*) ref. [66].

pared with previous determinations of ε'/ε obtained from the measurements of $|\eta_{00}|$ and $|\eta_{+-}|$ [67-69]. The data are compatible with the superweak model. In fig. 27 the average value of $\varepsilon'/\varepsilon = -0.0026 \pm 0.0045$ is compared with the standard-model predictions assuming the top mass m_t equal to 40 GeV. The agreement is not good, but the theoretical and experimental uncertainties are still large.

4·6. *Future experiments.* – An important experimental effort is now being made at CERN [70] and at FNAL [71] to improve the accuracy on ε'/ε.

The CERN SPS experiment [70] has started taking data in 1985, the decays into $\pi^0\pi^0$ and $\pi^+\pi^-$ being measured simultaneously. The K_S fraction of the beam is changed, displacing the proton target along the 50 m long decay region.

The use of a calorimetric technique based on a liquid-argon detector, and the use of high-energy K^0's, allows a precise determination of the pion energies and of the decay co-ordinates, and a larger acceptance with respect to magnetic measurements.

The measurement of the charged and neutral pions using the same geometry reduces acceptance errors.

In order to have $\Delta(\varepsilon'/\varepsilon) < 0.1\,\%$, the required accuracy for $|\eta_{00}|^2/|\eta_{+-}|^2$, derived by the measurement of the rate ratio

$$R = \frac{\Gamma(K_L \to \pi^0\pi^0)/\Gamma(K_L \to \pi^+\pi^-)}{\Gamma(K_S \to \pi^0\pi^0)/\Gamma(K_S \to \pi^+\pi^-)}, \tag{4.14}$$

is of a few parts per mille.

The new proposal for the FNAL Tevatron [71], with a high-energy beam and high statistics, aims at reaching an accuracy of $\Delta(\varepsilon'/\varepsilon) \approx 10^{-3}$.

It has recently been proposed to study *CP* violation effects [72] at the CERN LEAR facility by measuring the interference effects and the asymmetries of different decay amplitudes in the neutral-kaon system. The K^0 and $\overline{K}^0$ of known momentum and direction will be produced with large flux and equal magnitude in the annihilation of antiprotons at rest. Since the decay products will be measured with the same detector, the systematic errors cancel in the first approximation.

This experiment would allow a global overview of the whole *CP* problem.

4·7. *Conclusions.* – In conclusion, almost 40 years after the K^0 discovery the experimental and theoretical study of the K^0 system is still playing a very important role in the development of elementary-particle physics. The precise measurements of the K^0 decay can show hints of possible deviations from the standard model, even if the mass scale that can induce such deviations is expected to have a value much larger than the K^0 mass.

5. – The upper values of neutrino masses, and the search for neutrino oscillations and massive neutrinos.

In the standard model the quarks and leptons get a mass through the Higgs mechanism [5].

The study of the interaction of quarks with the Higgs field is based on the experimental knowledge of the quark masses and of the mixing angles that also fix the strength of the CC interactions (see sect. **3**).

In the standard model the neutrinos have zero mass, and no mixing matrix exists in the lepton sector of the CC Lagrangian. In the grand unified theories (GUTs) of strong, electromagnetic and weak interactions, since the neutrinos are put in multiplets together with quarks and charged leptons, it is « natural » that they have a mass.

The experimental knowledge of the neutrino masses and of the possible mixing angles between the lepton families is less advanced than in the case of the quarks. The masses of the muon-neutrino and tau-neutrino are known to be less than 0.49 MeV [73] and 70 MeV [74], respectively. There is an experimental determination of the mass of the electron-neutrino, obtained from the measurement of the spectrum of the beta-decay of tritium, corresponding to $20\ \text{eV} < m_{\nu_e} < 45\ \text{eV}$ [75], but this result must be confirmed by other experiments.

If neutrinos are massive, their weak (flavour) eigenstates ν_ℓ are linear combinations of the mass eigenstates ν_i [76]:

$$\nu_\ell = \sum U_{\ell i} \nu_i \qquad (\ell = \mathrm{e}, \mu, \tau, \ldots, \quad i = 1, 2, 3, \ldots), \tag{5.1}$$

where $U_{\ell i}$ are the elements of a unitary matrix.

The search for massive neutrinos has been made by investigating

1) the decay of mesons and nuclei,

2) the decay of massive neutrinos in neutrino beams,

3) the oscillation of neutrinos and

4) the double beta-decay of nuclei without neutrinos in the final state.

The last process is sensitive to the spinorial nature of neutrinos.

The measurement of the neutrino mass is important also for cosmological arguments. Stable neutrinos with masses of a few electronvolt can explain the large part of the Universe mass ($\approx 90\,\%$) which is not of a baryonic nature (the so-called dark matter of the Universe) [77].

5'1. *Study of the decay of mesons and nuclei.* – If neutrinos have a mass, the spectrum of charged particles produced with the neutrino in meson and nucleus

decays will be modified, compared with the case of zero mass [76]. In particular, the end-point of the momentum spectrum will be moved to lower values. In two-body decays, each mass eigenstate would show up as a peak in the lepton recoil spectrum (fig. 31), with intensity proportional to $|U_{li}|^2$. In three-body decays, the mixture of finite-mass eigenstates will cause kinks in the decay lepton spectrum because each eigenstate will have a different end-point energy.

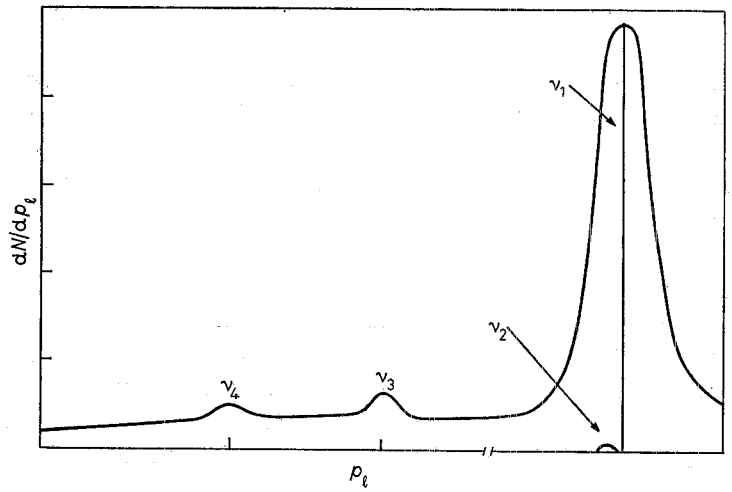

Fig. 31. – Schematic of a charged-lepton spectrum in meson decay $M \to l\nu$ if massive neutrinos exist.

The most accurate investigation of neutrinos with masses in the range of a few electronvolt, produced with an electron, has been done by analysing the energy distribution of the charged lepton produced in tritium decay [75]:

$$^3H \to {}^3He\, e^- \bar{\nu}_e . \tag{5.2}$$

The Q value of reaction (5.2) is 18.6 keV. The experiment was performed using the ITEP magneto-electrostatic spectrometer. The source was contained in molecules of valine ($C_5H_{11}NO_2$). The beta spectrum was scanned by varying the electrostatic field of the spectrometer while the magnetic field was kept constant. With this method there is no influence of detector efficiency on the shape of the beta spectrum.

Since the electrons are accelerated to an energy of 22 keV, which is above the end-point energy, the main background due to the tritium contamination of the spectrometer is strongly reduced, allowing the investigation of the beta spectrum up to ≈ 25 eV below the spectrum end-point.

The energy resolution of the spectrometer has been determined experimentally using monochromatic electron sources. The measured energy dis-

tribution for 18.430 keV electrons is shown in fig. 32. The FWHM is 22.3 eV. The accuracy of the absolute calibration is 5 eV.

Figure 33 shows the measured Kurie plots in the range close to the end-point for three sources of different thicknesses. The solid lines in the figure

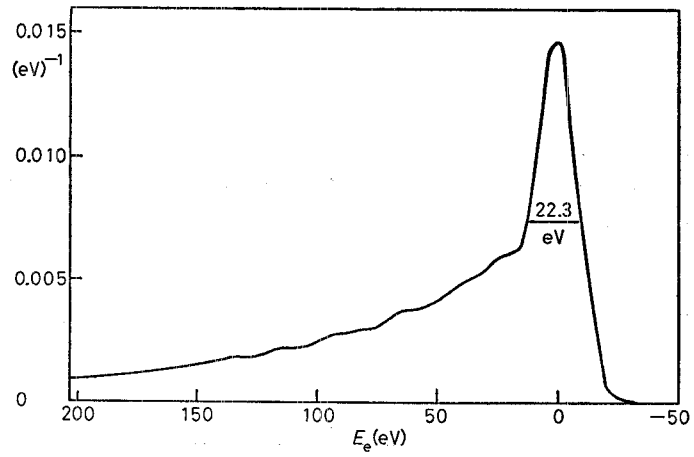

Fig. 32. – Resolution function corresponding to the energy $E_e = 18.430$ keV [75].

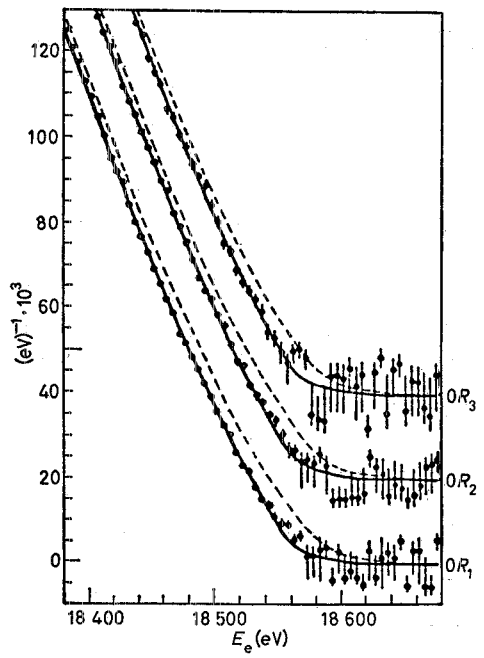

Fig. 33. – Kurie plots of experimental data close to the spectrum end-point measured with three sources (R_i). The solid lines are the best fits with the valine final-state spectrum. The dashed lines are fits with $m_\nu = 0$.

correspond to a fit to the data in the range $E_e > 16.8$ keV, having as parameters the neutrino mass m_ν, the end-point energy E_0 of the beta spectrum with $m_\nu = 0$ and a possible quadratic correction to the shape of the beta spectrum. In the fit, the calculated valine final-state spectrum (FSS) was used. The dashed lines in the figure show the expectations in the case of zero neutrino mass.

The dependence of the experimental results on the assumption about the FSS are reported in table V. The values are stable, changing the energy range fit of the data.

TABLE V. – *Dependence of the m_ν and E_0 parameter fit on the* FSS *assumptions* [75].

Parameters (eV)	Valine	Atom	Nucleus
m_ν	34.8 ± 1.9	$30.9 + 1.5/- 1.6$	$13.8 + 2.5/- 3.5$
E_0	$18\,584.2 \pm 1.6$	$18\,580.5 \pm 1.3$	$18\,567.4 \pm 1.0$

From the results reported in table V the authors obtained the model-independent result

$$m_{\nu_e} > 9 \text{ eV} \qquad (90\,\% \text{ c.l.}). \tag{5.3}$$

The most realistic result is the one coming from the valine FSS model; it corresponds to

$$20 \text{ eV} < m_{\nu_e} < 45 \text{ eV} \qquad (90\,\% \text{ c.l.}). \tag{5.4}$$

The value of $m_{^3\text{H}} - m_{^3\text{He}}$ obtained using the valine FSS assumption ($(18\,603.6 \pm \pm 6)$ eV) is in good agreement with a recent high-precision measurement ($(18\,599 \pm 3)$ eV) [78].

Assuming the existence of two massive neutrinos with mass m_{ν_1} and m_{ν_2}, the limits on the mixing angle U_{e2} as a function of m_{ν_2} are shown in fig. 34. In the fit, m_{ν_2} was fixed in the range $(0 \div 1.5)$ keV. The values of m_{ν_1} and E_0 obtained from this analysis do not differ much from the values obtained with the single mass fit.

A number of new tritium experiments are starting to take data or are being set up (for a review, see [79]). The most significant results should come from experiments that use tritium in the form of free atoms, for which the final states are well known [80].

A limit on the mass of the neutrinos produced with the muon in the π decay has been obtained at SIN, measuring the muon momentum from pions decaying in flight in the very forward direction [81].

To minimize the systematic errors, the π^- and μ^- momenta were measured in the same spectrometer, which consists of a 21° C-shaped magnet and four

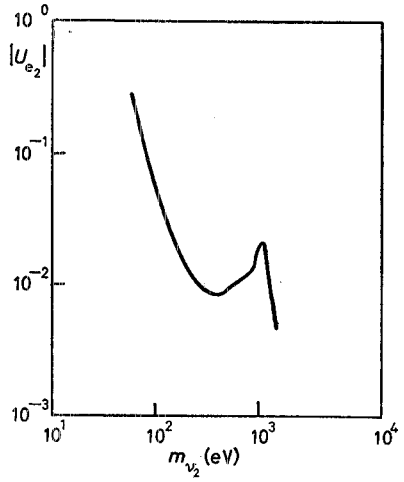

Fig. 34. – Limits at 90% c.l. on $|U_{e2}|^2$ as a function of m_{ν_2} obtained by the ITEP experiment [75].

very thin spark chambers. The decay angle was measured with two sets of proportional chambers, and the decay point by the time-of-flight technique.

The neutrino momentum, as determined from the vector difference between pion and muon momenta, was then compared with the momentum expected for a zero-mass neutrino; the limit obtained was

$$m_{\nu_\mu} < 0.50 \text{ MeV} \qquad (90\,\% \text{ c.l.}). \tag{5.5}$$

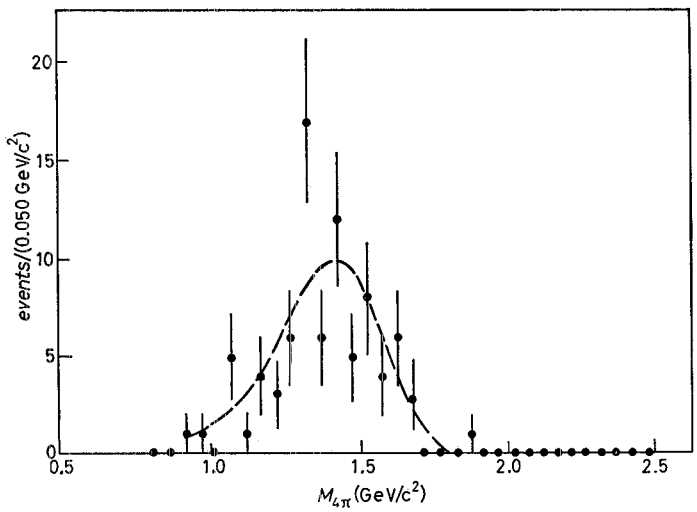

Fig. 35. – The $3\pi^{\pm}\pi^0$ invariant-mass distribution. The curve is for $m_{\nu_\tau} = 0$ and the assumption that the four-pion state is dominated by the ρ' resonance.

A second measurement comes from a study, again at SIN, of pion decay at rest [73]. The measurement of muon momentum gave

$$p_\mu = (29.7873 \pm 0.0008)\ \text{MeV}. \tag{5.6}$$

Combining this result with the pion mass measurement [82], the limit obtained on the neutrino mass was

$$m_{\nu_\mu} < 0.49\ \text{MeV} \qquad (90\,\%\ \text{c.l.}). \tag{5.7}$$

An upper limit was set on the mass of the neutrinos produced with the τ-lepton, studying the four-pion invariant-mass distribution in the decay

$$\tau \to 3\pi^\pm\pi^0\nu \tag{5.8}$$

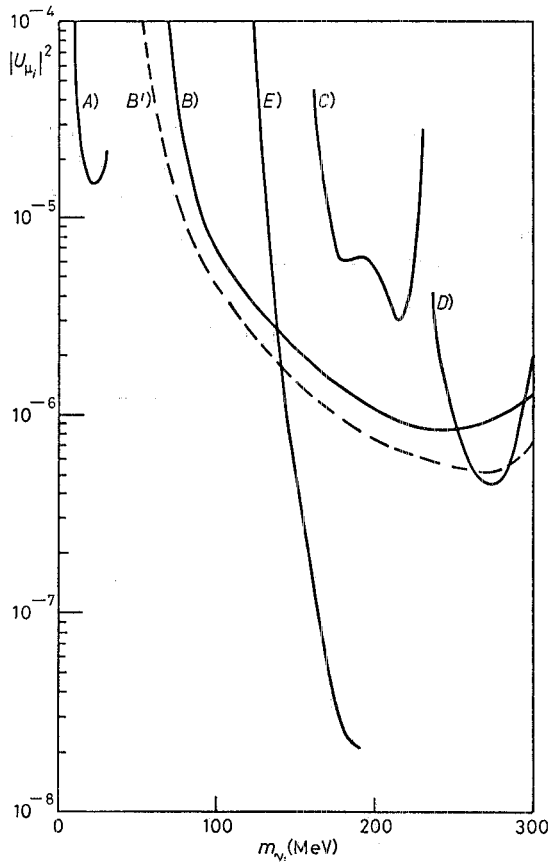

Fig. 36. – Limits on $|U_{\mu i}|^2$ at 90% c.l. as a function of m_{ν_i} from *A*) $\pi_{\mu 2}$ decay at SIN [83]; *B*), *B'*) $K_{\mu 2}$ decay at KEK [84, 85]; *C*) $K_{\mu 2}$ range at KEK [86]; *D*) $K \to \mu\nu\bar{\nu}\nu$ decay at LBL [87]; *E*) BEBC beam-dump experiment [88].

in the MARK II detector at PEP [89]. This decay mode is sensitive to the ν_τ mass, since the invariant mass of the four-pion state approaches the τ mass.

Figure 35 shows the measured invariant-mass distribution. The spectrum in the range $m_{4\pi} > 1.5$ GeV, containing 22 events, was compared with the expected behaviour for different values of the neutrino mass and different assumptions about the four-pion state. After including uncertainties in background, resolution and knowledge of the ρ' mass and width, an upper limit on the ν_τ mass was obtained

$$m_{\nu_\tau} < 143 \text{ MeV} \qquad (95\,\% \text{ c.l.}). \tag{5.9}$$

Recently the ARGUS Collaboration measured the ν_τ spectrum in the decay into $3\pi\nu_\tau$ of τ-leptons produced near $\sqrt{s} = 10$ GeV in DORIS II at DESY. From this energy spectrum an upper limit was derived [74]:

$$m_{\nu_\tau} < 70 \text{ MeV} \qquad (95\,\% \text{ c.l.}). \tag{5.10}$$

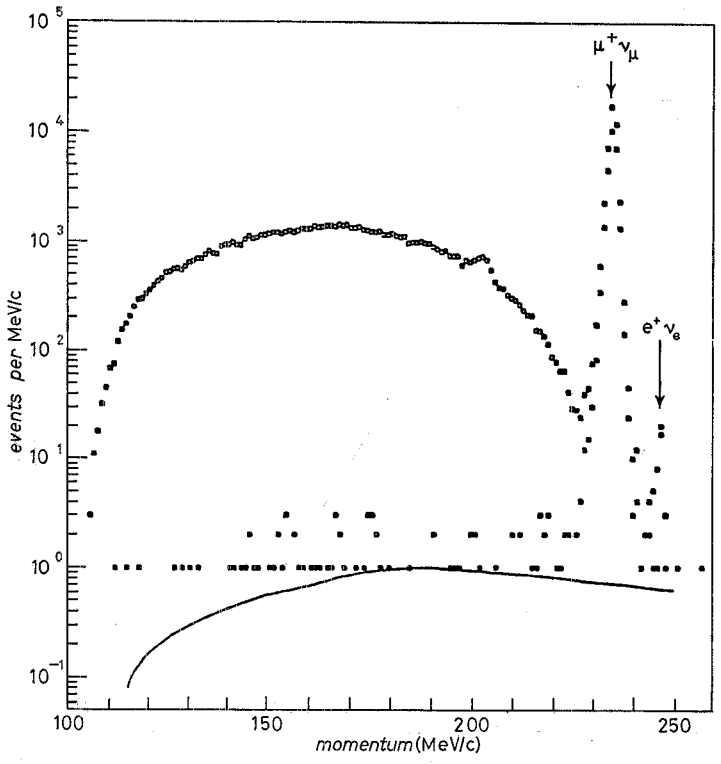

Fig. 37. – Momentum spectra of e^+ as measured in the KEK experiment [84]. The momentum dependence of the detector acceptance is also shown. □ Veto out, ■ veto in, ——— detector acceptance.

New results in the search for heavy neutrinos in $K_{\mu 2}$ decays have recently been obtained at KEK [84]. This experiment is sensitive to neutrino masses in the range of a few hundred MeV. No distinct peaks were observed in the muon spectrum below the peak corresponding to a zero neutrino mass, leading to the constraints in the plane $|U_{\mu i}|^2$-m_{ν_i} shown in fig. 36, where previous results obtained in the same detector are also shown [85]. Because of the better resolution the lower end of the neutrino mass was reduced to 40 MeV. The same figure shows the limits from different pion, kaon and neutrino decay experiments [83, 86-88].

In the KEK experiment [84] the electron spectrum of K decay was also measured. Figure 37 shows the e^+ spectra with and without photon veto (the veto allows rejection of the background due to the $K^+ \to e^+\nu\pi^0$ decay). There is no significant peak in this spectrum either. Constraints on $|U_{ei}|^2$ obtained from the same experiment in the mass range between 140 and 350 MeV are shown in fig. 38, as well as limits obtained from other experiments [90-94].

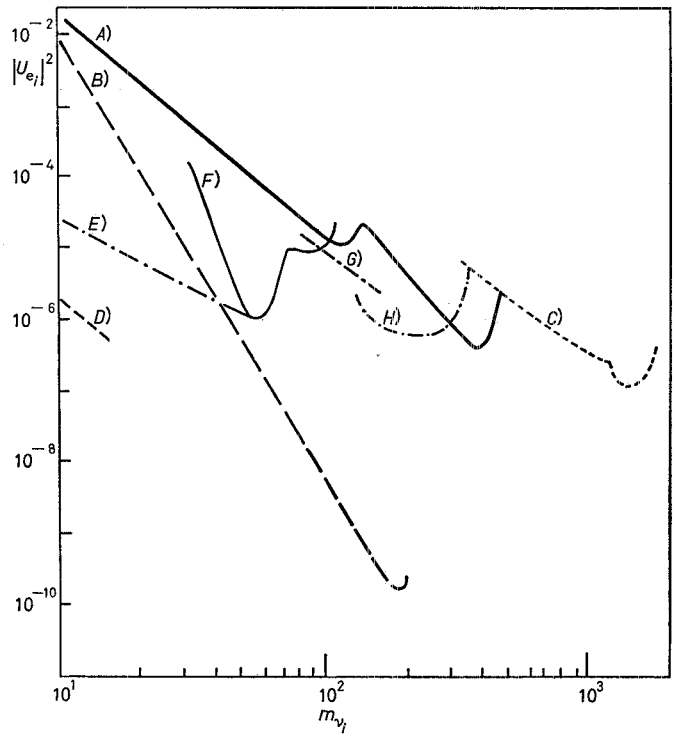

Fig. 38. – Limits on $|U_{ei}|^2$ at 90% c.l. as a function of the neutrino mass obtained from *A*) a WBB CHARM experiment [93], *B*) a BD CHARM experiment (F decay) [93], *C*) a BD CHARM experiment (D decay) [94], *D*) solar-neutrino experiments [90], *E*) measurement of the branching ratio of the $\pi \to e\nu$ decay [91], *F*) measurement of the electron spectrum in $\pi \to e\nu$ decay [91], *G*) measurement of the branching ratio $K \to e\nu$ [92], *H*) measurement of the electron spectrum in K decay [84].

5·2. *Decays of heavy neutrinos.* – If heavy neutrinos exist, a neutrino beam can contain, in addition to its major part of light neutrinos, a minor quantity of heavy ones [95]. As shown in fig. 39, such neutrinos may have originated in the decay of pseudoscalar mesons M (π, K, D, F, ...), produced by the interaction of protons with the target. Neutrino decays in the detector were looked for.

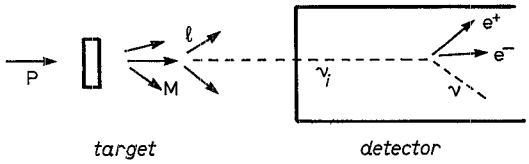

Fig. 39. – Production and decay of heavy neutrinos.

The production rate of heavy neutrinos compared to that of zero-mass neutrinos is [76, 95]

$$\frac{\Gamma(\mathrm{M} \to \nu_i [m] \ell \mathrm{X})}{\Gamma(\mathrm{M} \to \nu_i [0] \ell \mathrm{X})} = \varrho |U_{\ell i}|^2 . \tag{5.11}$$

The factor ϱ depends on the neutrino mass m. In the case of purely leptonic decay, it takes into account the fact that for finite neutrino mass there is less suppression due to helicity conservation than there is in the case of a zero-mass neutrino (*e.g.*, for a neutrino mass of 200 MeV, $\varrho \sim 10^5$ in the case of the $\mathrm{K} \to \mathrm{e}\nu$ decay and $\varrho \sim 4$ for the $\mathrm{K} \to \mu\nu$ decay).

Neutrinos with a mass larger than a few MeV can decay into a light neutrino and two electrons. For neutrinos with larger masses, other decay channels are open ($\nu_i \to \mathrm{e}\mu\nu$, $\nu_i \to \mathrm{e}\pi$, ...).

The number of heavy-neutrino decay events expected in the detector exposed to a heavy-neutrino flux φ is given by

$$N_{\mathrm{ev}} = \varphi P_{\mathrm{dec}} \approx |U_{\ell' i} U_{\ell i}|^2 , \tag{5.12}$$

where P_{dec} is the probability for the neutrino to decay in the detector; for a decay path much longer than the length L of the detector, P_{dec} is proportional to L. In eq. (5.12), $U_{\ell' i}$ and $U_{\ell i}$ are the neutrino mixing angles, defined in eq. (5.1), entering into the meson and the heavy-neutrino decay probability, respectively.

In the case of the decay

$$\nu_i \to \mathrm{e}^+\mathrm{e}^-\nu_{\mathrm{e}} , \tag{5.13}$$

the partial lifetime τ can be obtained from the μ lifetime according to the

expression

$$\tau_i = (m_\mu/m_i)^5 \tau_\mu / |U_{ei}|^2 . \tag{5.14}$$

Limits on $|U_{ei}|^2$ and $|U_{\mu i} U_{ei}|$ in the mass range 10 to 490 MeV have been set by the CHARM Collaboration searching for the chain of events

$$\pi, K \to \nu_i e(\nu_i \mu) , \quad \nu_i \to e^+e^-\nu_e \tag{5.15}$$

in a neutrino WBB experiment [93]. The events induced by the chain (5.15) would appear in the fine-grained CHARM calorimeter as muonless narrow showers; this is a characteristic of electromagnetic showers, with a small angle θ between the shower axis and the direction of the incoming neutrino beam and with two minimum-ionizing particles at the shower origin. The results of this analysis are presented as constraints at 90 % c.l. in the plane $|U_{ei}|^2$-m_{ν_i} and are shown in fig. 38. An upper limit of $\sim 10^{-6}$ on the square of the neutrino mixing angle was obtained for neutrino masses around 180 MeV. For $|U_{ti}|^2 > 0.1$ this experiment is not sensitive to neutrino masses larger than 350 MeV owing to the attenuation of the ν_i beam by its decay along the path ($\approx$ 900 m) from the target to the detector. Similar limits were obtained for $|U_{\mu i} U_{ei}|$.

The same collaboration also performed a dedicated search for the decay (5.13) in a neutrino beam, obtained by dumping 400 GeV protons on a solid copper target at the CERN SPS beam-dump (BD) [93]. Such a beam contains a larger fraction of neutrinos produced by short-lived high-mass particles (D, F, ...) than are contained in WBBs. Search for high-mass neutrinos (up to 1.6 GeV) can then be done with good sensitivity.

To minimize the background due to the neutrino interactions, the neutrino decays have been searched for in any empty region $3 \times 3 \times 35$ m^3 (fig. 40) parallel to the CDHS and CHARM neutrino detectors exposed to neutrinos produced by $2.4 \cdot 10^{18}$ protons on target.

None of the 21 000 events collected satisfied the expected signature of a heavy-neutrino decay into two electrons (one or two electromagnetic showers with their origin in the decay region). This absence of candidate events can be translated into a model-dependent limit on $|U_{ei}|^2$ (fig. 38) assuming that the τ produced via F decay couples mainly to a single-mass eigenstate neutrino. This assumption is justified by the present limit on the mass of neutrinos produced in τ decay (formula (5.9)).

Assuming the decay chain

$$D \to \ell\nu_i \ (D \to K\ell\nu_i) , \quad \nu_i \to e^+e^-\ell , \tag{5.16}$$

with $\ell = e$ and μ, a model-independent limit on the neutrino mixing angle equal to 10^{-7} has been obtained for neutrino masses around 1 GeV [94] (fig. 38).

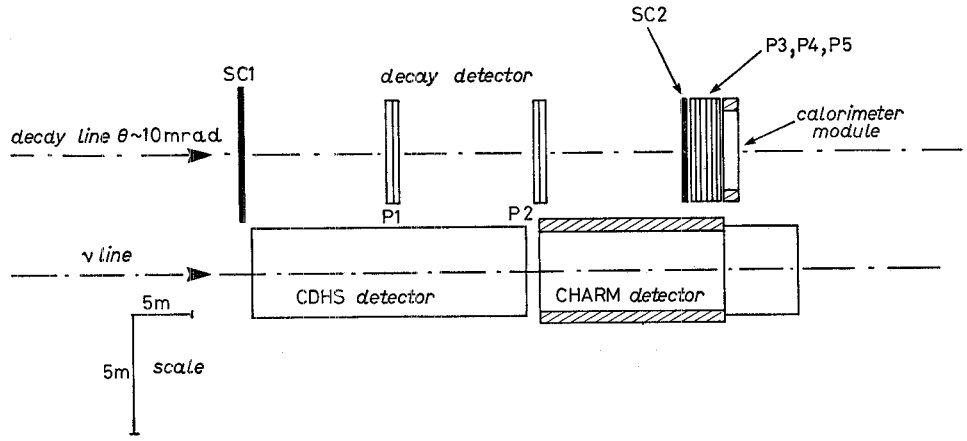

Fig. 40. – Layout of the decay beam-dump experiment of the CHARM Collaboration: SC1 and SC2 are scintillator planes (SC1 was used as a veto); P1 to P5 are sets of four planes of proportional drift tubes. The calorimeter module is 6 radiation lengths deep.

Because the heavy neutrinos can decay before reaching the detector, which is about 500 m from the target, the sensitivity of this experiment for large mixing angles is limited to small masses (*i.e.* for $|U_{\ell i}|^2 > 10^{-1}$ it is sensitive to $m_{\nu_i} < 1000$ MeV and for $|U_{\ell i}|^2 > 10^{-4}$ to $m_{\nu_i} < 1500$ MeV).

In the same beam a BEBC Collaboration [88] has searched for the decay chain

$$\text{(5.17)} \qquad \text{F} \to \nu_i \tau\,, \qquad \nu_i \to \mu e \nu\,.$$

Candidates for events induced by processes (5.17) have only one positively and one negatively charged track. In the analysis, electron and muon identification in unnecessary since the requirement $m_{\mu e} < 250$ MeV is sufficient to eliminate all candidates.

The limits shown in fig. 36 were set, assuming that the weak eigenstate ν_τ couples mainly with a single-mass eigenstate ν_i.

Heavy neutrinos produced via a NC flavour-changing interaction [96],

$$\text{(5.18)} \qquad \nu_\mu \mathcal{N} \to \nu_i \text{X}\,,$$

and decaying into a muon and hadrons,

$$\text{(5.19)} \qquad \nu_i \to \mu \text{X}\,,$$

were searched for in the CHARM calorimeter [94].

The topology of the events induced by reactions (5.18) and (5.19) would show up as two showers separated by a gap in the longitudinal direction and with a muon pointing to the vertex of the second shower.

The search for two showers in the CHARM detector imposes a short decay path (≈ 12 m) and the experiment is sensitive to masses of ≈ 2 GeV. The sensitivity to larger masses is limited by the threshold in the heavy-neutrino production and by the experimental acceptance.

One heavy-neutrino candidate event was detected, whilst the expected background due to the superposition of uncorrelated events occurring in the trigger gate time was 1.9 events. From this result the limits on $|U_{\mu i}|^2$ as a function of the neutrino mass shown in fig. 41 have been obtained.

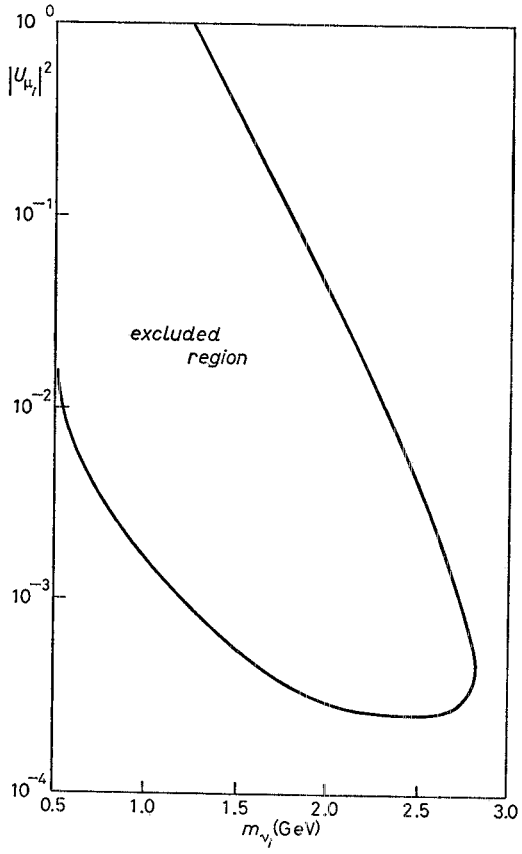

Fig. 41. – Limits at 90% c.l. on $|U_{\mu i}|^2$ as a function of the neutrino mass obtained by the CHARM Collaboration looking for heavy neutrinos produced in the detector by the reaction $\nu_\mu \mathcal{N} \to \nu_i X$ and decaying in the calorimeter into a muon and hadrons.

In the near future, improvements of 1 or 2 orders of magnitude in the mass range 10 to 450 MeV are expected from the CHARM Collaboration, which exposed the decay detector to the neutrino WBB, and from an experiment performed at the low-energy PS neutrino beam at CERN [97].

5·3. *Neutrino oscillation.* – If neutrinos have different masess, the mass eigenstates ν_i evolve in time as $\exp[-iE_i]$, where E_i is the ν_i energy [98].

In the case of two weak eigenstates ν_α and ν_β and two mass eigenstates ν_1 and ν_2, eq. (5.1) can be written, as for the quark case, in the form

$$\begin{cases} \nu_\alpha = \cos\theta\nu_1 + \sin\theta\nu_2 , \\ \nu_\beta = -\sin\theta\nu_1 + \cos\theta\nu_2 , \end{cases} \tag{5.20}$$

where θ is the mixing angle.

In this case the probability to have ν_β at a distance L starting with ν_α of energy E is given by

$$P(\nu_\alpha \to \nu_\beta) = \sin^2 2\theta \sin^2 (1.27\Delta m^2 L/E) , \tag{5.21}$$

where Δm^2 is the difference between the squares of the two neutrino masses ($\Delta m^2 = |m_1^2 - m_2^2|$). In eq. (5.21) the masses are in eV, the distance L in km (m), and the neutrino energy in GeV (MeV). The term $\sin^2 2\theta$ is the amplitude of the oscillation, and $Q = L/E$ gives the range of masses to which the experiment is sensitive. The maximum sensitivity is achieved when $1/Q \approx \Delta m^2$. Equation (5.21) is true in the limit m_1, $m_2 \ll E$.

In the case in which no effect has been detected, the limit on $P(\nu_\alpha \to \nu_\beta)$ sets correlated limits on the variables $\sin^2 2\theta$ and Δm^2 according to eq. (5.21).

For $\sin^2 2\theta = 1$ the minimum detectable value of Δm^2 is given by

$$\Delta m^2 = \frac{P(\nu_\alpha \to \nu_\beta)^{\frac{1}{2}}}{1.27Q} . \tag{5.22}$$

For large Δm^2 ($\Delta m^2 \gg 1/Q$) the finite size of the source and of the detector average out the oscillation, and the limit on $\sin^2 2\theta$ is given by

$$\sin^2 2\theta = 2P(\nu_\alpha \to \nu_\beta) . \tag{5.23}$$

Two kinds of experiments have been performed. Experiments looking for the « appearance » of some neutrino type ν_β in a relatively pure beam of another neutrino type ν_α are also called « exclusive ». They check the mixing between two types of neutrinos. The sensitivity is limited by background and by the contamination of ν_β at the source.

The « inclusive » or « disappearance » experiments look for the disappearance of a particular neutrino flavour. They check the mixing of this type of neutrino with any other neutrino type. The sensitivity is limited by the systematic uncertainties in the knowledge of the initial flux of the neutrino beam. To minimize this error, the ratio of the interaction rate measured with two detectors placed at different distances from the neutrino source is compared with the expected ratio in the case of no oscillation. Using two detectors the sensitivity is limited at large Δm^2 when the oscillation term averages to 0.5 in both detectors.

5·3.1. The appearance experiments. In the BNL-Columbia experiment the mixings $\nu_\mu \to \nu_e$ and $\nu_\mu \to \nu_\tau$ have been investigated in a neutrino WBB experiment at FNAL using the 15 ft bubble chamber [99]. The detector was placed (1200 ± 200) m away from the neutrino source. The dominant component in the beam consisted of ν_μ from π and K decay with an energy spectrum peaking around 30 GeV.

The $\nu_\mu \to \nu_e$ oscillations were investigated looking for ν_e in the beam in excess of the expected ν_e flux from K_{e3} decays. The measured number of ν_e interactions from anomalous ν_e sources is -85 ± 230. Comparing this number with the total number of ν_μ interactions $(69\,000 \pm 4000)$, a limit of $3 \cdot 10^{-3}$ at 90% c.l. for the $\nu_\mu \to \nu_e$ oscillations is obtained. The measurement also allows a limit to be set on $\nu_\mu \to \nu_\tau$ by considering the process $\nu_\tau \mathcal{N} e \to \tau^- X$, followed by the decay $\tau^- \to e^+ \nu_\tau \bar{\nu}_e$. The limit obtained is $2 \cdot 10^{-2}$ at 90% c.l. The corresponding limits in the plane Δm^2-$\sin^2 2\theta$ are shown, together with other results, in fig. 42 ($\nu_\mu \to \nu_\tau$) [99, 100] and fig. 43 ($\nu_\mu \to \nu_e$) [99, 101-103].

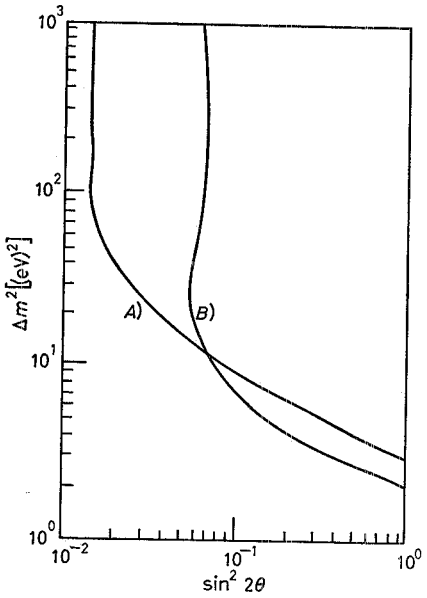

Fig. 42. – Limits on the plane Δm^2-$\sin^2 2\theta$ at 90% c.l. from the search for $\nu_\mu \to \nu_\tau$ oscillations performed by *A*) an emulsion experiment [100] and *B*) the BNL-Columbia bubble chamber experiment [99] at FNAL.

Another search for the oscillations of ν_μ into ν_τ was performed with a hybrid emulsion spectrometer exposed to the same beam [100]. The spectrometer consists of a 23 l nuclear-emulsion target, drift chambers on both sides of a large-aperture analysis magnet, time-of-flight hodoscopes for triggering and charged-particle identification, a lead-glass array, a coarse-grained hadron

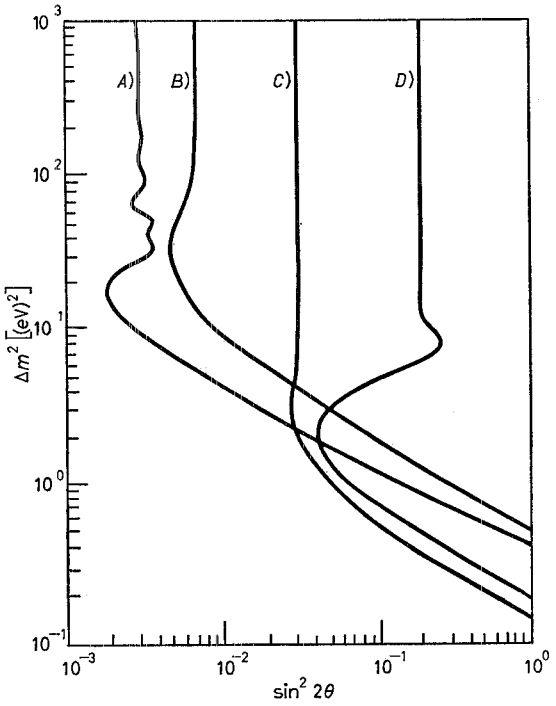

Fig. 43. – Limits on the plane Δm^2-$\sin^2 2\theta$ at 90% c.l. obtained from the search for the $\nu_\mu \to \nu_e$ oscillations performed by *A*) the BNL calorimeter experiment [103], *B*) the BNL-Columbia bubble chamber experiment [99], *C*) the APPW experiment at BEBC [102], *D*) the CHARM experiment [101].

calorimeter and two banks of counters behind steel for muon identification. The spectrometer was placed about 770 m from the neutrino source.

The interactions $\nu_\tau \mathcal{N} \to \tau^- X$ were searched for in a sample of 1241 neutrino interactions. The signature of the τ-lepton is its short lifetime ($\approx 3 \cdot 10^{-13}$ s) corresponding to a mean decay length of ≈ 500 μm detectable in the nuclear emulsion. No candidate event was found, giving a limit of 0.63% at 90% c.l. on the probability for a ν_μ to oscillate in ν_τ. This result corresponds to the limits on the plane Δm^2-$\sin^2 2\theta$ shown in fig. 42.

The CHARM Collaboration looked for the appearance of ν_e in a beam of ν_μ using two detectors running simultaneously [101]. The ν_μ were obtained by π and K decays produced by a proton beam of 19.2 GeV extracted from the CERN PS. Since there are no magnetic elements behind the target, the neutrino flux scales approximately as $1/L^2$ (L = distance from the neutrino source) for small angles. The mean neutrino energy is $\langle E_\nu \rangle = 1.5$ GeV. The estimated initial contamination of ν_e is less than 0.5%.

The close detector was placed at a distance $L = 123$ m from the target and the far one at $L = 900$ m. Figure 44 shows a sketch of the neutrino beam

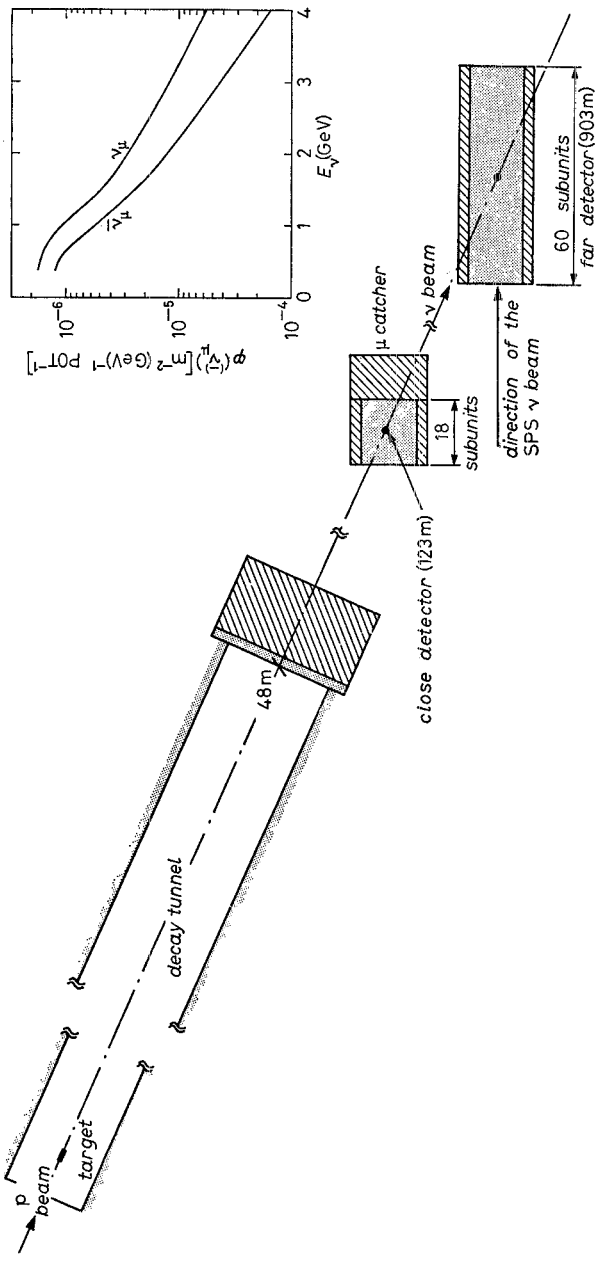

Fig. 44. – Sketch of the CERN PS neutrino beam and of the CHARM set-up [101]. The inset shows the computed $\nu_\mu^{\pi,K}$ and $\bar{\nu}_\mu$ fluxes at the far detector. ▨ iron, ⁞⁞ marble or concrete.

and of both detectors. The computed neutrino and antineutrino fluxes are also shown.

The ν_μ and ν_e CC events were identified in the two detecors. The ν_μ events were characterized by a clear isolated track originating in the detector volume, accompanied by at most some small hadronic activity at the origin; the ν_e CC events were characterized by a narrow and compact shower.

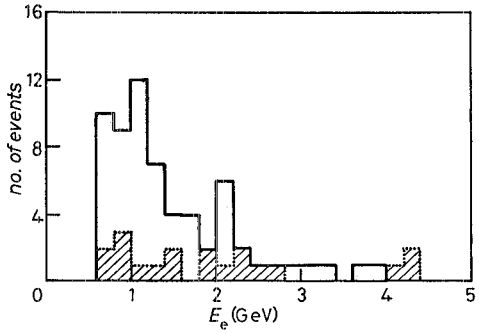

Fig. 45. – Distribution of the electron energy of ν_e candidates in the close (□) and in the far (▨) detector observed in the CHARM experiment [101].

The observed distributions of the electron energy of ν_e candidates, 19 in the far detector and 66 in the close one, are shown in fig. 45.

Subtracting the ratios of events identified as ν_e and ν_μ CC events in the close and in the far detector,

$$\begin{cases} R_C = (\nu_e/\nu_\mu)_C = [9.2 \pm 1.1\ (\text{stat.}) \pm 1.1\ (\text{syst.})]\%\,, \\ R_F = (\nu_e/\nu_\mu)_F = [8.9 \pm 2.0\ (\text{stat.}) \pm 1.0\ (\text{syst.})]\%\,, \end{cases} \tag{5.24}$$

one obtains an upper limit of 2.7 % at 90 % c.l. for the amount of $\nu_\mu \to \nu_e$ oscillation between these two detectors.

The comparison of the two electron candidate energy spectra (fig. 45) by a maximum-likelihood method, taking into account the computed beam energy spectrum and detector acceptances, provides the 90 % c.l. limits shown in fig. 43.

Preliminary results on $\nu_\mu \to \nu_e$ oscillations have been obtained by an APPW Collaboration using BEBC filled with a Ne-H_2 mixture [102]. The bubble chamber has been exposed to the low-energy horn-focused, PS neutrino beam ($\langle E_\nu \rangle = 2.5$ GeV). The detector was about 850 m away from the target.

The results, corresponding to one quarter of the final statistics, are shown in fig. 43.

A search for $\nu_\mu \to \nu_e$ oscillations has been also performed at BNL measuring the reactions

$$\nu_e n \to e^- p \tag{5.25}$$

and

(5.26) $$\nu_\mu n \to \mu^- p$$

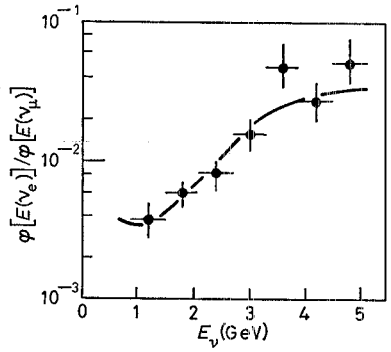

Fig. 46. – Plot of the flux ratio $\varphi[E(\nu_e)]/\varphi[E(\nu_\mu)]$ *vs.* E_ν [103]. The points represent the data; the solid line is calculated from a neutrino beam program.

in a detector located at 96 m from the neutrino source [103]. The mean neutrino energy was 1.5 GeV. Two samples of 418 events induced by reaction (5.25) and of 1370 events induced by reaction (5.26) were measured. These measurements yield directly the energy-dependent ratio of the neutrino fluxes (fig. 46). The difference between the measured ratio and the calculated one as a function of neutrino energy is shown in fig. 47. It is clear that no evidence for the oscillation $\nu_\mu \to \nu_e$ is present. The region in the Δm^2-$\sin^2 2\theta$ space excluded with 90 % c.l. by this experiment is shown in fig. 43.

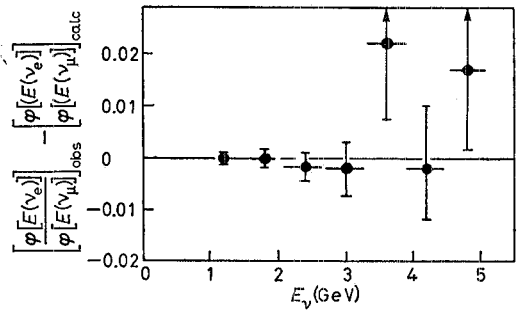

Fig. 47. – Plot of the difference between the observed and calculated flux ratios *vs.* E_ν (from ref. [103]).

5·3.2. The muon-neutrino disappearance experiments. A search for inclusive ν_μ oscillations has been performed in the FNAL neutrino NBB using two detectors running simultaneously at two different distances from the neutrino source [104].

Each neutrino detector consisted of a target calorimeter instrumented with scintillation counters and spark chambers, followed by an iron toroidal muon spectrometer. The close detector was located about 700 m from the target and the far detector at about 1100 m. The NBB configuration and the two detectors of the CCFR experiment are shown in fig. 48.

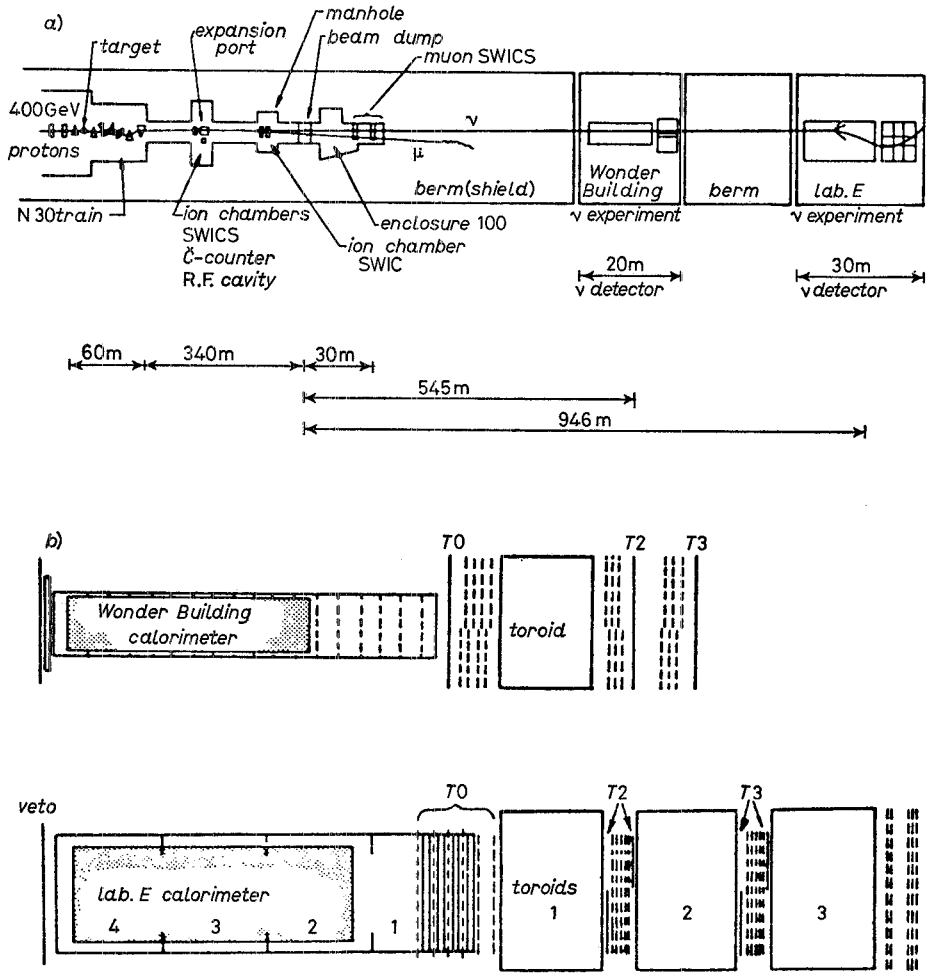

Fig. 48. – Layout of *a*) the NBB and *b*) the close (Wonder Bldg.) and far (lab. *E*) detectors of the CCFR experiment [104].

Charged-current ν_μ events were detected. In order for an event to be accepted, it was requested that the same event, when projected into the other detector, should also have triggered and passed all cuts. Events with total energy between 30 and 230 GeV were collected. The oscillation results were obtained, comparing the number of events in each of the two detectors as a

function of the neutrino energy. The data are consistent with there being no oscillation. The corresponding limits at 90 % c.l. on the plane Δm^2-$\sin^2 2\theta$ are shown, together with those found in other experiments, in fig. 49 [101, 102, 104, 105].

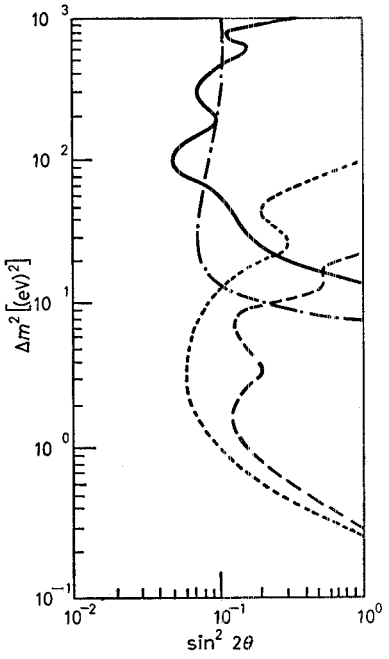

Fig. 49. – Limits on the plane Δm^2-$\sin^2 2\theta$ from the search of the oscillations $\nu_\mu \to \nu_x$ performed by ——— the CCFR experiment [104], – – – the CDHS experiment [105], — — — the CHARM experiment [101], —·—·— the Serpukhov experiment [102].

The disappearance of ν_μ has also been searched for by the CDHS Collaboration at the bare-target PS neutrino beam at CERN [105]. Two detectors were used, located 130 m and 885 m from the target. This experiment was sensitive to CC interactions for neutrino energies between 1 and 7 GeV, with an average of 3 GeV. The energy of neutrino events has been determined, measuring their projected range in iron along the detector axis.

After selection, about 22 000 events with a contamination of 50 cosmic-ray events were measured in the close detector. The corresponding rates in the far detector were $\approx$ 3300 neutrino and 290 cosmic-ray events. Figure 50 shows the ratios of the event rates in the close and in the far detector as a function of the event range in iron, corrected for the change of the neutrino flux between the two detectors. Also shown are curves indicating the expected behaviour of these ratios in the case of oscillations, for different choices of Δm^2 and $\sin^2 2\theta$.

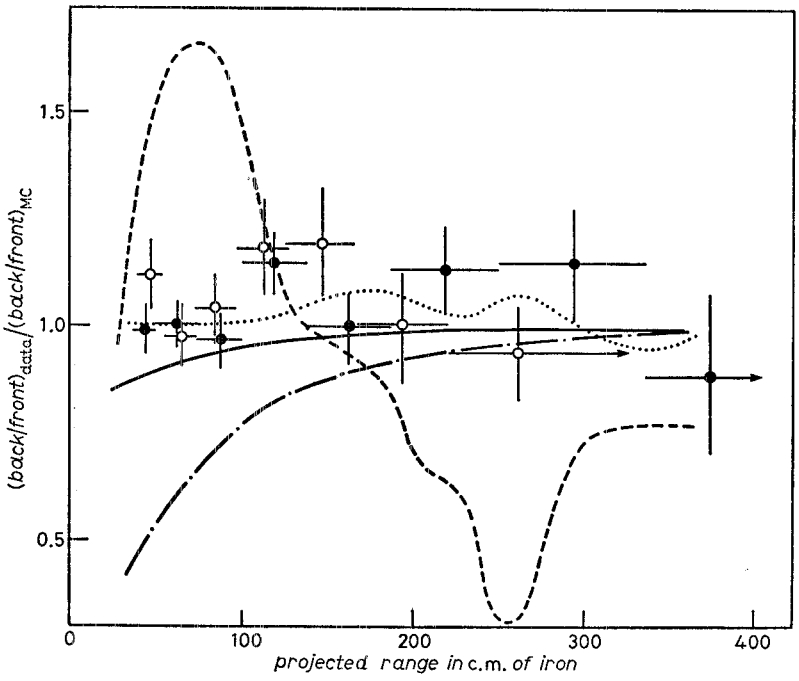

Fig. 50. – Ratio of the Monte Carlo corrected event rates in the close (front) and far (back) detectors of the CDHS experiment as a function of the projected range in iron [105]. The curves indicate the expectation for differents values of the neutrino mass and of the mixing angle: solid line, $\Delta m^2 = 1$ (eV)^2, $\sin^2 2\theta = 0.2$; dash-dotted line, $\Delta m^2 = 1$ (eV)^2, $\sin^2 2\theta = 1$; dashed line, $\Delta m^2 = 16$ (eV)^2, $\sin^2 2\theta = 1$; dotted line, $\Delta m^2 = 32$ (eV)^2, $\sin^2 2\theta = 0.2$. • Type-I modules, o type-II modules.

However, the data show no significant sign of an oscillation. Limits on the oscillation parameters Δm^2 *vs.* $\sin^2 2\theta$ from this experiment are shown in fig. 49.

The disappearance of ν_μ was also investigated in the CHARM experiment at the same beam [101]. The analysis is based on a sample of 2000 and 270 CC events collected in the far and in the close detector, respectively. The average energy of the selected events was 1.5 GeV. The events were subdivided into bins of the projected length l, and in each bin the observed ratio r_{obs} of the far to close detector rates per unit fiducial mass was computed.

In fig. 51 the measured ratio is compared with the expected one (r_{exp}). The results of this search are compatible with there being no disappearance of muon-neutrinos. The 90 % c.l. limits are shown in fig. 49.

Results on ν_μ oscillations have been obtained by an IHEP group at Serpukhov [102]. The disappearance of ν_μ was investigated, comparing the measured rate of CC events in a single detector with the expectations of the standard model. No deviation was found. The corresponding limits on the plane Δm^2-$\sin^2 2\theta$ are shown in fig. 49.

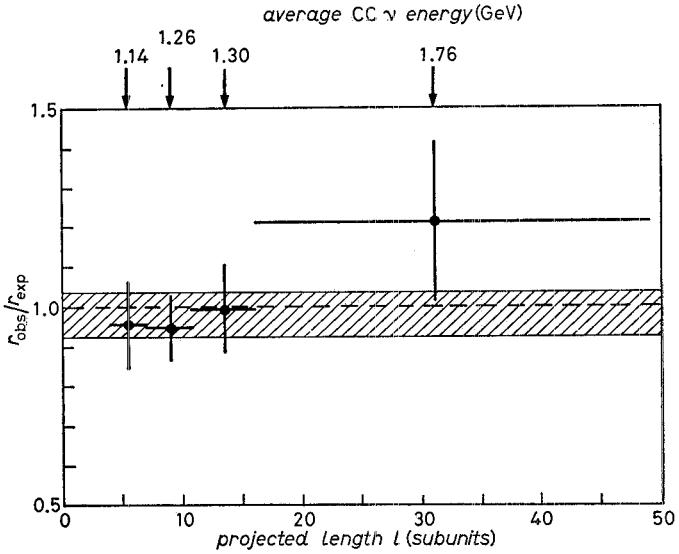

Fig. 51. – The ratio r_{obs}/r_{exp} measured in the CHARM disappearance experiment as a function of the length l (in number of detector subunits) of the events [101].

For a discussion of future experiments on neutrino oscillations at accelerators, see [106].

5·3.3. The electron-antineutrino disappearance experiments. The oscillation of $\bar{\nu}_e$ has been investigated in reactor experiments. The experimental method is based on the detection of the reaction

$$\bar{\nu}_e p \to e^+ n \,. \tag{5.27}$$

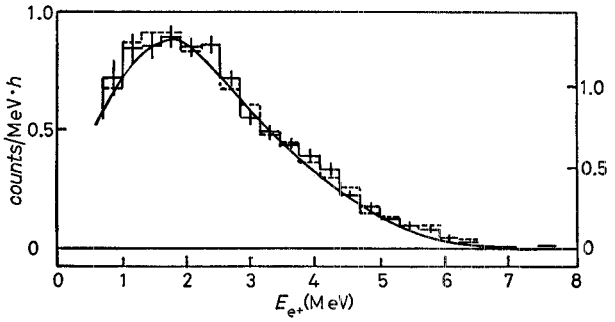

Fig. 52. – Experimental positron spectra measured at 45.9 m (solid line and left scale) and 37.9 m (dashed line and right scale) from the reactor neutrino source in the Gösgen experiment [107]. The curve represents the predicted positron spectra assuming no oscillation.

A recent experiment has been carried out, exposing to the power reactor at Gösgen (Switzerland) [107] a detector consisting of a sandwich of scintillation cells and ^{3}He wire chambers. A correlation in time and position between a positron and a neutron in the detector is required as a signature for a neutrino-induced event. In fig. 52 the positron spectra measured at two distances ($L = 37.9$ m and 45.9 m) from the reactor core are compared with the spectra predicted for the case of no oscillation. The ratio of the fluxes at the two distances is

$$R = 1.01 \pm 0.03 \text{ (stat.)} \pm 0.02 \text{ (syst.)}, \tag{5.28}$$

consistent with the absence of oscillation.

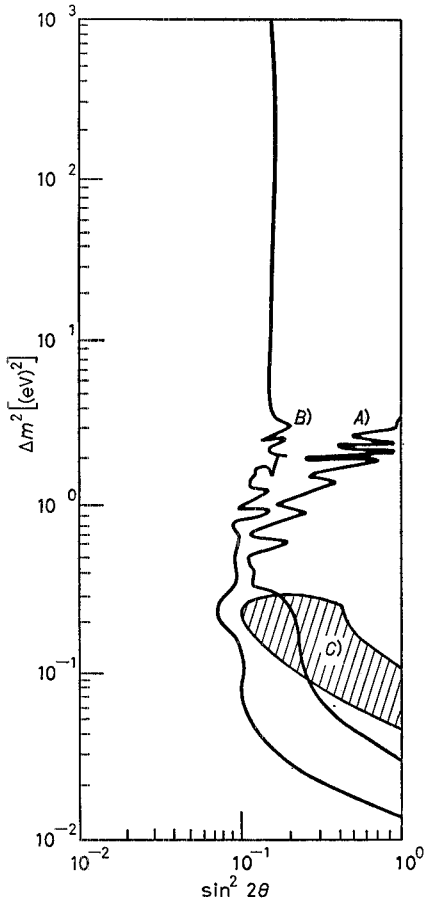

Fig. 53. – Curve *A*) represents the limits at 90% c.l. on Δm^2 as a function of $\sin^2 2\theta$ obtained in the Gösgen experiment [107] ($\bar{\nu}_e \to \nu_X$), using the data collected with the detector placed at 37.9, 45.9 and 8.76 m from the reactor core. Curve *B*) represents the limits, obtained in the same experiment, using also the computed reactor spectra. The shaded area *C*) defines the allowed region at 95.4% c.l. obtained by the Bugey experiment [108].

A comparison of the spectra obtained at 37.9, 45.9 and 8.76 m from the core gave the limits at 90 % c.l. shown in fig. 53. The measurement at 8.76 m was performed, exposing essentially the same detector, at the ^{235}U reactor of the Laue-Langevin Institute in Grenoble. Sensitivity to larger values of Δm^2 can be obtained by including in the analysis the information on the reactor neutrino spectrum. The limits are shown in fig. 53.

The energy spectra of electron-antineutrinos have also been measured at two distances, 13.6 and 18.3 m, from the core of a power reactor at Bugey in France [108]. The detector consists of five planes of six target cells each, filled with liquid scintillator sandwiched between four ^3He wire chambers. The liquid scintillator serves as a free proton target, prompt positron calorimeter and neutron moderator. The thermalized neutrons are detected in the ^3He chambers.

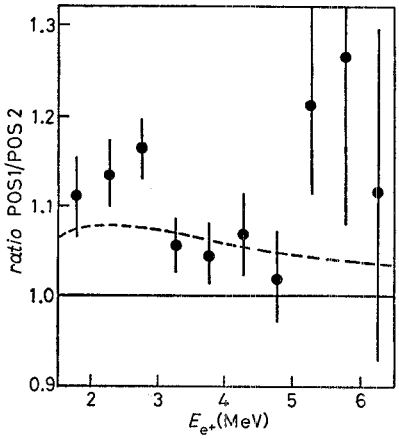

Fig. 54. – Ratio between the event yields measured at distances of 13.6 and 18.3 m at the Bugey reactor experiment as a function of positron energy, corrected for solid-angle difference and the fuel burn-up effect [108]. The dashed line shows the expected ratio for $\Delta m^2 = 0.2$ (eV)^2 and $\sin^2 2\theta = 0.25$.

The ratio of the experimental yields as a function of positron energy is shown in fig. 54. All the data points are higher than unity by 10 %, and the ratio of the integrated yields from 1.5 to 6.5 MeV is

$$R = 1.102 \pm 0.014 \pm 0.028 \,. \tag{5.29}$$

A chi-square test for the ratio of the integrated yields has two allowed regions around 0.8 (eV)^2 and 0.2 (eV)^2. Combining these results with the limits from the two positions of the Gösgen experiment, a region around $\Delta m^2 = 0.2$ (eV)^2 and $\sin^2 2\theta = 0.2$ is selected (fig. 53). The limits obtained by the Gösgen results, comparing the measured e^+ spectra with the predicted ones, are more

stringent (fig. 53). From the ratio of the experimental yields (fig. 54), the non-oscillation case cannot be excluded.

The Gösgen experiment is continuing to take data with the detector placed 65 m away from the reactor core. This measurement would be sensitive to the region in the plane Δm^2-$\sin^2 2\theta$ indicated by the Bugey experiment.

5·4 *Double-beta-decay experiments.* – The experiments described until now are not sensitive to the spinorial nature of neutrinos. The neutrino may be a Majorana particle (the neutrino and the antineutrino coincide) or a Dirac particle (the neutrino and antineutrino are different particles). In the first case the lepton number is not conserved.

The neutrinoless double beta-decay $(\beta\beta)_{0\nu}$ of isotopes of atomic mass A and atomic number Z,

$$[A, Z] \to [A, Z+2] + 2e\,, \tag{5.30}$$

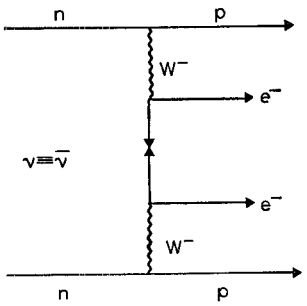

Fig. 55. – Neutrinoless double beta-decay diagram.

can occur only if neutrinos are Majorana particles. As shown in fig. 55, in fact, reaction (5.30) violates the lepton number conservation, requiring that the virtual $\bar{\nu}$ from the first e^- emission be reabsorbed as a ν in order to permit a second e^- to be emitted. The reabsorption is possible only if the neutrino has a mass or if the CCs have a right-handed component (RHC). The limits on the rates for $(\beta\beta)_{0\nu}$ decay can be turned into correlated limits on the neutrino mass and on the RHC.

If the $(\beta\beta)_{0\nu}$ decay is observed, the single-electron energy spectrum and the two-electron angular correlation can distinguish the two effects. The $0^+ \to 2^+$ transition is possible only through right-handed currents, whereas the $0^+ \to 0^+$ transition is possible in both mechanisms [109].

The Lagrangian describing process (5.30) is given by [110]

$$L_{(\beta\beta)_{0\nu}} = (G/\sqrt{2}\cos\theta_C)\,[\bar{e}_L\gamma_\mu\nu_L(\bar{u}_L\gamma^\mu d_L + \eta_{LR}\bar{u}_R\gamma^\mu d_R) + \\ + \bar{e}_R\gamma_\mu\nu'_R(\eta_{RR}\bar{u}_R\gamma^\mu d_R + \eta_{RL}\bar{u}_L\gamma^\mu d_L)]\,, \tag{5.31}$$

where η_{LR}, η_{RR} and η_{RL} are the couplings of the right-handed currents.

The decay rate of reaction (5.30) can be written as [111]

$$\Gamma_{(\beta\beta)_{0\nu}} = \varepsilon^2 F_{0\nu} |M_{GT}|^2 , \tag{5.32}$$

where M_{GT} is the Gamow-Teller matrix element, $F_{0\nu}$ is a kinematical factor, and ε is the lepton-number–violating amplitude. In the case in which the $(\beta\beta)_{0\nu}$ decay is due to the mass mechanism alone and only one massive neutrino contributes, then $\varepsilon = cm_\nu^2$, where c is a constant for a given $(\beta\beta)_{0\nu}$ decay nucleus.

Neutrinoless double beta-decay has been investigated in a large number of geochemical and counter experiments using elements such as ^{48}Cu, ^{76}Ge, ^{82}Se, ^{100}Mo, ^{130}Te and ^{150}Nd. No clear evidence for this decay has been found.

The interpretation of the experimental results in terms of limits on the neutrino mass and on the RHC is made difficult by the theoretical uncertainties in the computation of the transition matrix elements M_{GT} [112-114].

In the geochemical experiment the accumulation of double beta products over geological time periods ($\approx 10^9$ y) is measured. Such experiments are very sensitive but do not distinguish between reaction (5.30) and the double beta-decay with two electrons and two neutrinos in the final state $[(\beta\beta)_{2\nu}]$:

$$[A, Z] \to [A, Z+2] + 2e + 2\nu . \tag{5.33}$$

The experimental limits on the $(\beta\beta)_{0\nu}$ half-life, at two standard deviations, obtained from the geochemical measurements, and the corresponding values of the mass of neutrinos computed according to the models [113, 114], are reported in table VI [111]. The table also shows the limits on m_ν obtained by deriving the matrix elements from the geochemical data themselves.

TABLE VI. – *Experimental limits on the half-life of the* $(\beta\beta)_{0\nu}$ *decay and the corresponding limits on* m_ν *from geochemical experiments.*

Decay transition	Energy (MeV)	$T_{\frac{1}{2}}$ (years)	m_ν [114] (eV)	m_ν [113] (eV)	m_ν ([a]) (eV)
^{130}Te → ^{130}Xe	2.53	$> 2.15 \cdot 10^{21}$	< 9	< 46	< 107
^{128}Te → ^{128}Xe	0.87	$> 8.0 \cdot 10^{24}$	< 1	< 2	< 9
^{82}Se → ^{82}Kr	3.00	$> 1.1 \cdot 10^{20}$	< 74	< 76	< 176

([a]) Matrix element computed from geochemical data [111].

Assuming that $|M_{GT}|$ is equal for the $(\beta\beta)_{0\nu}$ decay of ^{128}Te and ^{130}Te [115], the following limit has been obtained [116]:

$$m_\nu < 5.7 \text{ eV} . \tag{5.34}$$

In the counter experiments it is in principle possible to distinguish between

the $(\beta\beta)_{0\nu}$ and $(\beta\beta)_{2\nu}$ and also between the $0^+ \to 0^+$ and $0^+ \to 2^+$ transitions. The most stringent limits come from the Mont Blanc experiment [117]. The set-up consists of two heavily shielded Ge(Li) crystals, with a fiducial volume of 115 cm^3 and 145 cm^3. A fraction of the germanium isotopes (7.76 %) is double-beta-decay active. Neutrinoless decay would manifest itself in a sharp line at 2040.9 keV ($0^+ \to 0^+$ transition) and at 1481.8 keV ($0^+ \to 2^+$ transition). The energy of the two electrons is measured with a resolution of 1 % at 1 MeV. The $(\beta\beta)_{2\nu}$ decays would produce a continuum spectrum superimposed on the background.

The main sources of background are cosmic rays, natural radioactivity of the environment and the internal radioactivity of the elements assembled in the detector. The background at 2 MeV gives $1.8 \cdot 10^{-3}$ counts per keV and hour in the first crystal and $0.37 \cdot 10^{-3}$ in the second.

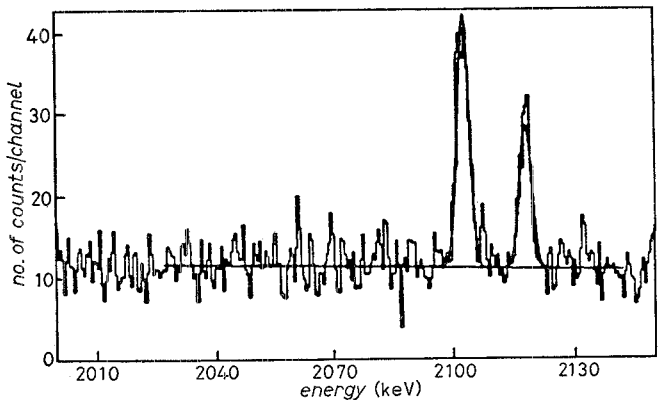

Fig. 56. – Energy spectrum as measured in the Mont Blanc experiment [117]. The background estimate is shown.

No evidence has been found for the $0^+ \to 0^+$ and $0^+ \to 2^+$ transitions. Figure 56 shows the spectrum obtained in $\approx 13\,500$ h of running time in the region of the transition $0^+ \to 0^+$.

The limits obtained for the $0^+ \to 0^+$ transitions were

$$\begin{cases} T_{\frac{1}{2}} > 7.2 \cdot 10^{22} \text{ y} & (68\% \text{ c.l.}), \\ T_{\frac{1}{2}} > 3.5 \cdot 10^{22} \text{ y} & (90\% \text{ c.l.}); \end{cases} \tag{5.35}$$

for the $0^+ \to 2^+$ transition the limit was

$$T_{\frac{1}{2}} > 1.2 \cdot 10^{22} \text{ y} \qquad (68\% \text{ c.l.}). \tag{5.36}$$

From the result for the $0^+ \to 0^+$ transition, the following limits, at 68 % c.l.,

were set:

$$\text{(5.37)} \qquad \begin{cases} m_\nu & < 5 \text{ eV}, \\ \eta_{RR}\langle \ell \rangle_{RL} & < 0.8 \cdot 10^{-5}, \\ \eta_{RL}\langle \ell \rangle_{RL} & < 1.3 \cdot 10^{-5}. \end{cases}$$

In formulae (5.37), $\langle \ell \rangle_{RL} = \sum \ell_k U^L_{ik} U^R_{ik}$, where U^L_{ik} (U^R_{ik}) are the coefficients of the expansions of the left (right) neutrino field coupled to the electron in terms of the $2n$ Majorana mass eigenstates.

A search for double beta-decay is being carried out in the low-background laboratory of the Baksan Neutrino Observatory (URSS) using ^{150}Nd [118].

The detector consists of four plastic-scintillator layers (50 cm $\times$ 25 cm $\times$ $\times$ 5 cm), each viewed by four photomultipliers. A method based on multi-dimensional analysis allows a distinction to be made between $(\beta\beta)_{0\nu}$ and $(\beta\beta)_{2\nu}$ events. The results are

$$\text{(5.38)} \qquad \begin{cases} T_{\frac{1}{2}}(\beta\beta)_{2\nu} & > 1.3 \cdot 10^{19} \text{ y} & (95\% \text{ c.l.}), \\ T_{\frac{1}{2}}(\beta\beta)_{0\nu} \ (m_\nu \neq 0) & > 1.2 \cdot 10^{21} \text{ y} & (95\% \text{ c.l.}), \\ T_{\frac{1}{2}}(\beta\beta)_{0\nu} \ (\eta \neq 0) & > 0.8 \cdot 10^{21} \text{ y} & (95\% \text{ c.l.}). \end{cases}$$

From the ratio of $(\beta\beta)_{0\nu}$ and $(\beta\beta)_{2\nu}$ lifetimes, the values

$$\text{(5.39)} \qquad m_\nu < 29 \text{ eV} \quad \text{and} \quad \eta < 2.2 \cdot 10^{-4}$$

were obtained, independently of the nuclear matrix element.

The half-life of the ^{82}Se $(\beta\beta)_{2\nu}$ decay was measured in an experiment performed with a cloud chamber [119]. The experimental result is

$$\text{(5.40)} \qquad T_{\frac{1}{2}}(\beta\beta)_{2\nu} = (1.0 \pm 0.4) \cdot 10^{19} \text{ y}.$$

This result is an order of magnitude smaller than the value obtained by geo-chemical measurements ($T_{\frac{1}{2}} = (1.7 \pm 0.3) \cdot 10^{20}$ y) [111].

The use of gas detectors would extend the study of double beta-decay to other nuclei such as ^{136}Xe [117]. A comparison of the energy resolution of the germanium detectors with that of gas detectors shows that the latter are worse, but the background can be rejected on a topological basis.

From the results of the ITEP experiment (eq. (5.4)) and the Mont Blanc experiment (eq. (5.37)), it is possible to conclude that the neutrinos are Dirac particles when there is a total absence of neutrino mixing. In the most general case of neutrino mixing in expression (5.32), the ε is a function of an effective mass that could be smaller than the actual masses of neutrinos [120].

In the future, a big improvement to the present limits could come from the

Santa Barbara-LBL experiment [121]. The detector, consisting of Ge crystals, has a fiducial volume eight times larger than the Mont Blanc one. In one year of running it would set a limit of $1 \cdot 10^{24}$ y on the transition $0^+ \to 0^+$. In the absence of right-handed currents this corresponds to a neutrino mass limit of $(1 \div 2)$ eV.

6. – Low-energy investigations of neutral-current interactions.

6·1. *Space-time structure of neutral currents.* – The space-time structure of the neutral currents can be determined in deep inelastic scattering of muon-neutrinos on nucleons,

$$\nu_\mu(\bar{\nu}_\mu)\mathcal{N} \to \nu_\mu(\bar{\nu}_\mu)\mathrm{X}\,, \tag{6.1}$$

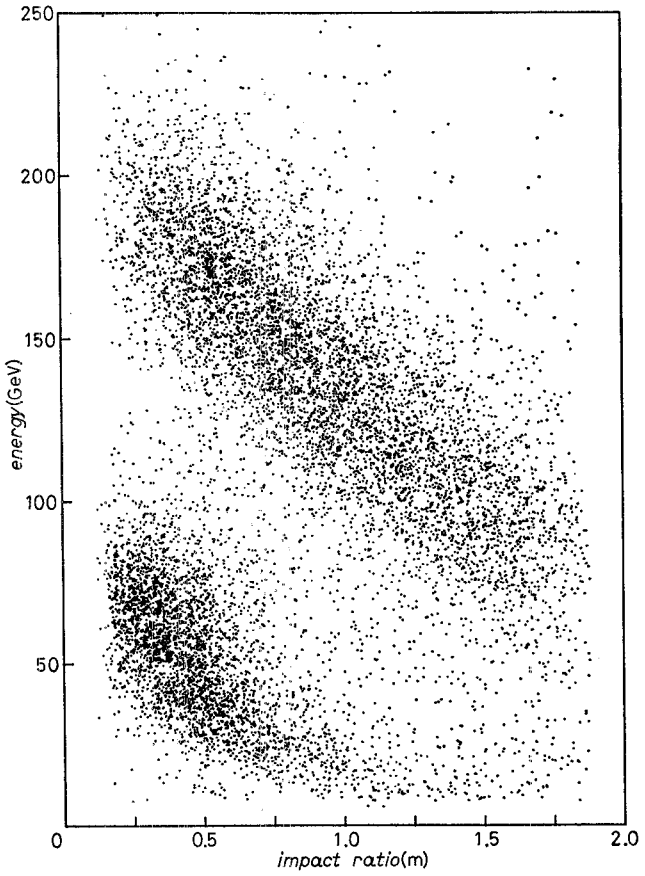

Fig. 57. – Relation between the energy and the radial co-ordinate of the interaction point of CC events as mesured in the CDHS detector exposed to the SPS 200 GeV NBB [40].

studying the differential cross-section as a function of the y variable (see definition (2.2)). Since the outgoing neutrino escapes detection, the y measurement requires knowledge of the incoming-neutrino energy, and the experiments have been made exposing the detectors to NBBs. In such a beam the neutrinos are produced by decays in flight of π's and K's with a selected momentum. The energy of the interacting neutrino is then determined, apart from the π-K ambiguity, from the radial position of the neutrino interaction in the detector (fig. 57).

If there are only V and A terms in the NC, a combination of a flat and a $(1-y)^2$ term is expected to contribute to the differential cross-section. The scalar (S) and pseudoscalar (P) terms would contribute equally to the neutrino and antineutrino interactions; as in the case of CC interactions (2.6) they would manifest themselves with a term proportional to y^2.

Results have been obtained by the CHARM Collaboration [122]. The neutrino and antineutrino differential cross-sections on an isoscalar target (a target with an equal number of quarks u and d) can be parametrized according to

$$\begin{cases} \mathrm{d}\sigma^{\nu}/\mathrm{d}y = A\,[(1-\alpha) + \alpha(1-y)^2] + By^2\,, \\ \mathrm{d}\sigma^{\bar{\nu}}/\mathrm{d}y = A\,[\alpha + (1-\alpha)(1-y)^2] + By^2\,, \end{cases} \tag{6.2}$$

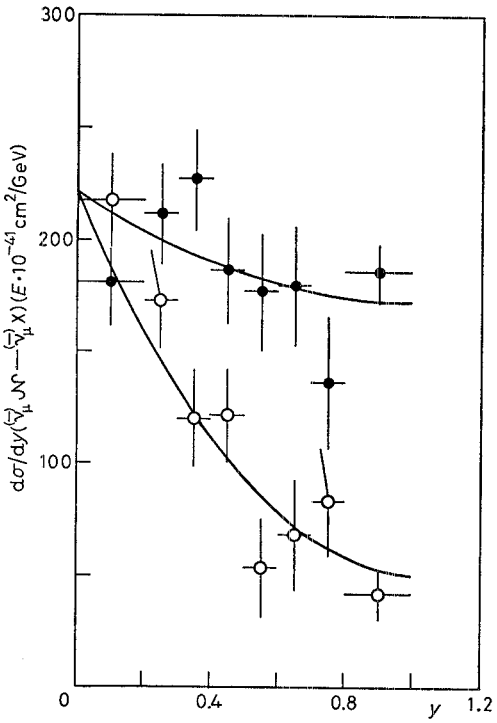

Fig. 58. – The differential cross-section, $\mathrm{d}\sigma/\mathrm{d}y$, of NC events after resolution unfolding and acceptance correction: o $\bar{\nu}$, • ν. The curves correspond to a two-parameter fit (A and α) [122].

where α is the average fraction of antiquarks in the nucleon. The ratio B/A gives the relative proportion of S and/or P, and V, A. A simultaneous fit of eqs. (6.2) to the data (fig. 58) gives $B/A = -0.05 \pm 0.05$, implying that

$$g^2_{SP}/g^2_{VA} < 0.03 \qquad (95\,\%\ \text{c.l.}), \tag{6.3}$$

where g^2_{SP} and g^2_{VA} are the SP and VA total coupling strengths.

6·2. *Flavour-changing neutral-current interactions.* – In all experimentally known processes involving NCs the flavour is conserved. In the standard model, the absence of flavour-changing neutral currents (FCNCs) is accounted for by the GIM mechanism [8].

The value of the ratio of the decay width of K^0_L into two muons to that of $K^\pm$ into a charged lepton and a neutrino [123],

$$\Gamma(K^0_L \to \mu^+\mu^-)/\Gamma(K^\pm \to \ell^\pm\nu) \approx (4 \pm 1)\cdot 10^{-9}, \tag{6.4}$$

represents strong evidence for the absence of FCNCs.

The search for wrong-sign muons in inclusive neutrino reactions has placed stringent limits on the cross-section of the flavour-changing reaction $\nu_\mu u \to \nu_\mu c$. The CDHS Collaboration [124] found

$$(\nu_\mu u \to \nu_\mu c)/(\nu_\mu \mathcal{N} \to \nu_\mu X) < 0.026 \qquad (90\,\%\ \text{c.l.}). \tag{6.5}$$

The IFIM Collaboration [125] obtained

$$(\bar\nu_\mu u \to \bar\nu_\mu c)/(\bar\nu_\mu \mathcal{N} \to \bar\nu_\mu X) < 0.04 \qquad (90\,\%\ \text{c.l.}). \tag{6.6}$$

This experiment searched for events with a single positron as a signature for charmed-particle decay. The result (6.6) was arrived at assuming a branching ratio $\mathrm{Br}\,(c \to e^+\nu_e X) = 0.1$.

At the SPEAR e^+e^- storage ring, charm-changing NCs have also been searched for in the decay of charmed particles [126]. It was found that

$$\Gamma(c \to e^+e^-X)/\Gamma(c \to e^+\nu X) < 0.02 \qquad (90\,\%\ \text{c.l.}). \tag{6.7}$$

A search for D^0-$\bar D^0$ mixing has been performed at SPEAR [127]. Mixing would lead to final states of D^0D^0 or $\bar D^0\bar D^0$ and hence to events with two electrons of equal charge from their semi-leptonic decays. The search gave an upper limit of

$$[N(e^+e^+) + N(e^-e^-)]/N(e^+e^-) < 0.05 \qquad (90\,\%\ \text{c.l.}). \tag{6.8}$$

Recently the CLEO Collaboration, studying the decay of beauty particles,

has found [128]

$$\Gamma(B \to e^+e^-X)/\Gamma(B \to \text{all}) < 0.003 \qquad (90\,\%\ \text{c.l.}). \tag{6.9}$$

6·3. *Determination of the fermion couplings to the* Z^0. – The NC coupling constants of the fermions to the Z^0 have been determined in

1) the interaction of neutrinos with electrons,

2) the interaction of neutrinos with quarks,

3) the interactions of charged leptons with quarks and

4) the electroweak interference in e^+e^- annihilation.

6·3.1. Neutrino-electron scattering. The scattering of neutrinos $(\nu_\mu(\bar{\nu}_\mu), \nu_e(\bar{\nu}_e))$ on electrons is of particular interest because of its theoretical simplicity. The neutrino-electron reactions involve only free pointlike particles, and the cross-sections can be computed in the standard model with high accuracy [129].

The following reactions have been studied:

$$\nu_e e \to \nu_e e\,, \tag{6.10}$$

$$\bar{\nu}_e e \to \bar{\nu}_e e\,, \tag{6.11}$$

$$\nu_\mu e \to \nu_\mu e\,, \tag{6.12}$$

$$\bar{\nu}_\mu e \to \bar{\nu}_\mu e\,. \tag{6.13}$$

Reactions (6.12) and (6.13) are induced only by NC interactions; NCs and CCs both contribute to the scattering of $\nu_e(\bar{\nu}_e)$ on electrons.

For centre-of-mass energy $\sqrt{s} \ll m_Z$, the Z^0 propagator is constant and the νe interactions behave as pointlike four-fermion interactions. The cross-sections of reactions (6.10) to (6.13) are proportional to the electron mass and, then, for a given neutrino energy, 3÷4 orders of magnitude smaller than the $\nu\mathcal{N}$ one. It follows that it is necessary to use high-intensity beams, massive detectors and a good discrimination of the events with a single electron in the final state to detect νe events.

The energy and the angle of the outgoing electron are related according to

$$E_e \theta_e^2 < 2m_e\,. \tag{6.14}$$

At high energy the angle of the recoil electron is very small (*e.g.*, for $E_e = 15$ GeV, $\theta_e < 8$ mrad). Provided there is a very good angular resolution, this feature can be used to discriminate the νe events from the electromagnetic background due to ν-nucleon interactions, which has a wider angular distribution.

The Lagrangian for the muon-neutrino (-antineutrino)-electron scattering

is given by

$$L^{(\nu_\mu e)} = (G/\sqrt{2})\{\bar{\nu}_{\mu L}\gamma_\mu \nu_{\mu L}[\varepsilon(e_L)\bar{e}_L\gamma_\mu e_L + \varepsilon(e_R)\bar{e}_R\gamma_\mu e_R]\}\,. \tag{6.15}$$

Assuming lepton universality of the weak interactions, the Lagrangian for the electron-neutrino (-antineutrino)-electron scattering $L^{(\nu_e e)}$ ($L^{(\bar{\nu}_e e)}$) is obtained from eq. (6.15) by replacing ν_μ with ν_e and $\varepsilon(e_L)$ with $\varepsilon(e_L)+1$ (the coupling of the CC is equal to one).

In the approximation of zero electron mass, the angular-momentum conservation determines the differential cross-sections $d\sigma/dy$ ($y = E_e/E_\nu$), as shown in fig. 2*a*) and *b*), where f=e. The weights of the left-handed and right-handed electron currents are $\varepsilon(e_L)$ and $\varepsilon(e_R)$, respectively.

The integral cross-sections are

$$\begin{cases} \sigma(\nu_\mu e) = (2G^2 E_\nu m_e/\pi)[\varepsilon(e_L)^2 + \varepsilon(e_R)^2/3]\,, \\ \sigma(\bar{\nu}_\mu e) = (2G^2 E_\nu m_e/\pi)[\varepsilon(e_R)^2 + \varepsilon(e_L)^2/3]\,, \\ \sigma(\nu_e e) = (2G^2 E_\nu m_e/\pi)\{[\varepsilon(e_L)+1]^2 + \varepsilon(e_R)^2/3\}\,, \\ \sigma(\bar{\nu}_e e) = (2G^2 E_\nu m_e/\pi)\{\varepsilon(e_R)^2 + [\varepsilon(e_L)+1]^2/3\}\,. \end{cases} \tag{6.16}$$

In the standard model $\varepsilon(e_L)$ and $\varepsilon(e_R)$ are functions of $\sin^2\theta_w$ (eq. (1.17)). Figure 59 shows the dependence of the cross-sections (6.16) on $\sin^2\theta_w$. For $\sin^2\theta_w = 0.25$, a destructive interference of $\approx 35\,\%$ of the CC cross-section is expected in the case of the $\nu_e e$ scattering and $\approx 25\,\%$ in the case of $\bar{\nu}_e e$.

The cross-section of the elastic scattering of electron-antineutrinos on electrons, reaction (6.11), has been measured using a 15.9 kg plastic scintillator target in a composite plastic NaI liquid scintillator detector exposed to a $\bar{\nu}_e$ flux of $2.2\cdot 10^{13}$ cm^{-2} s^{-1} produced by a fission reactor [130]. The results reported in table VII are given for two different electron energy regions.

TABLE VII. – *Results from the measurement of* $\sigma(\bar{\nu}_e e)$ [130].

Energy bin (MeV)	$\bar{\nu}_e e$ events	$\sigma_{obs}/\sigma(V-A)$
1.5 to 3	5.9 ± 1.4	0.87 ± 0.25
3 to 4.5	1.2 ± 0.25	1.70 ± 0.44

The background was due to the inverse beta-decay ($\bar{\nu}_e p \to e^+ n$) and to the interactions of neutrons and photons in the detector. The observation of the e^+ annihilation and the subsequent neutron capture allowed the rejection of events due to inverse beta-decay. Neutron and photon contamination was determined by varying the shielding, and was found to be less than 10%.

The observed cross-section, even if not incompatible with $V-A$, appears

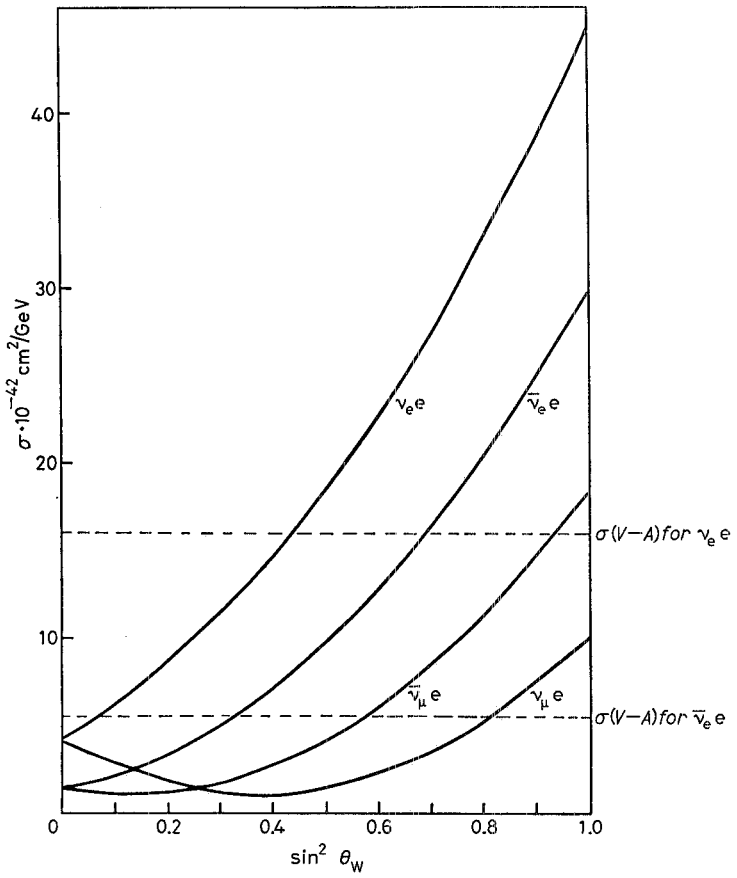

Fig. 59. – Dependence of $\nu_\mu e$, $\bar{\nu}_\mu e$, $\nu_e e$, $\bar{\nu}_e e$ cross-sections on $\sin^2\theta_w (\varrho = 1)$.

to favour the standard model with $\sin^2\theta_w = 0.29 \pm 0.05$, as quoted in ref. [130]. The interpretation of the result depends on the computation of the $\bar{\nu}_e$ beam. A new analysis of the data [131] gave a value of $\sin^2\theta_w$ equal to

$$\sin^2\theta_w = 0.23 \pm 0.05 . \tag{6.17}$$

The allowed regions at 68 % c.l. in the plane g_V^e-g_A^e obtained by the new analysis are shown in fig. 60 together with the limits from the $e^+e^- \to \ell^+\ell^-$ [132] (see subsect. **6**·3.4) and the $\nu_\mu e$ ($\bar{\nu}_\mu e$) cross-section measurements (see eqs. (6.20)).

First evidence for events induced by the scattering of electron-neutrinos on electrons (reaction (6.10)) has been obtained at LAMPF [133]. The neutrino beam contains an equal number of ν_μ, $\bar{\nu}_\mu$ and ν_e which originated in the $\pi^+ \to$ $\to \mu^+\nu_\mu$ decay followed by the $\mu^+ \to e^+\bar{\nu}_\mu\nu_e$ decay. The maximum ν_e energy is 53 MeV. The detector consists of alternate layers of thick plastic scintillators

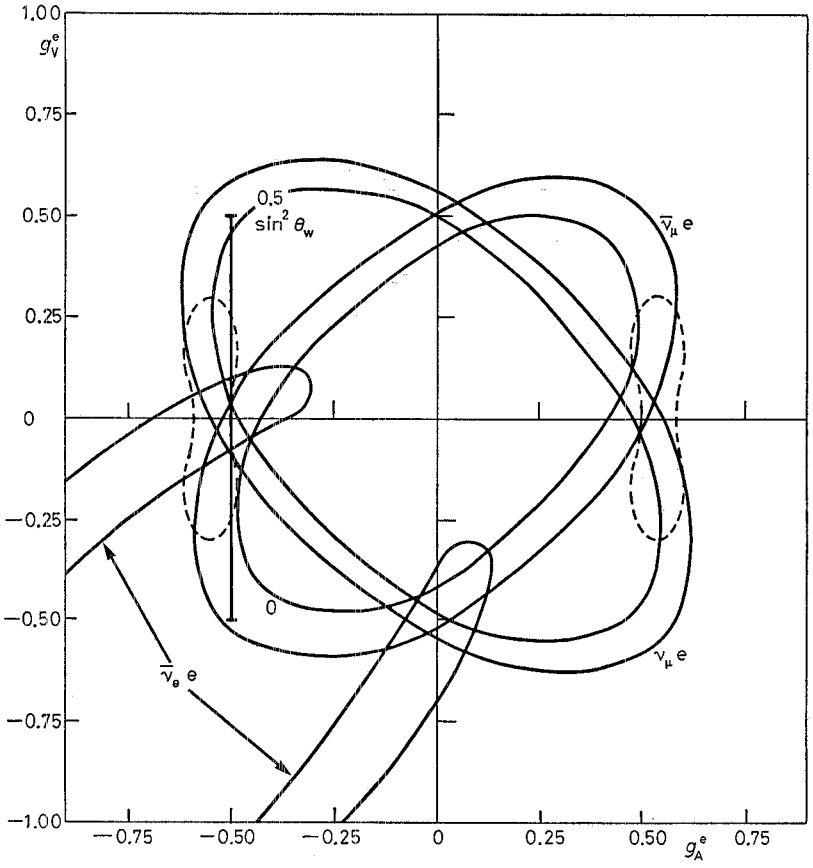

Fig. 60. – Allowed regions in the plane of the vector g_V^e and axial-vector g_A^e coupling constant $e^+e^- \to \ell^+\ell^-$ (— — —) [132], from $\bar{\nu}_e e$ scattering [131] and from $\nu_\mu e$ ($\bar{\nu}_\mu e$) scattering experiments.

and flash chambers to provide tracking information of the electron. It is surrounded by an active anticoincidence shield to provide suppression of cosmic-ray background. Preliminary results are shown in fig. 61. The candidate events are plotted against the cosine of the electron recoil angle. In the region $\cos\theta > 0.96$, a signal of (20.3 ± 7.3) events was obtained. This corresponds to a cross-section

$$\sigma(\nu_e e)/E_\nu = [10.6 \pm 4.6\ (\text{stat.}) \pm 1.9\ (\text{syst.})] \cdot 10^{-42}\ \text{cm}^2/\text{GeV}\,. \tag{6.18}$$

The indication is that the interference of NC and CC contributions is not constructive. From this measurement a preliminary value was obtained:

$$\sin^2\theta_w = 0.27^{+0.17}_{-0.18}\,. \tag{6.19}$$

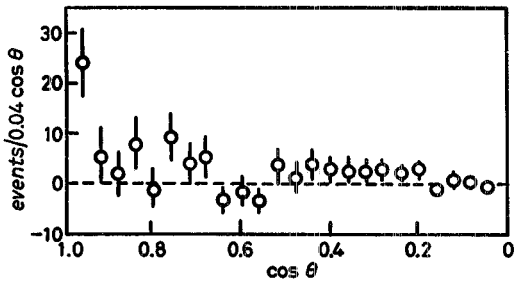

Fig. 61. – Candidate events *vs.* the cosine of the angle between the direction of the recoil particle and that of the neutrino beam. Neutrino-electron scattering events are expected to concentrate near $\cos\theta = 1$ [133].

The measurements of the $\nu_\mu e$ and $\bar{\nu}_\mu e$ cross-sections (reactions (6.12) and (6.13)) have been performed with high-energy neutrino beams produced in π and K decays. In such experiments the cosmic background is negligible and the main source of background is represented by ν interactions that can fake a single electron in the final state. The signal is separated from the background using the fact that the electron in the $\nu_\mu e$ ($\bar{\nu}_\mu e$) scattering is emitted at a very small angle with respect to the direction of the incoming neutrino.

Table VIII shows the results obtained from the measurements of the neutrino and antineutrino cross-sections [134-141]. The world averages of the σ's are

$$(6.20) \qquad \begin{cases} \langle \sigma_\nu / E_\nu \rangle = (1.55 \pm 0.20) \cdot 10^{-42} \text{ cm}^2/\text{GeV}, \\ \langle \sigma_{\bar{\nu}} / E_{\bar{\nu}} \rangle = (1.26 \pm 0.21) \cdot 10^{-42} \text{ cm}^2/\text{GeV}, \end{cases}$$

TABLE VIII. – *Results from the measurements of* $\sigma(\nu_\mu e)$ *and* $\sigma(\bar{\nu}_\mu e)$.

Neutrino $N_{tot} = 206$		
Experiment	Events	$\sigma_\nu(10^{-42}$ cm^2/GeV)
AP [134]	7	1.1 ± 0.6
GGM-SPS [135]	9	$2.4 + 1.2/-0.9$
FNAL [136]	22	1.6 ± 0.4
VPI [137]	34	1.4 ± 0.4
CHARM [138]	83	1.9 ± 0.6
E734 [139]	51	1.6 ± 0.4

Antineutrino $N_{tot} = 180$		
Experiment	Events	$\sigma_{\bar{\nu}}(10^{-42}$ cm^2/GeV)
GGM-PS [140]	3	$1.0 + 1.3/-0.6$
AP [134]	6	2.2 ± 1.0
CHARM [138]	112	1.5 ± 0.5
E734 [141]	59	1.2 ± 0.3

corresponding, in the hypothesis of $\varrho = 1$, to

$$\sin^2\theta_w = 0.22 \pm 0.03 \tag{6.21}$$

and

$$\sin^2\theta_w = 0.21^{+0.04}_{-0.06}, \tag{6.22}$$

respectively. The limits on the plane g_V^e-g_A^e at 68% c.l. are shown in fig. 60. The limits from neutrino and antineutrino reactions are represented by ellipses that intersect in four regions. Making use of the equations

$$\begin{cases} g_V^{e2} + g_A^{e2} = (2\pi/Gm_e)\,\frac{3}{8}\,[\sigma_\nu/E_\nu + \sigma_{\bar\nu}/E_{\bar\nu}]\,, \\ g_V \times g_A \;\; = (2\pi/Gm_e)\,\frac{3}{8}\,[\sigma_\nu/E_\nu - \sigma_{\bar\nu}/E_{\bar\nu}]\,, \end{cases} \tag{6.23}$$

of the limits obtained from the measurement of the $\bar\nu_e e$ cross-section [131] and of the angular asymmetry of leptons in the reactions $e^+e^- \to \ell^+\ell^-$ at PETRA and PEP [132], the following values of g_V^e and g_A^e were obtained:

$$\begin{cases} g_A^e = -0.494 \pm 0.026\,, \\ g_V^e = -0.050 \pm 0.052\,. \end{cases} \tag{6.24}$$

The measurement of the ratio $R = \sigma(\nu_\mu e)/\sigma(\bar\nu_\mu e)$ allows the determination of the weak angle in a way that is independent of ϱ. The ratio R depends on $\sin^2\theta_w$ according to the expression

$$R = 3\,\frac{1 - 4\sin^2\theta_w + 16/3\,\sin^4\theta_w}{1 - 4\sin^2\theta_w + 16\sin^4\theta_w}\,. \tag{6.25}$$

As shown in fig. 62, around $\sin^2\theta_w = 0.25$ the ratio R is very sensitive to $\sin^2\theta_w$ ($\Delta\sin^2\theta_w = (\Delta R/R)/8$).

If the two cross-sections are measured with the same detector, the ratio R is affected by a small systematic error. In fact, the uncertainty on the efficiency of the criteria applied to select the $\nu_\mu e$ ($\bar\nu_\mu e$) candidates cancels, the error in the background subtraction is strongly reduced, and the normalization is done with the ratio of the neutrino and antineutrino fluxes, avoiding the more difficult absolute flux measurement.

The value of $\sin^2\theta_w$ was determined from the measurement of the muon-neutrino and -antineutrino-electron scattering cross-sections at high neutrino energies with a single apparatus, first at the CERN SPS neutrino beam ($\langle E_\nu\rangle \approx$ $\approx$ 30 GeV) by the CHARM Collaboration [138], and later, at low energy, at the BNL AGS neutrino beam by the E734 experiment ($\langle E_\nu\rangle \approx 1.5$ GeV) [141].

In the CHARM experiment the electron-hadron separation was based on the different lateral profile of the showers. The $E^2\theta^2$ distributions of the neutrino and antineutrino candidate events, as shown in fig. 63, were used to separate the signal from the residual background. The signal in the region $E^2\theta^2 <$

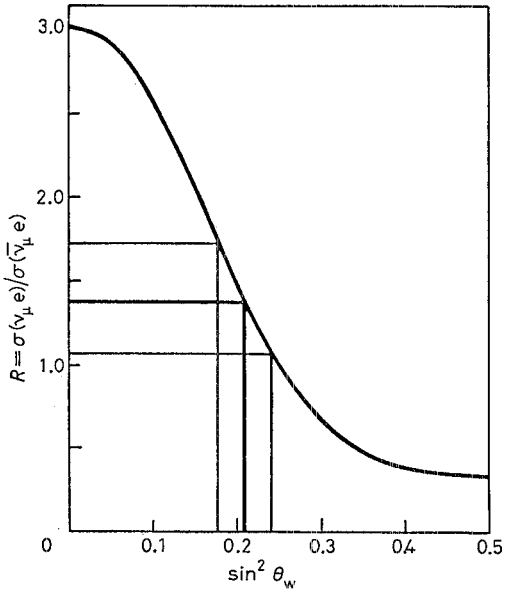

Fig. 62. – Dependence of $R = \sigma(\nu_\mu e)/\sigma(\bar{\nu}_\mu e)$ on $\sin^2\theta_w$. The experimental result of the E734 experiment [141] is compared with the standard-model prediction (curve), allowing a determination of $\sin^2\theta_w$.

< 0.12 (GeV)^2 was calculated extrapolating the background from the reference region $(0.12\ (\text{GeV})^2 < E^2\theta^2 < 0.54\ (\text{GeV})^2)$.

The background events with electromagnetic showers in the final state were produced by two sources: the quasi-elastic CC reactions induced by ν_e ($\bar{\nu}_e$) contamination of the beam on nucleons, and the NC reactions with a

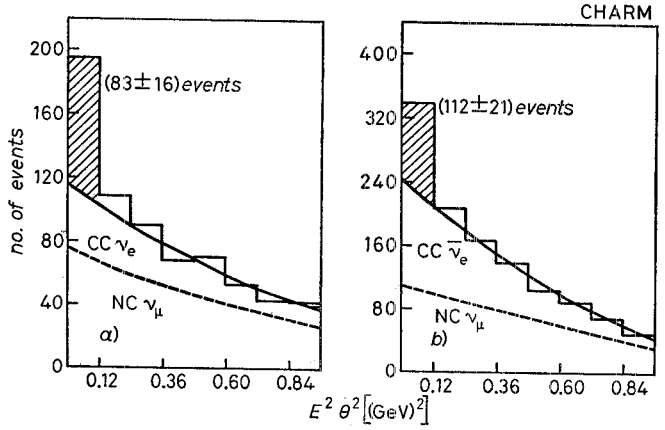

Fig. 63. – $E^2\theta^2$ distribution of *a*) $\nu_\mu e$ and *b*) $\bar{\nu}_\mu e$ candidate events in the CHARM experiment [138].

γ and/or a π^0 in the final state produced by coherent scattering of ν_μ ($\bar{\nu}_\mu$) on nuclei. Two signals, one of (83 ± 16) ν_μe events and the other of (112 ± 21) $\bar{\nu}_\mu$e events, were obtained. The normalization was done using the $\bar{\nu}_\mu$ quasi-elastic CC events and the deep inelastic events collected during the two exposures.

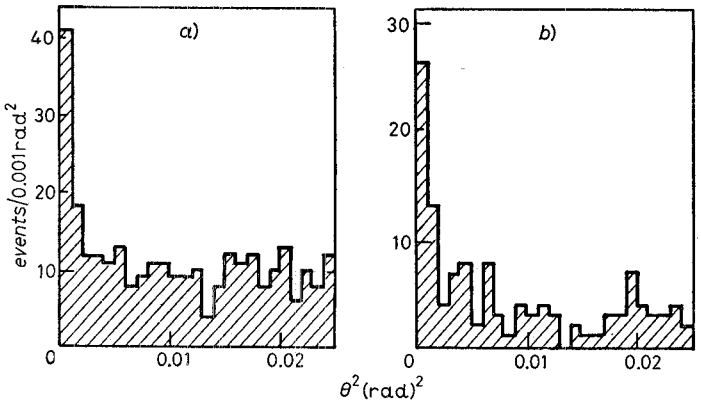

Fig. 64. – θ^2 distributions of *a*) $\bar{\nu}_\mu$e and *b*) ν_μe candidate events of the E734 experiment [141].

In the E734 experiment the hadron interactions are rejected on the basis of scanning criteria. The θ^2 distributions of the neutrino and antineutrino candidate events having 210 MeV $< E_e <$ 2100 MeV are shown in fig. 64. The signals of (51 ± 9) ν_μe and (58 ± 10) $\bar{\nu}_\mu$e were extracted in the region $\theta^2 < 0.01$ rad^2, subtracting the background normalized in the region 0.01 rad^2 $< \theta^2 <$ 0.032 rad^2. The background was assumed to be due to neutrino events with photons in the final state and to events induced by the inverse beta-decay reactions. The normalization was obtained using the $\nu_\mu n \to \mu^- p$ and $\bar{\nu}_\mu p \to \mu^+ n$ events collected during the two beam exposures.

Comparing the measured neutrino and antineutrino cross-section ratio with the expectations of the standard model (fig. 62), the following values of $\sin^2\theta_w$ were arrived at:

$$\begin{cases} \sin^2\theta_w = 0.215 \pm 0.032\ (\text{stat.}) \pm 0.012\ (\text{syst.}) & [\text{CHARM}], \\ \sin^2\theta_w = 0.209 \pm 0.029\ (\text{stat.}) \pm 0.013\ (\text{syst.}) & [\text{E734}]. \end{cases} \tag{6.26}$$

The average value of $\sin^2\theta_w$ obtained from the ratio measurements is

$$\sin^2\theta_w = 0.212 \pm 0.021\ (\text{stat.}) \pm 0.009\ (\text{syst.})\,. \tag{6.27}$$

The CHARM Collaboration also reported determinations of ϱ, g_A^e and g_V^e. The measured value of ϱ is

$$\varrho = 1.09 \pm 0.09\ (\text{stat.}) \pm 0.11\ (\text{syst.})\,. \tag{6.28}$$

The results for g_A^e and g_V^e are shown in fig. 65. The limits from the reaction $e^+e^- \to \ell^+\ell^-$ [132] and from $\bar{\nu}_e e$ scattering [131] select a unique solution:

$$(6.29) \qquad \begin{cases} g_A^e = -0.54 \pm 0.05 \text{ (stat.)} \pm 0.06 \text{ (syst.)}, \\ g_V^e = -0.08 \pm 0.07 \text{ (stat.)} \pm 0.03 \text{ (syst.)}. \end{cases}$$

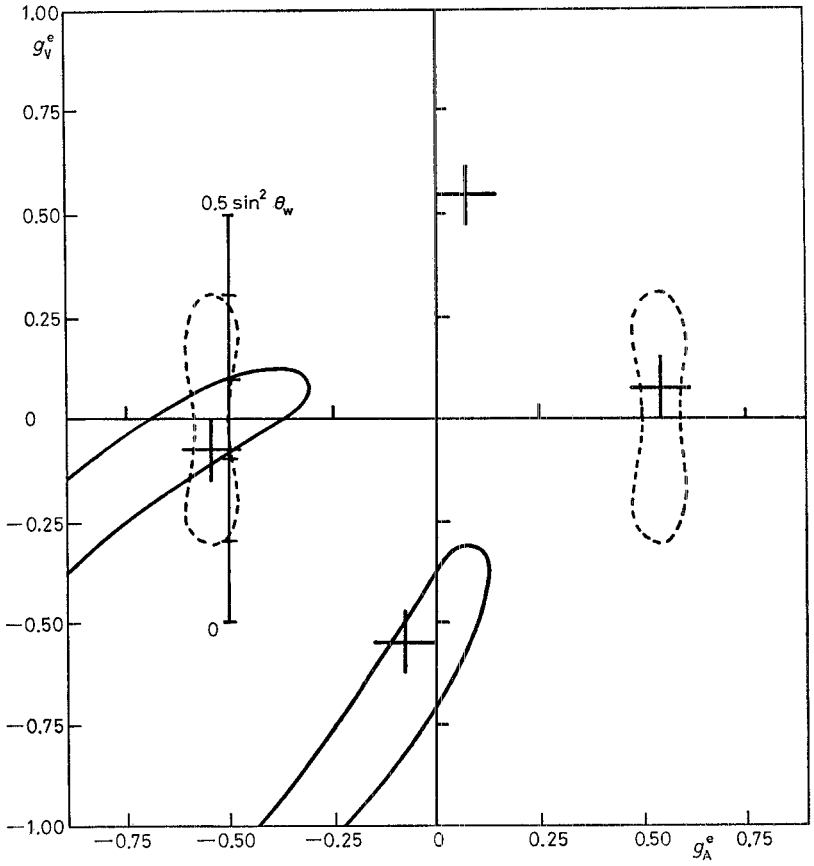

Fig. 65. – Allowed regions in the plane of the vector g_V^e and axial-vector g_A^e coupling constants from $e^+e^- \to \ell^+\ell^-$ [132], from the $\bar{\nu}_e e$ scattering [131] and from the measurement of the ratio $R = \sigma(\nu_\mu e)/\sigma(\bar{\nu}_\mu e)$ [138]: + CHARM experiment, ——— $\bar{\nu}_e e$ scattering limit, — — — $e^+e^- \to \ell^+\ell^-$ limits.

6·3.2. Neutrino-quark interactions.

6·3.2.1. Coupling constants of light quarks. – The light-quark NC couplings were determined by studying the interactions of neutrinos and antineutrinos with matter. Considering only V and A currents, the NC interactions of neu-

trinos with quarks is described by the following effective Lagrangian:

$$(6.30)\qquad L^{(\nu q)} = (G/\sqrt{2})\{\bar{\nu}_L\gamma_\mu\nu_L[\varepsilon(u_L)\bar{u}_L\gamma_\mu u_L + \varepsilon(d_L)\bar{d}_L\gamma_\mu d_L + \\ + \varepsilon(u_R)\bar{u}_R\gamma_\mu u_R + \varepsilon(d_R)\bar{d}_R\gamma_\mu d_R]\}\,.$$

The interaction Lagrangian can be also expressed in terms of the parameters α, β, γ and δ:

$$(6.31)\qquad L^{(\nu q)} = (G/\sqrt{2})\{[\bar{\nu}\gamma_\mu(1+\gamma_5)\nu]\tfrac{1}{2}[\bar{u}\gamma_\mu(\alpha+\beta\gamma_5)u - \bar{d}\gamma_\mu(\alpha+\beta\gamma_5)d] + \\ + \tfrac{1}{2}[\bar{u}\gamma_\mu(\gamma+\delta\gamma_5)u + \bar{d}\gamma_\mu(\gamma+\delta\gamma_5)d]\}\,.$$

The quantities α, β, γ and δ are related to the strong isospin properties of the NC: α = (strong) isovector vector coupling, β = (strong) isovector axial-vector coupling, γ = (strong) isoscalar vector coupling and δ = (strong) isoscalar axial-vector coupling. They are related to the chiral couplings according to

$$(6.32)\qquad \begin{cases} \varepsilon(u_L) = \tfrac{1}{4}(\alpha+\beta+\gamma+\delta)\,, & \varepsilon(u_R) = \tfrac{1}{4}(\alpha-\beta+\gamma-\delta)\,, \\ \varepsilon(d_L) = \tfrac{1}{4}(-\alpha-\beta+\gamma+\delta)\,, & \varepsilon(d_R) = \tfrac{1}{4}(-\alpha+\beta+\gamma-\delta)\,. \end{cases}$$

In terms of the weak mixing angle, we have

$$(6.33)\qquad \begin{cases} \alpha = 1 - 2\sin^2\theta_w\,, & \beta = 1\,, \\ \gamma = -\tfrac{2}{3}\sin^2\theta_w\,, & \delta = 0\,. \end{cases}$$

The NC coupling constants have been determined measuring the neutrino (antineutrino) CC and NC deep inelastic cross-sections:

$$(6.34)\qquad \nu_\mu(\bar{\nu}_\mu)\mathcal{N} \to \mu^-(\mu^+)X\,, \qquad \nu_\mu(\bar{\nu}_\mu)\mathcal{N} \to \nu_\mu(\bar{\nu}_\mu)X\,.$$

At high momentum transfer the processes (6.34) are described by the interaction of neutrinos with quarks. We will give the expressions of the cross-section in the case of an isoscalar target, ignoring the contribution of heavy quarks and assuming that the quarks in the nucleon are free.

The CC interactions are $V-A$ and the y differential cross-sections are (fig. 2*a*))

$$(6.35)\qquad \begin{cases} \mathrm{d}\sigma^{\nu CC}/\mathrm{d}y \approx (1-\alpha) + \alpha(1-y)^2\,, \\ \mathrm{d}\sigma^{\bar{\nu}CC}/\mathrm{d}y \approx (1-\alpha)(1-y)^2 + \alpha\,. \end{cases}$$

The quantity α is the fraction of antiquarks in the nucleon.

In the NC interactions the neutrinos (antineutrinos) interact with both helicity quarks with different couplings. The neutrino and antineutrino dif-

ferential cross-sections on an isoscalar target are (fig. 2*a*), *b*))

$$(6.36)\quad \begin{cases} \mathrm{d}\sigma^{\nu\mathrm{NC}}/\mathrm{d}y \approx \varepsilon(q_\mathrm{L})^2[(1-\alpha)+\alpha(1-y)^2]+\varepsilon(q_\mathrm{R})^2[(1-\alpha)(1-y)^2+\alpha], \\ \mathrm{d}\sigma^{\bar\nu\mathrm{NC}}/\mathrm{d}y \approx \varepsilon(q_\mathrm{L})^2[(1-y)^2(1-\alpha)+\alpha]+\varepsilon(q_\mathrm{R})^2[(1-\alpha)+\alpha(1-y)^2], \end{cases}$$

where $\varepsilon(q_\mathrm{L})^2 = \varepsilon(u_\mathrm{L})^2 + \varepsilon(d_\mathrm{L})^2$ and $\varepsilon(q_\mathrm{R})^2 = \varepsilon(u_\mathrm{R})^2 + \varepsilon(d_\mathrm{R})^2$. From eqs. (6.36) it follows that the measurements of the NC neutrino cross-sections on an isoscalar target do not allow a separate determination of the u and d couplings.

The integral cross-sections are

$$(6.37)\quad \begin{cases} \sigma^{\nu\mathrm{CC}} \approx 1-\tfrac{2}{3}\alpha, \\ \sigma^{\bar\nu\mathrm{CC}} \approx \tfrac{1}{3}+\tfrac{2}{3}\alpha, \end{cases}$$

and

$$(6.38)\quad \begin{cases} \sigma^{\nu\mathrm{NC}} \approx \varepsilon(q_\mathrm{L})^2[1-\tfrac{2}{3}\alpha]+\varepsilon(q_\mathrm{R})^2[\tfrac{1}{3}+\tfrac{2}{3}\alpha], \\ \sigma^{\bar\nu\mathrm{NC}} \approx \varepsilon(q_\mathrm{L})^2[\tfrac{1}{3}+\tfrac{2}{3}\alpha]+\varepsilon(q_\mathrm{R})^2[1-\tfrac{2}{3}\alpha]. \end{cases}$$

Introducing the ratios R and $\bar R$ of the NC and CC neutrino and antineutrino cross-sections and the ratio r of the antineutrino and neutrino CC cross-sections, we get

$$(6.39)\quad \begin{cases} R = \dfrac{\sigma^{\nu\mathrm{NC}}}{\sigma^{\nu\mathrm{CC}}} = \varepsilon(q_\mathrm{L})^2 + \varepsilon(q_\mathrm{R})^2 \times r, \\ \bar R = \dfrac{\sigma^{\bar\nu\mathrm{NC}}}{\sigma^{\bar\nu\mathrm{CC}}} = \varepsilon(q_\mathrm{L})^2 + \varepsilon(q_\mathrm{R})^2/r, \end{cases}$$

where $r = (1+2\alpha)/(3-2\alpha) = \sigma^{\bar\nu\mathrm{CC}}/\sigma^{\nu\mathrm{CC}}$.

When the corrections due to the QCD interactions of the quarks in the nucleon and to the contribution of heavy quarks are introduced, the largest uncertainties in the determination of the weak NC coupling constants are due to the distribution of strange quarks in the nucleon and to the knowledge of the mixing angle (3.2) defining the coupling of the s-quark in CC interactions [142].

Another set of equations can be used to obtain the NC coupling constants of light quarks:

$$(6.40)\quad R^\pm = \frac{\sigma^{\nu\mathrm{NC}} \pm \sigma^{\bar\nu\mathrm{NC}}}{\sigma^{\nu\mathrm{CC}} \pm \sigma^{\bar\nu\mathrm{CC}}}.$$

The quantities $R^\pm$ are less affected by the experimental cuts applied to the hadron energy in the analysis and by theoretical uncertainty (the sea contribution cancels) than are R and $\bar R$. The quantities R^+ and R^-, known as the Paschos-Wolfenstein ratios [143], are affected by a larger statistical error as compared with R for a given number of interacting protons.

In terms of the up and down coupling constants, we have

$$\begin{cases} R^+ = \varepsilon(u_L)^2 + \varepsilon(d_L)^2 + \varepsilon(u_R)^2 + \varepsilon(d_R)^2 , \\ R^- = \varepsilon(u_L)^2 + \varepsilon(d_L)^2 - \varepsilon(u_R)^2 - \varepsilon(d_R)^2 . \end{cases} \tag{6.41}$$

In the standard model, the weak angle is related to R, $\bar{R}$, $R^{\pm}$ and r according to

$$\begin{cases} R &= \frac{1}{2} - \sin^2\theta_w + \frac{5}{9}\sin^4\theta_w + \frac{5}{9}\sin^4\theta_w \times r , \\ \bar{R} &= \frac{1}{2} - \sin^2\theta_w + \frac{5}{9}\sin^4\theta_w + \frac{5}{9}\sin^4\theta_w / r , \\ R^- &= \frac{1}{2}(1 - 2\sin^2\theta_w) , \\ R^+ &= \frac{1}{2} - \sin^2\theta_w + \frac{10}{9}\sin^4\theta_w . \end{cases} \tag{6.42}$$

Experimentally the classification of the events as NC and CC has been made using different methods. In a bubble chamber experiment [144] and in the CHARM experiment [145] the identification has been done on an event-by-event basis. In the bubble chamber the muons have been tagged using counters located outside the chamber, the external muon identifier (EMI). In the CHARM detector, owing to the fine calorimeter granularity, the muons produced in a CC interaction appear as a penetrating track pointing to the shower vertex. In the CDHS [146] and the CCCFRR [147] experiments the separation of NC and CC events was made statistically on the basis of the measured length of the events in the detector. The NC events are characterized by the length of the hadronic shower, whilst the length of the CC events is given by the muon range, which in general is more penetrating than the hadronic shower.

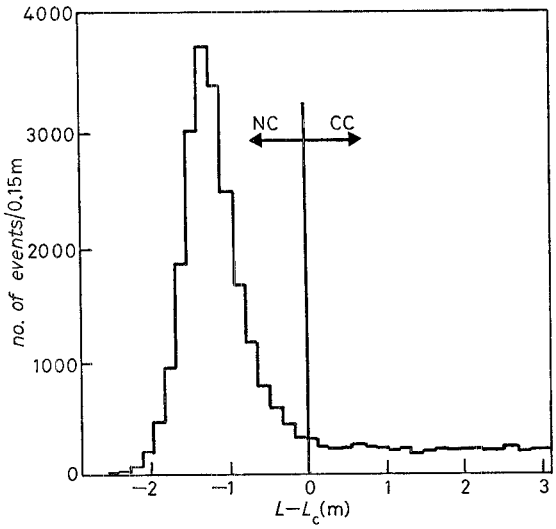

Fig. 66. – Length of neutrino events in metres of penetrated iron relative to L_c (see text) measured in the CDHS experiment [146].

In the CDHS experiment a cut length L_c, depending on the shower energy, has been introduced, so that 98% of all showers are contained within L_c. Figure 66 shows the distribution of $L - L_c$ for neutrino events.

The NC class contains the CC events for which a muon has either too low an energy or too large an angle for it to be able to penetrate longitudinally over a distance longer than L_c. In the CDHS experiment this correction is $\approx 20\%$. The misidentified CC events are always at large y. To reduce such a background in the CCCFRR experiment, a radius-dependent y cut has been applied. The measurement of the NC and CC ratio provided the most statistically significant determination of $\sin^2\theta_w$.

Table IX reports the measured values of $\sin^2\theta_w$, obtained assuming $\varrho = 1$. The table indicates the number of NC+CC events analysed, the hadron energy cuts applied, the method used, and whether first-order radiative corrections were applied. Only the experimental errors are quoted. An additional system-

TABLE IX. – *Results on the measurement of* $\sin^2\theta_w$ *in semi-leptonic neutrino interactions.*

Experiment	Events NC + CC	E_H cut (GeV)	Method	$\sin^2\theta_w$	Radiative corrections
BEBC(Ne) [144]	3178	9	R	0.182 ± 0.023	no
CHARM [145]	8864	2	R	0.220 ± 0.014	no
CDHS [146]	62400	10	R	0.226 ± 0.012	yes
CCCFRR [147]	13977	20	$R^{\pm}$	0.242 ± 0.012	yes

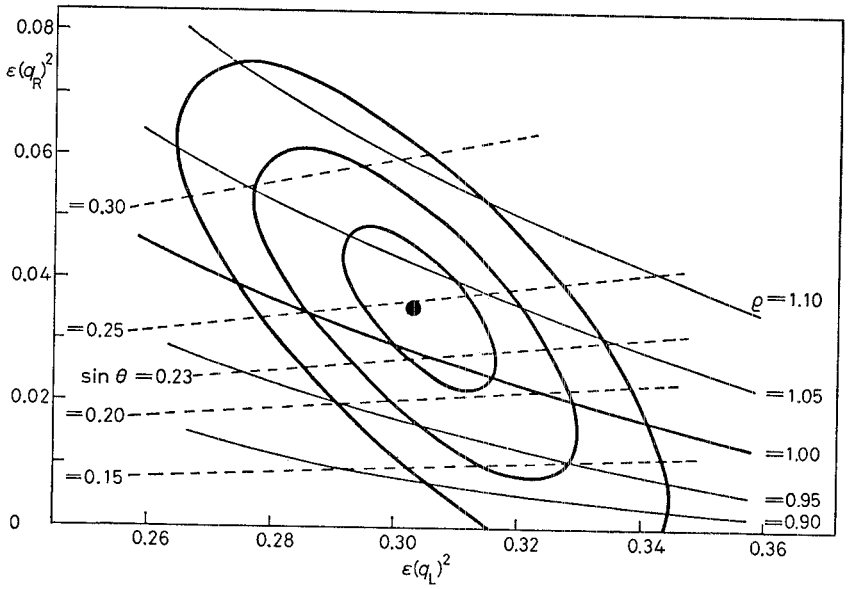

Fig. 67. – Limits on the plane $\varepsilon(q_R)^2$-$\varepsilon(q_L)^2$ obtained from the ratio of the NC and CC $\nu_\mu\mathcal{N}$ cross-sections [145]. Values of ϱ and $\sin^2\theta_w$ are also shown.

atic error of 0.009 on the value of $\sin^2\theta_w$, due the uncertainties on the model calculations, must be considered.

A two-parameter fit to the experimental data allowed a determination of $\varepsilon(q_L)^2$ and $\varepsilon(q_R)^2$. The limits obtained by the CHARM experiment [145] are shown in fig. 67. The average of the values of ϱ obtained by experiments reported in ref. [145] to [147] is

(6.43) $$\varrho = 1.01 \pm 0.01 .$$

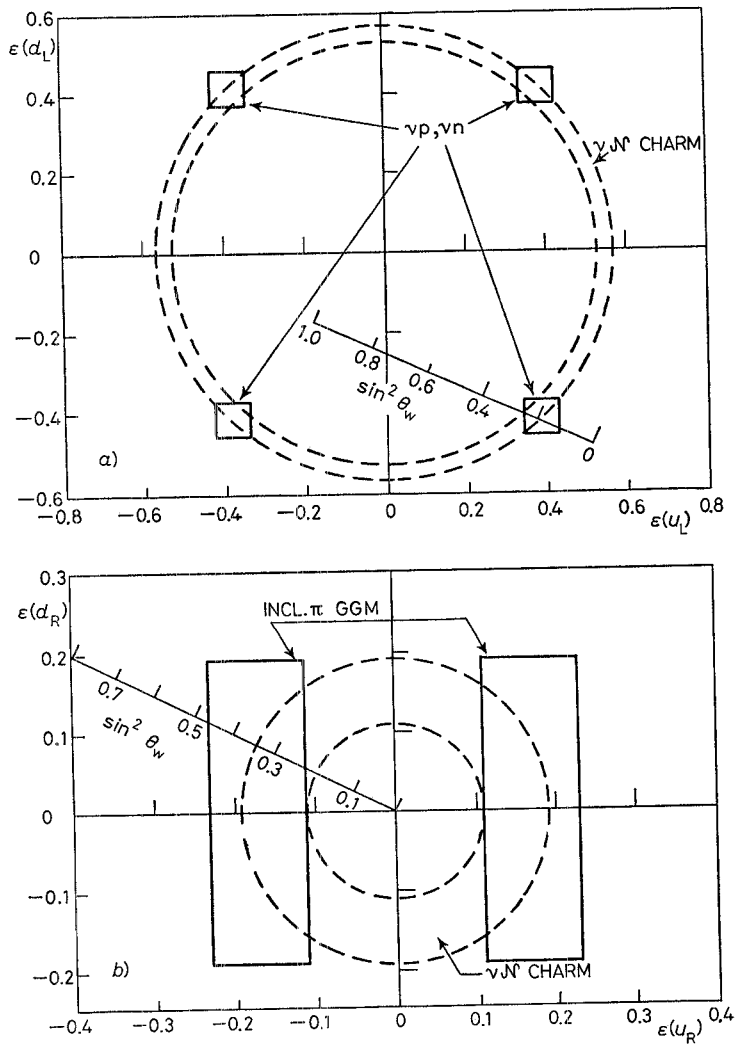

Fig. 68. – Allowed regions at 90% c.l. in the planes $\varepsilon(d_L)$-$\varepsilon(u_L)$ (a)) and $\varepsilon(d_R)$-$\varepsilon(u_R)$ (b)). The figure shows the limits from deep inelastic scattering on an isoscalar target, from deep inelastic scattering or protons and neutrons and from semi-inclusive π production.

The allowed regions in the planes $\varepsilon(u_L)$-$\varepsilon(d_L)$ and $\varepsilon(u_R)$-$\varepsilon(d_R)$, at 90 % c.l., are shown in fig. 68*a*), *b*) together with other limits obtained from measurements of neutrino interactions. Since $\varepsilon(u_R)$ and $\varepsilon(d_R)$ are small, the NCs are predominantly $V-A$. The possibility that $\varepsilon(u_R)$ and $\varepsilon(d_R)$ are both zero is ruled out.

Separate information on the couplings of u and d quarks has been obtained using a nonisoscalar target, such as a proton or a neutron target. Neglecting the sea quarks, the ratio between the number of u and d quarks is equal to 2 in the proton target and to $\frac{1}{2}$ in the neutron target.

The ratios of neutrino NC and CC cross-sections on protons (R_p) and neutrons (R_n) are

$$(6.44)\qquad \begin{cases} R_p = \dfrac{\sigma_p^{NC}}{\sigma_p^{CC}} = 2\varepsilon(u_L)^2 + \varepsilon(d_L)^2 + \frac{1}{3}[2\varepsilon(u_R)^2 + \varepsilon(d_R)^2]\,, \\ R_n = \dfrac{\sigma_n^{NC}}{\sigma_n^{CC}} = \{\varepsilon(u_L)^2 + 2\varepsilon(d_L)^2 + \frac{1}{3}[\varepsilon(u_R)^2 + 2\varepsilon(d_R)^2]\}/2\,. \end{cases}$$

The ratios $\bar{R}_p$ and $\bar{R}_n$ in the case of the antineutrino scattering are obtained by exchanging $\varepsilon(u_L)$ with $\varepsilon(u_R)$ and $\varepsilon(d_L)$ with $\varepsilon(d_R)$. For $\sin^2\theta_w = 0.25$ the standard-model expectations are $R_p = 0.42$, $R_n = 0.23$, $\bar{R}_p = 0.19$ and $\bar{R}_n = 0.09$. A measurement of R_n and $\bar{R}_n$ has been performed using deuterium as a target.

The reactions

$$(6.45)\qquad \begin{cases} \nu_\mu(\bar{\nu}_\mu)p \to \mu^-(\mu^+)X\,, & \nu_\mu(\bar{\nu}_\mu)p \to \nu(\bar{\nu})X\,, \\ \nu_\mu(\bar{\nu}_\mu)n \to \mu^-(\mu^+)X\,, & \nu_\mu(\bar{\nu}_\mu)n \to \nu(\bar{\nu})X \end{cases}$$

were measured simultaneously in BEBC [148]. The experiment was performed exposing BEBC, filled with deuterium, to the 400 GeV CERN SPS wide-band beam. The events are classified as CC if they contain at least one particle with momentum larger than 4 GeV/c identified by the EMI. Otherwise they are classified as NC. The interactions on protons are distinguished from the interactions on neutrons by measuring the charge multiplicity, excluding backward spectator protons: if it is even, the scattering is on neutrons, if it is odd, the scattering is on protons. The sample of NC candidates is contaminated by the background due to the interactions of neutrons and K_L^0 produced by neutrinos in the material in front of the chamber, and to the unidentified CC events caused by the inefficiency of the EMI. Both sources of background were strongly reduced by a cut in the total transverse momentum of the reaction products ($p_T > 1.5$ GeV/c). The corrected numbers of events attributed to the reactions (6.45) are reported in table X.

A summary of the experimental results [148-151] is reported in table XI. The limits on the chiral coupling constants of the u and d quarks, at 90 % c.l., obtained using the average of the results of the measurements of deep inelastic neutrino and antineutrino reactions on protons and neutrons are shown in fig. 68*a*).

TABLE X. – *Number of events measured in the* BEBC *experiment* [148].

Reaction	Events	Reaction	Events
$\nu p \to \mu^- X$	814 ± 41	$\bar{\nu} p \to \mu^+ X$	816 ± 33
$\nu n \to \mu^- X$	1801 ± 50	$\bar{\nu} n \to \mu^+ X$	355 ± 22
$\nu p \to \nu X$	399 ± 32	$\bar{\nu} p \to \bar{\nu} X$	211 ± 29
$\nu n \to \nu X$	458 ± 35	$\bar{\nu} n \to \bar{\nu} X$	202 ± 31

TABLE XI. – *Results on the measurement of* $R_p^{\bar{\nu}}$ *and* $R_n^{\bar{\nu}}$.

Experiment	Target	R_p^{ν}	R_n^{ν}	$R_p^{\bar{\nu}}$	$R_p^{\bar{\nu}}$
BEBC [148]	^{2}D	0.49 ± 0.05	0.25 ± 0.02	0.26 ± 0.04	0.57 ± 0.09
BEBC [149]	^{2}H	0.51 ± 0.04	—	—	—
15 feet BC [150]	^{2}D	0.49 ± 0.06	0.22 ± 0.03	—	—
BEBC [151]	^{2}H/^{2}H-Ne	0.47 ± 0.04	—	0.33 ± 0.04	—

Experiment	$\varepsilon(u_L)^2$	$\varepsilon(d_L)^2$	$\varepsilon(u_R)^2$	$\varepsilon(d_R)^2$
BEBC [148]	0.133 ± 0.030	0.192 ± 0.030	0.02 ± 0.02	0.00 ± 0.02
BEBC [149]	0.15 ± 0.04	0.19 ± 0.05	—	—
15 feet BC [150]	0.19 ± 0.06	0.13 ± 0.04	—	—
BEBC [151]	—	—	—	—

Another method of measuring the u and d couplings separately is to study the semi-inclusive NC pion production on isoscalar targets:

$$\nu_\mu(\bar{\nu}_\mu)\mathcal{N} \to \nu_\mu(\bar{\nu}_\mu)\pi^\pm X\,. \tag{6.46}$$

Indicating with D_u^+, D_u^- and D_d^+, D_d^- the probability for a u-quark and a d-quark to fragment into a π^+ or a π^-, the ratio of the π^+ and π^- produced in NC neutrino interactions is expressed in terms of the chiral coupling according to

$$(\pi^+/\pi^-)_\nu = \frac{[\varepsilon(u_L)^2 + \frac{1}{3}\varepsilon(u_R)^2]D_u^+ + [\varepsilon(d_L)^2 + \frac{1}{3}\varepsilon(d_R)^2]D_u^-}{[\varepsilon(u_L)^2 + \frac{1}{3}\varepsilon(u_R)^2]D_u^- + [\varepsilon(d_L)^2 + \frac{1}{3}\varepsilon(d_R)^2]D_u^+}\,. \tag{6.47}$$

In eq. (6.47) the strong isospin invariance ($D_d^+ = D_u^-$ and $D_d^- = D_u^+$) has been assumed. In the case of the antineutrino interaction the ratio $(\pi^+/\pi^-)_{\bar{\nu}}$ is obtained from $(\pi^+/\pi^-)_\nu$, replacing the left-handed couplings with the right-handed ones and *vice versa*. The quantities D_u^+, D_u^- and D_d^+, D_d^- can be obtained from the measurement of the semi-inclusive CC pion production reactions. In these interactions the flavour of the scattered quarks is fixed by the dynamics of the interaction. Neglecting the sea quarks and assuming $\cos\theta_C = 1$, we have

$$\nu_\mu d \to \mu^- u\,, \qquad \bar{\nu}_\mu u \to \mu^+ d\,. \tag{6.48}$$

The experimental results [152-154] are reported in table XII.

TABLE XII. – *Results obtained from the measurement of semi-inclusive pion production.*

Experiment	$(\pi^+/\pi^-)_\nu$	$(\pi^+/\pi^-)_{\bar{\nu}}$
GGM-PS [152]	0.77 ± 0.14	1.65 ± 0.33
ABCDLOS [153]	0.69 ± 0.22	1.37 ± 0.31
IFIM [154]	—	1.27 ± 0.22

Using the GGM bubble chamber data and taking into account the sea quarks, we obtain [155]

$$\begin{cases} |\varepsilon(u_R)| = 0.17 \pm 0.04 , \\ |\varepsilon(d_R)| = 0.00 \pm 0.12 . \end{cases} \tag{6.49}$$

Figure 68*b*) shows the allowed regions in the plane $\varepsilon(u_R)$-$\varepsilon(d_R)$ from the semi-inclusive pion production neutrino interactions.

Since $\varepsilon(d_R)^2 \approx 0$, all the measurements of deep inelastic reactions and of the semi-inclusive pion reactions leave us with an eightfold ambiguity on the sign of the helicity couplings:

$$\begin{cases} A: & \varepsilon(u_L) > 0 , & \varepsilon(u_R) < 0 , & \varepsilon(d_L) < 0 ; \\ B: & \varepsilon(u_L) > 0 , & \varepsilon(u_R) > 0 , & \varepsilon(d_L) < 0 ; \\ C: & \varepsilon(u_L) > 0 , & \varepsilon(u_R) < 0 , & \varepsilon(d_L) > 0 ; \\ D: & \varepsilon(u_L) > 0 , & \varepsilon(u_R) > 0 , & \varepsilon(d_L) > 0 ; \end{cases} \tag{6.50}$$

and four other solutions, A', B', C' and D', obtainable by changing the sign of the solutions A, B, C and D, respectively. The correspondence between these solutions and the values of α, β, γ and δ is

$$\begin{cases} A(A'): & \text{large } |\beta| ; \\ B(B'): & \text{large } |\alpha| ; \\ C(C'): & \text{large } |\delta| ; \\ D(D'): & \text{large } |\gamma| . \end{cases} \tag{6.51}$$

These ambiguities can be solved by making use of the experimental results obtained in exclusive neutrino reactions and studying the charged-lepton interactions.

The single-pion production in neutrino- and antineutrino-nucleon interactions via NC has been studied in two experiments performed in GGM exposed to the WBB at the CERN PS [156, 157]. The following reactions have been

measured:

$$
\begin{cases}
\nu_\mu(\bar{\nu}_\mu)\mathrm{p} \to \nu_\mu(\bar{\nu}_\mu)\mathrm{p}\pi^0, \\
\nu_\mu(\bar{\nu}_\mu)\mathrm{p} \to \nu_\mu(\bar{\nu}_\mu)\mathrm{n}\pi^+, \\
\nu_\mu(\bar{\nu}_\mu)\mathrm{n} \to \nu_\mu(\bar{\nu}_\mu)\mathrm{n}\pi^0, \\
\nu_\mu(\bar{\nu}_\mu)\mathrm{n} \to \nu_\mu(\bar{\nu}_\mu)\mathrm{p}\pi^-.
\end{cases} \tag{6.52}
$$

The shapes of the $N\pi$ invariant-mass distribution obtained in the experiments [156, 157] show mainly Δ production. This is particularly prominent in the channel $\nu p \to \nu p\pi^0$, which is less affected by distorsions due to reinteractions of the produced particles (fig. 69). The observation of a Δ resonance

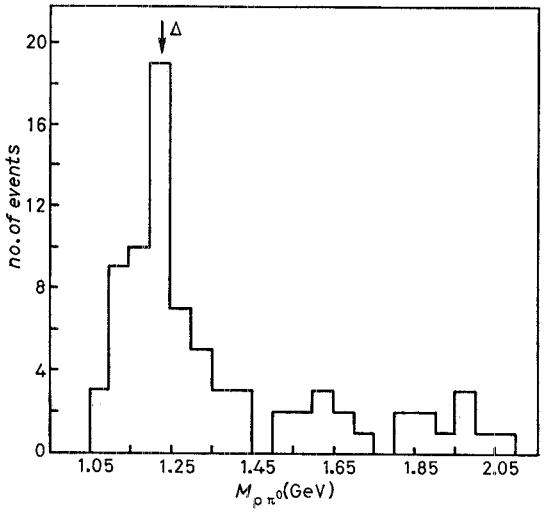

Fig. 69. – Invariant-mass distribution of the $p\pi^0$ system produced by the reaction $\nu p \to \nu p^0\pi$ measured in the GGM experiments [156] (selected sample, 80 events).

indicates qualitatively that there is a large isovector component in the hadronic NC. An analysis of the experimental data reported by FOGLI [158] obtained the following values for the couplings α, β, γ, δ:

$$
\alpha = 0.677^{+0.242}_{-0.452}, \quad \beta = 0.993^{+0.372}_{-0.452}, \quad \gamma = 0.202^{+0.077}_{-0.123}, \quad \delta = 0.007^{+0.103}_{-0.102}. \tag{6.53}
$$

These results clearly rule out solutions C and D in formulae (6.50).

The elastic scattering of neutrinos and antineutrinos on protons and neutrons,

$$
\nu_\mu(\bar{\nu}_\mu)\mathrm{p} \to \nu_\mu(\bar{\nu}_\mu)\mathrm{p}, \quad \nu_\mu(\bar{\nu}_\mu)\mathrm{n} \to \nu_\mu(\bar{\nu}_\mu)\mathrm{n}, \tag{6.54}
$$

also allows information to be obtained about the NC coupling constants. The hadronic matrix element in the case of the νp reaction is given by

$$(6.55)\qquad \langle p(K')|J_\mu^{NC}|p(K)\rangle = \\ = iu_p(K')\{\gamma_\mu G_E(Q^2) + i\sigma_{\mu\varrho}q_\varrho[G_M(Q^2) - G_E(Q^2)]/2m + \gamma_\mu\gamma_5 G_A(Q^2)\}u_p(K)\,,$$

where m is the proton mass, $q_\varrho = (K'-K)_\varrho$ is the transfer momentum, and Q^2 its square.

The form factors $G_E(Q^2)$, $G_M(Q^2)$ and $G_A(Q^2)$ at $Q^2 = 0$ have been predicted to be [159]

$$(6.56)\qquad \begin{cases} G_E(0) = \dfrac{1}{2}(\alpha + 3\gamma)\,, \\ G_M(0) = \dfrac{4.7}{2}(\alpha + 0.56\gamma)\,, \\ G_A(0) = \dfrac{1.25}{2}(\beta + \Lambda\delta)\,, \end{cases}$$

where Λ is the ratio of the isoscalar to the isovector axial-vector constants.

The experiment performed at the neutrino WBB at BNL [160] measured the reactions

$$(6.57)\qquad \nu(\bar\nu)p \to \nu(\bar\nu)p\,.$$

A fit to the differential cross-sections $d\sigma/dQ^2$ gave

$$(6.58)\qquad G_E(0) = 0.5^{+0.25}_{-0.50}\,,\quad G_M(0) = 1.0^{+0.35}_{-0.40}\,,\quad G_A(0) = 0.5^{+0.20}_{-0.15}\,.$$

The result favours solution A, which predicts $G_E(0) = 0$, $G_M(0) = 1.1$ and $G_A(0) = 0.6$, and rules out solution B, which has the following predictions: $G_E(0) = 0.55$, $G_M(0) = 2.2$ and $G_A(0) = 0.26$.

A fit to the standard model yields $\sin^2\theta_w = 0.26 \pm 0.04$. The quoted errors are only statistical. The systematic errors are estimated to be of the same order.

The experiment performed by the AP Collaboration at the CERN PS [161] measured the ratios

$$(6.59)\qquad R_p = \frac{\sigma(\nu_\mu p \to \nu_\mu p)}{\sigma(\nu_\mu n \to \mu^- p)}\,,\qquad R_n = \frac{\sigma(\nu_\mu n \to \nu_\mu n)}{\sigma(\nu_\mu n \to \mu^- p)}\,.$$

The measurement rules out the isoscalar-dominant solution C, and the isovector-dominant solution B is not favoured. The isoscalar-dominant solution D and the axial isovector-dominant solution A are in good agreement with data. The best value of $\sin^2\theta_w$ consistent with the data is $\sin^2\theta_w = 0.29 + 0.21/-0.12$.

A preliminary result on the value of $\sin^2\theta_w$, obtained from the fit of the Q^2 distribution of ≈ 3000 events induced by the reaction $\nu_\mu p \to \nu_\mu p$ (fig. 70), has recently been reported by the E734 Collaboration [162]. Assuming a value of $M_A = 1$ GeV, a value of

(6.60) $$\sin^2\theta_w = 0.26 \pm 0.04$$

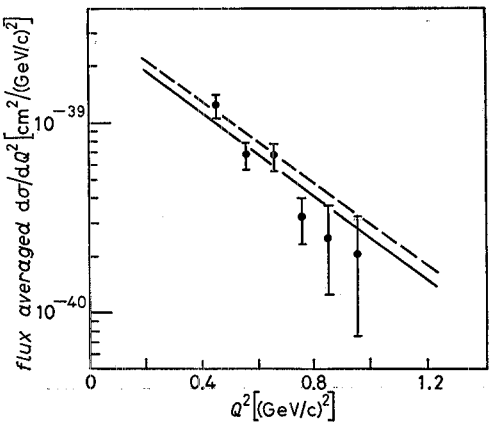

Fig. 70. – Observed Q^2 differential cross-section of the reaction $\nu p \to \nu p$; the solid line is the best fit to G_E, G_M and G_A, $M_A = 1.00$, $M_V = 0.84$: ——— $\sin^2\theta_w = 0.250$, — — — $\sin^2\theta_w = 0.200$ [162].

was obtained; M_A is the axial-vector mass that appears in the parametrization of the axial-vector form factor $F_A(Q^2) \approx (1 + Q^2/M_A^2)^{-2}$.

The reaction

(6.61) $$\bar{\nu}_e D \to \bar{\nu}_e np$$

induced by low-energy $\bar{\nu}_e$ depends only on the axial-vector term (Gamow-Teller type reaction). The measurement of the transition between the fundamental state ^3S of deuterium and its excited state ^1S allows the determination of $|\beta|$.

The measurement was performed at the 2000 MW fission reactor at the Savannah River Plant [163]. The target consisted of 268 kg of extremely pure (99.85 %) heavy water (D_2O). The detector was made of proportional counters filled with ^{3}He immersed in the D_2O. The neutrons were detected by observing the reaction $n^3He \to p^3H + 764$ keV. The entire detector was enclosed in Pb-Cd shielding and immersed in a 2200 l liquid-scintillator anticoincidence detector so as to reduce cosmic-ray and reactor background.

A cross-section of $(3.8 \pm 0.9) \cdot 10^{-45}$ cm^2 was measured, consistent with the dominant isovector solution of NC coupling ($\sigma_{exp}/\sigma_{th(A)} = 0.8 \pm 0.2$) and excluding the dominant isoscalar solution at a level of 2.5 standard deviations

$(\sigma_{exp}/\sigma_{th(B)} = 3.0 \pm 0.8)$. The experiment directly determines the isovector axial-vector coupling constant to be

$$|\beta| = 0.9 \pm 0.1 . \tag{6.62}$$

The NC coupling constants have also been determined studying the coherent production of neutral π^0 and η^0 by neutrinos (antineutrinos) on the nucleus

$$\nu_\mu(\bar{\nu}_\mu)A \to \pi^0 A \nu_\mu(\bar{\nu}_\mu) , \qquad \nu_\mu(\bar{\nu}_\mu)A \to \eta^0 A \nu_\mu(\bar{\nu}_\mu) . \tag{6.63}$$

Owing to the conserved-vector-current (CVC) hypothesis, only the axial-vector terms of the Lagrangian (6.31) contribute to reactions (6.63). The NC can be written in the form

$$J_\mu^{coh} = \beta J_\mu^{I=1} + \delta J_\mu^{I=0} , \tag{6.64}$$

where I is the isotopic spin of the current. The π^0 and the η^0 in the coherent scattering are expected at small angles with respect to the neutrino direction.

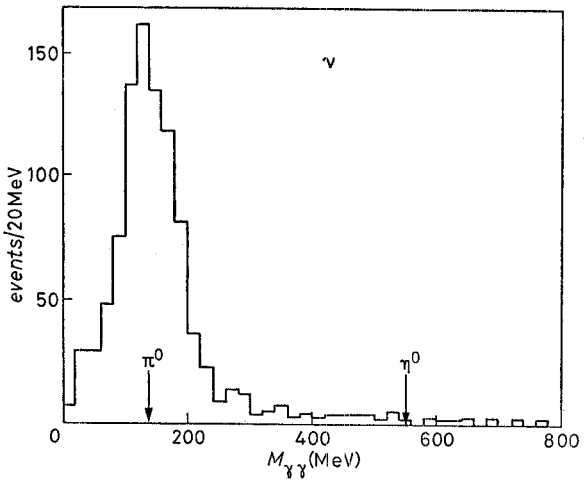

Fig. 71. – Invariant mass of forward-going 2γ events in the AP experiment [164].

Figure 71 shows the distribution of invariant mass $m_{\gamma\gamma}$ obtained in the AP spark chamber experiment [164] for the events in the forward region. The lack of η^0 and the presence of π^0 confirm that the isovector part is dominant. In fig. 72 is shown the $E\theta^2$ distributions of the ν and $\bar{\nu}$ candidate events obtained in the CHARM experiment [165]. The background is due to the reaction $\nu_\mu(\bar{\nu}_\mu)e \to \nu_\mu(\bar{\nu}_\mu)e$, to the quasi-elastic CC events induced by the ν_e and $\bar{\nu}_e$ contamination of the beams and to the NC events with high electromagnetic component. In this experiment the detection efficiency for η^0 is negligibly

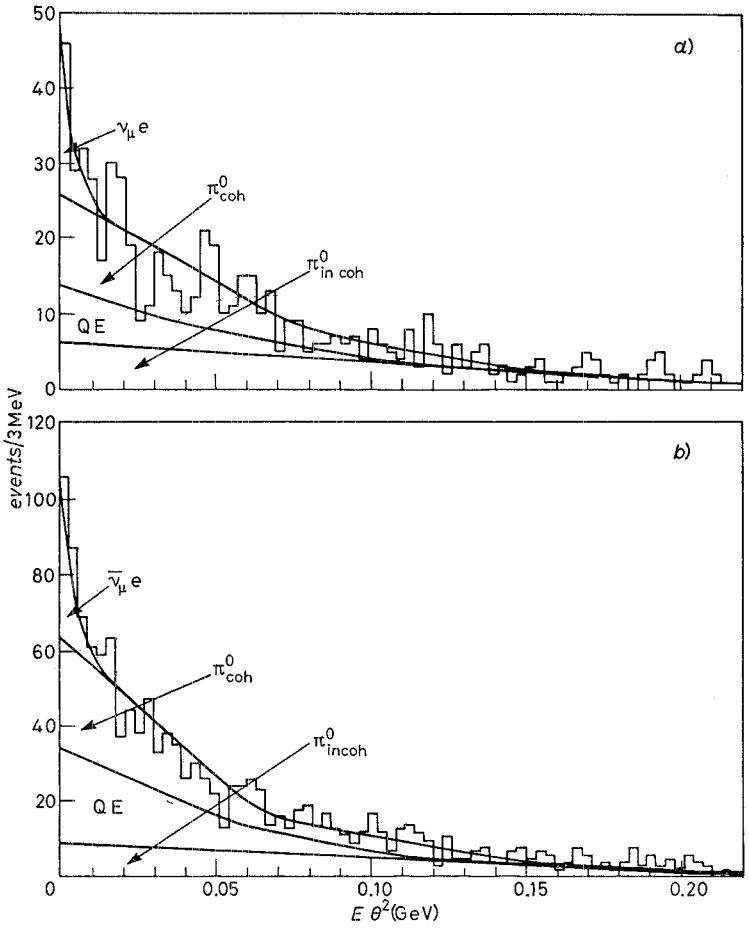

Fig. 72. – The $E\theta^2$ distribution of ν (a)) and $\bar{\nu}$ (b)) coherent π^0 candidate events observed in the CHARM experiment [165]. The background shapes are shown as curves.

small. Two signals of $223 \pm 72 \pm 53$ and $482 \pm 99 \pm 83$ events due to the π^0 coherent production reaction were obtained in the neutrino and antineutrino exposures, respectively. A comparison with the standard-model predictions [166] gave a value of

$$|\beta| = 1.08 \pm 0.24 \,. \tag{6.65}$$

All the experimental results described until now are compatible with solutions A and A' (large $|\beta|$). As we shall see, the distinction between the two solutions can be obtained from the measurements of the interference of the electromagnetic and weak interactions in charged lepton-hadron interactions.

The BEBC Collaboration, using solution A, which is the one predicted by

TABLE XIII. – *Experimental values of the light-quark chiral coupling constants.*

$\varepsilon(u_L)$	0.344 ± 0.026	α	0.533 ± 0.037
$\varepsilon(d_L)$	-0.419 ± 0.022	β	0.992 ± 0.037
$\varepsilon(u_R)$	-0.153 ± 0.022	γ	-0.152 ± 0.089
$\varepsilon(d_R)$	0.076 ± 0.041	δ	0.002 ± 0.049

the standard model, has made a recent fit to all ν and $\bar{\nu}$ data available in 1983, except those from elastic scattering [167]. The resulting values for the coupling constants are shown in table XIII. Figure 73 shows the allowed limits at 90% c.l. on the planes $[\varepsilon(u_L)$-$\varepsilon(d_L)]$, $[\varepsilon(u_R)$-$\varepsilon(d_R)]$, $[\alpha$-$\beta]$ and $[\gamma$-$\delta]$. In the figure the expectations of the standard model are shown.

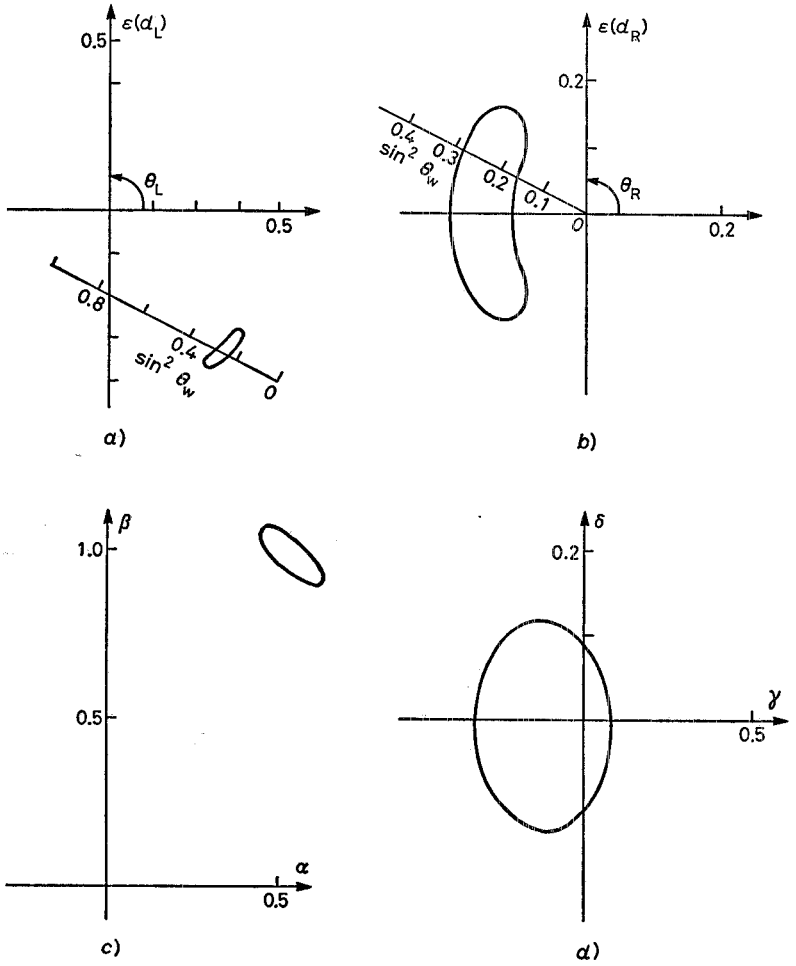

Fig. 73. – Global fit the to $\nu\mathcal{N}$ experiment (except elastic) for the chiral coupling constants. The contours correspond to a 90% c.l. limit.

6·3.2.2. Coupling constants of heavy quarks. – An attempt to extract the NC strange coupling from the global fit of the y distributions of CC and NC neutrino events on nuclei was carried out by the CHARM Collaboration [122].

Within the context of the quark-parton model and under the assumption that the weak currents contain only V and A terms, the differential cross-sections for deep inelastic scattering can be written as

$$
\left\{
\begin{aligned}
&\frac{\mathrm{d}\sigma^{\nu}}{\mathrm{d}y}(\mathrm{CC}) = B[(1-\alpha^{\nu}) + \alpha^{\nu}(1-y)^2]\,,\\
&\frac{\mathrm{d}\sigma^{\bar\nu}}{\mathrm{d}y}(\mathrm{CC}) = B[\alpha^{\bar\nu} + (1-\alpha^{\bar\nu})(1-y)^2]\,,\\
&\frac{\mathrm{d}\sigma^{\nu,\bar\nu}}{\mathrm{d}y}(\mathrm{NC}) = B\{[\varepsilon(u_{\mathrm{L(R)}})^2 + \varepsilon(d_{\mathrm{L(R)}})^2][(1-\alpha^{\bar\nu}) + \alpha^{\nu}(1-y)^2] +\\
&+[\varepsilon(u_{\mathrm{R(L)}})^2+\varepsilon(d_{\mathrm{R(L)}})^2][\alpha^{\nu}+(1-\alpha^{\bar\nu})(1-y)^2]+g_{\mathrm{S}}^2(\alpha^{\bar\nu}-\alpha^{\nu})[1+(1-y)^2]\},
\end{aligned}
\right. \tag{6.66}
$$

where B is a normalization constant. The quark structure of the nucleon is described by α^{ν} and $\alpha^{\bar\nu}$; for example, α^{ν} is the fractional momentum-weighted nonstrange quark content, and $\alpha^{\bar\nu} - \alpha^{\nu}$ is the fractional momentum-weighted strange quark-antiquark content. The quantity g_{S}^2 is defined by $g_{\mathrm{S}}^2 = \varepsilon(s_{\mathrm{L}})^2 + \varepsilon(s_{\mathrm{R}})^2$.

A fit of eqs. (6.66) to the measured y distributions (fig. 58) yields

$$
\frac{\varepsilon(s_{\mathrm{L}})^2 + \varepsilon(s_{\mathrm{R}})^2}{\varepsilon(d_{\mathrm{L}})^2 + \varepsilon(d_{\mathrm{R}})^2} = 1.39 \pm 0.43\,, \tag{6.67}
$$

in agreement with the universality predicted by the standard model for quarks of the same charge and different flavours.

The CDHS Collaboration has derived the NC charm-quark couplings from the study of the mass distribution of the neutrino events with two muons in the final state [168]:

$$
\nu_{\mu}(\bar\nu_{\mu})\,\mathcal{N} \to \mu^{+}\mu^{-}\mathrm{X}\,. \tag{6.68}
$$

The CDHS detector was exposed to the neutrino WBBs produced by 350 GeV and 400 GeV protons from the CERN SPS. Dimuon events were selected and the momenta of both muon tracks were measured by their curvature in the toroidal iron magnets of the calorimeter.

Figure 74 shows the invariant-mass spectrum of opposite-sign dimuon events with $E_{\mathrm{had}} < 10$ GeV. The distribution shows a peak centred at 3.26 GeV containing (45 ± 13) events. These events were attributed to diffractive J/ψ production via NC interactions.

Normalizing to the CC events, the following cross-section was obtained:

$$
\sigma(\nu\mathcal{N} \to \nu\psi\mathcal{N}) = (4.2 \pm 1.5)\cdot 10^{-41}\ \mathrm{cm}^2 \text{ per nucleon}\,, \tag{6.69}
$$

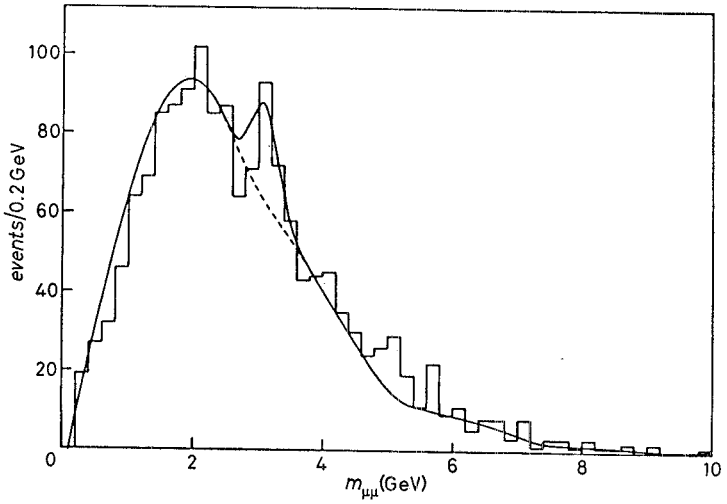

Fig. 74. – The mass spectrum of the neutrino-induced opposite-sign dimuon events as measured in the CDHS experiment [168].

in agreement with the predictions of the gluon fusion model. Comparing the neutrino-induced with the muon-induced dimuon events (in the J/ψ mass region) [169], and assuming the photon-gluon fusion mechanism for the muon-induced events, the following NC charm coupling is deduced from the experimental data:

$$\frac{\varepsilon(c_L^2)+\varepsilon(c_R^2)}{\varepsilon(u_L^2)+\varepsilon(u_R^2)} = 2.1 \pm 0.8 \,. \tag{6.70}$$

This result, within large errors, is also in agreement with the fermion weak universality.

6·3.3. Charged lepton-quark interactions. The interference between electromagnetic and weak interactions has been determined studying the interactions of charged leptons with quarks.

The scattering of charged leptons with matter is described in the first order of the theory by the graphs shown in fig. 75.

The order of magnitude of the electroweak interference for $Q^2 \ll m_{Z^0}^2$ is given with good approximation by

$$A_{e.m.} \times A_w / |A_{e.m.}|^2 = A_w / A_{e.m.} \approx GQ^2/e^2 \approx 137 \cdot 10^{-5} Q^2/4\pi \approx 10^{-4} Q^2 \,, \tag{6.71}$$

where $A_{e.m.}$ and A_w are the amplitudes of the electromagnetic and weak interactions, respectively, and Q (in GeV) is the transfer momentum involved in the reaction. The interactions of electrons with quarks have been studied at Q

values equal to 10^{-6} GeV (atomic physics) and around 1 GeV (scattering of polarized electrons on deuterium). At these Q values the electromagnetic interaction, which is parity-conserving, dominates. However, the tiny parity-violating effects (eqs. (6.71)) due to the interference between electromagnetic and weak interactions can be detected studying the dependence of measurable quantities on pseudoscalar variables, such as the dependence of the electron-hadron cross-section on the polarization state of the electron and the measurement of the light polarization in atomic transitions.

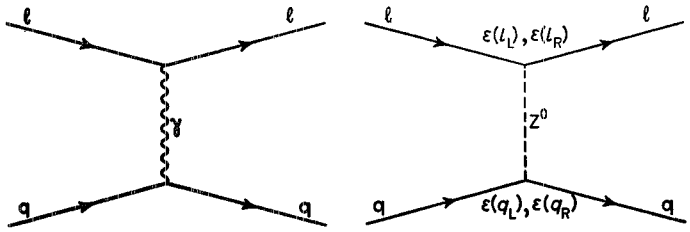

Fig. 75. – First-order diagrams for lepton production via γ and Z^0 in lepton-quark interactions.

The interference between electromagnetic and weak interactions has been studied also in the scattering of polarized muons on carbon at an average Q value around 20 GeV.

The weak effective Lagrangian describing the interactions of charged leptons ℓ with quarks q is

$$L^{(\ell q)} = (G/\sqrt{2})[\varepsilon(\ell_R)\bar{\ell}_R\gamma_\mu\ell_R + \varepsilon(\ell_L)\bar{\ell}_L\gamma_\mu\ell_L][\varepsilon(q_R)\bar{q}_R\gamma_\mu q_R + \varepsilon(q_L)\bar{q}_L\gamma_\mu q_L]\,. \tag{6.72}$$

The measurement of the electroweak interference makes it possible to determine the sign of the NC coupling of the light quarks (u and d) once the lepton couplings have been obtained from other measurements.

6˙3.3.1. Electron-quark interactions. – The scattering of longitudinally polarized electrons on unpolarized deuterium,

$$e_{L,R}D \to eX\,, \tag{6.73}$$

was studied in a celebrated SLAC experiment [170] at a value of the momentum transfer around 1 GeV/c^2 with an expected electroweak interference of $\approx 10^{-4}$ (eq. (6.71)).

The cross-section asymmetry is given by

$$A = \frac{\sigma_R - \sigma_L}{\sigma_R + \sigma_L}\,. \tag{6.74}$$

In eqs. (6.73) and (6.74) the symbols R and L indicate the helicity of the incoming electrons. As shown in fig. 76, the cross-section for left-handed and right-handed electrons is obtained as a sum of two terms with a y dependence ($y = E_X/E_e$) fixed by the conservation of the angular momentum. In the figure the weak amplitudes (A_w) depend on the chiral couplings according to

$$(6.75)\qquad \begin{cases} A_w^{(e_R)}(J=1) \approx \varepsilon(e_R)\,\varepsilon(u\,[d]_L)\,, \\ A_w^{(e_R)}(J=0) \approx \varepsilon(e_R)\,\varepsilon(u\,[d]_R)\,, \\ A_w^{(e_L)}(J=1) \approx \varepsilon(e_L)\,\varepsilon(u\,[d]_R)\,, \\ A_w^{(e_L)}(J=0) \approx \varepsilon(e_L)\,\varepsilon(u\,[d]_L)\,. \end{cases}$$

The sea-quark contributions are neglected.

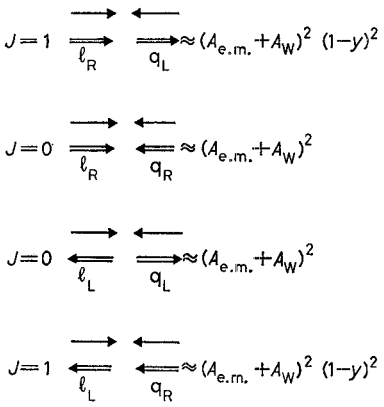

Fig. 76. – Helicity diagrams for ℓq reactions.

Using the fact that the deuterium has an equal number of quarks up and down (isoscalar target) and neglecting terms proportional to $1/m_Z^4$, the asymmetry A is given by the following parity-violating expression:

$$(6.76)\qquad A = Q^2\{a_1 + a_2[1-(1-y)^2]/[1+(1-y)^2]\}\,,$$

where $a_1 = B[\varepsilon(e_L) - \varepsilon(e_R)][\varepsilon(q_L) + \varepsilon(q_R)]$ and $a_2 = B[\varepsilon(e_L) + \varepsilon(e_R)][\varepsilon(q_L) - \varepsilon(q_R)]$, with $B = \frac{6}{5}\,G/\sqrt{2}\pi\alpha = 5.3\cdot10^{-4}$ (for Q^2 in $(\mathrm{GeV})^2$), and $\varepsilon(q_L) = \varepsilon(u_L) - \varepsilon(d_L)/2$ and $\varepsilon(q_R) = \varepsilon(u_R) - \varepsilon(d_R)/2$. In the standard model one has

$$(6.77)\qquad a_1 = B\left(-\frac{3}{8} + \frac{5}{6}\sin^2\theta_w\right), \qquad a_2 = B\left(-\frac{3}{8} + \frac{3}{2}\sin^2\theta_w\right).$$

By studying A as a function of y and Q^2 it is possible to determine a_1 and a_2.

Corrections to the asymmetry value, due to the scaling violation and to the sea-quark contribution, are small.

In the SLAC experiment [170] the target consisted of a 30 cm cell of liquid deuterium. The scattered electrons were observed at 4° using a single-arm spectrometer consisting of a Čerenkov counter filled with nitrogen and operating at atmospheric pressure and a lead-glass total-absorption shower counter. The average polarization of the incoming electrons was $P_e = 0.37$. The polarization was randomly reversed on a pulse-to-pulse basis to minimize systematic effects due to periodic changes in experimental parameters. The explored kinematic region for the inelastic scattering of electrons on deuterium was $0.9\ (\mathrm{GeV/c})^2 < Q^2 < 2\ (\mathrm{GeV/c})^2$ and $0.15 < y < 0.36$.

The measured asymmetry A_{exp} is related to the asymmetry A (eq. (6.74)) and to the beam polarization P_e according to $A_{exp} = P_e A$.

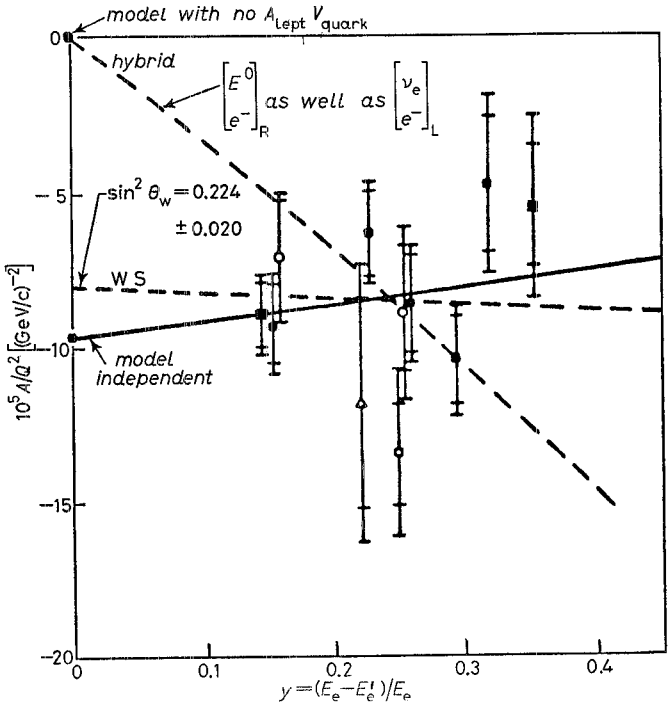

Fig. 77. – Asymmetry measurements in the $e_{L,R}D$ scattering as a function of y [170]. The data are compared with the predictions of different models [159]: ▪ $E_e = 19.4$ GeV, ▵ $E_e = 16.2$ GeV, ○ $E_e = 22.2$ GeV.

The results of 11 measurements are reported in fig. 77, where the ratio A/Q^2 is plotted *vs.* the kinematic variable $y = (E_e - E'_e)/E_e$ (E_e = energy of the incoming electron, E'_e = energy of the outgoing electron). The errors come mainly from statistics.

A two-parameter fit gave

$$a_1 = (-9.7 \pm 2.6)\cdot 10^{-5}\,(\mathrm{GeV})^{-2}, \qquad a_2 = (4.9 \pm 8.1)\cdot 10^{-5}\,(\mathrm{GeV})^{-2}. \tag{6.78}$$

The possibility of a right-handed electron forming a doublet with a heavy neutral lepton E^0 symmetrically with the usual left-handed doublet would lead to $a_1 = 0$ and is, therefore, excluded in a model-independent way by this result. The fit of the experimental data to the standard model (6.77) gives

$$\sin^2\theta_w = 0.224 \pm 0.020\,. \tag{6.79}$$

Owing to the intrinsic uncertainties in the quark-parton model the indetermination with respect to the value of $\sin^2\theta_w$ is ± 0.01.

The results obtained from the measurement of the scattering of polarized electrons on deuterium and from the measurement of g_V^e and g_A^e in the elastic scattering of neutrinos and antineutrinos on electrons select solution A of eq. (6.50). Using the results (6.24), solution A predicts $a_1 = -10.4\cdot 10^{-5}\,(\mathrm{GeV})^2$ in agreement with experimental results, whilst solution A' predicts $a_1 = +10.4\cdot 10^{-5}\,(\mathrm{GeV})^2$, which is completely ruled out by the experiment.

The interference between weak and electromagnetic interactions was also studied in atomic physics by measuring parity-violating transitions in heavy atoms. In terms of the vector and axial-vector coupling constants, the weak Lagrangian (eqs. (6.72)) can be written in the form

$$L^{(\mathrm{eq})} = (G/\sqrt{2})\,\{[\bar{e}(g_V^e + g_A^e\gamma_5)\,e][\bar{u}(g_V^u + g_A^u\gamma_5)\,u + \bar{d}(g_V^d + g_A^d\gamma_5)\,d]\,. \tag{6.80}$$

For heavy atoms (since the spins of the nucleon constituents in the nucleus tend to cancel) the term $g_V^e g_A^q$ (q = u, d) in eq. (6.80) is negligible with respect $g_A^e g_V^q$. The parity-violating potential is then proportional to the « weak charge » Q_w defined by

$$Q_w^{(Z,N)} = -2g_A^e[g_V^u(2Z + N) + g_V^d(2N + Z)]\,, \tag{6.81}$$

where N and Z are the numbers of neutrons and protons in the nucleus, respectively. Since $N \approx Z$ the « weak charge » is proportional to Z.

The presence of parity-violating interactions implies that the atomic levels are not pure eigenstates of parity. As a result, a dominant transition (for example $M1$) can mix with an opposite-parity transition with a coupling proportional to

$$\langle k|H_{pv}|i\rangle/(E_i - E_k)\,, \tag{6.82}$$

where $|i\rangle$ is the dominant-parity state, $|k\rangle$ is the opposite-parity state due to

the parity-violating potential, and $E_i - E_k$ is the difference between the energies of the two levels.

Since Q is of the order of $1/R_{\text{atom}} \approx m_e/137$, the parity-violating effects in atomic physics are of the order of 10^{-15}. Such effects are too small to be detected. The parity-violating effects can be enhanced in three ways: *a*) since the potential H_{pv} is proportional to Z^3 [171], by using heavy atoms such as bismuth or cesium ($Z^3 \approx 10^5$); *b*) by studying a suppressed-parity-conserving transition; and *c*) by overlapping a pair of levels of opposite parity using an external magnetic field to adjust the hyperfine splitting. The mixing coefficient (6.82) is in fact proportional to the inverse of the difference between the energies of the states.

Parity-violating effects are proportional to the quantity $X^{pv} = \text{Im}\,(E1^{pv})/M1$, where $E1^{pv}$ and $M1$ are the parity-violating electric-dipole amplitude and the parity-conserving magnetic-dipole amplitude, respectively. In allowed magnetic-dipole transitions, $X^{pv} \sim 10^{-7}$ for Tl, Pb and Bi, and $\sim 10^{-8}$ for Cs. The main experimental problem in the measurement of such transitions is represented by systematic effects. In forbidden magnetic transitions, $X^{pv} \sim 10^{-4}$ for Cs and 10^{-3} for Tl. In the study of these transitions the systematic errors are suppressed, but the statistics are very low.

Parity-violating interactions in atoms have been investigated, measuring the rotation of the polarization plane of a laser light ($\Delta\varphi$) and the asymmetry in the absorption cross-section of right and left circularly polarized laser beams,

$$A' = \frac{\sigma_{RC} - \sigma_{LC}}{\sigma_{RC} + \sigma_{LC}}. \tag{6.83}$$

The physical origin of $\Delta\varphi$ is the difference between the refractive indices of right and left circularly polarized light. The rotation angle follows a sharp dispersionlike dependence on the light frequency around the resonant value. This behaviour is essential to the discrimination of the signal from the background. As pointed out by KRIPLOVICH [172], the effect can be measured by studying allowed magnetic transitions. The measurement of $\Delta\varphi$ was performed in bismuth [173-175] and lead [176] (the electroweak interference effects were enhanced by using method *a*) above).

The asymmetry A was studied by measuring forbidden magnetic transitions in thallium [177, 178] and in cesium [179, 180]. In these experiments the electroweak interference effects were enhanced by using methods *a*) and *b*). To reduce the isotropic background due to molecular and collisional effects, the experiments have been performed in an external static electric field. The experiment reported in ref. [177] measured $\text{Im}\,(E1^{pv})/M1$. In the other three experiments the measured quantity was $\text{Im}\,(E1^{pv})/\beta$, where β is the vector polarizability of the element which is caused by the external electric field.

The experimental results are reported in table XIV together with the atomic

TABLE XIV. – *Results on parity violation in atoms.*

Optical rotation				
Experiment	Element	λ (nm)	$10^8\,\mathrm{Im}(E1^{pv})/M1$	Theory
Novosibirsk [173]	bismuth	648	-20.2 ± 2.7	
Oxford [174]	bismuth	648	-9.3 ± 1.5	-13 ± 3
Moscow [174]	bismuth	648	-7.8 ± 1.8	
Seattle [175]	bismuth	876	-10.4 ± 1.7	-10 ± 2.5
Seattle [176]	lead	1280	-9.9 ± 2.5	-13 ± 2

Forbidden magnetic transitions			
Experiment	Element	Im $(E1^{pv})/\beta$ (mV/cm)	Theory
Berkeley (1981) [177]	thallium	$-1.80 + 0.65/-0.60$	-1.2 ± 0.3
Berkeley (1984) [178]	thallium	-1.73 ± 0.33	
Paris (1982) [179]	cesium	-1.34 ± 0.33	-1.6 ± 0.2
Paris (1984) [180]	cesium	-1.78 ± 0.38	

transition studied and the theoretical predictions, whose uncertainties are of the order of $(25 \div 30)\,\%$ [174]. A value of Im $(E1^{pv})/M1$ is also reported for the Berkeley experiment [177]. The value was derived using β from ref. [181].

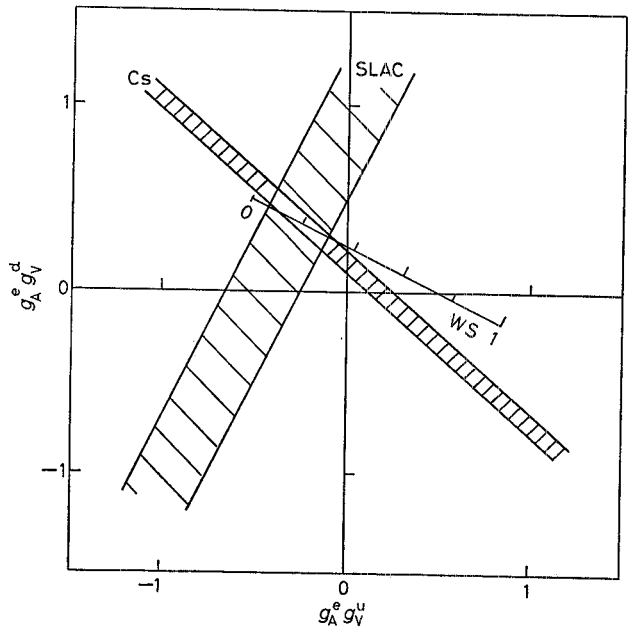

Fig. 78. – Regions of $g_A^e g_V^d$ and $g_A^e g_V^u$ allowed at 90% c.l. by the cesium [179, 180] and the $e_{L,R}D$ [170] (SLAC) experiments. The standard-model predictions (WS) are shown.

The allowed regions at 90 % c.l. in the plane $g_A^e g_V^u - g_A^e g_V^d$ from the cesium [179, 180] and the $e_{R,L}$ deuterium scattering experiments [170] are shown in fig. 78. The value of $\sin^2\theta_w$ obtained from the cesium experiment is

$$\sin^2\theta_w = 0.205 \pm 0.035 \pm 0.025 . \tag{6.84}$$

The systematic error due to the atomic-physics uncertainties is ± 0.045.

Information on both the vector and the axial-vector coupling constants of u and d quarks, free from theoretical uncertainties, can be obtained by making very difficult experiments in hydrogen and deuterium [182]. In such experiments the parity violation effect is enhanced by using method *c*).

6·3.3.2. Muon-quark interactions. – The electroweak interference has been experimentally proved also in the deep inelastic scattering of longitudinally polarized muons on carbon nuclei,

$$\mu^{\pm}C \to \mu^{\pm}X . \tag{6.85}$$

The high-energy, high-intensity CERN SPS muon beam allows the exploration of the effects at momentum transfers Q^2 ranging from 15 to 100 $(\mathrm{GeV})^2$, the muon energy being 120 and 200 GeV.

The cross-section for the reaction depends on the charge and on the polarization λ of the incoming muon.

The BCDMS Collaboration measured the cross-section asymmetry in the scattering of positive and negative muons, with left and right polarization, on carbon nuclei [183],

$$B = \frac{\sigma_L^+ - \sigma_R^-}{\sigma_L^+ + \sigma_R^-}, \tag{6.86}$$

where the indices $+$, $-$ and R, L indicate the charge and the longitudinal polarization of the muons.

The σ_L^+ and σ_R^- are obtained, as in the case of the polarized-electron scattering, by the sum of two terms with a fixed y distribution ($\mathrm{d}\sigma/\mathrm{d}y \approx 1$ and $\mathrm{d}\sigma/\mathrm{d}y \approx (1-y)^2$).

For a given initial angular momentum, the weak amplitudes are related to the NC chiral coupling constants according to

$$\begin{cases} A_w^{(\mu_L^+)}(J=1) \approx \varepsilon(\mu_R)\,\varepsilon(u, [d]_R) , \\ A_w^{(\mu_L^+)}(J=0) \approx \varepsilon(\mu_R)\,\varepsilon(u, [d]_L) , \\ A_w^{(\mu_R^-)}(J=1) \approx \varepsilon(\mu_R)\,\varepsilon(u, [d]_L) , \\ A_w^{(\mu_R^-)}(J=0) \approx \varepsilon(\mu_R)\,\varepsilon(u, [d]_R) . \end{cases} \tag{6.87}$$

If we neglect the terms proportional to $1/m_Z^4$, the asymmetry B is given by

$$B = -Q^2 a \{[1-(1-y)^2]/[1+(1-y)^2]\}\, \varepsilon(\mu_R) \cdot \cdot \{\varepsilon(d_R) - \varepsilon(d_L) - 2[\varepsilon(u_R) - \varepsilon(u_L)]\}, \tag{6.88}$$

where $a = 6G/\pi\alpha\sqrt{2} = 2.15 \cdot 10^{-4}\ (\mathrm{GeV})^{-2}$. Equation (6.88) shows that B is almost parity-conserving, since the quark term is axial-vector and the dominant part of the μ term is also axial-vector.

The charge asymmetry is affected by higher-order electromagnetic contributions. They compensate part of the electroweak effect and are predominantly due to interference between one- and two-photon exchange and between lepton and hadron bremsstrahlung.

In fig. 79 the measured B values corrected for higher-order electromagnetic and electroweak effects are shown as a function of

$$g(y)\,Q^2 = Q^2[1-(1-y)^2]/[1+(1-y)^2]\,. \tag{6.89}$$

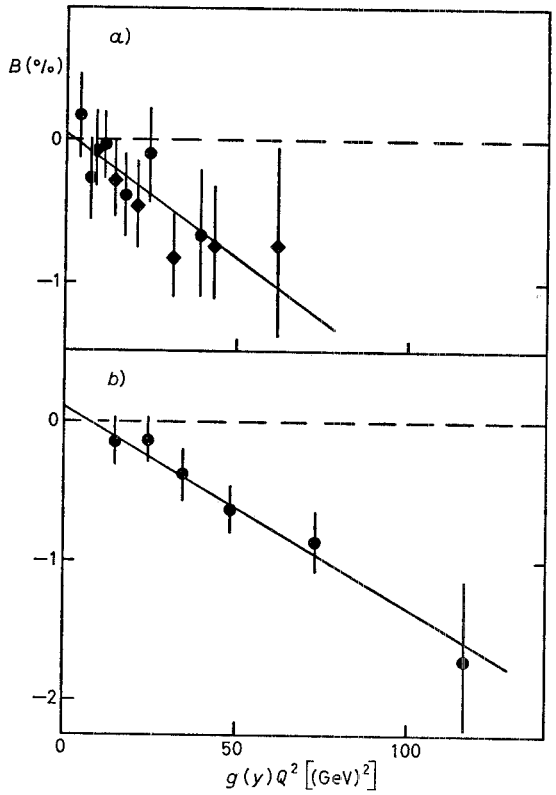

Fig. 79. – The measured B asymmetries after radiative corrections at *a*) 120 and *b*) 200 GeV μ beam energies. The points represent 120 GeV data with $Q^2 > 15$ GeV. Solid lines are straight-line fits.

Straight-line fits to the two data samples ($B = a + bg(y)Q^2$) give

$$
\begin{cases}
E_\mu = 200 \text{ GeV}: & \\
\qquad a = (0.15 \pm 0.15)\cdot 10^{-2}, & \\
\qquad b = (-0.147 \pm 0.037)\cdot 10^{-3} \text{ (GeV)}^{-2}; & \\
E_\mu = 120 \text{ GeV}: & \\
\qquad a = (0.06 \pm 0.17)\cdot 10^{-2}, & \\
\qquad b = (-0.174 \pm 0.075)\cdot 10^{-3} \text{ (GeV)}^{-2}; &
\end{cases} \tag{6.90}
$$

where only statistical errors are quoted. The estimated systematic errors on b are $\Delta b = 0.02\cdot 10^{-3}$ (GeV)$^{-2}$ (200 GeV) and $\Delta b = 0.03\cdot 10^{-3}$ (GeV)$^{-2}$ (120 GeV).

The mixing angle of the standard model derived from the measured slope b is

$$
\sin^2\theta_w = 0.23 \pm 0.07 \text{ (stat.)} \pm 0.04 \text{ (syst.)}. \tag{6.91}
$$

If we took into account the sea quarks, $\sin^2\theta_w$ would increase by 0.01. The sensitivity is not large, since the axial term dominates. Assuming $\sin^2\theta_w = 0.23$, the following value of the weak coupling of a right-handed muon was obtained:

$$
I_R^3(\mu) = 0.00 \pm 0.06 \text{ (stat.)} \pm 0.06 \text{ (syst.)}. \tag{6.92}
$$

This result rules out the existence of a neutral right-handed lepton M^0 associated with a muon in a right-handed isospin doublet.

Using the results obtained in the PETRA experiments, ARGENTO *et al.* [183] found a value of

$$
g_V^\mu = -0.12 \pm 0.14 \text{ (stat.)} \pm 0.08 \text{ (syst.)}, \tag{6.93}
$$

corresponding to $\sin^2\theta_w = 0.19 \pm 0.07$ (stat.) ± 0.04 (syst.).

6·3.4. Electroweak interference in e^+e^- interactions. The interference between electromagnetic and weak interactions has been investigated at the e^+e^- rings PETRA (DESY) and PEP (SLAC) at high values of the momentum transfer ($Q^2 \approx 1000$ (GeV)^2). The following reactions have been studied:

$$
\begin{cases}
e^+e^- \to e^+e^-, & \\
e^+e^- \to \mu^+\mu^-, & \\
e^+e^- \to \tau^+\tau^-, &
\end{cases} \tag{6.94}
$$

$$
\begin{cases}
e^+e^- \to c\bar{c}, & \\
e^+e^- \to b\bar{b}. &
\end{cases} \tag{6.95}
$$

The weak NC effective Lagrangian describing interactions (6.86) and (6.87) is given by

$$(6.96) \qquad L^{(e^+e^-\to f\bar{f})} = (G/\sqrt{2})\,[\varepsilon(e_L)\bar{e}_L\gamma_\mu e_L + \varepsilon(e_R)\bar{e}_R\gamma_\mu e_R][\varepsilon(f_L)\bar{f}_L\gamma_\mu f_L + \varepsilon(f_R)\bar{f}_R\gamma_\mu f_R]\,,$$

where f=e, μ, τ, c and b.

The constants $\varepsilon(f_L)$ and $\varepsilon(f_R)$ have been measured by studying the magnitude and the energy dependence of the cross-section of reactions (6.94) and the forward-backward asymmetry in the angular distribution of the final fermions produced in reactions (6.94) and (6.95).

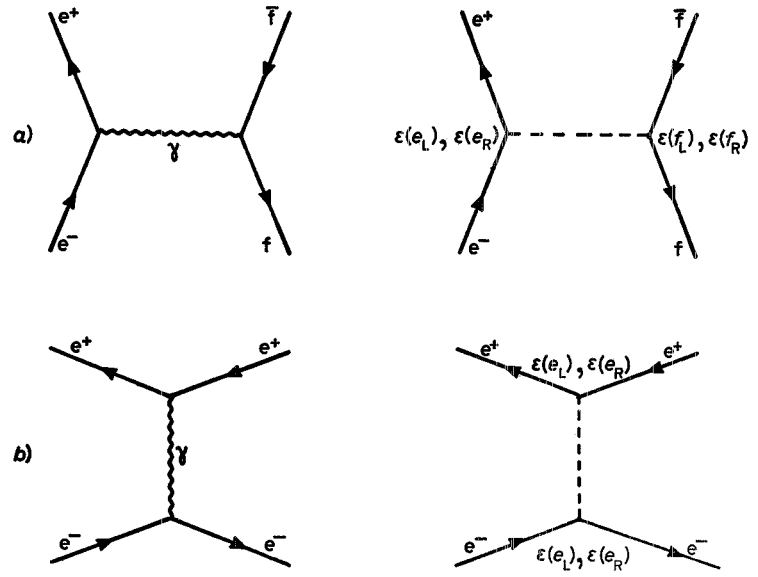

Fig. 80. – First-order diagrams for fermion production in e^+e^- interactions via γ and Z^0 exchange: *a*) *s*-channel, *b*) *t*-channel.

In the lowest order of the theory, the reaction $e^+e^- \to f\bar{f}$ is described by the sum of the electromagnetic and weak amplitudes (fig. 80*a*)). If f = e, the *t*-channels (fig. 80*b*)) must also be taken into account. Using eq. (6.71), the effects induced by the interference between the electromagnetic and weak interactions, at PETRA and PEP energies, are expected to be $\approx 10\,\%$. The angular distribution of the fermion-antifermion pair in the e^+e^- annihilation can be obtained from the angular-momentum conservation (fig. 81). Here θ is the angle between the fermion in the final state and the electron. The differential cross-section is then proportional to

$$(6.97) \qquad \frac{\mathrm{d}\sigma}{\mathrm{d}\cos\theta} = a(1+\cos\theta)^2 + b(1-\cos\theta)^2\,.$$

For $a = b$, corresponding to the case in which only the electromagnetic interaction contributes, or $g_A = 0$,

$$\frac{d\sigma}{d\cos\theta} \approx 1 + \cos^2\theta \,. \tag{6.98}$$

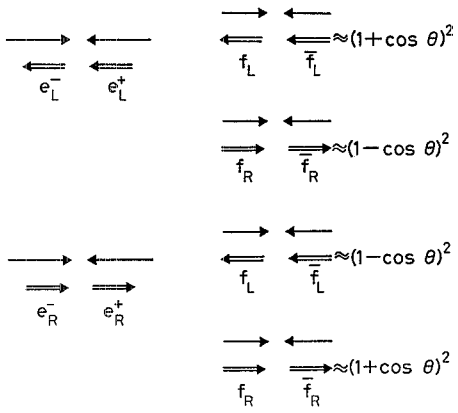

Fig. 81. – Helicity diagrams for the $e^+e^- \to f\bar{f}$ reactions.

Neglecting the square of the contribution of the Z^0 exchange, we get

$$\frac{d\sigma}{d\cos\theta} = \frac{\alpha^2}{4s}\,[c_1(1 + \cos\theta^2) + c_2\cos\theta]\,, \tag{6.99}$$

where

$$c_1 = q_f^2 - 2cq_f[\varepsilon(e_L) + \varepsilon(e_R)][\varepsilon(f_L) + \varepsilon(f_R)]\,,$$
$$c_2 = -\,4cq_f[\varepsilon(e_L) - \varepsilon(e_R)][\varepsilon(f_L) - \varepsilon(f_R)]\,,$$

with

$$c = \frac{\varrho G m_Z^2}{2\sqrt{2}\pi\alpha}\,\frac{s}{s - m_Z}\,, \tag{6.100}$$

or

$$c = \frac{1}{4\sin^2\theta_w\cos^2\theta_w}\,\frac{s}{m_Z^2 - s}\,, \tag{6.101}$$

where s is the centre-of-mass energy squared and q_f is the charge of the produced fermions. The $\cos\theta$ term is due to the weak electromagnetic interference. However, in the cross-section there is also a term proportional to $\cos\theta$; this is due to higher-order electromagnetic interactions [184], which must be subtracted in order to estimate the weak effect. Integrating over the solid angle,

we obtain

$$(\sigma_{\mathrm{QED}} - \sigma)/\sigma_{\mathrm{QED}} = 2cq_f[\varepsilon(e_{\mathrm{L}}) + \varepsilon(e_{\mathrm{R}})][\varepsilon(f_{\mathrm{L}}) + \varepsilon(f_{\mathrm{R}})] . \tag{6.102}$$

It follows that only the vector coupling constants of the fermions to the Z^0 contribute to the change of the cross-section with respect to the quantum electrodynamics (QED) expectations.

The term proportional to $\cos\theta$ in eq. (6.99) leads to a backward-forward asymmetry:

$$A = \frac{F - B}{F + B} = -1.5c[\varepsilon(e_{\mathrm{L}}) - \varepsilon(e_{\mathrm{R}})][\varepsilon(f_{\mathrm{L}}) - \varepsilon(f_{\mathrm{R}})]/q_f . \tag{6.103}$$

The axial-vector couplings are responsible for the asymmetry in the angular distribution.

As the fermion electric charge q_f enters in the denominator, asymmetries are expected to be larger for quarks than for leptons. Equation (6.100) is not very sensitive to the mass of the Z^0. Using this expression and assuming $\varrho = 1$, the measurement of A makes it possible to determine the product of the axial-vector coupling constants $g_{\mathrm{A}}^{\mathrm{e}} g_{\mathrm{A}}^{f}$. Expression (6.101) is free from any assumption regarding the ϱ parameter. Taking for g_{A}^{f} the standard-model predictions, it allows the relation (1.35) between $\sin^2\theta_{\mathrm{w}}$ and the Z^0 mass to be tested.

In the standard model, in the case of lepton production we have

$$\begin{cases} [\varepsilon(e_{\mathrm{L}}) + \varepsilon(e_{\mathrm{R}})][\varepsilon(f_{\mathrm{L}}) + \varepsilon(f_{\mathrm{R}})] = \frac{1}{4}(1 - 4\sin^2\theta_{\mathrm{w}})^2 , \\ [\varepsilon(e_{\mathrm{L}}) - \varepsilon(e_{\mathrm{R}})][\varepsilon(f_{\mathrm{L}}) - \varepsilon(f_{\mathrm{R}})] = \frac{1}{4} . \end{cases} \tag{6.104}$$

Because the value of $\sin^2\theta_{\mathrm{w}}$ obtained from other experiments is $\approx \frac{1}{4}$, the fractional deviation from the QED cross-section is expected to be very small.

6˙3.4.1. Lepton neutral-current couplings. – The most precise data come from the measurements of the asymmetry of μ pair production. The experimental signature for the events induced by the reaction $e^+e^- \to \mu^+\mu^-$ is two penetrating minimum-ionizing particles with momentum close to that of the beam, emerging almost back to back from the beam interaction. The background due to cosmic rays, Bhabha scattering, μ pair production from $\gamma\gamma$ scattering and τ decay is negligible and easily subtracted.

The asymmetry was measured at PETRA at $\langle\sqrt{s}\rangle = 34.5$ GeV by CELLO [185], JADE [186], MARK J [187], PLUTO [188] and TASSO [189, 190] and at $\langle\sqrt{s}\rangle = 41.6$ GeV by CELLO, JADE, MARK J and TASSO [191]; at PEP the measurements were performed at $\sqrt{s} = 29$ GeV by MAC [192, 193], MARK II [194] and HRS [195]. The muon angular distributions from the PETRA experiments are shown in fig. 82. The full curves represent the fit results, whilst the dashed curves show the prediction of QED. The experi-

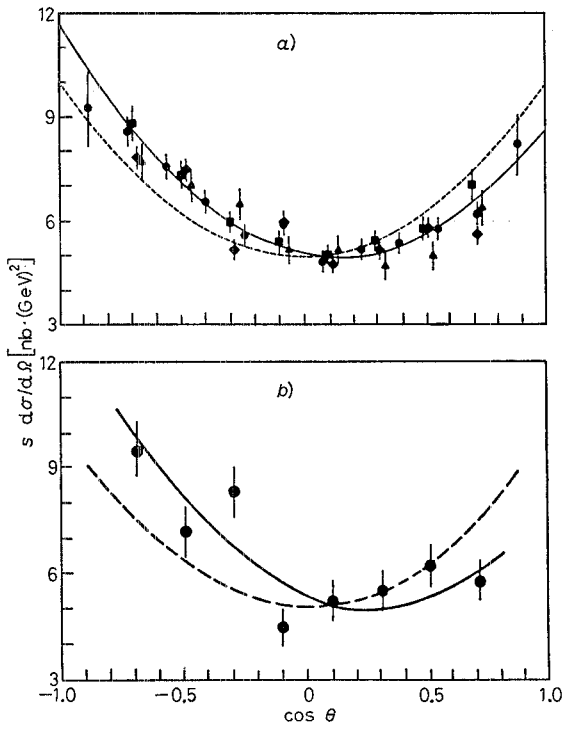

Fig. 82. – Differential cross-sections for the reaction $e^+e^- \to \mu^+\mu^-$ at *a*) $\sqrt{s} = 34.5$ GeV: • JADE, ◆ MARK I, ▲ PLUTO, ■ TASSO; *b*) $\sqrt{s} = 41.6$ GeV, from some PETRA experiments CELLO + JADE + TASSO. ——— QED + weak, — — — QED.

TABLE XV. – *Asymmetries in μ pair production.*

Experiments (a)	$\sqrt{s}$ (GeV)	$N_{\mu\mu}$	$A_{\mu\mu}$ (%)	Standard-model prediction (%)
MAC	29	10258	$-5.8 \pm 1.0 \pm 0.3$	-6.3
MARK II	29	5312	-7.1 ± 1.7	-6.3
HRS [195]	29	5057	$-4.9 \pm 1.5 \pm 0.5$	-6.3
CELLO	34.2	387	-6.4 ± 6.4	-9.2
JADE	34.4	3400	$-11.0 \pm 1.8 < 1.0$	-9.3
MARK J	34.6	3658	$-11.7 \pm 1.7 < 1.0$	-9.5
PLUTO	34.7	1550	$-12.4 \pm 3.1 < 1.0$	-9.4
TASSO	34.5	2673	$-9.1 \pm 2.3 \pm 0.5$	-9.4
CELLO	42.5	108	-13.4 ± 9.4	-15.6
JADE	41.5	444	-14.6 ± 4	-14.9
MARK J	41.1	480	-15.8 ± 5.3	-14.4
TASSO	42.4	174	-13.1 ± 8.8	-15.6

(*a*) The PETRA results are taken from ref. [191]; the PEP results (except HRS) are from ref. [132].

mental results are reported in table XV. The PETRA and the PEP results (apart from HRS) are updated to the time of the 1984 Vanderbilt Symposium [191] and the 1983 Ithaca Conference [132], respectively. In the table the expectations from the standard model are also reported. The averages of the $A_{\mu\mu}$ values are shown in fig. 83 as a function of the centre-of-mass energy squared [196].

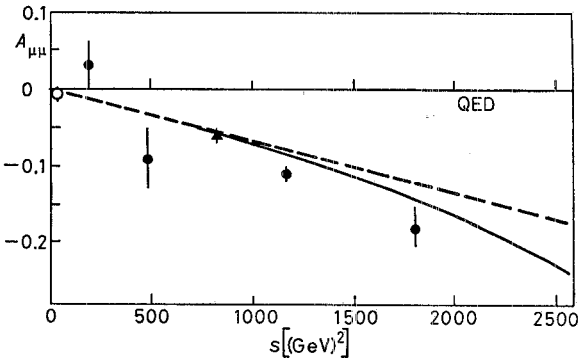

Fig. 83. – The μ asymmetry results: • PETRA, ▲ PEP; ——— $m_Z = 93.7$ GeV, $\sin^2\theta_w = 0.22$; — — — $m_Z = \infty$. The figure also shows the results from MARK I (○) [196].

Measurements of the asymmetry of τ pairs have also been done but with less accuracy. The signature of events induced by the reaction $e^+e^- \to \tau^+\tau^-$ is not as clear as that of μ pair production. The τ decays partly into electrons and pions that interact in the material of the detector, and partly into neutrinos that escape. It follows that, compared with the μ pair measurements, the systematic uncertainties are larger and the statistics are lower.

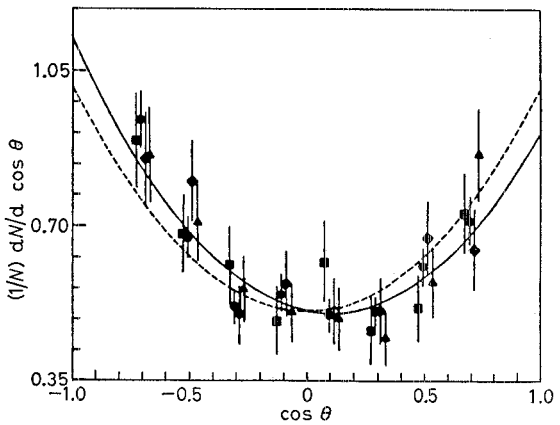

Fig. 84. – Differential cross-sections for the reaction $e^+e^- \to \tau^+\tau^-$ at $\sqrt{s} = 34.5$ GeV, from PETRA experiments: ■ CELLO, ◆ JADE, • MARK I, ▲ TASSO; ——— QED + + weak, – – – QED.

The τ pair asymmetry has been measured at PETRA at $\langle\sqrt{s}\rangle = 34.5$ GeV by CELLO [197], JADE [186], MARK J [187] and TASSO [189] and at $\sqrt{s} = 42.5$ GeV by CELLO [196]; at PEP the measurements were made at $\sqrt{s} = 29$ GeV by MAC [132, 193], MARK II [194] and HRS [198]. The angular distributions of the τ pairs from the PETRA experiments are shown in fig. 84. The experimental results, together with the standard-model expectations, are reported in table XVI, where the PETRA results at $\langle\sqrt{s}\rangle = 34.5$ GeV are updated to the time of the 1984 Vanderbilt Symposium [191].

TABLE XVI. – *Asymmetries in τ pair production.*

Experiment (a)	$\sqrt{s}$ (GeV)	$N_{\tau\tau}$	$A_{\tau\tau}$ (%)	Standard-model predictions (%)
HRS [198]	29	3243	$-6.1 \pm 2.3 \pm 0.5$	-6.3
MAC [132]	29	1247	-1.3 ± 2.9	-6.3
MARK II [132]	29	3714	-4.2 ± 2.0	-6.3
CELLO	34.2	434	-10.3 ± 5.2	-9.2
JADE	34.6	1612	-7.6 ± 2.7	-9.5
MARK J	34.6	860	-7.8 ± 4.0	-9.5
TASSO	34.4	517	-5.4 ± 4.5	-9.3
CELLO [197]	42.5	133	-16.7 ± 9.0	-14.5

(a) Results that are not referenced are from ref. [191].

The results from the MAC and MARK II experiments come from ref. [132]. The averages of the $A_{\tau\tau}$ values are shown in fig. 85 [196].

In the determination of the NC coupling constants from the asymmetry measurements, radiative corrections were taken into account [199]. The most important corrections come from graphs involving photons. The angular asymmetry changes by $+1$ to $+2$ % depending on the experimental cuts.

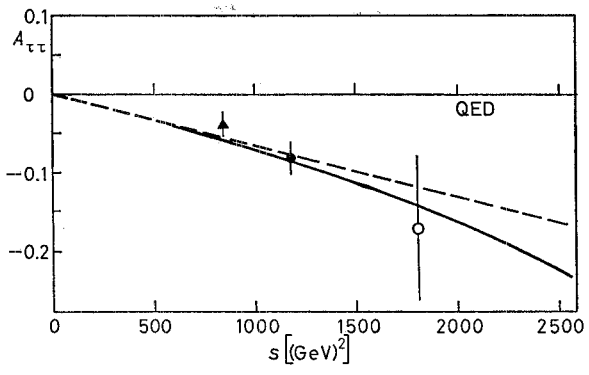

Fig. 85. – The τ asymmetry results from PETRA (•) and PEP (▲) experiments, o CELLO; ——— $m_Z = 93.7$ GeV, $\sin^2\theta_w = 0.22$; — — — $m_Z = \infty$.

TABLE XVII. – *Results on electroweak axial-vector couplings for leptons.*

$\sqrt{s}$ (GeV)	$g_A^e g_A^\mu$	$g_A^e g_A^\tau$
29	0.23 ± 0.03	0.21 ± 0.05
34.5	0.295 ± 0.029	0.22 ± 0.05
41.5	0.274 ± 0.060	—
42.5	—	—

Table XVII shows the values of the product of the axial-vector coupling constants from eqs. (6.103), using as input the average value of the Z^0 mass obtained by the UA1 and UA2 experiments. The values at $\sqrt{s} = 29$ GeV come from the MAC experiment that has the most statistically significant results at that energy ($N(\mu^+, \mu^-) = 16\,139$, $N(\tau^+, \tau^-) = 9\,905$) [193]. The PETRA results are quoted in ref. [191].

Using for g_A^e the value (6.24) obtained from the $\nu_\mu(\bar{\nu}_\mu)$e experiments, we get

$$\begin{cases} g_A^\mu = -0.51 \pm 0.05\,, \\ g_A^\tau = -0.44 \pm 0.07\,. \end{cases} \tag{6.105}$$

Both coupling constants turn out to be consistent with the value predicted by the standard model ($-\frac{1}{2}$) and thus confirm e-μ-τ universality. If universality is assumed, we obtain

$$\begin{cases} g_A^\mu = -0.50 \pm 0.02\,, \\ g_A^\tau = -0.46 \pm 0.04\,. \end{cases} \tag{6.106}$$

The allowed region in the plane g_A-g_V obtained from the measurement of the lepton asymmetry at PETRA and PEP for the case in which lepton universality is assumed [132] can be seen in fig. 60 and 65.

Figure 86 shows the allowed region in the $\sin^2\theta_w$-m_Z plane for the combined μ pair data from PETRA and PEP using the asymmetry (the expression of c is that defined in eq. (6.101)) as well as the cross-section measurements. In this figure the results obtained from the UA1 and UA2 experiments are also shown. The dash-dotted line represents the standard-model predictions (1.35). For $m_Z = (93 \pm 2)$ GeV the combined fit gives $\sin^2\theta_w = 0.18 \pm 0.02$ [191].

The sensitivity of the Bhabha cross-section to the electroweak effect is small owing to the presence of the t-channel, which reduces the deviations from QED. For $\sin^2\theta_w = 0.25$ the expected deviations from QED are of the order of $(2 \div 3)\%$ and are then very difficult to measure.

High-statistics data for $e^+e^- \to e^+e^-$ exist from CELLO [200], JADE [201], MARK J [187] and TASSO [190] at PETRA at an average c. m. energy of 35.4 GeV and from HRS [132], MAC [193] and MARK II [194] at PEP at $\sqrt{s} = 29$ GeV. The data agree well both with QED and the standard-model

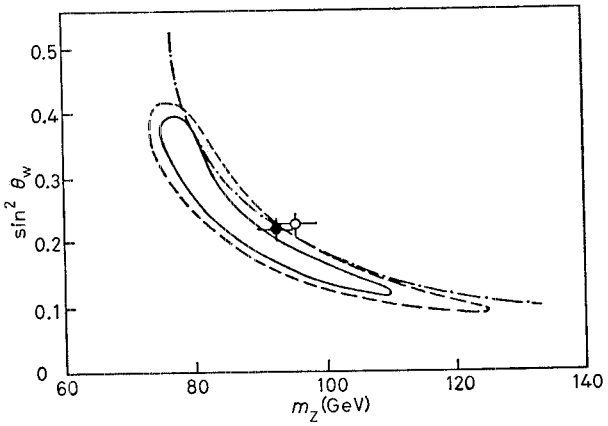

Fig. 86. – Contours of allowed regions in the plane $\sin^2\theta_w$-m_Z from $e^+e^- \to \mu^+\mu^-$ results obtained at PETRA and PEP. The results from UA1 (○) and UA2 (●) are shown together with the standard-model prediction. ——— 68% c.l. contour, — — — 95% c.l. contour, both in PETRA + PEP; —·—·— standard theory.

predictions. Figure 87 shows a typical result obtained in the MAC experiment. The TASSO experiment at $\sqrt{s} = 42.3$ GeV [191] found $g_A^{e2} = 0.15 \pm 0.14$ and $g_V^{e2} = 0.01 \pm 0.16$, or $\sin^2\theta_w = 0.28 + 0.10/-0.14$ (preliminary results). The result of the MAC experiment [193] was $g_A^{e2} = 0.33 \pm 0.24$ and $g_V^{e2} = 0.09 \pm 0.14$.

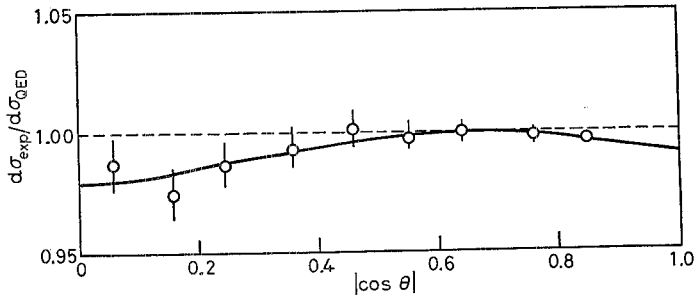

Fig. 87. – Differential cross-section for the reaction $e^+e^- \to e^+e^-$ measured in the MAC experiment [193]: — — — QED, ——— electroweak.

6·3.4.2. Heavy-quark neutral-current couplings. – The couplings of heavy quarks (c and b) have also been investigated in e^+e^- interactions studying reactions (6.95). The expected values of the charm-quark and bottom-quark asymmetries are

$$A_{cc}(29\ \text{GeV}) \approx -9\,\%, \qquad A_{cc}(34\ \text{GeV}) \approx -14\,\%,$$

$$A_{bb}(29\ \text{GeV}) \approx -18\,\% \quad \text{and} \quad A_{bb}(34\ \text{GeV}) \approx -28\,\%.$$

Two techniques have been used to identify the $\frac{4}{11}$ and $\frac{1}{11}$ of all multihadronic events that come from a primary $c\bar{c}$ and $b\bar{b}$ quark pair, respectively. The first consists in the reconstruction of resonances containing heavy quarks. The charm quark was tagged by measuring the $D^{*\pm}$ and the D^0 mesons. Reconstructed B-mesons have not been used for bottom-quark tagging.

The HRS [193], JADE [202] and TASSO [203] Collaborations identified the events generated from the fragmentation of c-quarks, looking for

$$D^{*\pm} \to D^0\pi^\pm, \tag{6.107}$$

with the subsequent decays

$$D^0 \to K^-\pi^+, \quad D^0 \to K^-\pi^+\pi^0, \quad D^0 \to K^-\pi^+\pi^-\pi^+. \tag{6.108}$$

The mass difference $\Delta = m_{K\pi\pi} - m_{K\pi}$ due to the small Q value of this reaction is expected to peak around the π mass. In the HRS experiment [193] the angular asymmetry has also been measured for inclusive D production decaying into K and π. Figure 88 shows *a*) the Δ and *b*) the $m_{K\pi}$ distributions measured in this experiment.

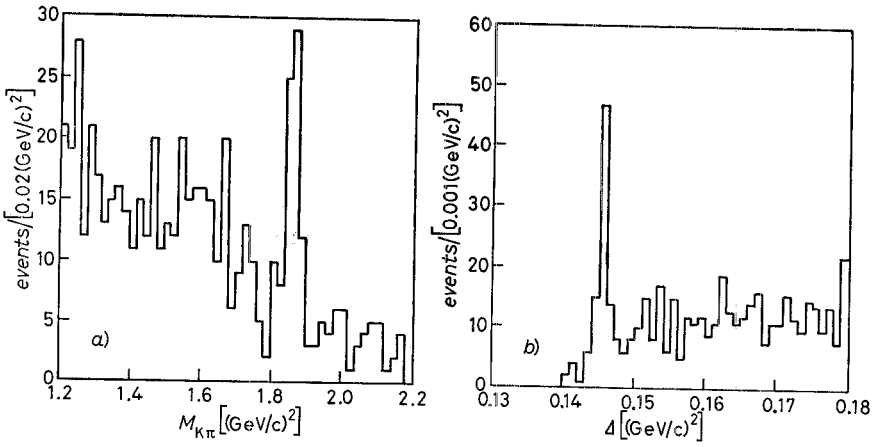

Fig. 88. – Distributions of *a*) $\Delta = m_{K\pi\pi} - m_{K\pi}$ and *b*) $m_{K\pi}$ measured in the HRS experiment [193].

The direction of the charm quark is assumed to be equal to that of the D-meson. The measured angular distributions from JADE [202] and TASSO [203] are shown in fig. 89. The full curves show the fit results. The values of the results from these three experiments are reported in table XVIII.

The second method of tagging heavy quarks consists in observing the semi-

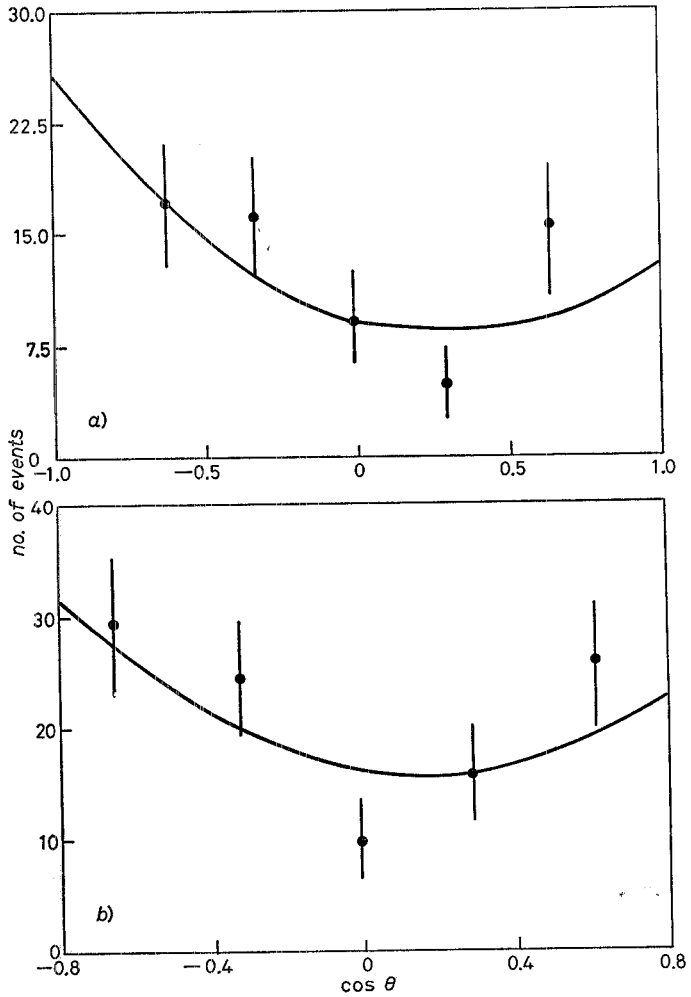

Fig. 89. – Angular distribution of c-quarks identified by the reconstruction of the D* in the JADE (*a*)) [202] and TASSO (*b*)) [203] experiments, $\sqrt{s} = 34.5$ GeV.

leptonic decays

(6.109) $$c \to \ell\nu X\,, \qquad b \to \ell\nu X\,.$$

Hadronic events with leptons in the final states, indicating the decays of the quarks into μ's and e's, have been studied in the TASSO [204], MARK II [205] and TPC [193] experiments. The experiments MARK J [206], JADE [207] and MAC [132] have searched for c and/or b decays into muons.

The heavy-flavour tagging by the leptonic decays gives a larger statistical sample of events than the D reconstruction but with a more important systematic error. Muons have backgrounds due to punch-through and to decays in flight

of $K^{\pm}$ and $\pi^{\pm}$. Electrons have backgrounds due to hadronic showers and converted photons. The leptonic-decay tagging gives only a statistical separation between c and b quarks. In order to reduce the backgrounds and to separate the c and b decays, a cut was introduced on the transverse momentum p_T of the final-state lepton with respect to the jet axis. Because of their larger mass, the b-quarks produce a harder p_T spectrum than that produced by c-quarks. The hadron jet axis is used to reconstruct the quark direction. Figure 90 shows the p_T distribution for inclusive muon events obtained in the MARK J experiment [206]. The predictions for the c and b contributions are shown.

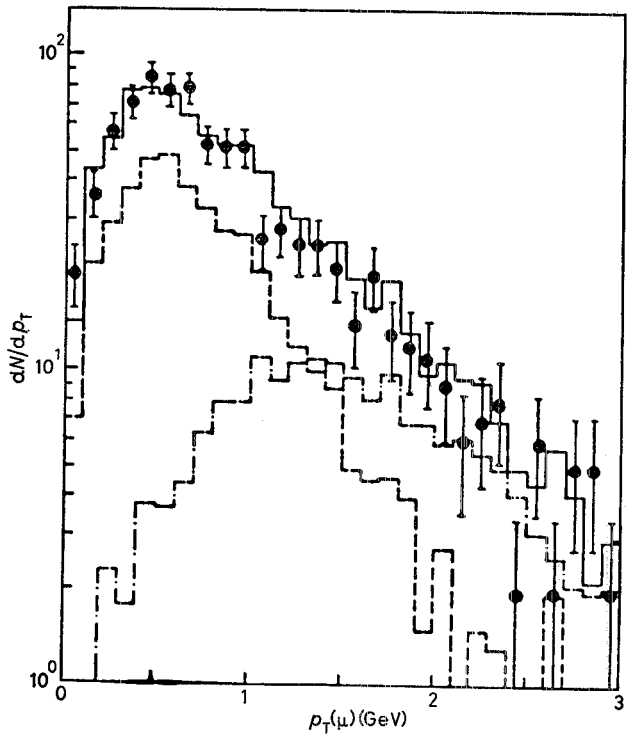

Fig. 90. – The p_T distribution for inclusive muons from the MARK J experiment at $\sqrt{s} = 34.5$ GeV. Monte Carlo predictions for the contributions from the c-quark (dashed line) and the b-quark (dash-dotted line) are shown. The full histogram shows the sum of the two and includes also the background (from ref. [132]).

Figure 91 shows the angular distributions of the events that were identified as coming from c and b fragmentation in the MARK II experiment [205]. In the figure the fits to the data (solid lines) are compared with the expectation without electroweak effects (dashed lines).

The experimental results are reported in tables XVIII and XIX. In these tables the heavy-quark coupling constants g_A^c and g_A^b are extracted assuming

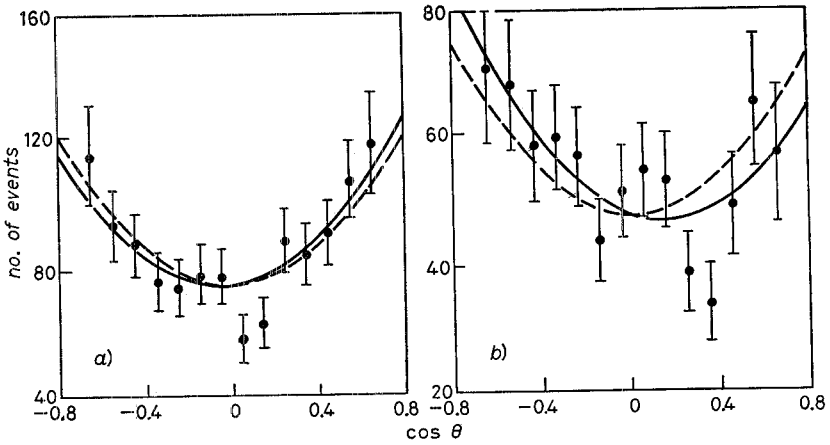

Fig. 91. – Angular distributions of c (a)) and b (b)) quarks obtained by measuring the inclusive muon and electron events in the MARK II experiment [205]. The full lines give fits allowing for an asymmetry. The dashed lines are without the electroweak effect.

that $g_A^c = -\frac{1}{2}$. The average axial-vector coupling constants obtained for the c and b quarks are

$$\begin{cases} g_A^c = +0.55 \pm 0.17 , \\ g_A^b = -0.54 \pm 0.12 , \end{cases} \tag{6.110}$$

in good agreement with the expectations of the standard model.

A determination of $\sin^2\theta_w$ can be obtained studying the energy dependence of the ratio $R = \sigma(e^+e^- \to q\bar{q})/\sigma(e^+e^- \to \mu^+\mu^-)$ (see eq. (6.102)). Results have been reported by the MARK J, TASSO and JADE Collaborations [208]. The best determination coming from JADE is

$$\sin^2\theta_w = 0.23 \pm 0.05 . \tag{6.111}$$

TABLE XVIII. – *Charm-quark asymmetry and axial-vector couplings.*

Experiment	$\sqrt{s}$ (GeV)	A_{cc} [a] (%)	g_A^c	Method
HRS [193]	29	-12 ± 8	—	D*, D⁰
MAC [132]	29	-5 ± 11	0.8 ± 1.8	μ
TPC [193]	29	—	$0.7 \pm 0.6 \pm 0.3$	μ
TPC [193]	29	—	$1.2 \pm 0.7 \pm 0.5$	e
JADE [192]	34.4	-14 ± 9	0.5 ± 0.3	D*
TASSO [203]	34.4	-13 ± 10	0.5 ± 0.4	D*
MARK J [206]	34.6	$-18 \pm 9 \pm 5$	0.6 ± 0.3	μ
TASSO [204]	34.6	$+5 \pm 24$	-0.2 ± 0.9	e

(a) The values expected for the PETRA and the PEP experiments are −14% and −9%, respectively.

TABLE XIX. – *Bottom-quark asymmetry and axial-vector couplings.*

Experiment	$\sqrt{s}$ (GeV)	A_{bb} [a] (%)	g_A^b	Method
MARK II [205]	29	—	$-0.75 + 0.35/-0.3$	μ, e
MAC [132]	29	-7 ± 9	-0.3 ± 0.35	μ
TPC [193]	29	—	$-0.6 \pm 0.45 \pm 0.1$	μ
TPC [193]	29	—	$-1.0 \pm 0.95 \pm 0.25$	e
JADE [207]	34.4	$-22.8 \pm 6 \pm 2.3$	-0.5 ± 0.2	μ
TASSO [204]	34.5	-37.5 ± 27.5	-0.8 ± 0.6	μ
TASSO [204]	34.5	-25 ± 22	-0.5 ± 0.4	e
MARK J [206]	34.6	$-23 \pm 20 \pm 15$	-0.5 ± 0.4	μ

(a) The values expected for PETRA and PEP experiments are $-28\,\%$ and $-19\,\%$, respectively.

6·3.5. Summary of the experimental results and comments on future experiments. In this subsection the experimental results are summarized and compared with the expectations of the standard model.

In the standard model the axial-vector coupling constants are fixed by the representation of the fermion in the weak-spin isotopic space. Table XX re-

TABLE XX. – *Fermion axial-vector couplings.*

Fermion	g_A^f	Standard-model predictions
u	0.50 ± 0.03	0.5
d	-0.49 ± 0.05	-0.5
c	0.55 ± 0.17	0.5
s	—	-0.5
b	-0.54 ± 0.12	-0.5
e	-0.49 ± 0.03	-0.5
μ	-0.51 ± 0.05	-0.5
τ	-0.44 ± 0.07	-0.5

ports the measured values of g_A^f and the standard-model expectations. Within the errors, all the results are in agreement with the theory. The g_A^u and g_A^d are obtained from the measurements of the chiral coupling constants in neutrino interactions. The g_A^μ and g_A^τ are obtained from the $A_{\mu\mu}$ and $A_{\tau\tau}$ measurements using the value of g_A^e from the measurement of the ν_μe scattering.

Table XXI gives the experimental values of the ratio of the overall strength of NC and CC neutrino interactions (ϱ).

TABLE XXI. – *Measurement of* ϱ.

Process	ϱ
deep inelastic	1.01 ± 0.01
ν_μe	0.99 ± 0.05
$e^+e^- \to \mu^+\mu^-$	1.17 ± 0.09

In the standard model, at first order of the theory, ϱ is predicted to be equal to one.

The value of $\sin^2\theta_w$ has been obtained in many experiments. The results are summarized in table XXII; in fig. 92 they are shown together with the result from the measurements of the W and Z^0 masses (see sect. 7). As expected at first order in the standard model, all the determinations of $\sin^2\theta_w$ coincide within the experimental errors.

TABLE XXII. – *Measurements of* $\sin^2\theta_w$.

Process	$\sin^2\theta_w$
$\nu_\mu e$	0.21 ± 0.02
νN	0.226 ± 0.007
νp	0.26 ± 0.04
eD	0.22 ± 0.02
atomic physics	0.205 ± 0.04
μC	0.23 ± 0.08
$e^+e^- \to \mu^+\mu^-$	0.18 ± 0.02
$e^+e^- \to q\bar{q}$	0.23 ± 0.05

A new, precise determination of $\sin^2\theta_w$ would come from the measurement of the NC and CC neutrino-nucleon cross-sections. The data were collected at CERN in 1984 by the CHARM and CDHS Collaborations. The expected experimental uncertainty on the determination of $\sin^2\theta_w$ is $\Delta(\sin^2\theta_w) = \pm 0.005$ [209, 210].

Experiment E734 [141] will increase the statistics of the $\nu_\mu e$ and $\bar{\nu}_\mu e$ events, reaching ≈ 150 events for each channel. This should allow a determination of $\sin^2\theta_w$ with a precision of ± 0.01 [211].

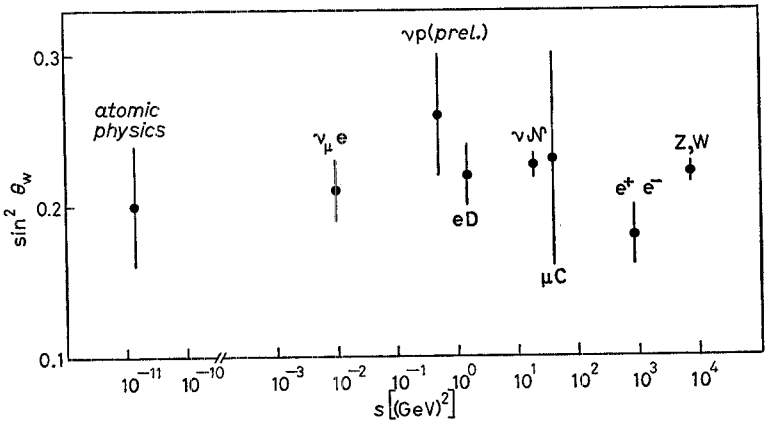

Fig. 92. – Experimental results on $\sin^2\theta_w$ obtained from different measurements.

A new experiment, dedicated to the measurement of the $\bar{\nu}_\mu e$ reactions, will start to take data at CERN in 1986 [212]. A total of 200 events are expected to be collected for the neutrino and antineutrino reactions, which would give a determination of $\sin^2\theta_w$, from a purely leptonic reaction, with a precision of ± 0.005.

7. – The discovery of the intermediate vector bosons.

As described in sect. **1**, the masses of the intermediate bosons are unambiguously predicted by the standard model of the electroweak interactions provided the weak mixing angle θ_w is known (eqs. (1.34) and (1.35)). Using the experimental value of $\sin^2\theta_w$ obtained in low-energy, high-accuracy $\nu\mathcal{N}$ experiments (table XXII), one gets

$$\begin{cases} m_W = (82.4 \pm 1.1)\ \text{GeV}, \\ m_Z = (93.3 \pm 0.9)\ \text{GeV}. \end{cases} \tag{7.1}$$

The intermediate vector bosons (IVBs) decay rapidly, mainly into a fermion-antifermion pair. The W decays into leptons and quarks according to the reactions

$$\begin{cases} W^- \to \ell\bar{\nu}_\ell, & \ell\bar{\nu}_\ell = (e^-\bar{\nu}_e),\ (\mu^-\bar{\nu}_\mu),\ (\tau^-\bar{\nu}_\tau), \\ W^- \to q'\bar{q}, & q'\bar{q} = (d'\bar{u}),\ (s'\bar{c}),\ (b'\bar{t}), \end{cases} \tag{7.2}$$

where d′, s′ and b′ are related to the quark mass eigenstates by a unitary transformation (see sect. **3**). The decay modes of W^+ are obtained by replacing the particles with the antiparticles and *vice versa*. The W decay into bt is allowed if the sum of the bottom and top masses is assumed to be smaller than the W mass.

The widths of the W decays into the different channels are obtained using the CC Lagrangian defined in (1.5). Neglecting the lepton and quark masses with respect to the W mass, one obtains

$$\Gamma(W \to \ell\nu) = g^2 m_W/48\pi = G m_W^3/6\pi\sqrt{2} \approx 180\ \text{MeV} \tag{7.3}$$

and

$$\Gamma(W \to q'q) = 3\Gamma(W \to \ell\nu)|U_{qq'}|^2, \tag{7.4}$$

where $|U_{qq'}|$ are the elements of the mixing matrix defined in (1.10), and the factor 3 is due to the colour symmetry of strong interactions. Assuming six leptons and six quarks, the total width of W is

$$\Gamma = \sqrt{2}/\pi\, G m_W^3 \approx 2.2\ \text{GeV}. \tag{7.5}$$

Taking into account the mass of the top quark m_t and the QCD effects [213], we have

$$(7.6) \qquad \Gamma(\mathrm{W} \to \text{hadrons}) = 3\Gamma(\mathrm{W} \to \ell\nu)(3 - 3m_t^2/2m_W^2)[1 + \alpha_s(m_W^2)/\pi],$$

where $\alpha_s(m_W^2)$ is the strong-coupling constant at mass scale m_W.

The Z^0 can decay into lepton and quark pairs: $Z \to \ell^+\ell^-$, $Z \to \bar{q}q$. Using the NC Lagrangian (1.15) and neglecting the fermion masses, one obtains

$$(7.7) \qquad \Gamma(Z \to \text{all}) = (m_Z g^2/48\pi \cos^2\theta_w)\left[\sum_\ell (g_V^{\ell 2} + g_A^{\ell 2}) + 3\sum_q (g_V^{q 2} + g_A^{q 2})\right],$$

where $g_V^{\ell,q}$ and $g_A^{\ell,q}$ are, respectively, the vector and axial-vector coupling constants of leptons and quarks.

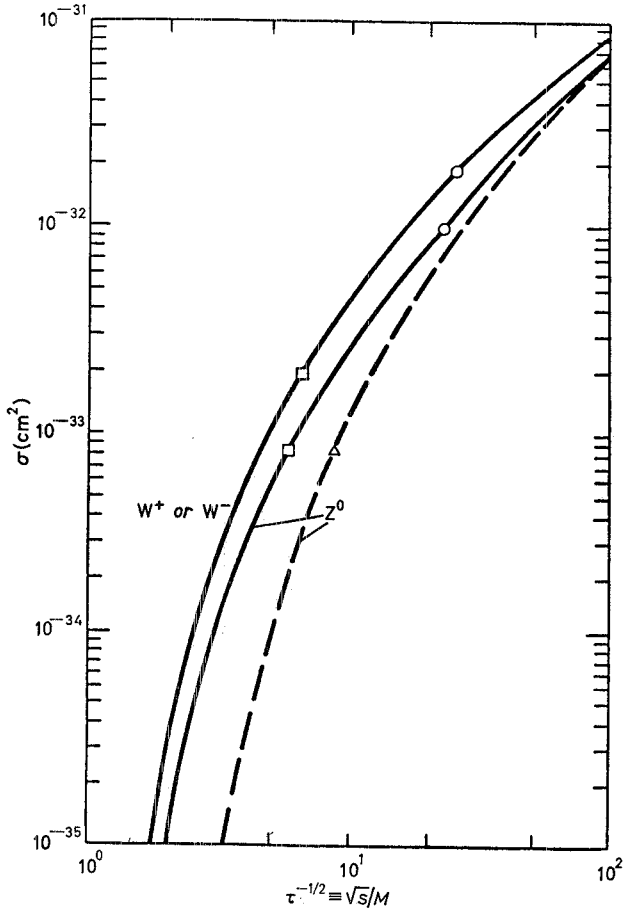

Fig. 93. – Predicted production cross-sections for $W^\pm$ and Z^0 in pp (dashed curve) and $p\bar{p}$ (solid curves) collisions [214, 215]: ○ $\sqrt{s} = 2000$ GeV, □ $\sqrt{s} = 540$ GeV, △ $\sqrt{s} = 800$ GeV.

Assuming six quarks and six leptons and using a value of $\sin^2\theta_w = 0.23$, one obtains

$$\Gamma(Z \to \text{all}) \approx 2.2 \text{ GeV}. \tag{7.8}$$

The QCD corrections to the quark-antiquark decay modes amount to factors of the type $1 + \alpha_s(m_Z^2)/\pi$, as for the W decay. Finite-mass effects on the decay width in $t\bar{t}$ have been investigated in ref. [213] and [216].

The IVBs have been detected [3] at the CERN $p\bar{p}$ Collider. In the quark-parton model scheme, the production cross-section of the vector bosons is given in terms of the quark distributions in the nucleons and the resonant quark cross-section:

$$\sigma(p\bar{p} \to W[Z]X) = \int_0^1 dx_1 \int_0^1 dx_2 \sigma(x_1, x_2) f(x_1, x_2), \tag{7.9}$$

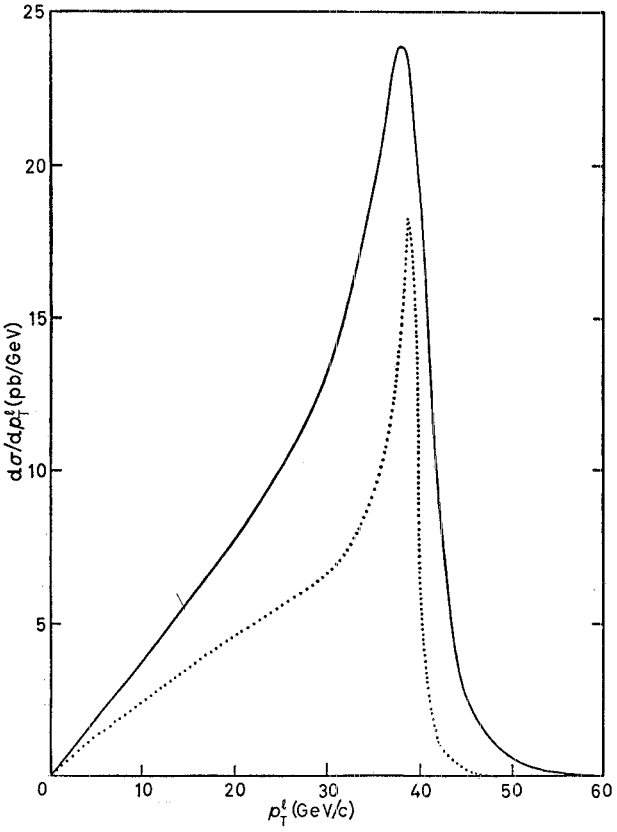

Fig. 94. – The predicted p_T spectrum of the charged lepton from $p\bar{p} \to W(\to e\nu)X$ at $\sqrt{s} = 540$ GeV [215, 216]. The dotted line shows the expected distribution in the case of a resonant cross-section. The full QCD-corrected distribution is shown by the solid curve.

where x_1 and x_2 are the fractions of momentum brought by the interacting quarks in the nucleons.

In the case of W production, the resonant cross-section is given by

$$\sigma_{\mathrm{W}}(x_1, x_2) = \sqrt{2}\, G^2 \pi m_{\mathrm{W}}^2 \delta(x_1 x_2 s - m_{\mathrm{W}}^2)\,, \tag{7.10}$$

where s is the centre-of-mass energy of the $\mathrm{p\bar{p}}$ system squared. The quark and antiquark distribution in eq. (7.9) is given by

$$f(x_1, x_2) = W^+(x_1, x_2) = \tfrac{1}{3}\{[u(x_1)\bar{d}(x_2) + \bar{d}(x_1)u(x_2)]\cos^2\theta_{\mathrm{C}} + [u(x_1)\bar{s}(x_2) + \bar{s}(x_1)u(x_2)]\sin^2\theta_{\mathrm{C}}\}\,. \tag{7.11}$$

For the W^- production the quark and antiquark distributions must be interchanged.

In the Z^0 case we have

$$\sigma_{\mathrm{Z}}(x_1, x_2) = (G^2\pi/\sqrt{2})\, m_{\mathrm{Z}}^2\, \delta(x_1 x_2 s - m_{\mathrm{Z}}^2) \tag{7.12}$$

and

$$f(x_1, x_2) = Z(x_1, x_2) = \tfrac{1}{3}\{[u(x_1)\bar{u}(x_2) + u(x_2)\bar{u}(x_1)]\cdot [\tfrac{1}{4} - \tfrac{2}{3}\sin^2\theta_{\mathrm{w}} + \tfrac{8}{9}\sin^4\theta_{\mathrm{w}}] + [d(x_1)\bar{d}(x_2) + d(x_2)\bar{d}(x_1) + s(x_1)s(x_2) + s(x_2)s(x_1)][\tfrac{1}{4} - \tfrac{1}{3}\sin^2\theta_{\mathrm{w}} + \tfrac{2}{9}\sin^2\theta_{\mathrm{w}}]\}\,. \tag{7.13}$$

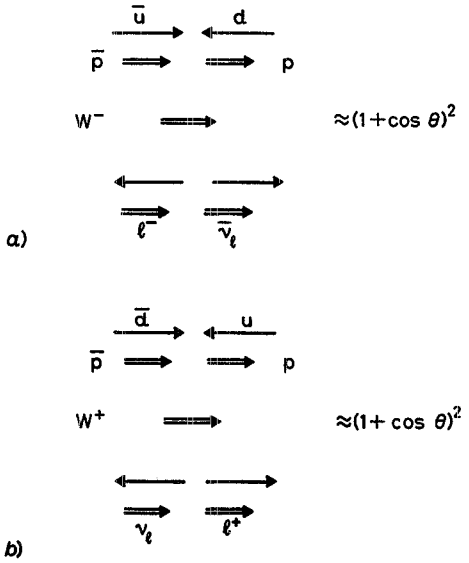

Fig. 95. – Production of *a*) W^- and *b*) W^+ in proton-antiproton interactions. The W polarizations due to the $V - A$ coupling of the quarks and the preferred direction of the charged lepton produced in the purely leptonic decay of the W are shown.

Higher-order QCD corrections modify the predictions (7.10) and (7.12). Figure 93 shows the expected cross-sections for IVB production in $p\bar{p}$ interactions as a function of $\sqrt{s}/m_{W,Z}$ [214, 215]. At the CERN $p\bar{p}$ Collider the centre-of-mass energy is $\sqrt{s} = 540$ GeV, and one gets

$$\begin{cases} \sigma_{W^+} = \sigma_{W^-} \approx 2 \cdot 10^{-33} \text{ cm}^2, \\ \sigma_Z \approx 10^{-33} \text{ cm}^2. \end{cases} \tag{7.14}$$

Until now the IVBs have been identified by looking for purely leptonic decays [3]:

$$W^+ \to \ell^+ \nu_\ell, \quad W^- \to \ell^- \bar{\nu}_\ell \tag{7.15}$$

and

$$Z^0 \to \ell^+ \ell^-, \tag{7.16}$$

with $\ell = e, \mu$.

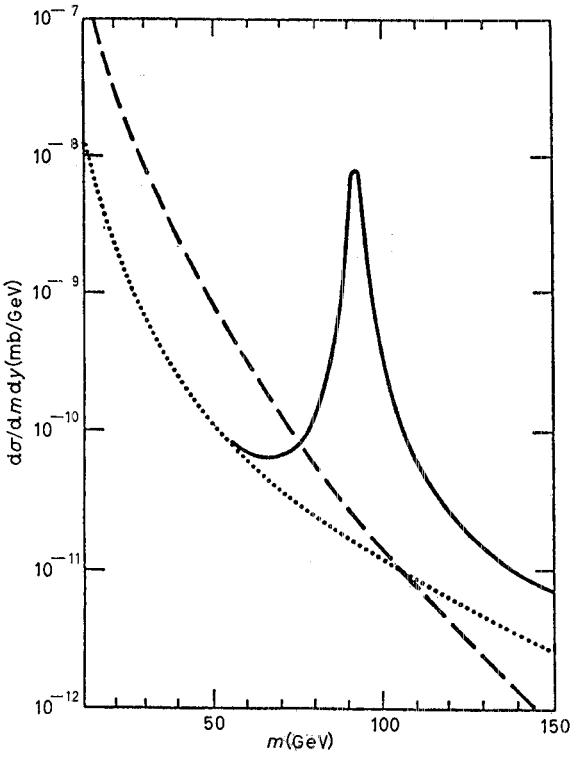

Fig. 96. – Expected invariant-mass distribution of the charged lepton pairs from the reaction $p\bar{p} \to Z^0(\to \ell^+\ell^-)X$ at $\sqrt{s} = 540$ GeV and $y = \frac{1}{2}\ln(x_1/x_2) = 1$ (solid line). The spectra of the events induced by heavy-quark decays (dashed line) and Drell-Yan reactions (dotted line) are shown [217].

The purely leptonic decays of the $W^{\pm}$ are characterized by the detection of a charged lepton with large transverse momentum, and of a large missing energy brought by a neutrino in the direction opposite to that of the charged lepton. Since the W decays into two bodies, the p_T spectrum of the charged lepton peaks at $p_T = m_W/2$ (fig. 94). Both the resonant (dotted line) and the full QCD-corrected distributions (solid line) are shown [215, 216].

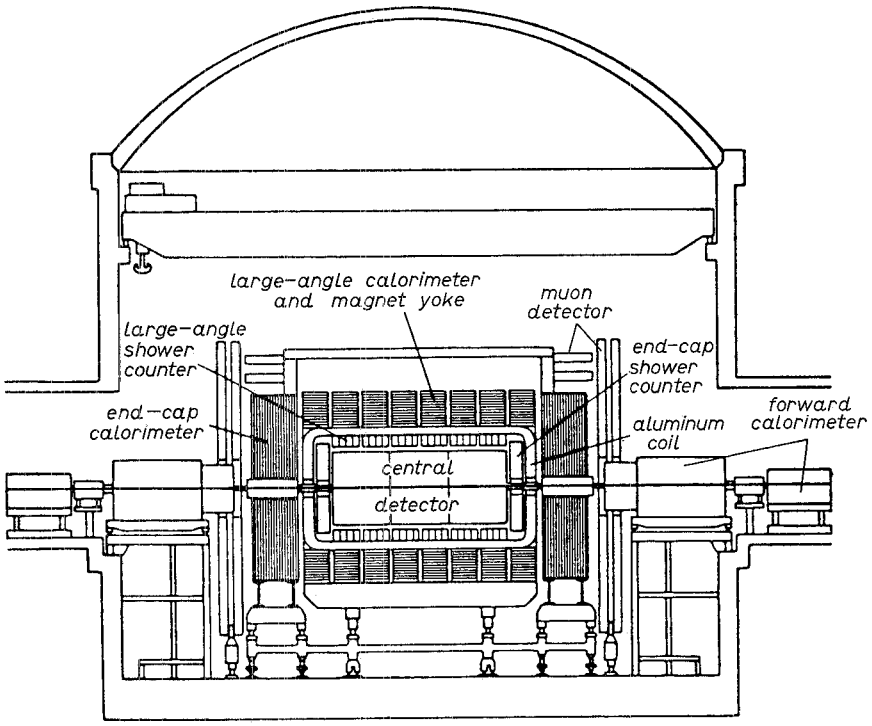

Fig. 97. – Side view of the UA1 detector.

Another signature of process (7.15) is that negative leptons are preferentially emitted along the direction of the incoming proton and positive leptons along the direction of the incoming antiprotons. This is related to the $V - A$ structure of the CCs and is explained by applying angular-momentum conservation to the elementary qq process (fig. 95). In this figure it has been assumed that only the valence quarks interact. The angle θ refers to the direction of the outgoing charged lepton in the centre of mass, with respect to the proton direction.

The Z^0, decaying into a pair of charged leptons (7.16), can be directly identified through a peak in the dilepton invariant mass (fig. 96). The negligible background due to heavy-quark leptonic decay and to Drell-Yan production of lepton pairs [217] is shown in this figure.

Evidence of the existence of IVBs was recorded by the detectors of the UA1 and UA2 experiments. The layout of the UA1 experiment is shown in fig. 97. The apparatus [218] consists of a 4π solid-angle detector for identifying and measuring the energy of electrons, muons and hadrons. The energy of neutrinos is deduced from the missing-energy measurement. There is a central detector (CD) made of drift chambers, located in a magnetic-dipole field (0.7 T) perpendicular to the beam direction. The CD, which allows the track position and the energy loss (dE/dx) of charged particles to be measured, is surrounded by an electromagnetic calorimeter of the lead/scintillator sandwich type. The hadronic calorimeter is contained in the segmented iron yoke equipped with scintillators. The energy and the direction of neutrinos are obtained from the missing-energy and missing-momentum measurements. The muons are identified by an array of proportional chambers placed outside the magnet.

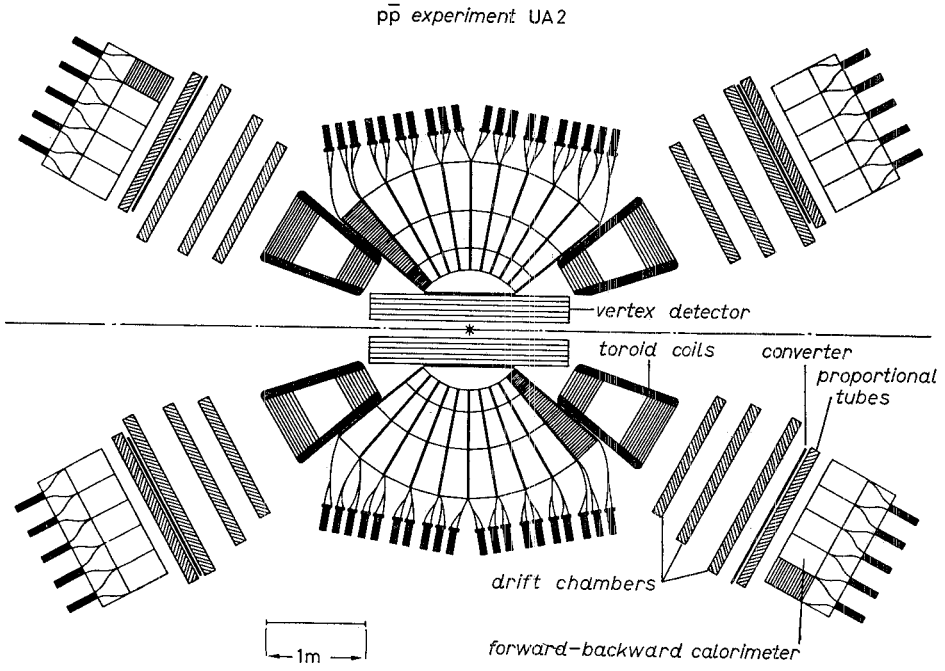

Fig. 98. – The UA2 detector: schematic cross-section in the vertical plane containing the beam.

The UA2 detector (fig. 98) [218] is instrumented to identify electrons and measure their energy over a polar angle interval $20° < \theta < 160°$. Magnetic spectrometers are placed in the region $20° < \theta < 37.5°$ and $142.5° < \theta < 160°$ in order to measure the asymmetry in the purely leptonic W decay. The muons are not identified. The vertex detector is a system of cylindrical chambers

which measures charged-particle trajectories. It is surrounded by a 1.5 r.l. tungsten converter followed by a proportional chamber. The central calorimeter contains an electromagnetic part and an hadronic part. The two forward magnetized regions (0.38 T) are equipped with drift chambers and electromagnetic and hadronic calorimeters.

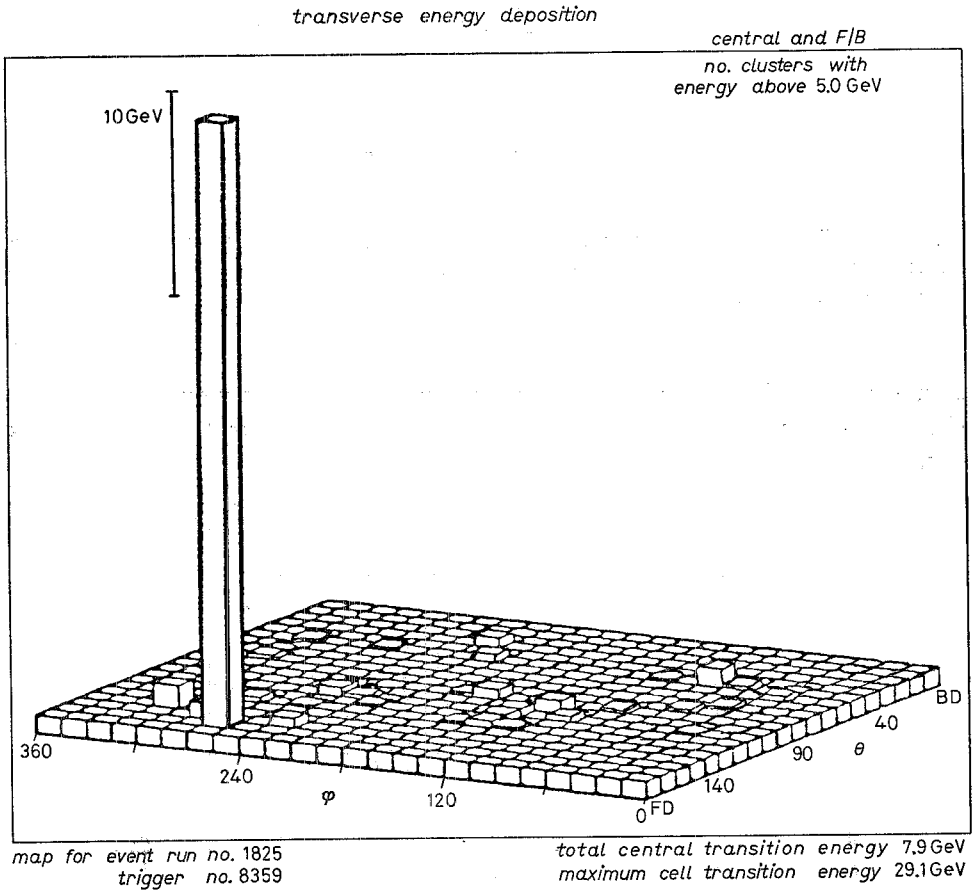

Fig. 99. – Plot of the electromagnetic energy flow in the UA2 calorimeter cells for a W event.

The UA1 and UA2 detectors took data in 1982-83 for an integrated luminosity of 136 nb^{-1}. A total of 57 W candidate events (43 decaying into $e\nu$ and 14 into $\mu\nu$) have been detected by the UA1 experiment. The UA2 experiment observed 37 W decaying into $e\nu$. Figure 99 shows the calorimeter cell energy distribution for one of these events in the UA2 detector. The E_T distribution of the electrons peaks at high E_T values, as can be seen in fig. 100 (UA1). The events show clearly a missing transverse energy of the same mag-

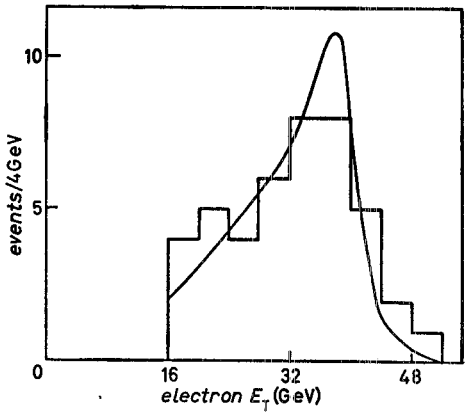

Fig. 100. – The electron transverse-energy distribution of the 43 candidate events observed in the UA1 detector: ——— $W \to ev$. The curve represents the result of a Monte Carlo simulation.

nitude as the electron transverse energy, with the vector momentum of the charged lepton and of the neutrino balanced almost exactly back to back (fig. 101).

The sign of the electron was determined for a subsample of these events

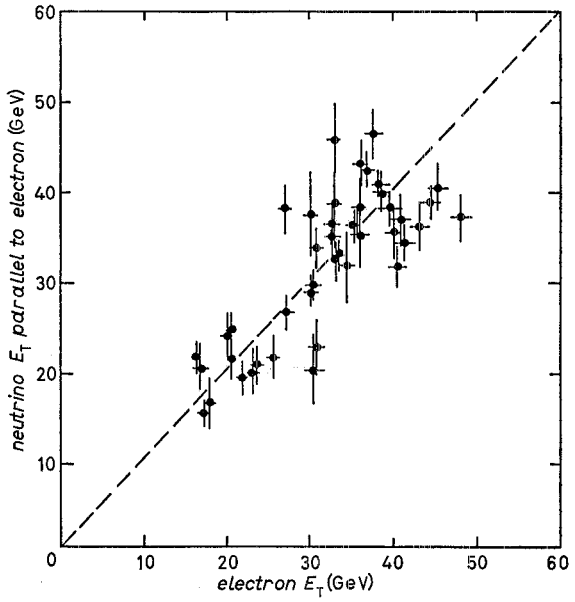

Fig. 101. – Correlation between the electron and « neutrino » transverse energies (43 events in UA1). The missing-energy component along the electron direction is plotted against the electron transverse energy.

(29 in UA1 and 8 in UA2). In fig. 102 the angular distribution of the electron in the rest frame of the W is shown together with the prediction.

The following mass values have been obtained [3] from the total samples of W decaying into νe:

$$(7.17)\qquad \begin{cases} m_{\mathrm{W}} = [80.9 \pm 1.5\ (\mathrm{stat.}) \pm 2.4\ (\mathrm{syst.})]\ \mathrm{GeV} & [\mathrm{UA1}], \\ m_{\mathrm{W}} = [83.1 \pm 1.9\ (\mathrm{stat.}) \pm 1.3\ (\mathrm{syst.})]\ \mathrm{GeV} & [\mathrm{UA2}]. \end{cases}$$

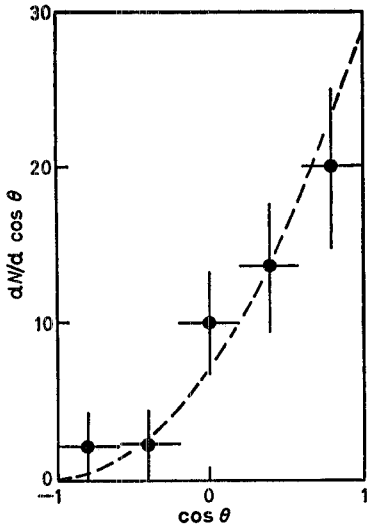

Fig. 102. – The angular distribution of the electron emission angle θ in the rest frame of the W after correction for experimental acceptance (UA1). Only those events in which the electron charge is determined have been used. The dashed line shows the $(1 + \cos\theta)^2$ function.

The values of the product between the measured W cross-section and the decay branching ratio of $\mathrm{W} \to \mathrm{e}\nu$ (Br^{e}) are

$$(7.18)\qquad \begin{cases} (\sigma\,\mathrm{Br}^{\mathrm{e}})_{\mathrm{W}} = [0.53 \pm 0.08\ (\mathrm{stat.}) \pm 0.09\ (\mathrm{syst.})]\ \mathrm{nb} & [\mathrm{UA1}], \\ (\sigma\,\mathrm{Br}^{\mathrm{e}})_{\mathrm{W}} = [0.53 \pm 0.10\ (\mathrm{stat.}) \pm 0.10\ (\mathrm{syst.})]\ \mathrm{nb} & [\mathrm{UA2}], \end{cases}$$

in agreement with the standard-model expectations ($\sigma B = 0.39$ nb).

Analysing the 14 W candidates decaying into μν, the UA1 Collaboration found

$$(7.19)\qquad m_{\mathrm{W}} = 81^{+6}_{-7}\ \mathrm{GeV}\,.$$

The measured value of $(\sigma\,\mathrm{Br}^{\mu})_{\mathrm{W}}$ is

$$(7.20)\qquad (\sigma\,\mathrm{Br}^{\mu})_{\mathrm{W}} = [0.67 \pm 0.17\ (\mathrm{stat.}) \pm 0.15\ (\mathrm{syst.})]\ \mathrm{nb}\,.$$

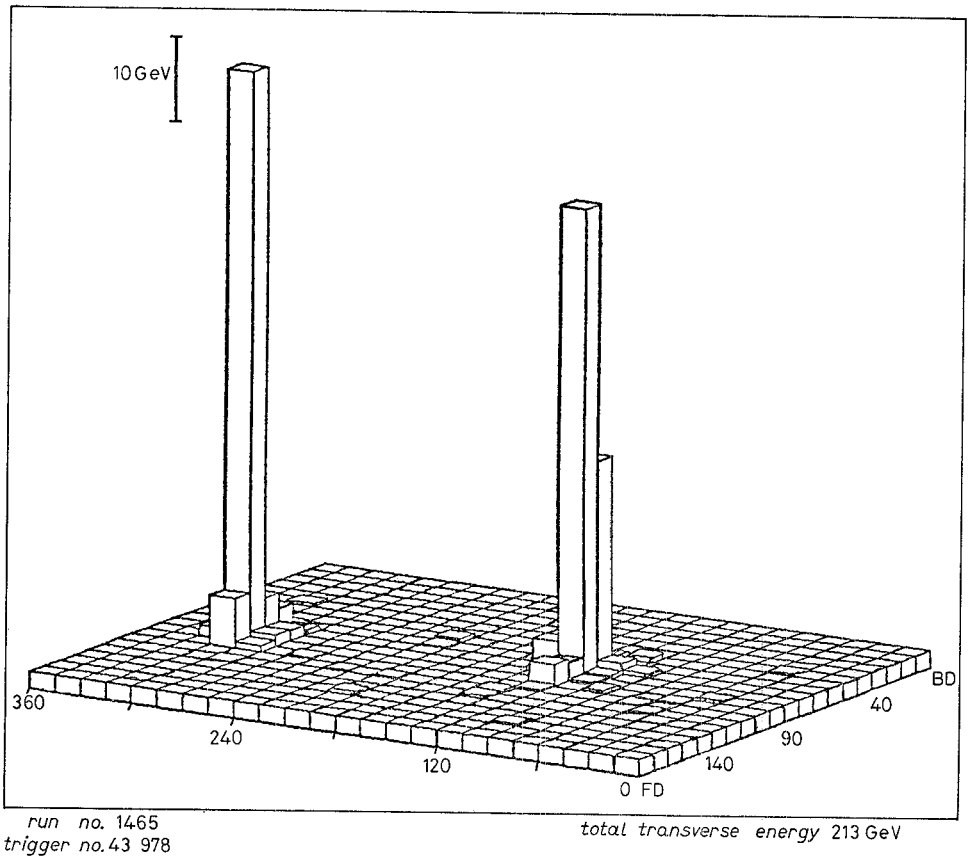

Fig. 103. – Plot of the electromagnetic energy flow in the UA2 calorimeter cells for a Z^0 event. CERN $p\bar{p}\sqrt{s} = 540$ GeV.

A total of five Z^0 candidate events (four decaying into electrons and one into muons) have been detected by the UA1 experiment. The UA2 experiment observed eight Z^0 decays into the electron channel. Figure 103 shows the calorimeter cell energy distribution as a function of polar and azimuthal angles for one of these events observed in the UA2 experiment. The mass distribution of the lepton pairs is shown in fig. 104*a*) (UA1) and fig. 104*b*) (UA2). For the Z^0 mass the following values were obtained:

$$(7.21)\qquad \begin{cases} m_Z = [95.6 \pm 1.4\ (\text{stat.}) \pm 2.9\ (\text{syst.})]\ \text{GeV} & [\text{UA1}], \\ m_Z = [92.7 \pm 1.7\ (\text{stat.}) \pm 1.4\ (\text{syst.})]\ \text{GeV} & [\text{UA2}]. \end{cases}$$

The measured values of $(\sigma\,\text{Br}^e)_Z$ are

$$(7.22)\qquad \begin{cases} (\sigma\,\text{Br}^e)_Z = [0.050 \pm 0.020\ (\text{stat.}) \pm 0.009\ (\text{syst.})]\ \text{nb} & [\text{UA1}], \\ (\sigma\,\text{Br}^e)_Z = [0.110 \pm 0.040\ (\text{stat.}) \pm 0.020\ (\text{syst.})]\ \text{nb} & [\text{UA2}]. \end{cases}$$

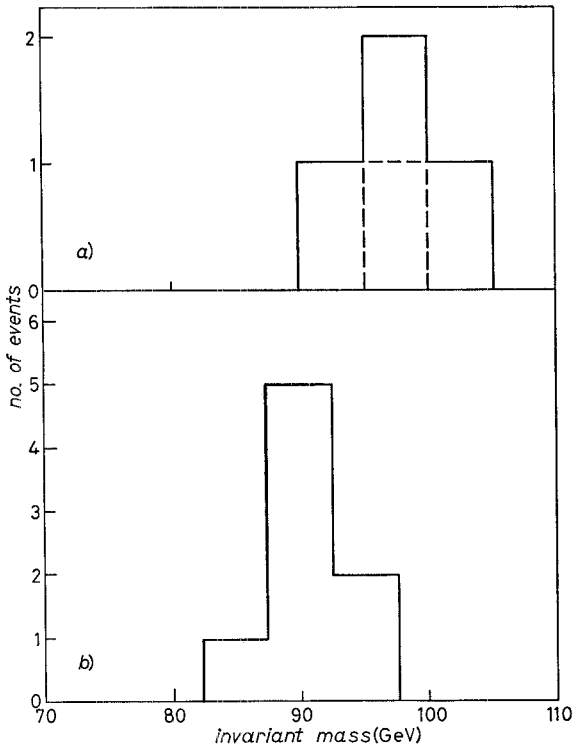

Fig. 104. – Invariant-mass distribution of charged lepton pairs: *a*) UA1 results (5 events), — — — $Z^0 \to \mu^+\mu^-$ 1 event, ——— $Z^0 \to e^+e^-$ 4 events; *b*) UA2 results (8 events).

The average values of the measured W and Z^0 masses are

$$\begin{cases} m_W = (82.2 \pm 1.8)\ \text{GeV}, \\ m_Z = (93.6 \pm 1.8)\ \text{GeV}, \end{cases} \tag{7.23}$$

in good agreement with the values (7.1). In eqs. (7.22) the statistical and the systematic errors are added in quadrature. Table XXIII shows the values

TABLE XXIII. – *Comparison between the values of* $\sin^2\theta_w$, ϱ *and* Δr *obtained at low and high energies.*

Parameters	W and Z^0 measurements	Low-energy $\nu\mathcal{N}$ experiment
$\sin^2\theta_w$, eq. (1.31)	0.232 ± 0.008	0.220 ± 0.006
$\sin^2\theta_w$, eq. (1.34)	0.221 ± 0.010	0.220 ± 0.006
$\sin^2\theta_w$, eq. (1.35)	0.218 ± 0.012	0.220 ± 0.006
ϱ, eq. (1.37)	0.988 ± 0.029	1.01 ± 0.01
Δr, eq. (1.36)	0.120 ± 0.088	0.0696 ± 0.0020

of $\sin^2\theta_w$, ϱ and Δr obtained from the measurement of the W and Z^0 masses (eqs. (1.31), (1.34)-(1.37)) and from low-energy measurements. The agreement between the experimental results provides strong support for the standard model.

The measurement of the width of the Z^0 (Γ_z) allows limits to be put on the number of additional types of light neutrinos Δn_ν. Combining the UA1 and UA2 results, it was found [219] that

$$\Delta n_\nu < 15 \qquad (90\,\%\ \text{c.l.}). \tag{7.24}$$

The quantity Γ_z can be also determined from the ratio of the number of $Z^0 \to e^+e^-$ and $W^\pm \to e\nu$ events. The UA2 Collaboration found

$$\Delta n_\nu = 0 \qquad (90\,\%\ \text{c.l.}). \tag{7.25}$$

During 1984 the UA1 and UA2 Collaborations increased the statistics by a factor of about 4. In the forthcoming years, before the shutdown of the Collider foreseen to take place in 1987 with a view to improving the luminosity (the antiproton collector (ACOL) project), an improvement in statistics by a factor of about 15 is expected. This would allow a determination of the W and Z^0 masses with an error of $(1 \div 2)\,\%$ due essentially to the systematic uncertainties. The error in the determination of $\sin^2\theta_w$ obtained from eq. (1.34) and combining the two experimental results would be $\Delta(\sin^2\theta_w) \approx 0.005$. The systematic errors almost cancel in the mass ratio and would allow a determination of $\sin^2\theta_w$ from eq. (1.31) with an error $\Delta(\sin^2\theta_w) \approx \pm 0.009$.

8. – The search for Higgs particles.

A neutral scalar Higgs particle is introduced in the standard model [9] by the spontaneous symmetry-breaking mechanism of the electroweak theory [5] (see subsect. I·1). The Higgs couples to each elementary particle with a strength proportional to the mass of the particle (eqs. (1.25) and (1.29)). In contrast with the mass of the IVBs, the mass of the Higgs boson is a free parameter of the theory. In other models [220] more Higgs particles are expected, including the charged ones, H^+ and H^-. The charged Higgs decay predominantly (as do the neutral ones) into the heaviest quarks and leptons that are kinematically allowed. In some models, such as the technicolour one [221], the gauge symmetry breaking is realized dynamically, and the resulting bosons, called technipions, are a condensate of new fundamental fermions. The coupling of the technipions to fermions is proportional to the fermion mass that has been predicted to be in the range $(5 \div 14)$ GeV [222].

The standard neutral Higgs particle can be produced in the radiative decay

of heavy quarkonia:

$$(8.1) \qquad QQ \to \gamma H^0 .$$

The expected branching ratio [223] is

$$(8.2) \qquad \mathrm{Br}\,(QQ \to \gamma H^0) = (G m_{QQ}^2/4\sqrt{2}\alpha\pi)(1 - m_{H^0}^2/m_{QQ}^2)\,\mathrm{Br}\,(QQ \to \mu^+\mu^-) .$$

Since $\mathrm{Br}\,(J/\psi \to \mu^+\mu^-) = 0.07$ and $\mathrm{Br}\,(\Upsilon \to \mu^+\mu^-) = 0.03$, if Higgs masses are negligible with respect to those of the quarkonia, one finds

$$(8.3) \qquad \begin{cases} \mathrm{Br}(J/\psi \to \gamma H^0) = 6 \cdot 10^{-5}, \\ \mathrm{Br}(\Upsilon \to \gamma H^0) = 2.5 \cdot 10^{-4}. \end{cases}$$

The CUSB Group searched for monochromatic photon signals from Υ and Υ' decay at CESR, both in inclusive photon from multihadron final states and in final states consisting of two charged particles [224]. No signal was observed. The 90 % c.l. upper limit on $\mathrm{Br}\,(\Upsilon \to \gamma H^0) \times \mathrm{Br}\,(H^0 \to \mathrm{had})$ obtained from the inclusive measurements is shown in fig. 105 as a function of the Higgs mass. The experimental constraints are still much larger than the theoretical predictions (8.3).

Extensive searches for charged Higgs were done mainly at PETRA and PEP in e^+e^- reactions. At the energies investigated, the differential cross-

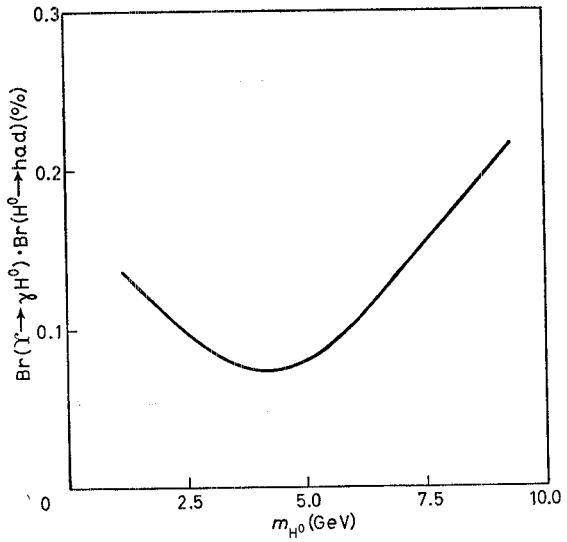

Fig. 105. – Limits at 90% c.l. on the product of the branching ratios $\mathrm{Br}(\Upsilon \to \gamma H^0)$ and $\mathrm{Br}(H^0 \to \mathrm{had})$ as a function of the Higgs mass [224].

section is

$$d\sigma/d\Omega = \alpha^2/8s\beta^3 \sin^2\theta \,, \tag{8.4}$$

where β is the velocity of the $H^{\pm}$ in the centre-of-mass system, and θ is the production angle with respect to the beam axis. The ratio of the leptonic and hadronic decay rates depends on the specific assumptions [225] used. Figure 106 shows the expected event patterns for $e^+e^- \to H^+H^-$. The reaction

$$e^+e^- \to H^+H^- \to (\tau\nu)(\tau\nu) \tag{8.5}$$

studied by CELLO [226], JADE [227], MARK II [228], MARK J [229] and

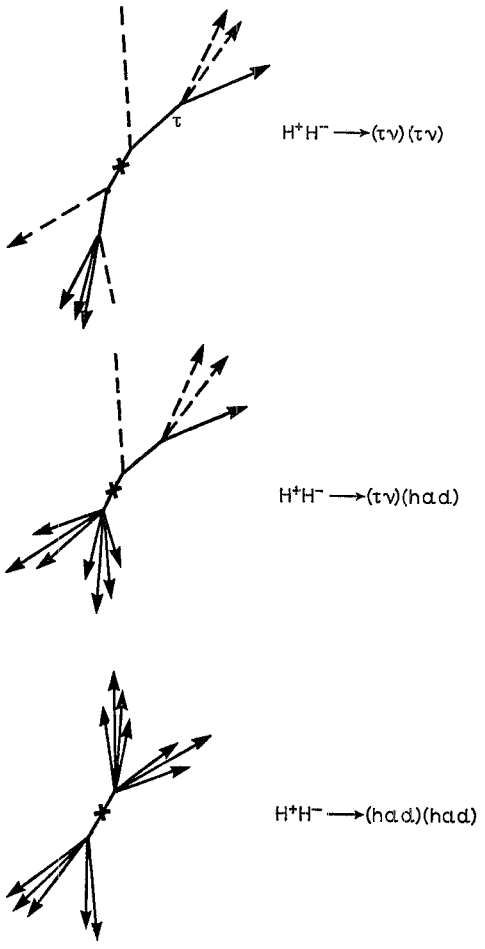

Fig. 106. – Event patterns for $e^+e^- \to H^+H^-$ reactions for different decay modes of $H^{\pm}$. The dashed lines represent neutrinos.

MAC [230] should give an excess in τ pair production over the QED yield. If the mass of the Higgs particle is high, reaction (8.5) should produce an acoplanar τ pair because of the energy carried away by neutrinos.

In the case of the reaction

$$e^+e^- \to H^+H^- \to (\tau\nu)(\text{had}) , \tag{8.6}$$

there will be multihadron events with the missing energy and total momentum unbalanced, owing to the undetected neutrino. For light $H^\pm$ masses, a single lepton from the τ decay would be emitted against a hadron jet. These reactions have been studied by JADE [227], MARK II [228], MARK J [229] and MAC [230].

The final state from the process

$$e^+e^- \to H^+H^- \to (\text{had})(\text{had}) \tag{8.7}$$

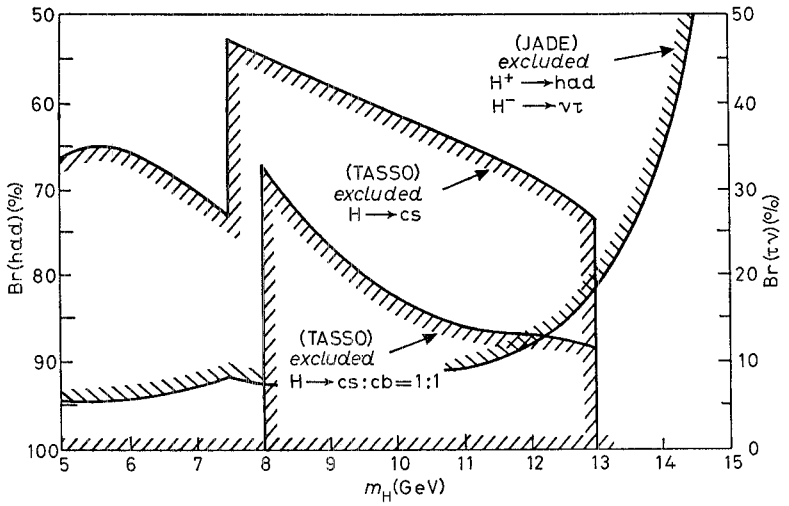

Fig. 107. – Limits on the leptonic (hadronic) branching ratio as a function of the $H^\pm$ mass obtained by JADE [227], studying the reactions $e^+e^- \to H^+H^- \to (\nu\tau)(\nu\tau)$ and $e^+e^- \to H^+H^- \to (\nu\tau)(\text{had})$, and by TASSO [231] studying the reaction $e^+e^- \to H^+H^- \to$ $\to$ [had)(had). The shaded regions are excluded at 95% c.l.

would consist of four hadronic jets. Two decay processes were studied by TASSO [231]:

$$\begin{cases} e^+e^- \to H^+H^-, & H^+ \to c\bar{s} , & H^- \to \bar{c}s , \\ e^+e^- \to H^+H^-, & H^+ \to c\bar{s}(c\bar{b}) , & H^- \to \bar{c}s(\bar{c}b) . \end{cases} \tag{8.8}$$

Experimental bounds on the masses of charged Higgs as a function of the leptonic (hadronic) branching ratio obtained by JADE [227] studying reactions (8.5) and (8.6), and from TASSO [231] studying reaction (8.7), are shown in fig. 107.

* * *

We wish to thank our colleagues in the CHARM Collaboration at CERN: I. ABT, J. V. ALLABY, U. AMALDI, J. ASPIAZU, A. BARONCELLI, L. BARONE, M. BAUBILLIER, B. BORGIA, C. BOSIO, C. BUSI, F. W. BÜSSER, A. CAPONE, H. DAUMANN, M. DIEMOZ, U. DORE, F. FERRONI, W. FLEGEL, D. GALL, P. GORBUNOV, G. GRANCAGNOLO, E. GRIGORIEV, T. HEBBEKER, V. KAFTANOV, V. KHOVANSKY, L. LANCERI, E. LONGO, L. LUMINARI, M. METCALF, P. MONACELLI, S. MORGANTI, G. NIEBERGALL, C. NIEUWENHUIS, F. DE NOTARISTEFANI, J. PANMAN, R. PLUNKETT, A. ROSANOV, P. SCHÜTT, P. STÄHELIN, L. TORTORA, V. VALENTE and K. WINTER.

Thanks are also due to all the people in the field who let us use figures and information.

We are grateful to G. COCCONI, D. HAIDT and H. WAHL for their critical reading of the manuscript.

We also wish to acknowledge the help of the CERN Data Handling Division's specialists in SCRIPT, the Scientific Reports Copy Editing Service (Documentation Department) and the Drawing Offices in the preparation of this review.

APPENDIX

List of abbreviations.

Laboratories

BNL:	Brookhaven National Laboratory, Upton, N.Y., USA.
CERN:	European Organization for Nuclear Research, Geneva, Switzerland.
DESY:	Deutsches Elektronen-Synchrotron, Hamburg, Fed. Rep. Germany.
FNAL:	Fermi National Accelerator Laboratory, Batavia, Ill., USA (also known as Fermilab).
IHEP:	Institute for High-Energy Physics, Serpukhov, USSR.
ITEP:	Institute for Theoretical and Experimental Physics, Moscow, USSR.
KEK:	National Laboratory for High-Energy Physics, Ibaraki-ken, Japan.
LBL:	Lawrence Berkeley Laboratory, Berkeley, Cal., USA.
SIN:	Schweizeriches Institut für Nuklearforschung, Villigen, Switzerland.
SLAC:	Stanford Linear Accelerator Center, Stanford, Cal., USA.
TRIUMF:	Tri-University Meson Facility, Vancouver, BC, Canada.

Machines

AGS:	BNL alternating-gradient synchroton.
CESR:	Cornell electron storage ring.
DORIS II:	Doppel Ring Speicher No. II (Double e^+e^- storage ring No. II).
LAMPF:	Los Alamos meson physics facility.
LEAR:	CERN low-energy antiproton ring.
LEP:	Large electron-positron storage ring.
PEP:	Positron-electron project.
PETRA:	Positron-electron tandem ring accelerator.
PS:	CERN proton synchrotron.
SLC:	SLAC linear collider.
SPEAR:	SLAC positron-electron accelerator ring.
SPS:	CERN super proton synchrotron.

Experiments and collaborations

ABCDLOS:	Aachen-Bonn-CERN-Demokritos-London-Oxford-Saclay.
AP:	Aachen-Padua.
APPW:	Athens-Padua-Pisa-Wisconsin.
ARGUS:	DESY-Dortmund-Heidelberg-Canada-Kansas-Ljubljana-Moscow-Columbia.
BCDMS:	Bologna-CERN-Dubna-Munich-Saclay.
BEBC:	Big European Bubble Chamber.
CCCFRR:	Chicago-CalTech-Columbia-Fermilab-Rochester-Rockefeller.
CCFR:	Chicago-Columbia-Fermilab-Rochester.
CDHS:	CERN-Dortmund-Heidelberg-Saclay.
CELLO:	DESY-Karlsruhe-Munich-Orsay-Paris-Saclay.
CHARM:	CERN-Hamburg-Amsterdam-Rome-Moscow.
CLEO:	Syracuse-Vanderbilt-Cornell-Ithaca-Harvard-Ohio-Rochester-Rutgers.
CUBS:	Stony Brook-Columbia-Cornell-Louisiana-Munich.
DELCO:	Los Angeles-SLAC-Irvine-Stony Brook.
E734:	BNL-Brown-KEK-Osaka-Pennsylvania-Stony Brook.
GGM:	Gargamelle Bubble Chamber.
HRS:	Purdue-Argonne-Indiana-Michigan-LBL-SLAC.
IFIM:	Fermilab-IHEP-ITEP-Michigan.
JADE:	Japan-Deutschland-England.
MAC:	Colorado-Frascati-Houston-Northeastern-SLAC-Utah-Wisconsin.
MARK J:	Aachen-DESY-Annecy-Massachusetts-Madrid-Amsterdam-Beijing.
MARK I:	SLAC-LBL.
MARK II:	SLAC-LBL-Harvard.
PLUTO:	Aachen-Bergen-DESY-Glasgow-Hamburg-Maryland-Siegen-Tel Aviv-Wuppertal.
TASSO:	Aachen-Bonn-DESY-Hamburg-London-Oxford-RAL-Siegen-Weizmann Institute-Wisconsin.
TPC:	LBL-Los Angeles-Riverside-Baltimore-Massachusetts-Tokyo-Yale.
UA1:	Underground Area Expt. No. 1 (Aachen-Annecy-Birmingham-CERN-Harvard-Helsinki-London-Amsterdam-Paris-Riverside-Rome-RAL-Saclay-Vienna-Wisconsin).
UA2:	Underground Area Expt. No. 2 (Berne-CERN-Copenhagen-Orsay-Pavia-Saclay).
VPI:	Virginia-Maryland-Washington-Oxford-Beijing.
WA2:	Bristol-Geneva-Heidelberg-Orsay-RAL-Strasbourg.

REFERENCES

[1] S. L. GLASHOW: *Nucl. Phys.*, **22**, 579 (1961); S. WEINBERG: *Phys. Rev. Lett.*, **19**, 1264 (1967); A. SALAM: *Elementary particle theory*, in *Proceedings of the VIII Nobel Symposium, Aspenäsgarden, 1968*, edited by N. SVARTHOLM (Almqvist and Wiksell, Stockholm, 1968), p. 367.

[2] F. J. HASERT *et al.*: *Phys. Lett. B*, **46**, 121 (1973).

[3] For the experimental evidence for the Z^0, see G. ARNISON *et al.*: *Phys. Lett. B*, **126**, 398 (1983); P. BAGNAIA *et al.*: *Phys. Lett. B*, **129**, 130 (1983). Experimental results on the W have been reported by G. ARNISON *et al.*: *Phys. Lett. B*, **122**, 103 (1983); M. BANNER *et al.*: *Phys. Lett. B*, **122**, 476 (1983); G. ARNISON *et al.*: *Phys. Lett. B*, **129**, 273 (1983); P. BAGNAIA *et al.*: *Z. Phys. C*, **24**, 1 (1984); G. ARNISON *et al.*: *Phys. Lett. B*, **134**, 469 (1984).

[4] G. W. 'T HOOFT: *Nucl. Phys. B*, **83**, 173 (1971).

[5] P. W. HIGGS: *Phys. Lett.*, **12**, 132 (1964); *Phys. Rev.*, **145**, 1156 (1966).

[6] M. KOBAYASHI and K. MASKAWA: *Prog. Theor. Phys.*, **49**, 652 (1973).

[7] N. CABIBBO: *Phys. Rev. Lett.*, **10**, 531 (1963).

[8] S. L. GLASHOW, J. ILIOPOULOS and L. MAIANI: *Phys. Rev. D*, **2**, 1285 (1970).

[9] S. WEINBERG: *Phys. Rev. D*, **19**, 1277 (1979).

[10] D. A. ROSS and M. VELTMAN: *Nucl. Phys. B*, **95**, 135 (1975).

[11] W. J. MARCIANO and A. SIRLIN: *Phys. Rev. Lett.*, **46**, 163 (1981).

[12] See, for example, G. MARTINELLI: CERN TH 3971 (1984), and references quoted therein.

[13] A. SIRLIN: *Phys. Rev. D*, **22**, 971 (1980); W. J. MARCIANO and A. SIRLIN: *Phys. Rev. D*, **22**, 2695 (1980).

[14] S. SARANTAKOS, A. SIRLIN and W. MARCIANO: *Nucl. Phys. B*, **217**, 84 (1983).

[15] A. SIRLIN: *Phys. Rev. D*, **29**, 89 (1984); W. J. MARCIANO and A. SIRLIN: *Phys. Rev. D*, **29**, 945 (1984).

[16] H. ABRAMOWICZ *et al.*: *Z. Phys. C*, **12**, 225 (1982).

[17] M. A. BEG, R. V. BUDNY, R. MOHAPATRA and A. SIRLIN: *Phys. Rev. Lett.*, **38**, 1252 (1977); M. GELL-MANN, P. RAMOND and R. SLANSKY: *Rev. Mod. Phys.*, **50**, 721 (1978).

[18] R. L. KINGSLEY, F. WILCZEK and A. ZEE: *Phys. Rev. D*, **10**, 2216 (1974).

[19] B. KAYSER, G. T. GARVEY, E. FISCHBACH and S. P. ROSEN: *Phys. Lett. B*, **52**, 385 (1974).

[20] M. JONKER *et al.*: *Z. Phys. C*, **17**, 211 (1983).

[21] C. JARLSKOG: *Lett. Nuovo Cimento*, **1**, 337 (1970).

[22] F. BERGSMA *et al.*: *Phys. Lett. B*, **122**, 465 (1983).

[23] N. ARMENISE *et al.*: *Phys. Lett. B*, **84**, 137 (1979).

[24] M. JONKER *et al.*: *Phys. Lett. B*, **93**, 203 (1980).

[25] B. BAIKE *et al.*: Berkeley preprint LBL-18320 (1984); H. M. STEINER: in *Proceedings of the XXII International Conference on High-Energy Physics, Leipzig, 1984*, edited by A. MEYER and E. WIECZOREK (Akad. Wissensch. DDR, Leipzig, 1984), Vol. **1**, p. 208.

[26] W. BACINO *et al.*: *Phys. Rev. Lett.*, **42**, 749 (1979).

[27] A. ALI and Z. Z. AYDIN: *Nuovo Cimento*, **43**, 270 (1978).

[28] H. ABRAMOWICZ *et al.*: *Z. Phys. C*, **15**, 19 (1982).

[29] M. JONKER *et al.*: *Phys. Lett. B*, **107**, 241 (1981).

[30] G. ARNISON *et al.*: *Phys. Lett. B*, **147**, 493 (1984).
[31] H. D. POLITZER: *Phys. Rep. C*, **14**, 129 (1974).
[32] L. MAIANI: in *International Symposium on Lepton and Photon Interactions at High Energies, Hamburg 1977* (DESY, Hamburg, 1977), p. 877
[33] K. L. GIOVANNETTI *et al.*: *Phys. Rev. D*, **29**, 343 (1984).
[34] D. H. WILKINSON: *Symmetries and nuclei*, in *Nuclear Physics with Heavy Ions and Mesons*, Vol. **2**, edited by R. BALIAN, M. RHO and G. RIPKA (North-Holland Publ. Co., Amsterdam, 1978).
[35] M. BOURQUIN *et al.*: *Z. Phys. C*, **21**, 27 (1983).
[36] R. E. SHROCK and L. L. WANG: *Phys. Rev. Lett.*, **41**, 1692 (1978); R. E. SHROCK, S. B. TREIMAN and L. L. WANG: *Phys. Rev. Lett.*, **42**, 1589 (1979).
[37] E. A. PASCHOS and U. TURKE: *Phys. Lett. B*, **116**, 360 (1982).
[38] M. BOURQUIN *et al.*: *Z. Phys. C*, **12**, 307 (1982); **21**, 1, 17 (1983).
[39] C. J. CHRISTENSEN *et al.*: *Phys. Rev. D*, **5**, 1628 (1972); J. BYRNE *et al.*: *Phys. Lett. B*, **92**, 274 (1980).
[40] J. G. H. DE GROOT *et al.*: *Z. Phys. C*, **1**, 143 (1979).
[41] W. BACINO *et al.*: *Phys. Rev. Lett.*, **43**, 1073 (1979).
[42] R. SCHINDLER *et al.*: *Phys. Rev. D*, **24**, 78 (1981).
[43] N. REY: in *Proceedings of the International Symposium on Lepton and Photon Interactions at High Energies, Ithaca, 1983*, edited by G. D. CASSEL and L. KREINICK (Cornell University, Ithaca, N. Y., 1983), p. 244.
[44] J. LEE-FRANZINI: in *Proceedings of the Europhysics Conference on Flavour Mixing in Weak Interactions, Erice, 1984*, edited by L. L. CHAU (Plenum Press, New York, N. Y., London, 1984), p. 217.
[45] M. HOLDER *et al.*: *Phys. Lett. B*, **70**, 396 (1977); J. G. H. DE GROOT *et al.*: *Phys. Lett. B*, **86**, 103 (1979); K. NISHIKAWA *et al.*: *Phys. Rev. Lett.*, **46**, 1555 (1981); T. TRINKO *et al.*: *Phys. Rev. D*, **23**, 1889 (1981); M. JONKER *et al.*: *Phys, Lett. B*, **107**, 241 (1981).
[46] K. KLEINKNECHT: in *Proceedings of the XII International Neutrino Conference, Balatonfüred*, 1982, Vol. **1** (Central Res. Inst. Physics, Budapest, 1982), p. 115.
[47] C. KLOPFENSTEIN *et al.*: *Phys. Lett. B*, **130**, 444 (1983).
[48] A. CHEN *et al.*: *Phys. Rev. Lett.*, **52**, 1084 (1984).
[49] J. LEE-FRANZINI: in *Proceedings of the XXII International Conference on High-Energy Physics, Leipzig, 1984*, Vol. **1**, edited by A. MEYER and E. WIECZOREK (Akad. Wissensch. DDR, Leipzig, 1984), p. 150.
[50] N. S. LOCKYER *et al.*: *Phys. Rev. Lett.*, **51**, 1316 (1983).
[51] G. WOLF: in *Proceedings of the XXII International Conference on High-Energy Physics, Leipzig, 1984*, Vol. **1**, edited by A. MEYER and E. WIECZOREK (Akad. Wissensch. DDR, Leipzig, 1984), p. 175.
[52] M. K. GAILLARD and L. MAIANI: in *Proceedings of the Summer Institute on Quarks and Leptons, Cargèse, 1979* (Plenum Press, New York, N. Y., 1980), p. 433.
[53] J. P. ALBANESE *et al.*: preprint CERN-EP/85-76 (1985).
[54] K. KLEINKNECHT and B. RENK: *Phys. Lett. B*, **130**, 459 (1983).
[55] G. D. ROCHESTER and C. C. BUTLER: *Nature (London)*, **160**, 855 (1947).
[56] M. GELL-MANN: *Phys. Rev.*, **92**, 833 (1953); T. NAKANO and K. NISHIJIMA: *Prog. Theor. Phys.*, **10**, 581 (1953).
[57] T. D. LEE and C. N. YANG: *Phys. Rev.*, **104**, 254 (1956).
[58] J. J. AUBERT *et al.*: *Phys. Rev. Lett.*, **33**, 1404 (1974); J. E. AUGUSTIN *et al.*: *Phys. Rev. Lett.*, **33**, 1406 (1974); C. BACCI *et al.*, B. BARTOLI *et al.*, G. BARBARINO *et al.*: *Phys. Rev. Lett.*, **33**, 1408 (1974).
[59] J. CHRISTENSON J. W. CRONIN, V. L. FITCH and R. TURLAY: *Phys. Rev. Lett.*, **13**, 138 (1964).

[60] L. WOLFENSTEIN: *Phys. Rev. Lett.*, **13**, 563 (1964).
[61] See, for instance, J. W. CRONIN: *Rev. Mod. Phys.*, **53**, 373 (1981); I. MANNELLI: in *Fifty Years of Weak-Interaction Physics, Bologna, 1984*, edited by A. BERTIN, R. A. RICCI and A. VITALE (Italian Physical Society, Bologna, 1984), p. 297.
[62] F. NIEBERGALL *et al.*: *Phys. Lett. B*, **49**, 103 (1974).
[63] See *Review of Particle Properties*, *Rev. Mod. Phys.* **56**, No. 2, Part 2, S16(1984).
[64] F. J. GILMAN and J. S. HAGELIN: *Phys. Lett. B*, **133**, 443 (1983).
[65] B. WINSTEIN: in *Proceedings of the XI International Conference on Nuetrino Physics and Astrophysics, Nordkirchen, 1984*, edited by K. KLEINKNECHT and E. A. PASCHOS (World Scientific, Singapore, 1984), p. 627.
[66] J. K. BLACK *et al.*: *Measurement of the CP-violating parameter* ε'/ε, to be published in *Phys. Rev. Lett.* See also K. NISHIKAWA: in *Proceedings of the XXII International Conference on High-Energy Physics, Leipzig, 1984*, Vol. **1**, edited by A. MEYER and E. WIECZOREK (Akad. Wissensch. DDR, Leipzig, 1984), p. 163.
[67] M. HOLDER *et al.*: *Phys. Lett. B*, **40**, 141 (1972).
[68] M. BANNER *et al.*: *Phys. Rev. Lett.*, **28**, 1597 (1972).
[69] J. H. CHRISTENSON *et al.*: *Phys. Rev. Lett.*, **43**, 1209 (1979).
[70] D. CUNDY *et al.*: proposal CERN/81-110, SPSC/P174 (1981).
[71] G. GOLLIN *et al.*: Fermilab proposal No. 749 (1983).
[72] L. ADIELS *et al.*: proposal CERN/PSCC/85-6, PSCC/P82 (1985).
[73] R. ABELA *et al.*: SIN Newsletter 15, 26.
[74] P. WAGNER: private communication.
[75] V. LUBIMOV: in *Proceedings of the XXII International Conference on High-Energy Physics, Leipzig, 1984*, Vol. **1**, edited by A. MEYER and E. WIECZOREK (Akad. Wissensch. DDR, Leipzig, 1984), p. 259.
[76] See, for example, R. E. SHROCK: *Phys. Rev. D*, **24**, 1232 (1981).
[77] G. STEIGMAN: preprint BA-84-43 (1984).
[78] E. LIPMAA *et al.*: *Pis'ma Ž. Èksp. Teor. Fiz.*, **39**, 529 (1984).
[79] S. P. ROSEN: in *Proceedings of the Moriond Workshop on Massive Neutrinos in Astrophysics and Particle Physics, La Plagne, 1984*, edited by J. TRAN THANH VAN (Editions Frontières, Gif-sur-Yvette, 1984), p. 483.
[80] R. G. H. ROBERTSON: in *Proceedings of the Moriond Workshop on Massive Neutrinos in Astrophysics and Particle Physics, La Plagne, 1984*, edited by J. TRAN THANH VAN (Editions Frontières, Gif-sur-Yvette, 1984), p. 253.
[81] H. B. ANDERHUD *et al.*: *Phys. Lett. B*, **114**, 76 (1982).
[82] D. C. LU *et al.*: *Phys. Rev. Lett.*, **45**, 1066 (1980).
[83] R. ABELA *et al.*: *Phys. Lett. B*, **105**, 263 (1981).
[84] Y. YAMAZAKI: in *Proceedings of the XXII International Conference on High-Energy Physcs, Leipzig, 1984*, Vol. **1**, edited by A. MEYER and E. WIECZOREK (Akad. Wissensch. DDR, Leipzig, 1984), p. 262.
[85] R. S. HAYANO *et al.*: *Phys. Rev. Lett.*, **49**, 1305 (1982).
[86] Y. ASANO *et al.*: *Phys. Lett. B*, **104**, 84 (1981).
[87] C. Y. PANG *et al.*: *Phys. Rev. D*, **8**, 1989 (1973).
[88] A. M. SARKAR-COOPER: in *Proceedings of the XXII International Conference on High-Energy Physics, Leipzig, 1984*, Vol. **1**, edited by A. MEYER and E. WIECZOREK (Akad. Wissensch. DDR, Leipzig, 1984), p. 163.
[89] C. MATTEUZZI *et al.*: *Phys. Rev. Lett.*, **52**, 1869 (1984). Updated results were presented by W. R. INNES: in *Proceedings of the XXII International Conference on High-Energy Physics, Leipzig, 1984*, Vol. **1**, edited by A. MEYER and E. WIECZOREK (Akad. Wissensch. DDR, Leipzig, 1984), p. 364.
[90] D. TOUSSAINT and F. WILCZEK: *Nature (London)*, **289**, 777 (1981).
[91] D. A. BRYMAN *et al.*: TRIUMF preprint TRI-PP-82-43 (1982).

[92] See D. BERGHOFER *et al.*: in *Proceedings of the International Conference on Neutrino Physics and Astrophysics, Maui, Hawaii, 1981*, Vol. **2**, edited by R. J. CENCE, E. MA and A. ROBERTS (University of Hawaii, Honolulu, 1981), p. 67.
[93] F. BERGSMA *et al.*: *Phys. Lett. B*, **128**, 361 (1983).
[94] F. BERGSMA *et al.*: *Search for heavy neutrinos in the mass range* (500÷2800) MeV, preprint CERN in preparation.
[95] M. GRONAU: Stanford preprint SLAC-PUB-2967 (1982).
[96] M. GRONAU, C. N. LEUNG and J. L. ROSNER: *Phys. Rev. D*, **29**, 2359 (1984), and references quoted therein.
[97] D. PERRET-GALLIX *et al.*: proposal CERN/PSCC/83-12, PSCC/P67 (1983).
[98] B. PONTECORVO: *Ž. Èksp. Teor. Fiz.*, **34**, 247 (1958) (English translation: *Sov. Phys. JETP*, **7**, 172 (1958)); *Ž. Èksp. Teor. Fiz.*, **53**, 1725 (1967) (English translation: *Sov. Phys. JETP*, **26**, 984 (1968)).
[99] N. J. BAKER *et al.*: *Phys. Rev. Lett.*, **47**, 1576 (1981).
[100] U. USHIDA *et al.*: *Phys. Rev. Lett.*, **47**, 1694 (1981).
[101] F. BERGSMA *et al.*: *Phys. Lett. B*, **142**, 251 (1984).
[102] See U. DORE: in *Proceedings of the XXII International Conference on High-Energy Physics, Leipzig, 1984*, Vol. **1**, edited by A. MEYER and E. WIECZOREK (Akad. Wissensch. DDR, Leipzig, 1984), p. 265.
[103] L. A. AHRENS *et al.*: *Phys. Rev. D*, **31**, 2732 (1985).
[104] I. E. STOCKDALE *et al.*: *Phys. Rev. Lett.*, **52**, 1384 (1984).
[105] F. DYDAK *et al.*: *Phys. Lett. B*, **134**, 281 (1984).
[106] J. WOTSCHACK: in *Proceedings of the XI International Conference on Neutrino Physics and Astrophysics, Nordkirchen, 1984*, edited by K. KLEINKNECHT and E. A. PASCHOS (World Scientific, Singapore, 1984), p. 117.
[107] J. L. VUILLEUMIER *et al.*: *Phys. Lett. B*, **114**, 298 (1982); K. GABATHULER *et al.*: *Phys. Lett. B*, **138**, 449 (1984).
[108] J. F. CAVAIGNAC *et al.*: *Phys. Lett. B*, **148**, 387 (1984).
[109] S. P. ROSEN: in *Proceedings of the International Conference on Neutrino Physics and Astrophysics, Maui, Hawaii, 1981*, Vol. **2**, edited by R. J. CENCE, E. MA and A. ROBERTS (University of Hawaii, Honolulu, 1981), p. 76.
[110] H. NISHIURA: report RIFP-453 Kyoto University (1981); M. DOI, T. KOTANI, H. NISHIURA and E. TOKASUGI: *Prog. Theor. Phys.*, **69**, 602 (1983).
[111] T. KIRSTEN: in *Proceedings of the XI International Conference on Neutrino Physics and Astrophysics, Nordkirchen, 1984*, edited by K. KLEINKNECHT and E. A. PASCHOS (World Scientific, Singapore, 1984), p. 145.
[112] W. HAXTON and G. J. STEPHENSON: Los Alamos preprint LA-UR-84-396 (1984).
[113] H. V. KLAPDOR and K. GROTZ: *Phys. Lett. B*, **142**, 323 (1984).
[114] W. HAXTON, G. STEPHENSON and D. STROTTMAN: *Phys. Rev. Lett.*, **47**, 153 (1981).
[115] B. PONTECORVO: *Sov. Phys. JETP*, **26**, 984 (1968).
[116] T. KIRSTEN, H. RICHTER and E. JESSBERGER: *Phys. Rev. Lett.*, **50**, 474 (1983).
[117] E. BELLOTTI: in *Proceedings of the XI International Conference on Neutrino Physics and Astrophysics, Nordkirchen, 1984*, edited by K. KLEINKNECHT and E. A. PASCHOS (World Scientific, Singapore, 1984), p. 171.
[118] A. A. POMANSKY: in *Proceedings of the XI International Conference on Neutrino Physics and Astrophysics, Nordkirchen, 1984*, edited by K. KLEINKNECHT and E. A. PASCHOS (World Scientific, Singapore, 1984), p. 161.
[119] M. K. MOE and D. D. LOWENTHAL: *Phys. Rev. C*, **22**, 2186 (1980).
[120] B. KAYSER: in *Proceedings of the Moriond Workshop on Massive Neutrinos in Astrophysics and Particle Physics, La Plagne, 1984*, edited by J. TRAN THANH VAN (Editions Frontières, Gif-sur-Yvette, 1984), p. 11.

[121] R. EISBERG: in *Proceedings of the Moriond Workshop on Massive Neutrinos in Astrophysics and Particle Physics, La Plagne, 1984*, edited by J. TRAN THANH VAN (Editions Frontières, Gif-sur-Yvette, 1984), p. 439.
[122] M. JONKER *et al.*: *Phys. Lett. B*, **102**, 67 (1981).
[123] *Review of Particle Properties, Rev. Mod. Phys.*, **56**, No. 2, Part 2, S12 (1984).
[124] M. HOLDER *et al.*: *Phys. Lett. B*, **74**, 277 (1978).
[125] V. EFREMENKO *et al.*: *Phys. Lett. B*, **88**, 181 (1979).
[126] C. BALTAY: *Phys. Rev. Lett.*, **39**, 62 (1977).
[127] See, for example, K. WINTER: in *Proceedings of the* JINR-CERN *School of Physics, Dobogoko, Hungary, 1979*, Vol. **1** (Hungarian Acad. Sci. and Central Research Inst. for Physics, Budapest, 1980), p. 1.
[128] See S. STONE: in *Proceedings of the International Symposium on Lepton and Photon Interactions at High Energies, Ithaca, 1983*, edited by D. G. CASSEL and L. KREINICK (Cornell University, Ithaca, N. Y., 1983), p. 203.
[129] G. W. 'T HOOFT: *Phys. Lett. B*, **37**, 195 (1971).
[130] F. REINES, H. S. GURR and H. W. SOBEL: *Phys. Rev. Lett.*, **37**, 315 (1976).
[131] W. KRENZ: Aachen preprint PITHA 82/26 (1982).
[132] B. NAROSKA: in *Proceedings of the International Symposium on Lepton and Photon Interactions at High Energies, Ithaca, 1983*, edited by D. G. CASSEL and L. KREINICK (Cornell University, Ithaca, N. Y., 1983), p. 96.
[133] K. C. WANG: in *Proceedings of the XI International Conference on Neutrino Physics and Astrophysics, Nordkirchen, 1984*, edited by K. KLEINKNECHT and E. A. PASCHOS (World Scientific, Singapore, 1984), p. 322.
[134] H. FAISSNER *et al.*: *Phys. Rev. Lett.*, **41**, 213 (1978).
[135] N. ARMENISE *et al.*: *Phys. Lett. B*, **86**, 225 (1979).
[136] A. M. CNOPS *et al.*: *Phys. Rev. Lett.*, **41**, 6 (1978). See also M. J. MURTAGH: in *Proceedings of the XI International Conference on Neutrino Physics and Astrophysics, Nordkirchen, 1984*, edited by K. KLEINKNECHT and E. A. PASCHOS (World Scientific, Singapore, 1984), p. 290.
[137] R. H. HEISTERBERG *et al.*: *Phys. Rev. Lett.*, **44**, 635 (1980).
[138] F. BERGSMA *et al.*: *Phys. Lett. B*, **147**, 481 (1984).
[139] L. A. AHRENS *et al.*: *Phys. Rev. Lett.*, **51**, 1514 (1984).
[140] J. BLIETSCHAU *et al.*: *Nucl. Phys. B*, **114**, 189 (1976).
[141] L. A. AHRENS *et al.*: *Phys. Rev. Lett.*, **55**, 1814 (1985).
[142] C. H. LLEWELLYN SMITH: Oxford preprint OUTP 83-005.
[143] F. PASCHOS and L. WOLFENSTEIN: *Phys. Rev.*, **70**, 91 (1973).
[144] P. C. BOSETTI *et al.*: *Nucl. Phys. B*, **217**, 1 (1983).
[145] M. JONKER *et al.*: *Phys. Lett. B*, **99**, 265 (1981).
[146] J. KNOBLOCH: in *Proceedings of the XXII International Conference on High-Energy Physics, Leipzig, 1984*, Vol. **1**, edited by A. MEYER and E. WIECZOREK (Akad. Wissensch. DDR, Leipzig, 1984), p. 235.
[147] A. BODEK: in *Proceedings of the XXII International Conference on High-Energy Physics, Leipzig, 1984*, Vol. **1**, edited by A. MEYER and E. WIECZOREK (Akad. Wissensch. DDR, Leipzig, 1984), p. 234.
[148] D. ALLASIA *et al.*: *Phys. Lett. B*, **133**, 129 (1983).
[149] J. BLIETSCHAU *et al.*: *Phys. Lett. B*, **88**, 381 (1979).
[150] T. KAFKA *et al.*: *Phys. Rev. Lett.*, **48**, 910 (1982).
[151] N. ARMENISE *et al.*: *Phys. Lett. B*, **122**, 448 (1983).
[152] H. KLUTTIG, J. G. MORFIN and W. VAN DONINCK: *Phys. Lett. B*, **71**, 446 (1977).
[153] H. DEDEN: in *Proceedings of the International Conference on Neutrino Weak Interactions and Cosmology, Bergen, 1979*, Vol. **2**, edited by A. HAATUFT and C. JARLSKOG (University of Bergen, Bergen, 1979), p. 397.

[154] B. P. ROE: in *Proceedings of the International Conference on Neutrino Weak Intreactions and Cosmology, Bergen, 1979*, Vol. **2**, edited by A. HAATUFT and C. JARLSKOG (University of Bergen, Bergen, 1979), p. 592.
[155] L. M. SEHGAL: *Phys. Lett. B*, **71**, 99 (1977).
[156] W. KRENZ *et al.*: *Nucl. Phys. B*, **135**, 45 (1978).
[157] Q. ERRIQUEZ *et al.*: *Nucl. Phys. B*, **176**, 37 (1980).
[158] G. L. FOGLI: *Nucl. Phys. B*, **207**, 322 (1982).
[159] See, for example, P. Q. HUNG and J. J. SAKURAI: *The structure of neutral currents*, Berkeley preprint LBL-12364 (1981).
[160] A. ENTENBERG *et al.*: *Phys. Rev. Lett.*, **42**, 1198 (1979).
[161] H. FAISSNER *et al.*: *Phys. Rev. D*, **21**, 21 (1980).
[162] M. D. MARX: in *Proceedings of the XI International Conference on Neutrino Physics and Astrophysics, Nordkirchen, 1984*, edited by K. KLEINKNECHT and E. A. PASCHOS (World Scientific, Singapore, 1984), p. 280.
[163] E. PASIERB *et al.*: *Phys. Lett.*, **43**, 96 (1979).
[164] H. FAISSNER *et al.*: *Phys. Lett. B*, **125**, 230 (1983).
[165] F. BERGSMA *et al.*: preprint CERN-EP/85-37, to be published in *Phys. Lett.*
[166] D. REIN and L. M. SEHGAL: *Nucl. Phys. B*, **223**, 29 (1983).
[167] See A. PULLIA: in *Fifty Years of Weak-Interaction Physics, Bologna, 1984*, edited by A. BERTIN, R. A. RICCI and A. VITALE (Italian Physical Society, Bologna, 1984), p. 333.
[168] H. ABRAMOWICZ *et al.*: *Phys. Lett. B*, **109**, 115 (1982).
[169] A. R. CLARK *et al.*: *Phys. Rev. Lett.*, **43**, 187 (1979); J. J. AUBERT *et al.*: *Phys. Rev. Lett.*, **89**, 267 (1980).
[170] C. Y. PRESCOTT *et al.*: *Phys. Lett. B*, **77**, 347 (1978); **84**, 524 (1979).
[171] M. A. BOUCHIAT and C. BOUCHIAT: *Phys. Lett. B*, **48**, 111 (1974); *J. Phys.*, **35**, 899 (1974); **36**, 493 (1975).
[172] I. B. KRIPLOVICH: *JETP Lett.*, **20**, 315 (1974).
[173] L. M. MARKOV and M. S. ZOLOTOREV: *Phys. Lett. B*, **85**, 308 (1979).
[174] C. A. PIKETTY: in *Proceedings of the XI International Conference on Neutrino Physics and Astrophysics, Nordkirchen, 1984*, edited by K. KLEINKNECHT and E. A. PASCHOS (World Scientific, Singapore, 1984), p. 308.
[175] J. H. HOLLISTER *et al.*: *Phys. Rev. Lett.*, **46**, 643 (1981).
[176] T. P. EMMONS *et al.*: *Phys. Rev. Lett.*, **51**, 2089 (1983).
[177] P. BUCKSBAUM *et al.*: *Phys. Rev. Lett.*, **46**, 640 (1981); *Phys. Rev. D*, **24**, 1134 (1981).
[178] P. S. DRELL and E. D. COMMINS: preprint University of California, Berkeley, Cal. (May 1984).
[179] M. A. BOUCHIAT *et al.*: *Phys. Lett. B*, **117**, 358 (1982) (Erratum, **121**, 456 (1983)).
[180] M. A. BOUCHIAT *et al.*: *Phys. Lett. B*, **134**, 463 (1984).
[181] D. V. NEUFFER and E. D. COMMINS: *Phys. Rev. A*, **16**, 844 (1977).
[182] R. R. LEWIS and W. L. WILLIAMS: *Phys. Lett. B*, **59**, 70 (1975); E. A. HINDS and V. W. HUGHES: *Phys. Lett. B*, **67**, 480 (1977).
[183] A. ARGENTO *et al.*: *Phys. Lett. B*, **120**, 245 (1983).
[184] F. M. RENARD: *Basics of Electron-Positron Collisions* (Editions Frontières, Gif-sur-Yvette, 1981).
[185] H. J. BEHREND *et al.*: *Z. Phys. C*, **14**, 283 (1982).
[186] W. BARTEL *et al.*: *Phys. Lett. B*, **108**, 140 (1982).
[187] B. ADEVA *et al.*: *Phys. Rev. Lett.*, **48**, 1701 (1982); preprint MIT-LNS 128 (1983).
[188] C. BERGER *et al.*: *Z. Phys. C*, **14**, 283 (1982).
[189] R. BRANDELIK *et al.*: *Phys. Rev. Lett. B*, **110**, 173 (1982).

[190] M. ALTHOFF *et al.*: *Z. Phys. C*, **22**, 13 (1984).
[191] H. U. MARTYN: *Weak interactions*: PETRA *results*, preprint DESY 84-048 (1984), invited talk given at *The Symposium on High-Energy* e^+e^- *Interactions, Vanderbilt University, Nashville, Tenn.* (1984).
[192] E. FERNANDEZ *et al.*: *Phys. Rev. Lett.*, **50**, 1238 (1983).
[193] R. PREPOST: in *Proceedings of the XXII International Conference on High-Energy Physics, Leipzig, 1984*, Vol. **1**, edited by A. MEYER and E. WIECZOREK (Acad. Wissensch. DDR, Leipzig, 1984), p. 227.
[194] M. E. LEVI *et al.*: Stanford preprint SLAC-PUB-3177 (1983).
[195] M. DERRICK *et al.*: ANL-HEP-PR-84-71, UM HE 84-20, PU-84-521, IUHEE-59 (1984).
[196] C. K. BOWDERY: in *Proceedings of the XXII International Conference on High-Energy Physics, Leipzig, 1984*, Vol. **1**, edited by A. MEYER and E. WIECZOREK (Akad. Wissensch. DDR, Leipzig, 1984), p. 229.
[197] H. J. BEHREND *et al.*: *Phys. Lett. B*, **114**, 391 (1982).
[198] K. K. GAN *et al.*: PU-84-522, ANL-HEP-PR-84-89, IUHEE-60, UM HE 84-23 (1984).
[199] F. A. BERENDS *et al.*: *Nucl. Phys. B*, **63**, 381 (1973); **177**, 237 (1981); F. A. BERENDS and R. KLEISS: preprint DESY 80-66 (1980); F. A. BERENDS, R. KLEISS and S. JADACH: *Nucl. Phys. B*, **202**, 63 (1982); G. PASSARINO and M. VELTMAN: *Nucl. Phys. B*, **160**, 151 (1979); G. PASSARINO: *Nucl. Phys. B*, **204**, 237 (1982); M. GRECO *et al.*: *Nucl. Phys. B*, **171**, 118 (1979); **197**, 543 (1982); R. W. BROWN, R. DECKER and E. A. PASCHOS: *Phys. Rev. Lett.*, **52**, 1192 (1984); M. BOHM and W. HOLLIK: *Nucl. Phys. B*, **204**, 45 (1982); preprint DESY 83-060 (1983); W. WETZEL: Heidelberg University preprint (May 1983).
[200] H. J. BEHREND *et al.*: *Z. Phys. C*, **16**, 301 (1983).
[201] W. BARTEL *et al.*: *Z. Phys. C*, **19**, 197 (1983).
[202] W. BARTEL *et al.*: DESY preprint 84-059 (1984).
[203] M. ALTHOFF *et al.*: *Phys. Lett. B*, **126**, 493 (1983); **138**, 318 (1984).
[204] M. ALTHOFF *et al.*: *Z. Phys. C*, **22**, 219 (1984); DESY preprint 84-061 (1984).
[205] M. E. NELSON *et al.*: *Phys. Rev. Lett.*, **50**, 1542 (1983); SLAC-PUB-3059 (1983).
[206] B. ADEVA *et al.*: preprint MIT-LNS 131 (1983).
[207] W. BARTEL *et al.*: DESY preprint 84-068 (1984).
[208] D. P. BARBER *et al.*: *Phys. Rev. Lett.*, **46**, 1663 (1981); R. BRANDELIK *et al.*: *Phys. Lett. B*, **113**, 499 (1982); W. BARTEL *et al.*: *Phys. Lett. B*, **129**, 145 (1983).
[209] F. DYDAK *et al.*: proposal CERN-SPSC/83-49, SPSC/P188 (1983).
[210] F. BERGSMA *et al.*: proposal CERN/SPSC/84-1, SPSC/P194 (1984).
[211] M. J. MURTAGH: in *Proceedings of the XI International Conference on Neutrino Physics and Astrophysics, Nordkirchen, 1984*, edited by K. KLEINKNECHT and E. A. PASCHOS (World Scientific, Singapore, 1984), p. 290.
[212] C. BUSI *et al.*: proposal CERN/SPSC/83-24, SPSC/P186 (1983).
[213] D. ALBERT, W. J. MARCIANO, Z. PARSA and D. WYLER: *Nucl. Phys. B*, **166**, 460 (1980); W. J. MARCIANO and Z. PARSA: in *Proceedings of the 1982* DPF *Summer Study on Elementary Particle Physics and Future Facilities, Snowmass, 1982* (AIP, New York, N. Y., 1983), p. 155.
[214] P. AURENCHE and J. LINDFORS: *Nucl. Phys. B*, **185**, 274 (1981).
[215] P. AURENCHE and R. KINNUNEN: Annecy report LAPP-TH-78 (1983); F. E. PAIGE: Brookhaven preprint BNL-27066 (1979).
[216] W. J. MARCIANO and Z. PARSA: Cornell report CNLS 81-485 (1981).
[217] S. PAKVASA, M. DECHANTSREITER, F. HALZEN and D. M. SCOTT: *Phys. Rev. D*, **20**, 2862 (1979).

[218] For a description of the UA1 and UA2 detectors, see E. RADERMACHER: preprint CERN-EP/84-41 (1984).
[219] See A. ROTHENBERG: in *Proceedings of the Moriond Workshop on Massive Neutrinos in Astrophysics and Particle Physics, La Plagne, 1984*, edited by J. TRAN THANH VAN (Editions Frontières, Gif-sur-Yvette, 1984), p. 453.
[220] E. GOLOWICH and T. C. YANG: *Phys. Lett. B*, **80**, 245 (1979); L. N. CHANG and J. E. KIM: *Phys. Lett. B*, **81**, 233 (1979); H. E. HABER, G. L. KANE and T. STERLING: *Nucl. Phys. B*, **161**, 493 (1979); G. BARBIELLINI *et al.*: DESY preprint 79-027 (1979).
[221] S. WEINBERG: *Phys. Rev. D*, **13**, 974 (1976); **19**, 1277 (1979); L. SUSSKIND: *Phys. Rev. D*, **20**, 2619 (1979); S. DIMOPOULOS and L. SUSSKIND: *Nucl. Phys. B*, **155**, 137 (1979); E. EICHTEN and K. LANE: *Phys. Lett. B*, **90**, 125 (1980).
[222] S. DIMOPOULOS: *Nucl. Phys. B*, **168**, 69 (1980); M. E. PESKIN: *Nucl. Phys. B*, **175**, 197 (1980); J. PRESKILL: *Nucl. Phys. B*, **177**, 21 (1981); S. CHADHA and M. E. PESKIN: *Nucl. Phys. B*, **185**, 61 (1981); **187**, 529 (1981).
[223] F. WILCZEK: *Phys. Rev. Lett.*, **40**, 279 (1978).
[224] M. SIVERTZ *et al.*: *Phys. Rev. D*, **26**, 717 (1982); S. YOUSSEF *et al.*: *Phys. Lett. B*, **139**, 322 (1984). See also P. FRANZINI: in *Proceedings of the XXII International Conference on High-Energy Physics, Leipzig, 1984*, Vol. **1**, edited by A. MEYER and E. WIECZOREK (Akad. Wissensch. DDR, Leipzig, 1984), p. 205.
[225] J. ELLIS, M. K. GAILLARD, D. V. NANOPOULOS and P. SIKIVIE: *Nucl. Phys. B*, **182**, 529 (1981).
[226] H. J. BEHREND *et al.*: *Phys. Lett. B*, **114**, 287 (1982).
[227] W. BARTEL *et al.*: *Phys. Lett. B*, **114**, 211 (1982).
[228] C. A. BLOCKER *et al.*: *Phys. Rev. Lett.*, **49**, 517 (1982).
[229] B. A. ADEVA *et al.*: *Phys. Lett. B*, **115**, 345 (1982).
[230] D. M. RITSON: in *Proceedings of the XXI International Conference on High-Energy Physics, Paris, 1982, J. Phys.* (*Paris*), C **3**, 52 (1982).
[231] M. ALTHOFF *et al.*: *Phys. Lett. B*, **122**, 95 (1983).

Direttore responsabile: RENATO ANGELO RICCI

Stampato in Bologna dalla Tipografia Compositori
coi tipi della Tipografia Monograf

Questo fascicolo è stato licenziato dai torchi il 5-V-1986

Questo periodico
è iscritto
all'Unione Stampa
Periodica Italiana

LAST PUBLISHED PAPERS

P. G. BIZZETI – Weak interactions in nuclei.

M. ADEMOLLO – Cabibbo theory and current algebra.

A. PULLIA – Structure of charged and neutral weak interactions at high energy.

G. ALTARELLI – Future perspectives in particle physics.

G. GOGGI – Gauge vector bosons and unified electroweak interaction.

M. GIFFON and E. PREDAZZI – High-energy physics after the SPS collider.

A. DEVOTO and D. W. DUKE – Table of integrals and formulae for Feynman diagram calculations.

A. BERTIN and A. VITALE – Pure Leptonic Weak Processes.

A. BERTIN and A. VITALE – Strangeness-conserving semi-leptonic weak processes.

F. PALMONARI – Nonleptonic weak interactions.

G. F. BIGNAMI – Galactic high-energy astrophysics after the gamma-ray astronomy mission of the ESA COS-B satellite.

G. IADONISI – Electron-phonon interaction: effects on the excitation spectrum of solids.

G. GIACOMELLI - Magnetic monopoles.

E. BUSSOLETTI – Interstellar grains.

C. TOMASI and F. TROMBETTI – Absorption and emission by minor atmospheric gases in the radiation balance of the Earth.

P. FURLAN – Conformal quantum electrodynamics and nondecomposable representation.

M. M. GIANNINI – Photoreactions above the giant dipole resonance.

P. RUGGIERO and M. ZANNETTI–Stochastic quantization at finite temperature.

C. A. DOMINGUEZ – The Goldberger-Treiman relation: a probe of the chiral symmetries of quantum chromodynamics.

I. MANNELLI – Neutral K-K mixing and *CP* violation.

D. V. NANOPOULOS – Superunification.

B. OLIVO-MELCHIORRI and F. MELCHIORRI - Progress in cosmology.

V. N. PERVUSHIN – The vacuum in gauge theories.

S. TWAREQUE ALI – Stochastic localization, quantum mechanics on phase space and quantum space-time.

A. DUPASQUIER and A. ZECCA – Atomic and solid-state physics experiments with slow-positron beams.

E. GATTI and P. F. MANFREDI – Processing the signals from solid-state detectors in elementary-particle physics.

FORTHCOMING PAPERS (in alphabetical order)

I. A. BATALIN and E. S. FRADKIN – Operator quantization and Abelization of dynamical systems subject to first-class constraints.

S. A. BONOMETTO and A. MASIERO – Phase transitions in the early Universe.

V. BORTOLANI and A. C. LEVI – Atom-surface scattering theory.

C. CASO and M. C. TOUBOUL – Measurements of heavy-flavour lifetimes.

G. COSTA and F. ZWIRNER – Baryon and lepton number nonconservation.

M. DOBROWOLNY – The TSS project: electrodynamics of long metallic tethers in the ionosphere.

G. L. FOGLI – Neutrino-induced deep inelastic scattering and the structure of the neutral current. A review and an updated analysis.

H. GRUPPELAAR, P. NAGEL and P. E. HODGSON – Pre-equilibrium processes in nuclear-reaction theory: the state of the art and beyond.

C. LEONARDI, F. PERSICO and G. VETRI – Dicke model and the theory of driven and spontaneous emission.

V. R. MANFREDI – Old and new results in statistical nuclear spectroscopy.

E. RECAMI – Classical tachyons.

LA RIVISTA DEL NUOVO CIMENTO della società italiana di fisica

Quote di abbonamento alla *Rivista del Nuovo Cimento* per l'anno 1986:

Per i Soci in Italia	L. 175.000
Per i non Soci in Italia	L. 220.000

Abbonamento cumulativo al *Nuovo Cimento*, Sezioni A, B, C e D, *Rivista del Nuovo Cimento*:

Per i Soci in Italia	L. 1.280.000
Per i non Soci in Italia	L. 1.610.000

La *Rivista del Nuovo Cimento* è in vendita anche in fascicoli separati al prezzo di lire 20.000 ciascuno; per ordini cumulativi di almeno 10 copie sarà concesso uno sconto del 10% sul prezzo complessivo.
Le somme per l'abbonamento e per l'acquisto dei fascicoli vanno versate (direttamente o per mezzo di un libraio) a **Editrice Compositori, viale XII Giugno, 1 - 40124 Bologna,** alla quale occorre rivolgersi anche per l'acquisto di volumi arretrati o numeri isolati. Trascorsi 3 mesi dalla data di pubblicazione, non saranno piú accettati reclami per i fascicoli non pervenuti.

Subscriptions to *Rivista del Nuovo Cimento* for the year 1986:

To members abroad	$ 165.00
To nonmembers abroad	$ 210.00

Combined subscription to *Il Nuovo Cimento*, Sections A, B, C and D, *Rivista del Nuovo Cimento:*

To members abroad	$ 1220.00
To nonmembers abroad	$ 1520.00

Subscribers who wish to receive their issues by air mail will be charged extra postage. The airmail postage for 1986 amounts to $ 20.00.
Single issues of *Rivista del Nucvo Cimento* may be purchased at the price of US $ 15.00 each; 10% discount on this price will be allowed for bulk orders of 10 copies or more. Subscriptions and purchase orders should be sent, either directly or through a bookseller, to **Editrice Compositori, viale XII Giugno, 1 - I 40124 Bologna (Italy).** Requests for back numbers or single copies should be directed to the same address.
3 months after publication we will not consider complaints for issues not received.

Per qualsiasi ordinazione rivolgersi a
For any order please write to

EDITRICE COMPOSITORI Viale XII Giugno, 1 I 40124 Bologna (Italy)

Autorizzazione del Tribunale di Bologna n. 3382 del 24 dicembre 1968

La Rivista del Nuovo Cimento

volume 9 serie 3 numero 2 1986

Experimental Status of Weak Interactions.

G. BARBIELLINI and C. SANTONI

Price of this issue $15.00
10 % discount for bulk orders
of 10 copies or more

Prezzo del fascicolo lire 20.000
sconto 10 % per ordini
cumulativi di almeno 10 copie